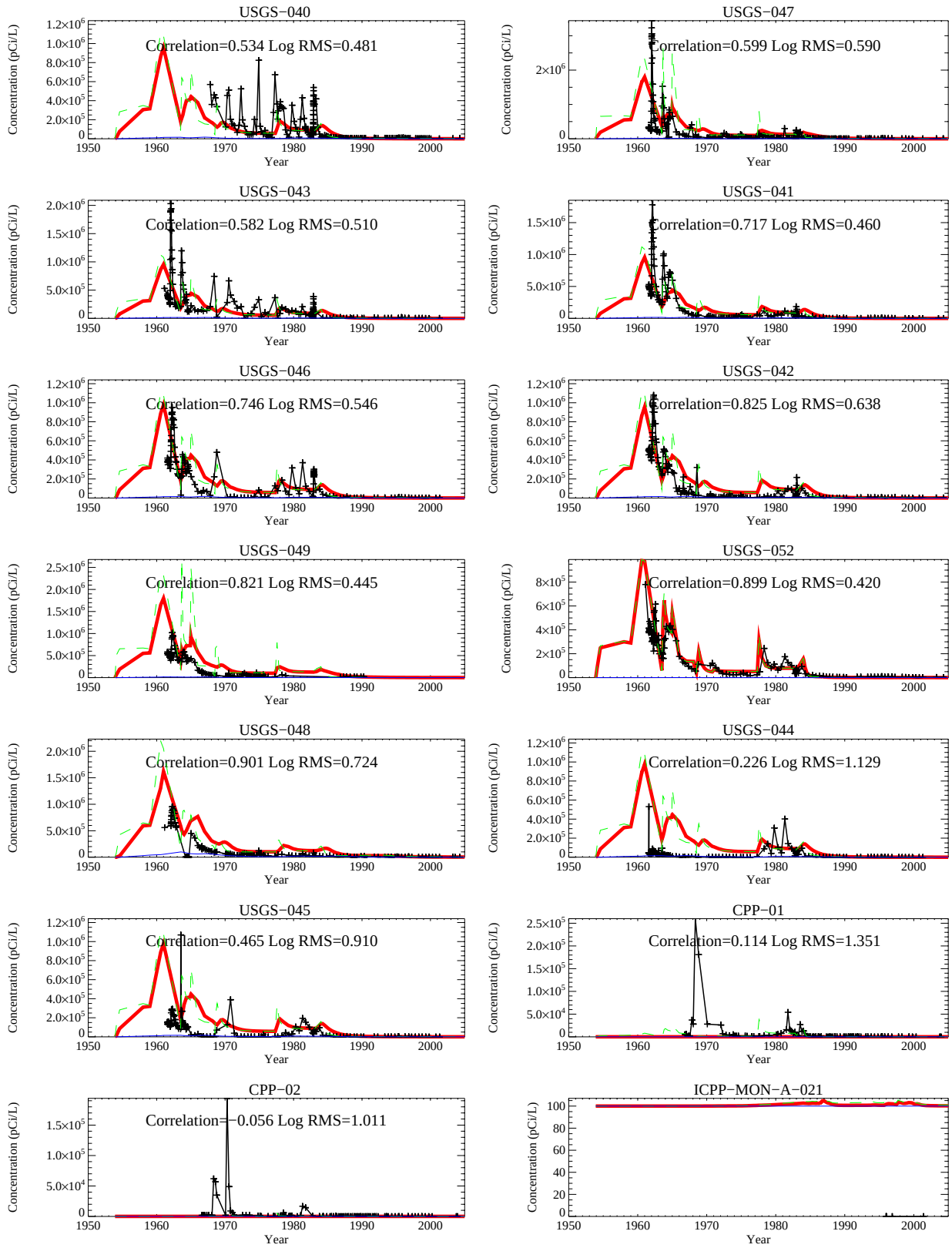

Figure A-8-13. Simulated and observed tritium concentration histories (pCi/L) (measured = black crosses, thick red = model at screen center, dashed green = model top, blue = model bottom).

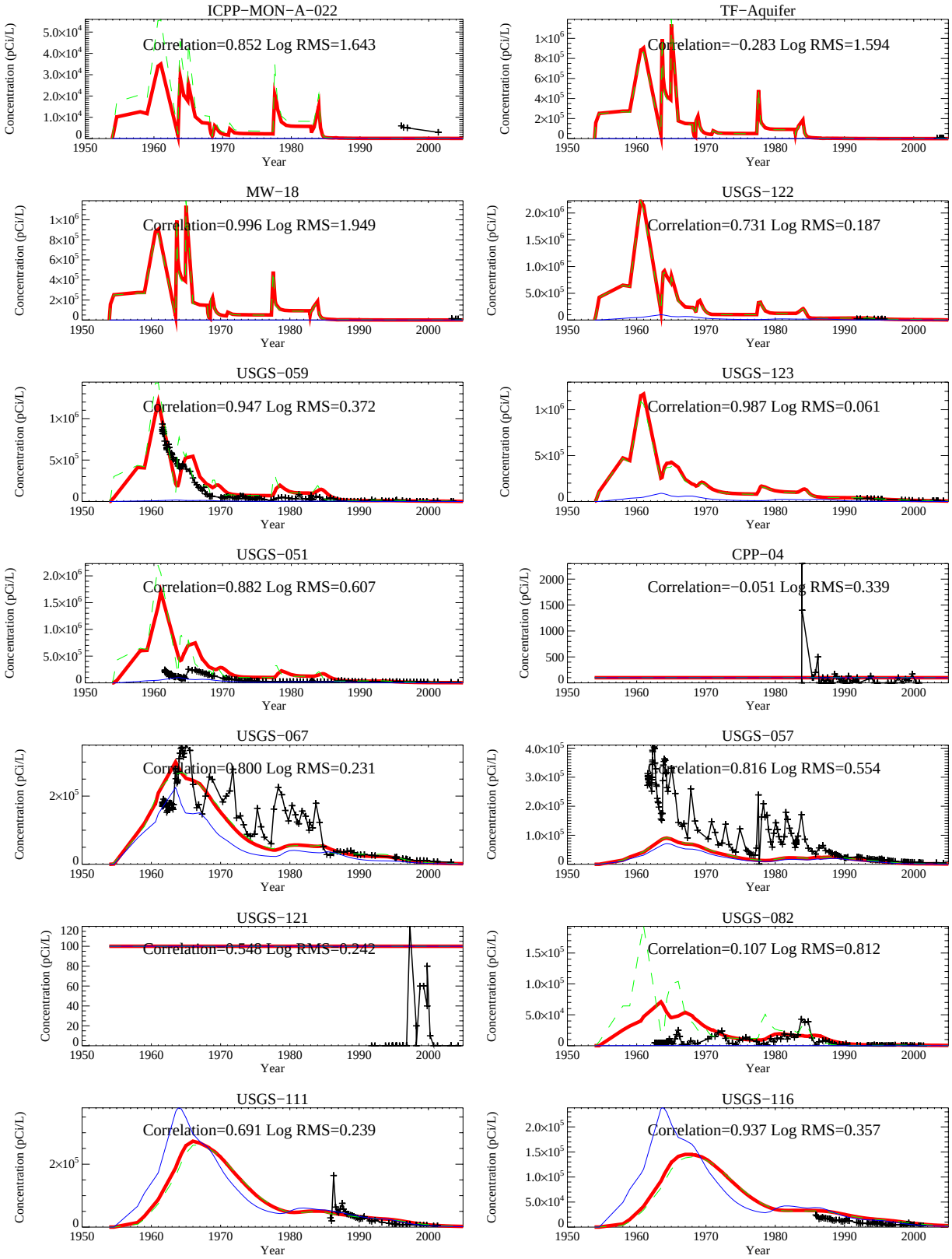

Figure A-8-14. Simulated and observed tritium concentration histories (pCi/L) (measured = black crosses, thick red = model at screen center, dashed green = model top, blue = model bottom).

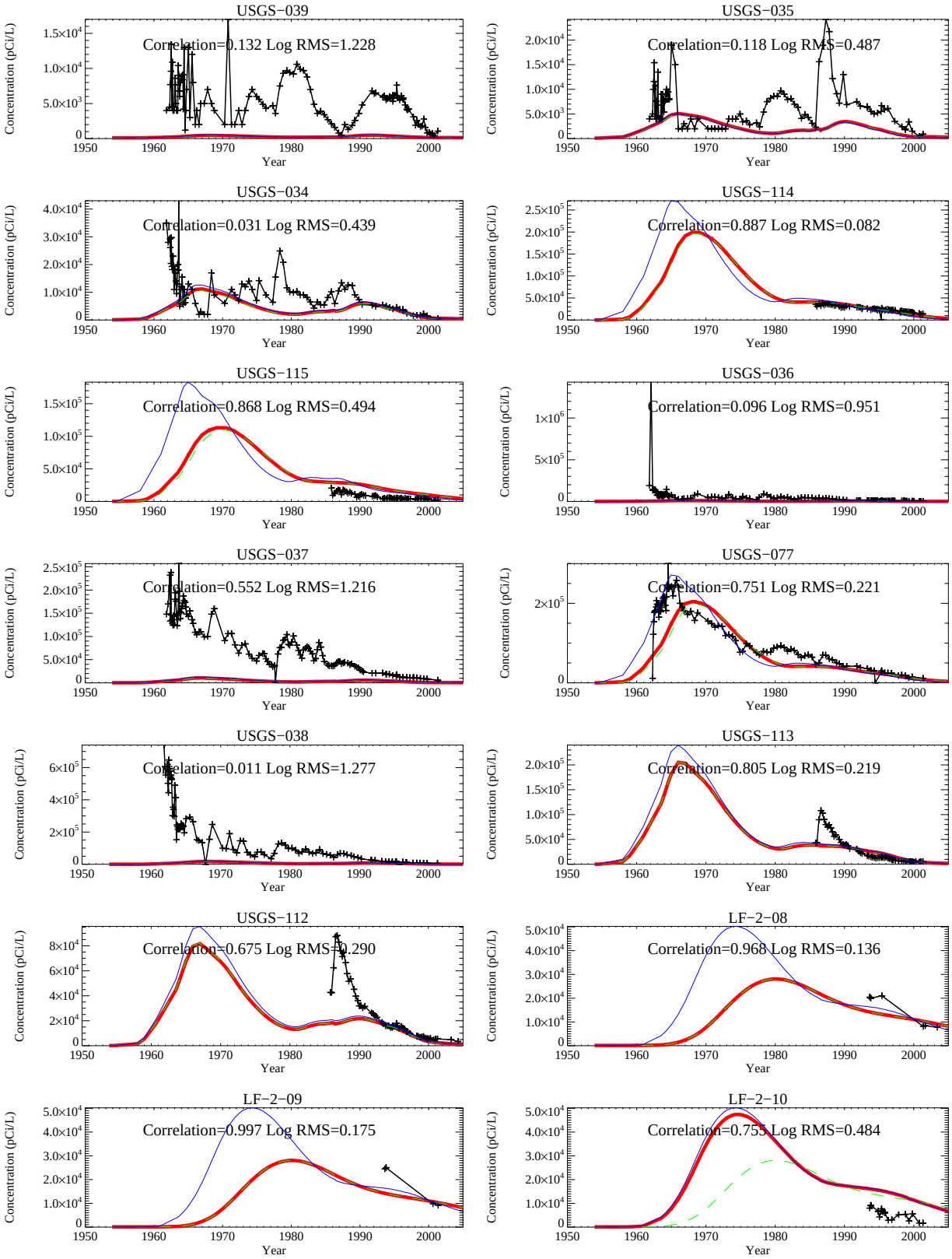

Figure A-8-15. Simulated and observed tritium concentration histories (pCi/L) (measured = black crosses, thick red = model at screen center, dashed green = model top, blue = model bottom).

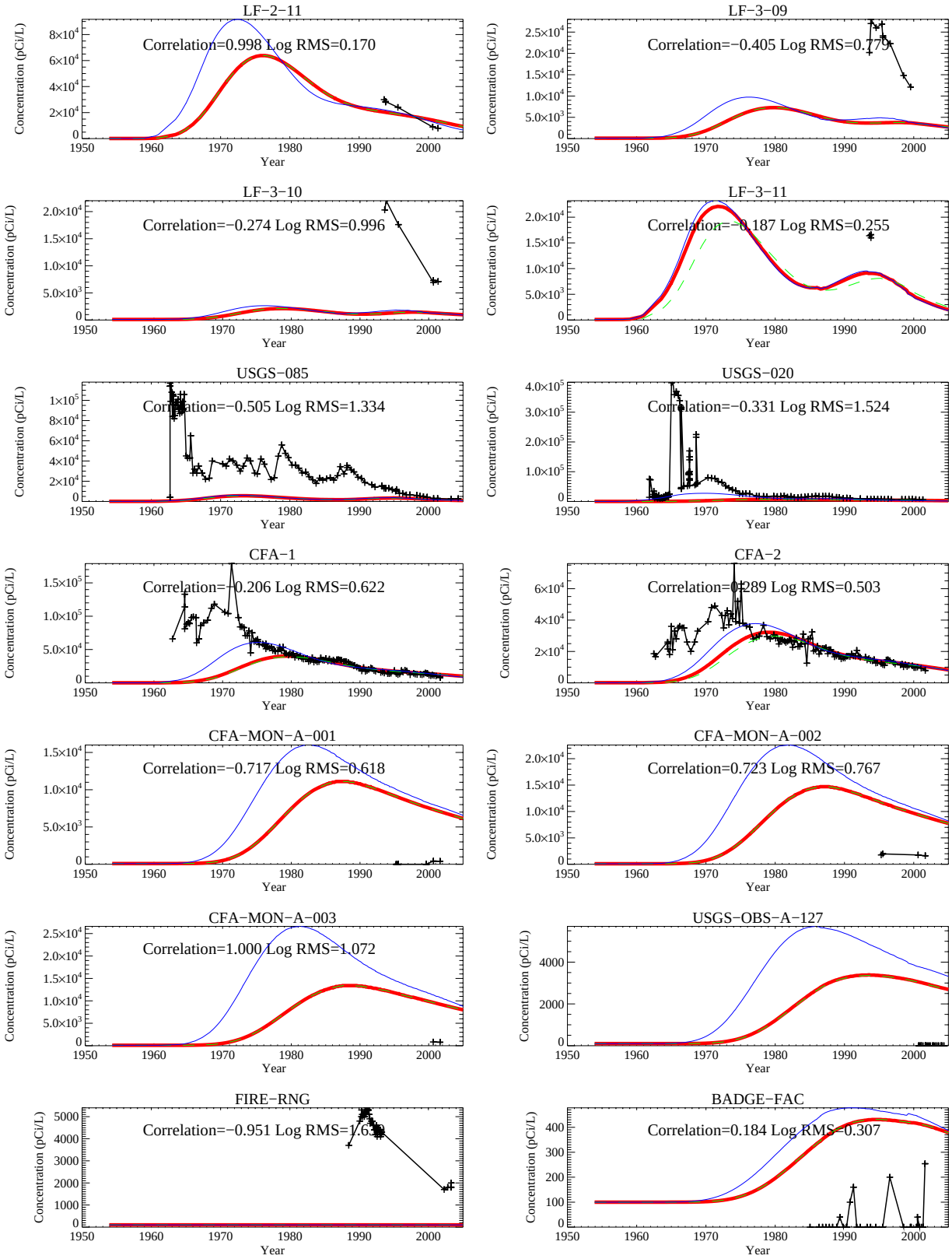

Figure A-8-16. Simulated and observed tritium concentration histories (pCi/L) (measured = black crosses, thick red = model at screen center, dashed green = model top, blue = model bottom).

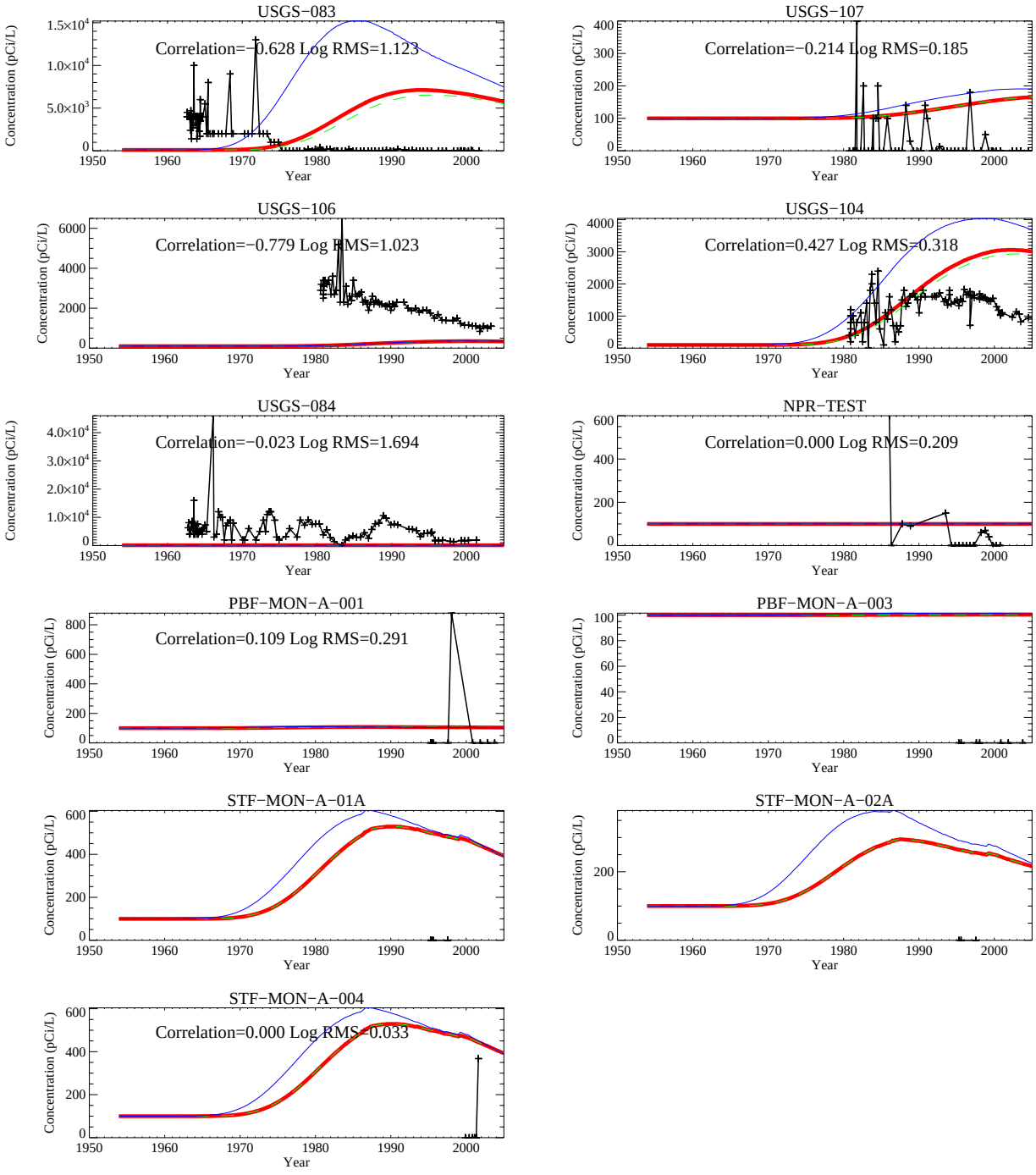

Figure A-8-17. Simulated and observed tritium concentration histories (pCi/L) (measured = black crosses, thick red = model at screen center, dashed green = model top, blue = model bottom).

A-8.3.2 Technetium-99 in the Aquifer

Calibration targets for Tc-99 included matching downgradient concentrations resulting from CPP-3 injection well discharges and matching the current high concentrations resulting from the tank farm releases. The maximum observed Tc-99 concentration was 3,160 pCi/L in 2003 and was recorded in the TF-Aquifer well. With the exception of the TF-Aquifer well, higher concentrations occur south and southeast of the tank farm. The maximum observed concentration in well USGS-52 was 339 pCi/L in 2004, and the maximum observed concentration in well MW-18 was 589 pCi/L in 2003.

Figures A-8-18 and A-8-19 show the contour plot of simulated maximum Tc-99 concentration at any depth averaged over a 15-m well screen for the refined model grid near INTEC and the base grid, respectively. The year 1999 is shown here because that is the time period when the model is predicting the highest concentrations in the aquifer. The peak aquifer concentration corresponds to the arrival of the highest predicted fluxes from the vadose zone. There are two high concentration areas in Figure A-8-19, one within the INTEC fence line and the other one nearer CFA. The high concentrations near INTEC are due to tank farm releases, which began arriving at the aquifer during the mid-1980s. The second high-concentration area is due to service waste discharges in the CPP-03 injection well.

The peak Tc-99 concentration occurring anywhere within the aquifer averaged over a 15-m well screen is shown in Figure A-8-20. The early high concentrations are the result of the injection well operation. The concentration peak occurring in the year 1999 is due to tank farm releases and corresponds to the high flow year of the Big Lost River. The overall variability is due to the fluctuations in the injection well discharge rates, variability in the Big Lost River flow, and, in part, due to the peak value being taken from any location within the model as opposed to representing a single location. The peak concentration only briefly exceeds the MCL in 1999. This is inconsistent with the maximum measured Tc-99 concentration seen in the TF-Aquifer well and the recently drilled ICPP-2020 and ICPP-2021 wells. The vadose zone model may be overestimating the attenuation occurring within the vadose zone or may have underestimated the Tc-99 source term. Possible causes include the following: 1) using a source smaller than the actual source, 2) overestimating dilution and dispersion in the vadose zone, and 3) underestimating or not accounting for preferential arrival from high concentration regions in the vadose zone. However, the simulated concentrations were similar to the measured concentrations in the vertical profile wells, which are located south of the INTEC (Figure A-8-21). This indicates dilution dispersion in the aquifer model was adequately parameterized, because the source of the Tc-99 currently seen in these wells is from the CPP-3 injection well.

The vertical profile of observed and simulated data is given in Figure A-8-21 for 2003 in the ICPP-179x series wells located between the INTEC and the CFA. The simulated and observed Tc-99 concentration history plots presented in Figures A-8-22 through A-8-28 indicate that the wells were sampled too infrequently to allow identification of the first arrival or peak concentration in most wells. Sampling in these wells began in the mid-1990s at most locations and other sampling began in 2000. The presented concentrations correspond to the values obtained from the base grid, which is 400 by 400 m. The TETRAD software reports model results for a base grid and for each refined area in separate data files. The concentration histories were created by reading the base grid data files, which correspond to the average over the refined grid blocks within each base grid block. This results in a lower reported base grid concentration because of the large averaging volume.

Figure A-8-18. Simulated maximum Tc-99 concentrations (pCi/L) near INTEC averaged over a 15-m well screen in 1999 (MCL=thick red line, 10*MCL=thin red line, MCL/10=thin black line, MCL/100=dashed black line).

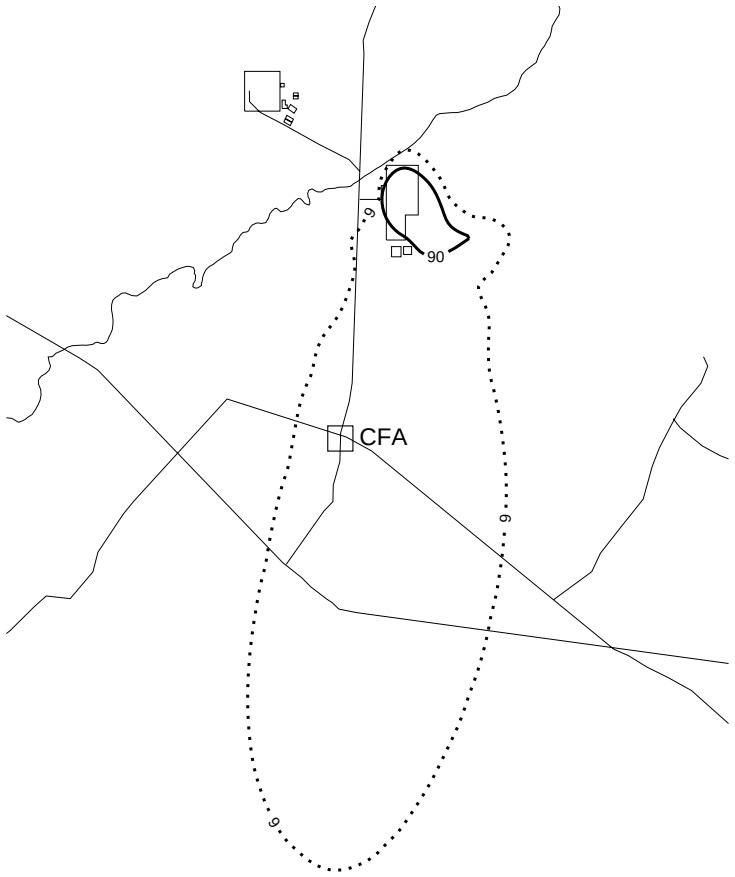

Figure A-8-19. Simulated maximum Tc-99 concentrations (pCi/L) in base grid averaged over a 15-m well screen in 1999 (MCL=thick red line, 10*MCL=thin red line, MCL/10=thin black line, MCL/100=dashed black line).

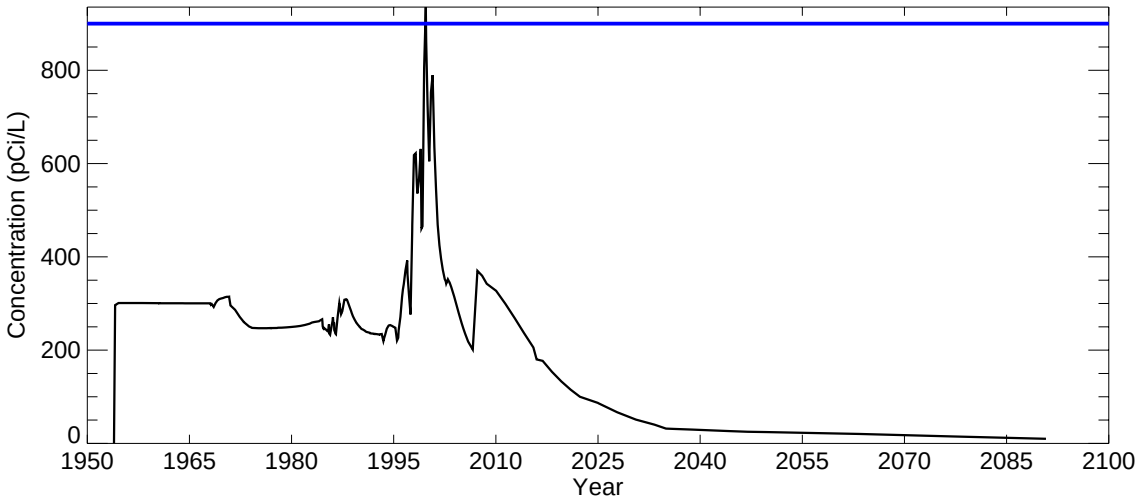

Figure A-8-20. Simulated Tc-99 peak aquifer concentrations averaged over a 15-m well screen (pCi/L).

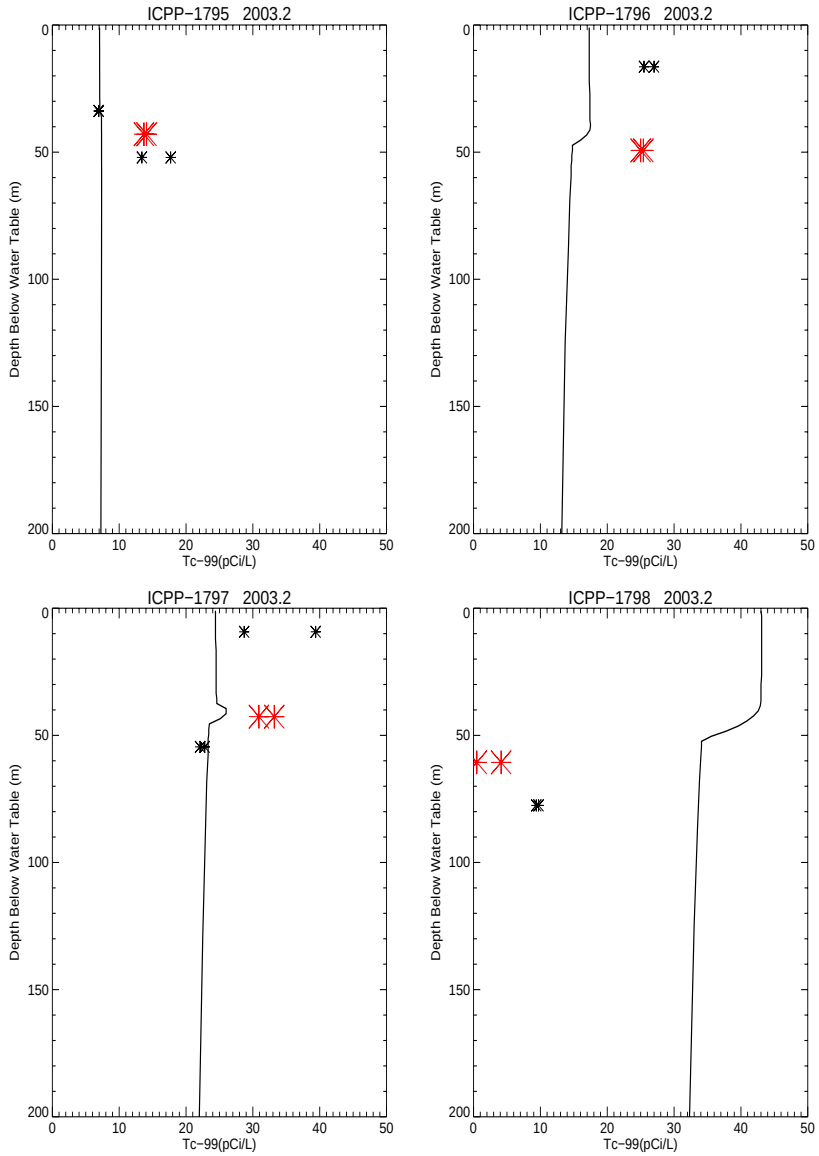

Figure A-8-21. Simulated and measured Tc-99 vs. depth at vertical boreholes in 2003 (pCi/L) (simulated data = solid line, small asterisk = data taken in basalt, large red asterisk = data taken in the HI interbed).

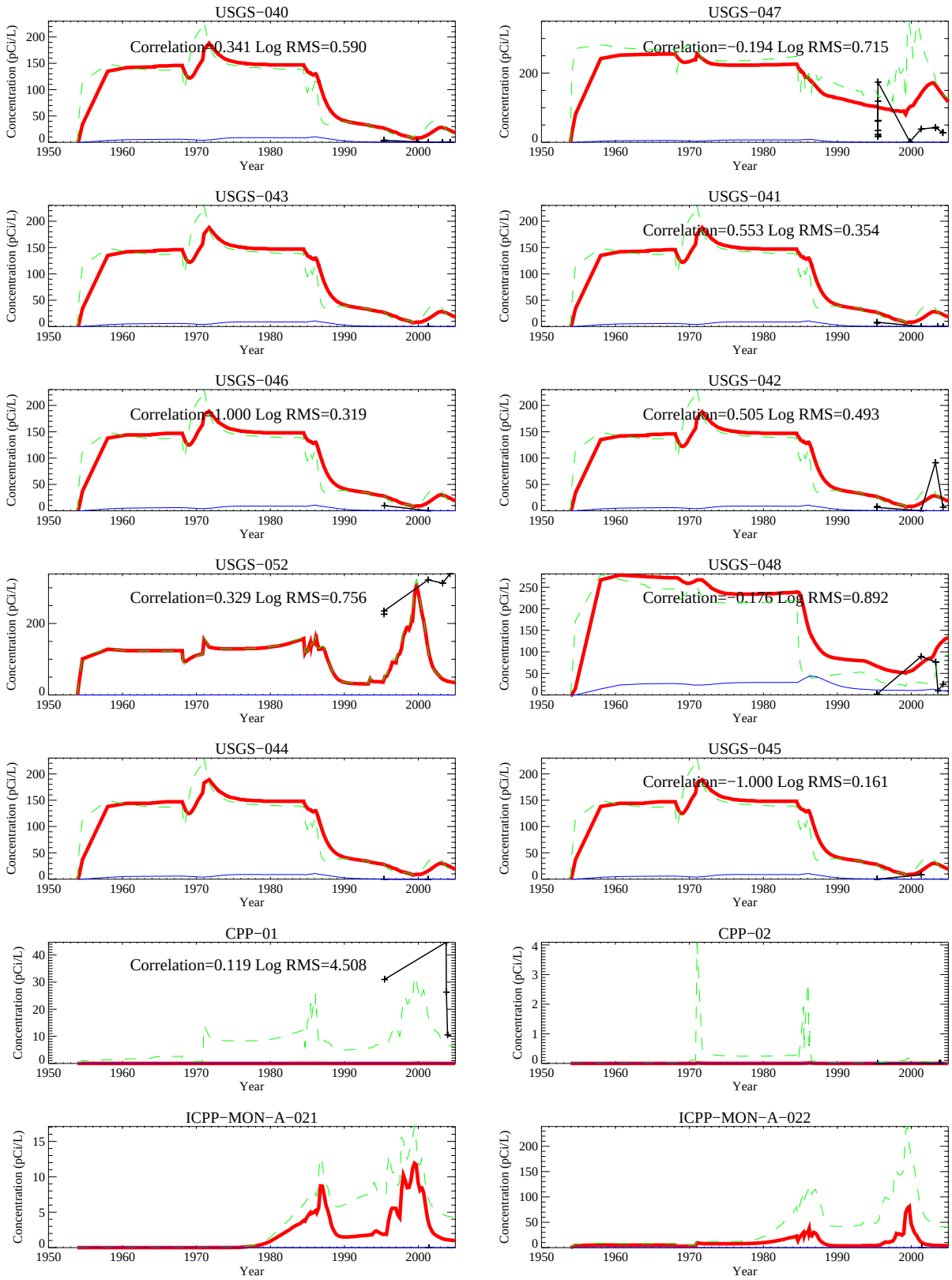

Figure A-8-22. Simulated and observed Tc-99 concentration histories (pCi/L) (measured = black crosses, thick red = model at screen center, dashed green = model top, blue = model bottom).

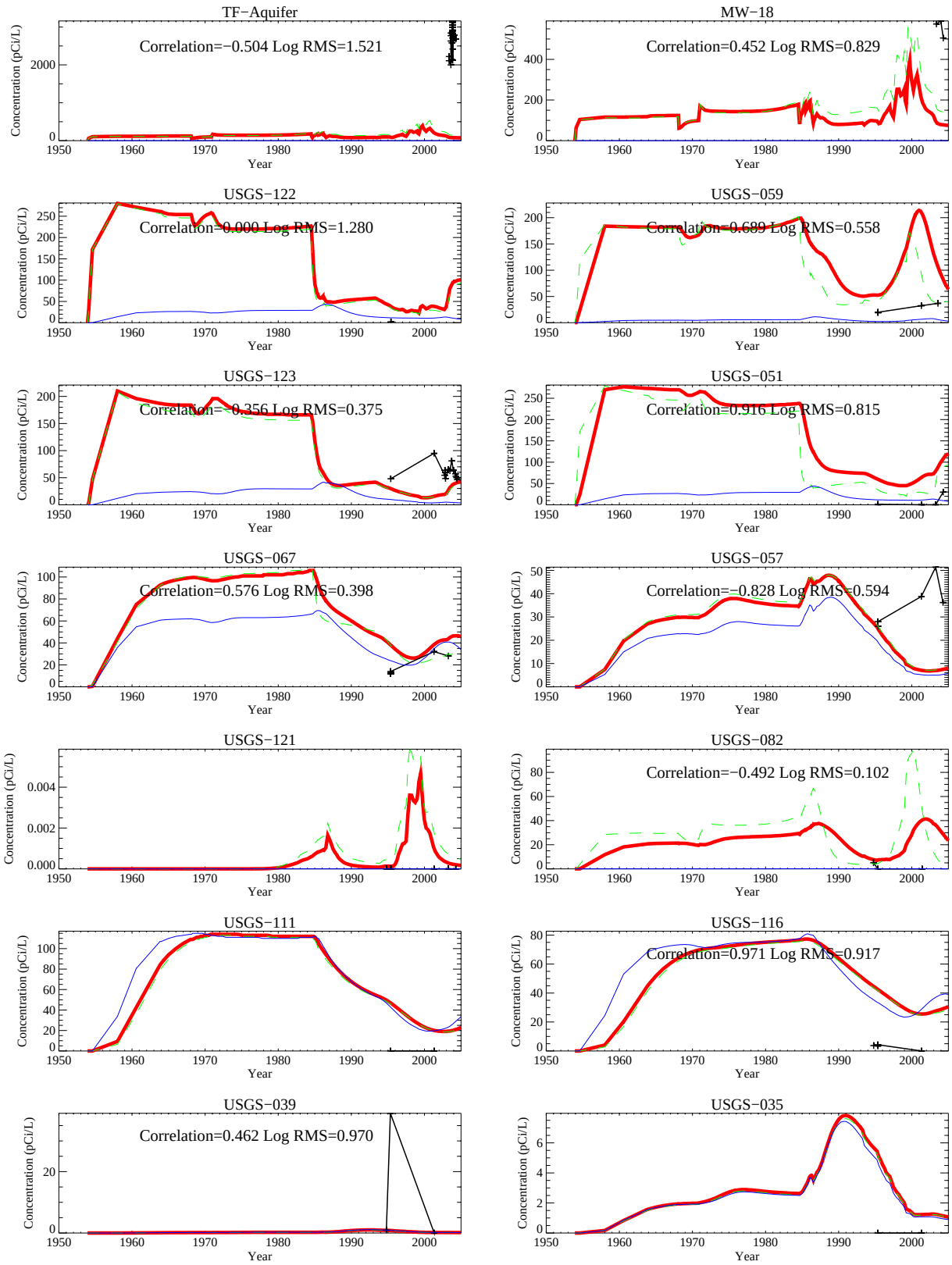

Figure A-8-23. Simulated and observed Tc-99 concentration histories (pCi/L) (measured = black crosses, thick red = model at screen center, dashed green = model top, blue = model bottom).

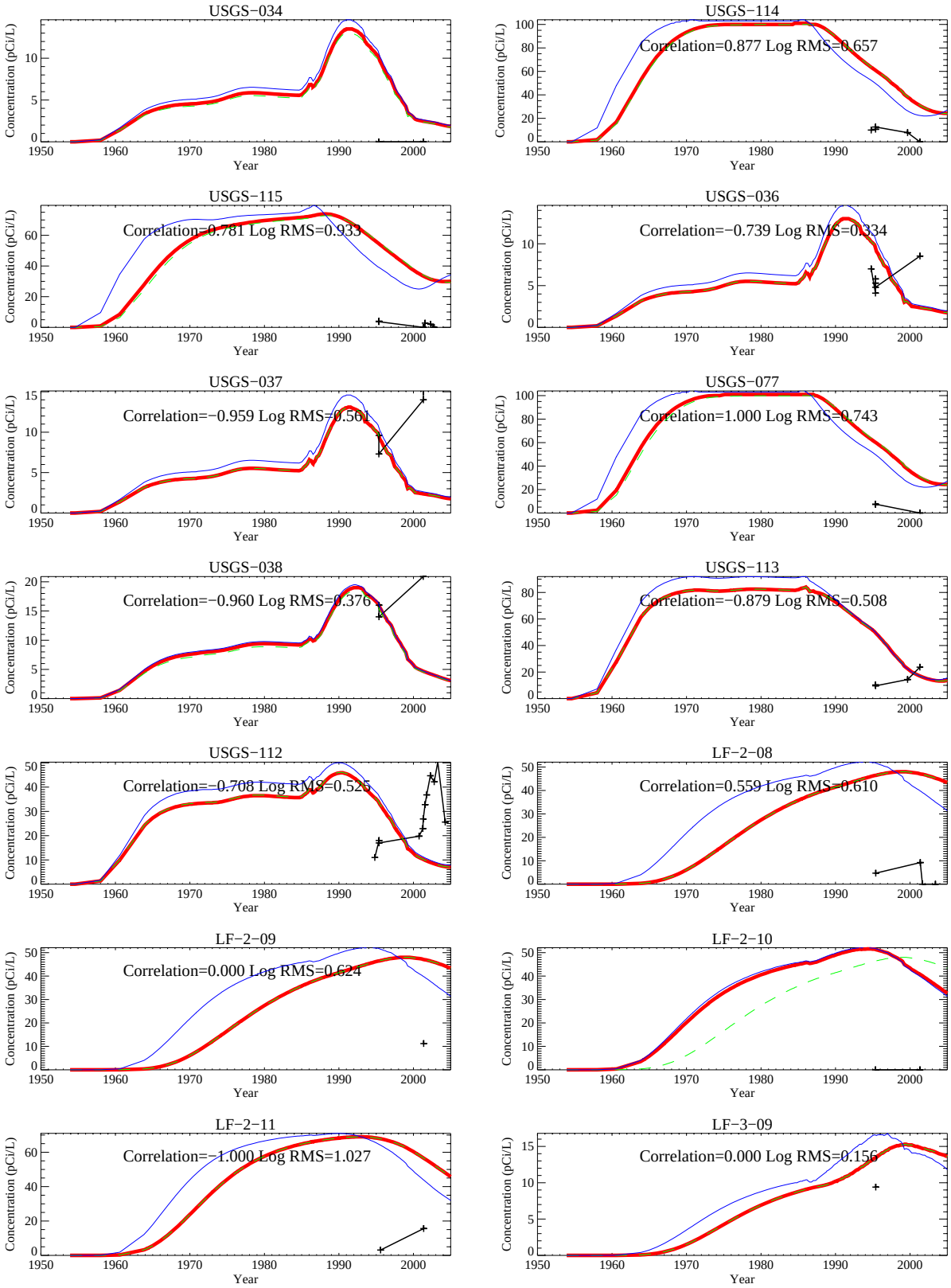

Figure A-8-24. Simulated and observed Tc-99 concentration histories (pCi/L) (measured = black crosses, thick red = model at screen center, dashed green = model top, blue = model bottom).

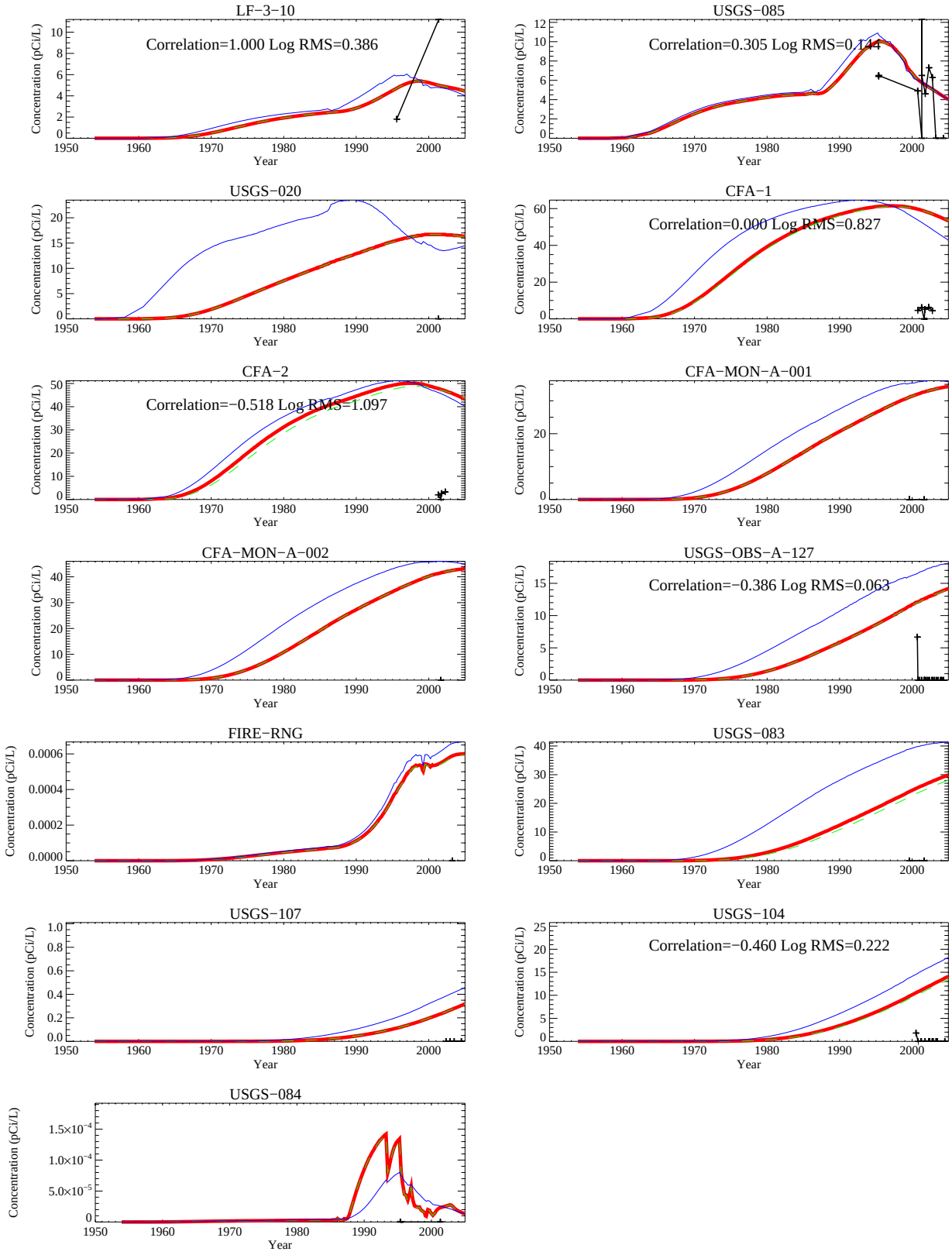

Figure A-8-25. Simulated and observed Tc-99 concentration histories (pCi/L) (measured = black crosses, thick red = model at screen center, dashed green = model top, blue = model bottom).

A-8.3.3 Iodine-129 in the Aquifer

The aquifer model was not calibrated to I-129 concentrations, but comparisons to observed data are presented. It was not used as a calibration target because the service waste disposal records were only available from 1976 through 1985. Prior to 1976, the source term used in this report was simply an estimate. The uncertainty associated with the estimated releases in the injection well were thought to be too large to use I-129 as a primary calibration target. In addition, field observations of I-129 are more sparse than data for the other calibration targets.

The aquifer model predicts that peak I-129 concentrations originating from the injection well operation reached CFA around mid-2002, as shown in Figure A-8-26. On the average, concentrations of I-129 were overpredicted in wells downgradient of CPP-3. The highest concentration observed in the most recent sampling campaign was 1.06 pCi/L and was located approximately 400 m west of CFA. Figure A-8-27 illustrates the simulated and observed vertical concentrations for 2003 in the ICPP-179x series wells located between INTEC and CFA. Figures A-8-28 through A-8-32 illustrate the simulated and observed concentrations at each well location with I-129 sampling results. There were 64 wells with observed I-129 data, but most wells have very few data points. There is more variability in the I-129 concentrations than in the injection well source term because the aquifer concentrations are also influenced by the transient injection well water disposal rate, vadose zone water flux, and arrival of the vadose zone I-129 sources. The concentration spikes seen in the measured I-129 in Wells USGS-40, 42, 44, 45, 46, and 52 may be due to an increase I-129 disposal in 1978, which coincided with low recharge from the Big Lost River. Between 1982 and 1986 the Big Lost River recharge was higher than average and waste water disposal to the injection well was stopped in 1984, thereby reducing concentrations.

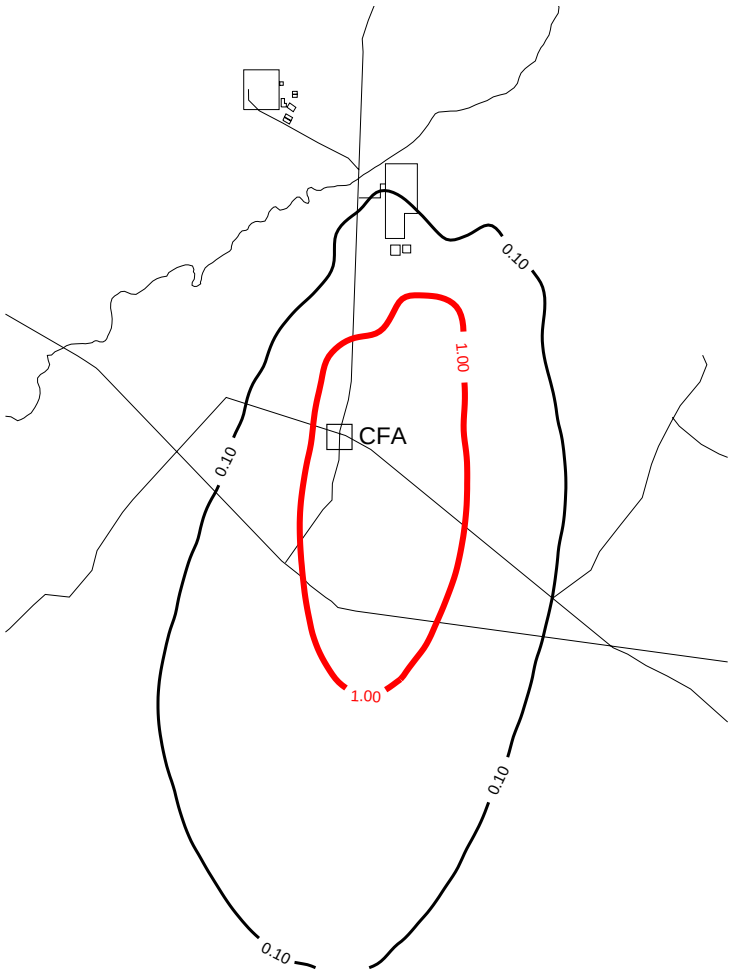

Figure A-8-26. Maximum simulated I-129 concentrations (pCi/L) in base grid averaged over a 15m well screen in 2004 (MCL=thick red line, 10*MCL=thin red line, MCL/10=thin black line, MCL/100=dashed black line).

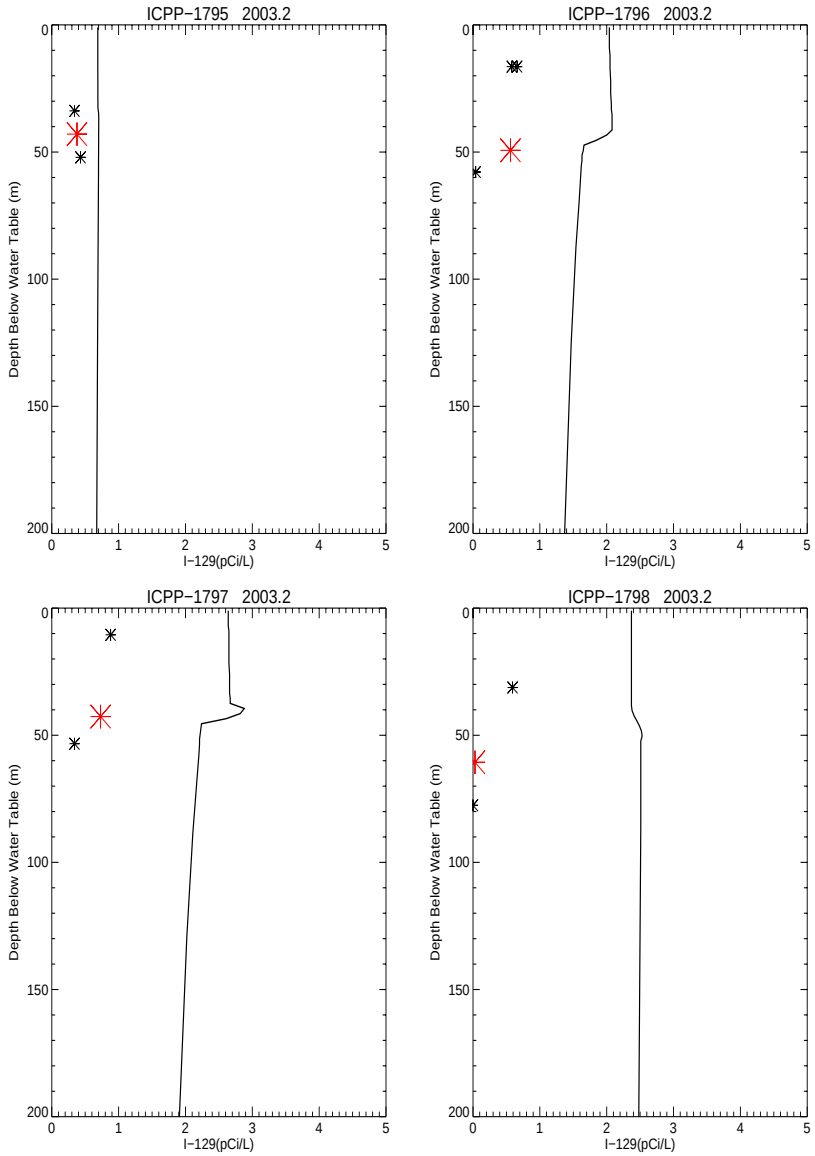

Figure A-8-27. Simulated and observed I-129 concentrations vs. depth at vertical boreholes in 2003 (simulated data = solid line, small asterisk = data taken in basalt, large red asterisk = data taken in the HI interbed, pCi/L).

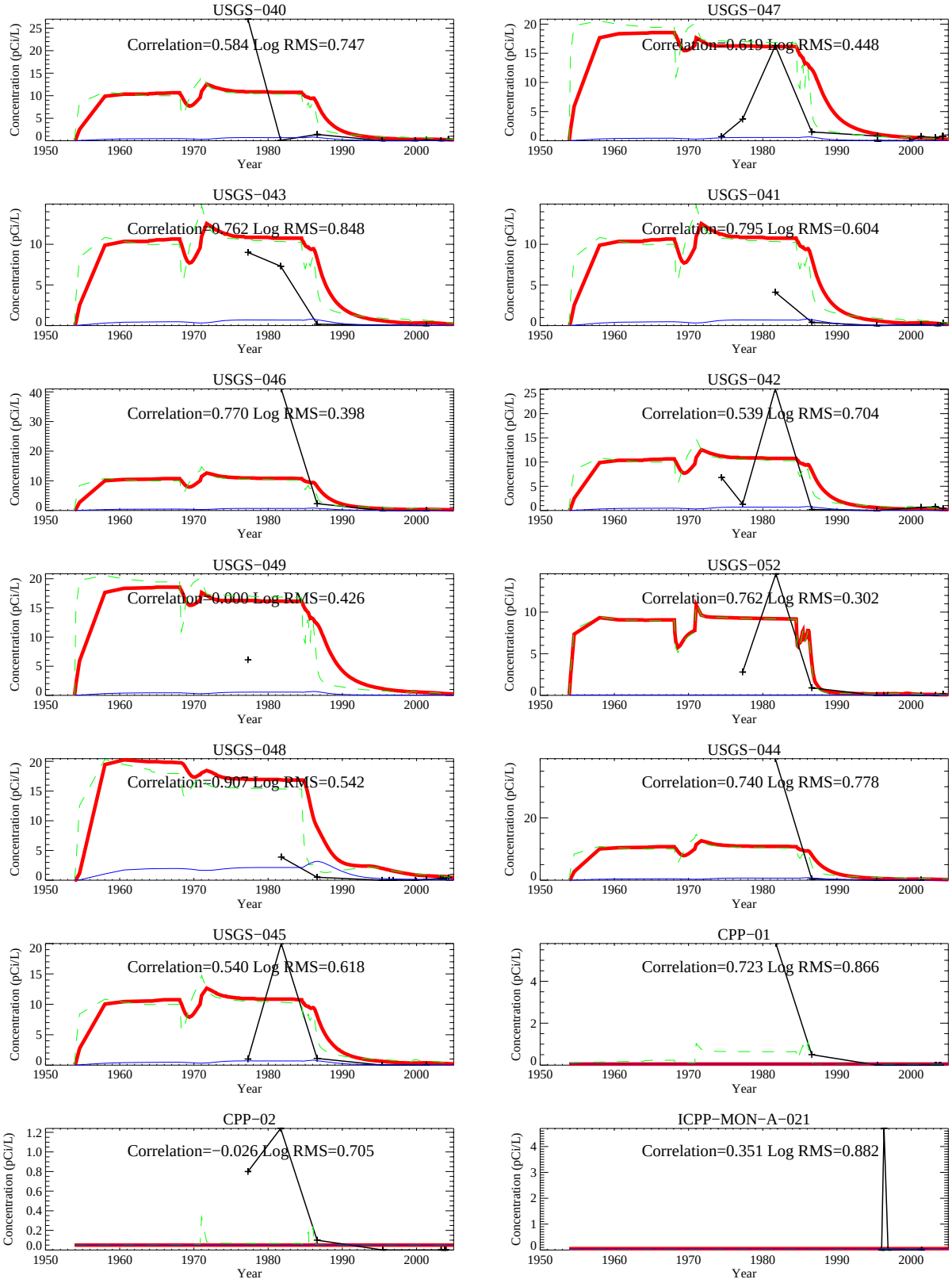

Figure A-8-28. Simulated and observed I-129 concentration histories (pCi/L) (measured = black crosses, thick red = model at screen center, dashed green = model top, blue = model bottom).

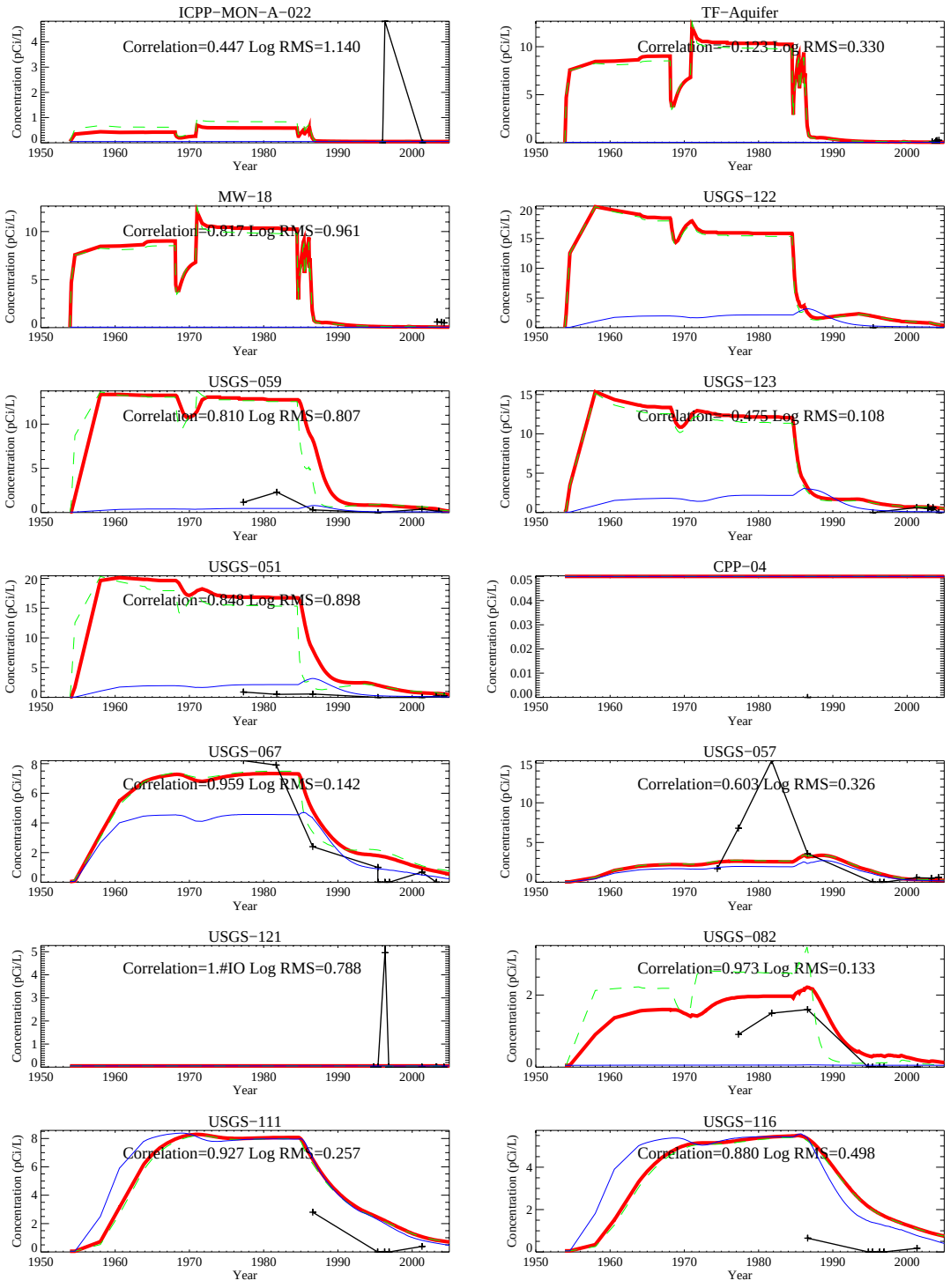

Figure A-8-29. Simulated and observed I-129 concentration histories (pCi/L) (measured = black crosses, thick red = model at screen center, dashed green = model top, blue = model bottom).

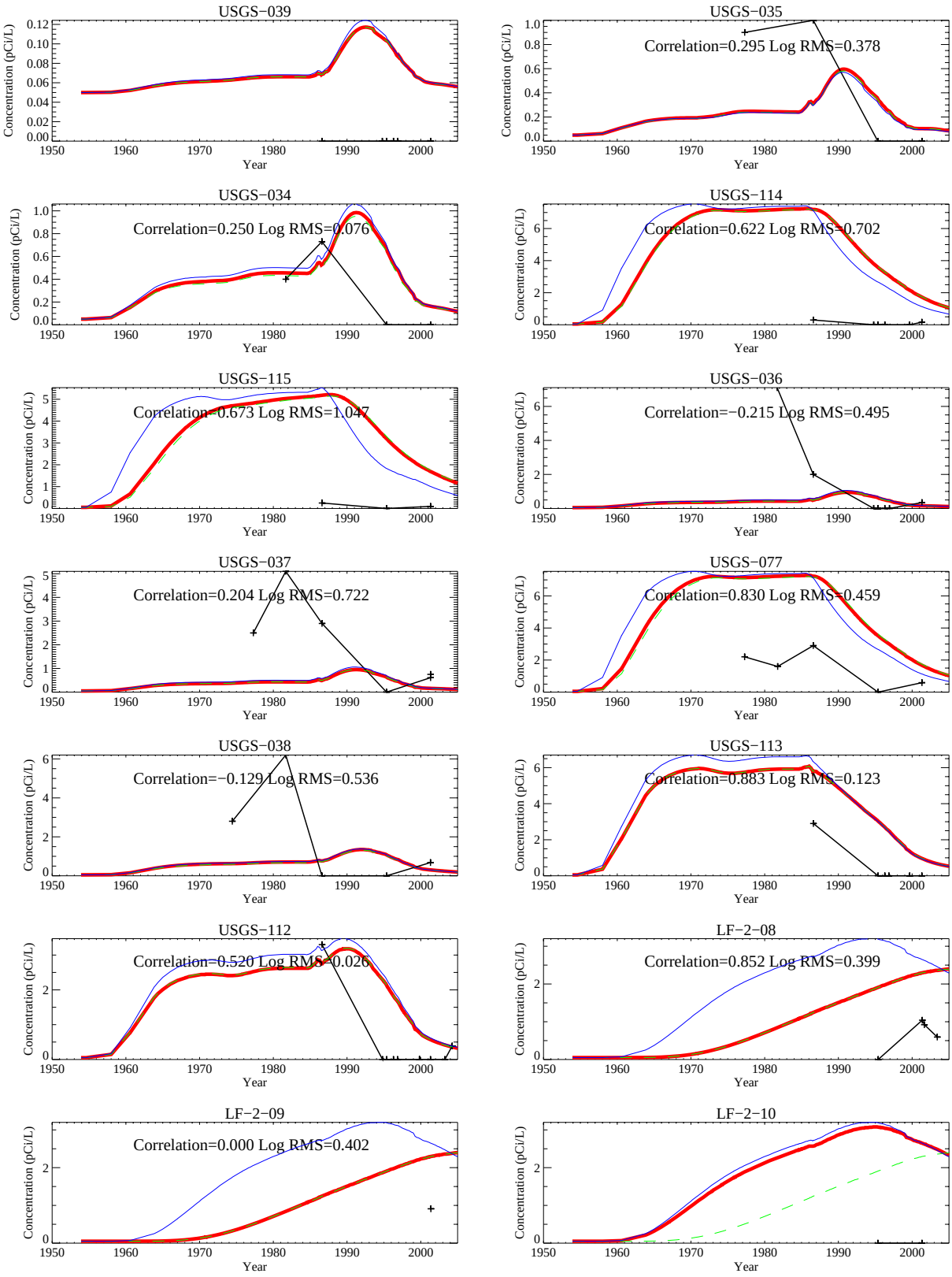

Figure A-8-30. Simulated and observed I-129 concentration histories (pCi/L) (measured = black crosses, thick red = model at screen center, dashed green = model top, blue = model bottom).

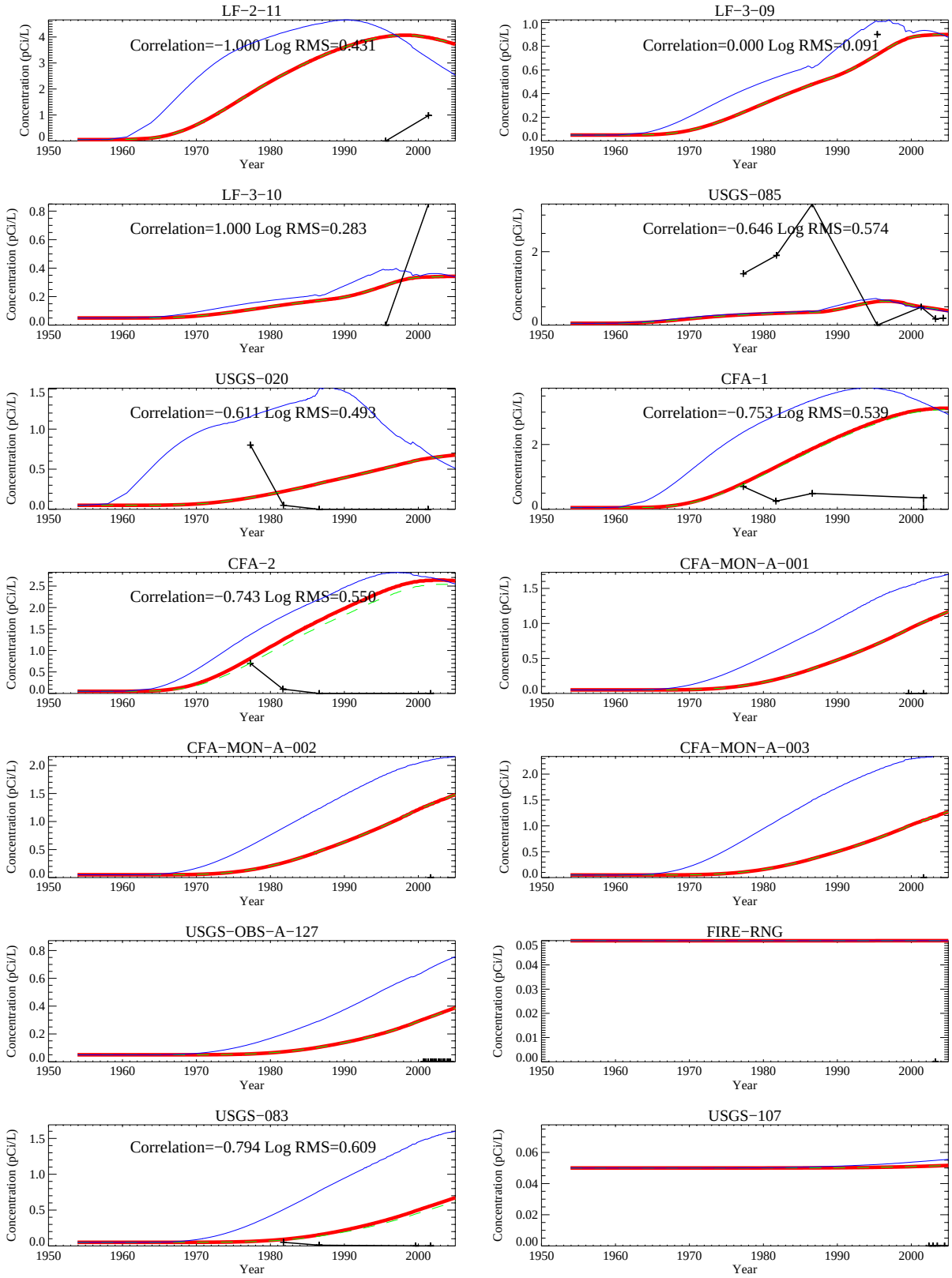

Figure A-8-31. Simulated and observed I-129 concentration histories (pCi/L) (measured = black crosses, thick red = model at screen center, dashed green = model top, blue = model bottom).

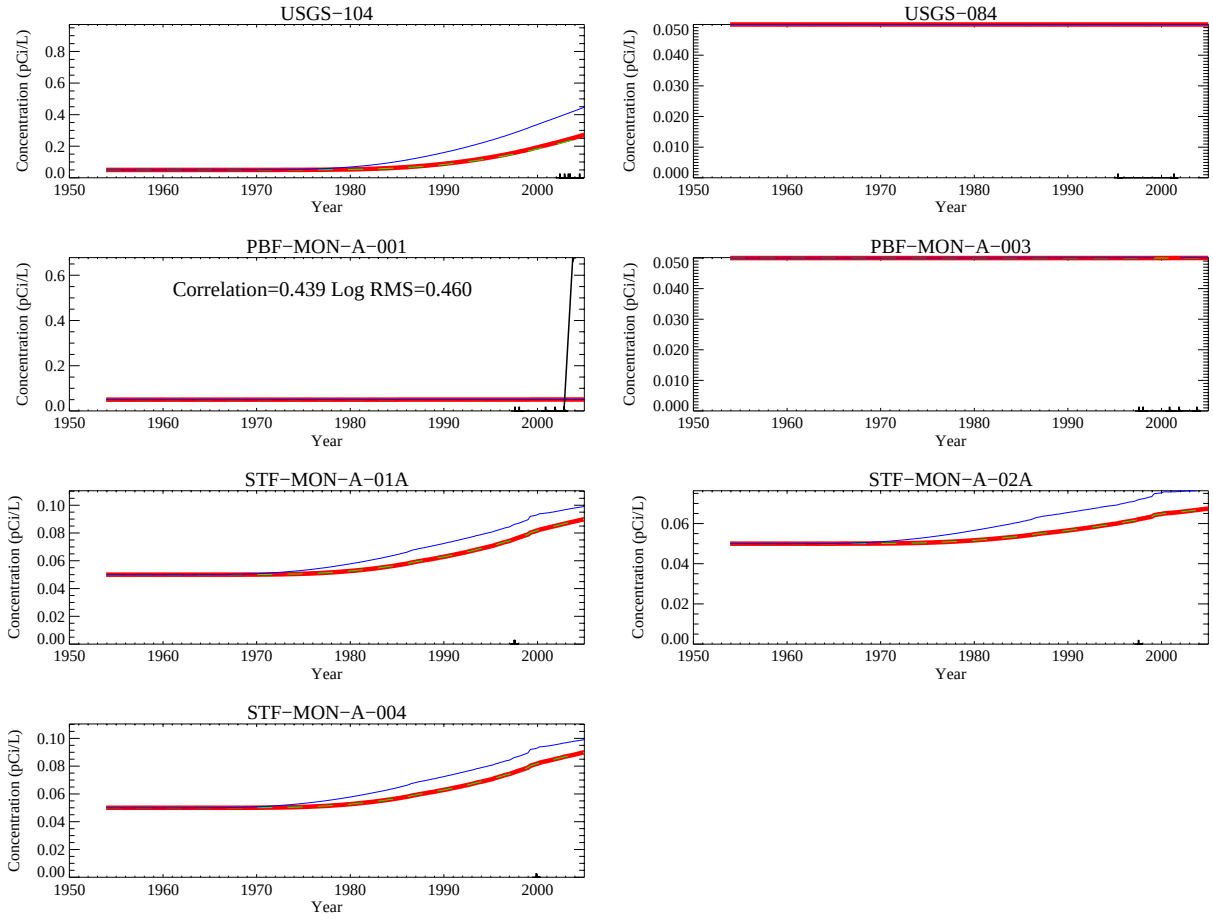

Figure A-8-32. Simulated and observed I-129 concentration histories (pCi/L) (measured = black crosses, thick red = model at screen center, dashed green = model top, blue = model bottom).

A-8.3.4 Nitrate in the Aquifer

The background concentration for nitrate is approximately 1.5-mg/L as N in the Snake River Plain Aquifer and surface waters near the INL Site (Orr et al. 1991). The simulated concentrations were adjusted to account for the background concentrations by adding this amount to the simulated value.

As with the I-129, the aquifer model was not calibrated to nitrate concentrations, but comparisons of predicted and observed data are presented. Service waste disposal records for nitrate were not kept, and the amounts used in these simulations were estimated based on discharge water volumes and average concentrations measured in 1981 (see Section A-5 of the main document). Field sampling for nitrate began during the mid-1990s in most of the aquifer wells, which is much later than the discharges in the injection well would have arrived at most downstream locations. Observed concentrations were assigned a zero value if the nitrate sample analysis was recorded as nondetect. These zero values should have been assigned the background concentration to be consistent with the upward adjustment of the simulation results by the background value. Overall, the model tends to overpredict nitrate concentrations, suggesting actual releases were smaller than the values used in these simulations. Figure A-8-33 illustrates the horizontal extent of the maximum concentration at any depth averaged over a 15-m well screen in 2004. Figures A-8-34 through A-8-36 illustrate the simulated and observed nitrate concentration history at each aquifer well with reported nitrate.

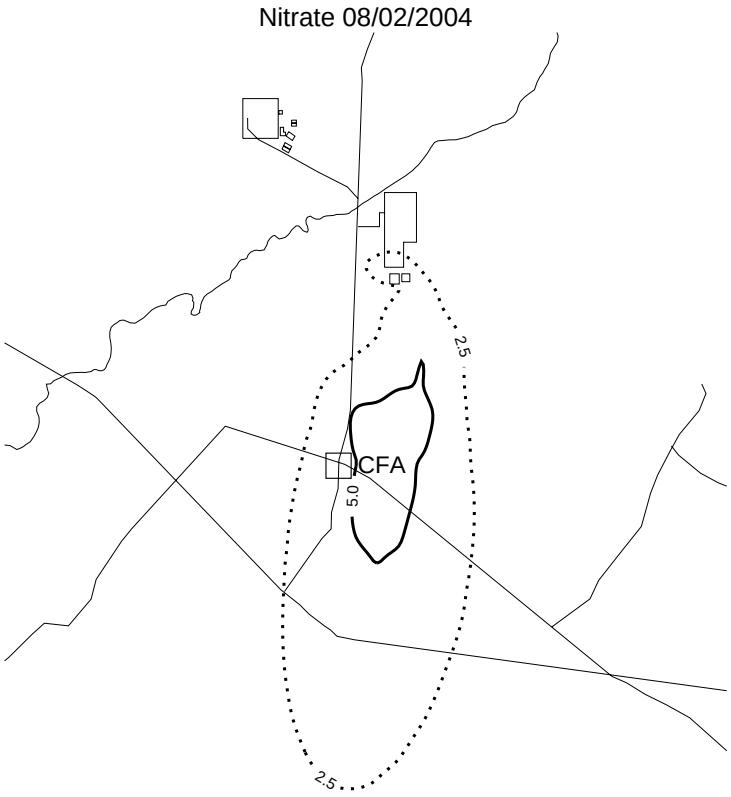

Figure A-8-33. Maximum simulated nitrate concentration (mg/L as N) in base grid averaged over a 15m well screen in 2004 (MCL=thick red line, 10*MCL=thin red line, MCL/5=thin black line, MCL/4=dashed black line).

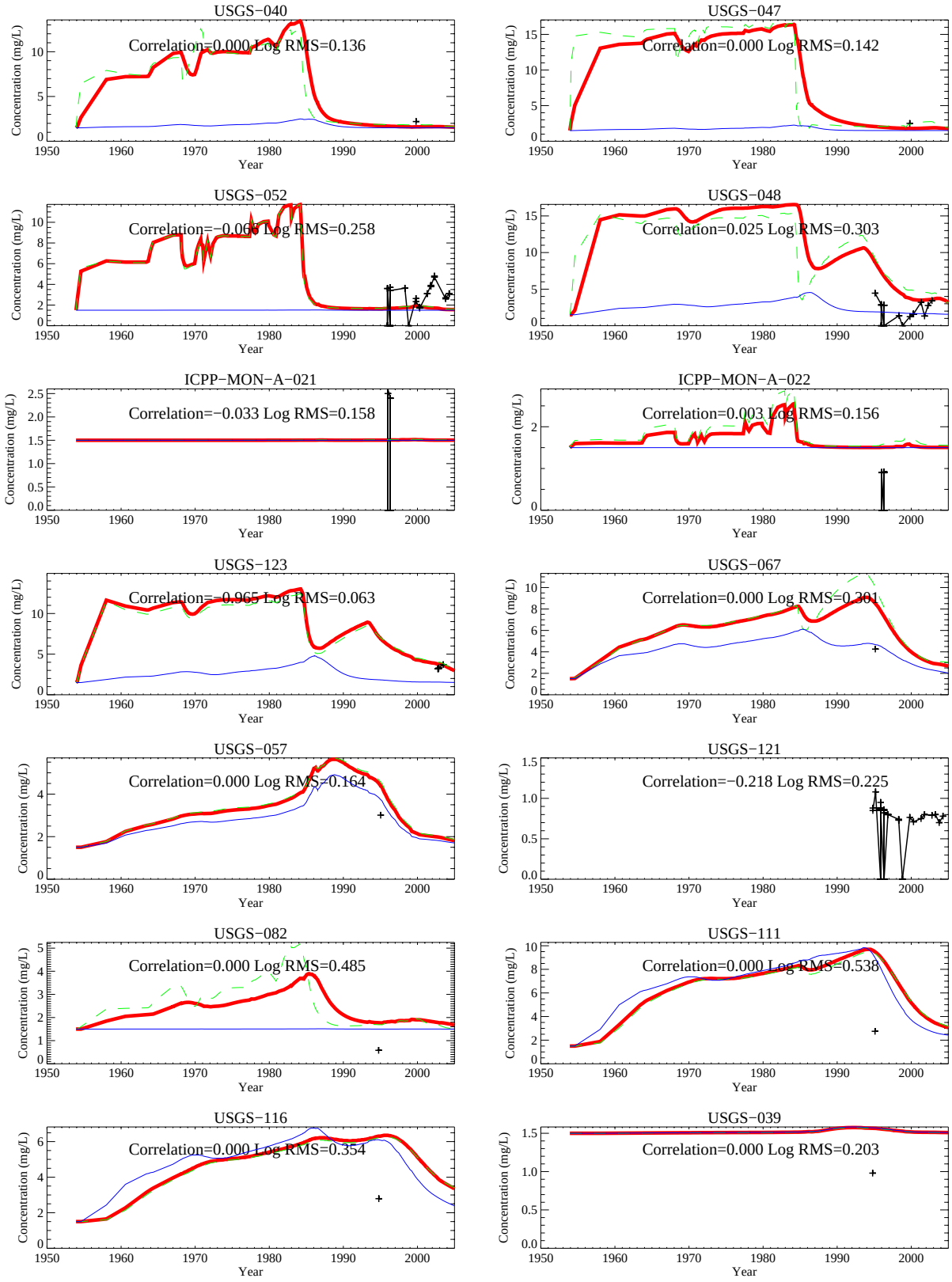

Figure A-8-34. Simulated and observed nitrate concentration histories (mg/L as N) (measured = black crosses, thick red = model at screen center, dashed green = model top, blue = model bottom).

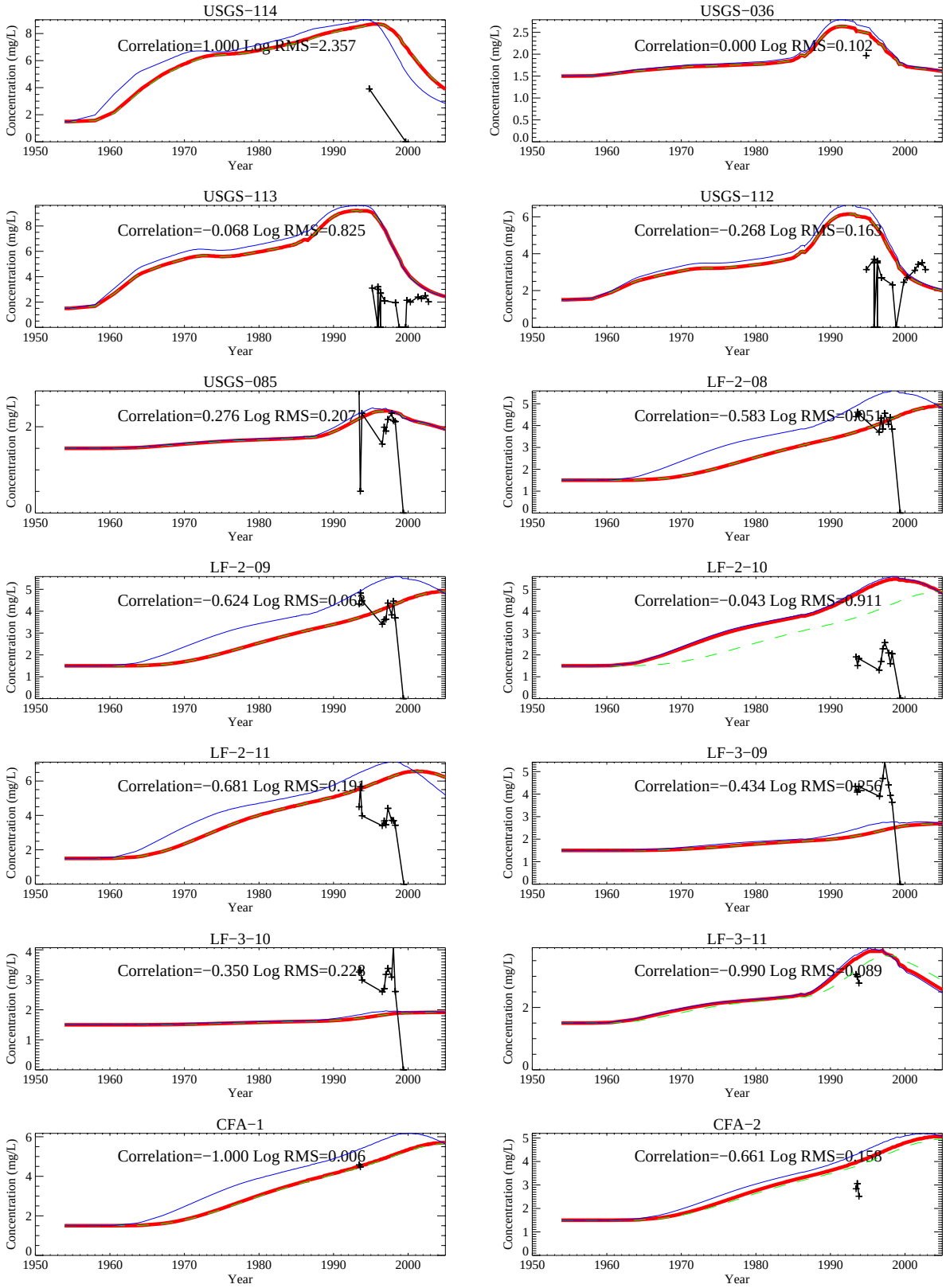

Figure A-8-35. Simulated and observed nitrate concentration histories (mg/L as N) (measured = black crosses, thick red = model at screen center, dashed green = model top, blue = model bottom).

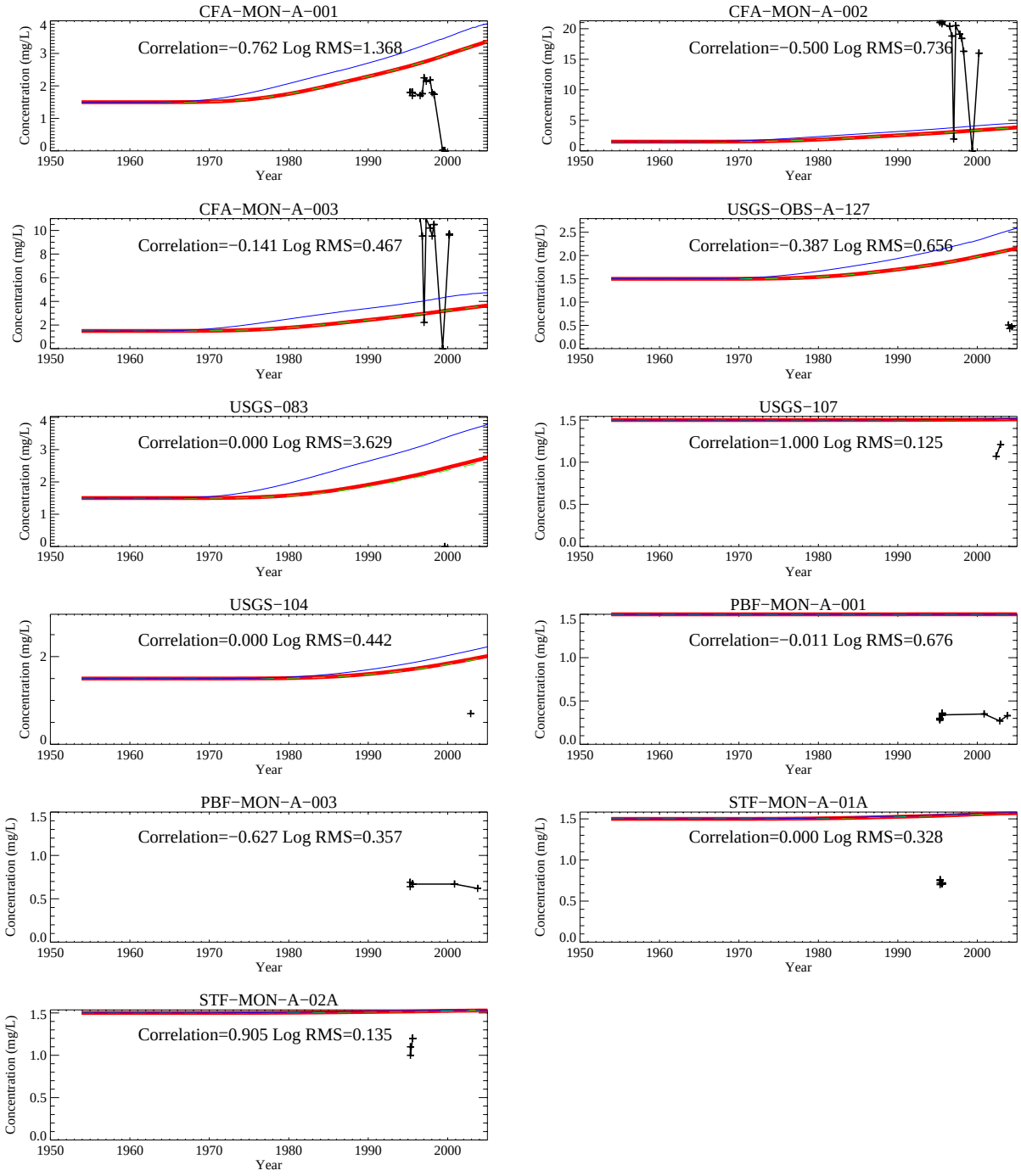

Figure A-8-36. Simulated and observed nitrate concentration histories (mg/L as N) (measured = black crosses, thick red = model at screen center, dashed green = model top, blue = model bottom).

A-8.3.5 Aquifer Flow Model Calibration Conclusions

The simulated large-scale aquifer gradient near the INTEC is southerly with a local eastern component below the INTEC facility footprint. This matches the large-scale regional gradient predicted in the summer 2004 water level measurements and is consistent with the small-scale flow directions observed in several INTEC aquifer wells from recent observations of colloid movement. The local eastern component may be due to a high-permeability zone running southeast under northern INTEC. The aquifer is relatively flat west of INTEC, and this is due to higher aquifer permeability in this area, which was confirmed by aquifer pump test data. The HI interbed may act as a weak dividing layer separating the contamination in the H and I basalt. The simulated and observed vertical concentrations suggest this is occurring. The large-scale aquifer gradient should keep the INTEC contamination east of the Subsurface Disposal Area.

A-8.3.6 Aquifer Transport Model Calibration Conclusions

The current tritium, Tc-99, I-129 and nitrate observed in the aquifer near INTEC are the result of vadose zone contaminant sources now reaching the aquifer. The CPP-3 injection well was closed in 1984 and the aquifer velocity between INTEC and the CFA is approximately 0.5 m/day.

The current model has better agreement with the observed tritium than with the other contaminants. This was because the tritium sources were well known and there was sufficient downgradient data to discern the arrival of specific peak concentrations. For these reasons, more emphasis was placed on matching the tritium data.

The current high Tc-99 concentrations occurring in the TF-Aquifer well could not be matched with either the vadose zone or aquifer models. The vadose zone model may be overestimating the attenuation occurring within the vadose zone or may have underestimated the vadose zone Tc-99 source term. The simulated concentrations seen in the vertical profile wells midway between INTEC and CFA matched the measured concentrations. This indicates dilution dispersion in the aquifer model was adequately parameterized because the source of the Tc-99 currently seen in these wells is from the CPP-3 injection well.

A-8.4 Summary of Aquifer Model Assumptions

The following list contains the primary assumptions used in developing the aquifer flow and transport models:

- The aquifer model domain is assumed to be fully saturated, and the response to pumping and recharge is assumed to behave as if confined. However, a transient water and contaminant flux is placed as an upper boundary condition.

- Production in the CPP-1, -2, and -4 wells is steady state.

- Injection in the CPP-3 well is transient.

- The Big Lost River loss rate between the INL Site diversion dam and the Lincoln Boulevard bridge gauging station represents the loss rate near INTEC, and quarterly averages adequately represent transient river recharge.

- The Big Lost River recharge prior to 1985 and after 2004 is steady state and is adequately represented by the long-term average between 1965 through 1987.

- Three material types (H basalt, HI interbed, and I basalt) and spatially varying H basalt permeability adequately represent aquifer heterogeneity.

- The observed isothermal temperature pofile with depth adequately denotes the thickness of the actively flowing portion of the aquifer.

- Flow in the fractured basalt was controlled by the fracture network and could be represented by a high-permeability, low-porosity equivalent porous medium.

- Water levels measured in summer 2004 are representative of the long-term natural gradient.

- All contaminant (except Site CPP-31 Sr-90 within the alluvium) sorption processes can be lumped into a single contaminant-specific soil/water distribution coefficient (K_d) parameter.

- There is sufficient accuracy in the contaminant source terms and sufficient number of concentration observations for aquifer flow model calibration.

- The aquifer model can be linked to the vadose zone model through a transient water and contaminant flux.

- There is no gaseous-phase contaminant transport to the aquifer.

A-9 GROUNDWATER PATHWAY RISK PREDICTION

In this section, predictions of the future baseline groundwater concentrations are presented. In view of the large number of COPCs, a screening analysis was performed to reduce the number of contaminants incorporated into the full 3-D vadose zone and aquifer models. The screening analysis used very simple, but conservative assumptions. The screening analysis procedure and results are presented in Section A-9.1. The contaminant source terms used in the modeling are presented in Section A-9.2, and the simulation results are presented in Section A-9.3.

A-9.1 Screening Analysis

An extensive screening of groundwater COPCs was performed in the OU 3-13 RI/BRA (DOE-1997). The OU 3-13 COPC list was used as the starting point for the OU 3-14 screening process. The list was reviewed using process knowledge and new data collected since the OU 3-13 RI/BRA to determine if any additional COPCs from the OU 3-14 tank farm sites needed to be added to this list. As a result of the review, nitrate and C-14 were added to the list of COPCs. C-14 was added to the list of COPCs because it is an activation product in spent nuclear fuel.

All of the OU 3-14 alluvium samples collected in 2004 were analyzed for C-14. All sample results were nondetect except for the duplicate sample collected from the 36-40-ft depth in CPP-31 (the primary sample was nondetect and the duplicate was 3 pCi/g). Tank farm waste has been analyzed for C-14, but it has never been detected. The ORIGEN code was used to predict the ratio of C-14 to Cs-137 in the fuel and it is approximately 10^{-9} (see Table A-9-1). The C-14 in the waste is likely much lower than in the fuel because it would be oxidized and released as CO_2 during the fuel dissolution process. INTEC perched water and Snake River Plain Aquifer samples have been analyzed for C-14. The maximum C-14 concentrations measured in the Snake River Plain Aquifer in 2004 were less than 1% of the Snake River Plain Aquifer MCL. The maximum C-14 measured in the perched water in 2004 was approximately 4% of the Snake River Plain Aquifer MCL. Although C-14 was not expected to be a final COC for the tank farm soils and groundwater, it was part of the groundwater COPC screening because it had not been part of the previous screening conducted in OU 3-13.

All of the OU 3-14 COPCs were then evaluated using the GWSCREEN model (Rood 1999) and conservative parameters. The initial list of COPCs and screening results are provided in Table A-9-2. The GWSCREEN model was developed to address CERCLA sites at the INL Site. The code, coupled with a set of default parameter values identified in the CERCLA Track 2 risk assessment process (DOE-ID 1994), provides conservative estimates of groundwater concentrations and ingestion doses at the INL Site.

The GWSCREEN conceptual model is illustrated in Figure A-9-1. Contaminants are mixed homogeneously with an assumed volume of soil. One-dimensional transport in the unsaturated zone is assumed. The dimensions of the source were assumed to be $100 \times 100 \times 0.5$ m. The horizontal dimensions are based on the minimum area of the computational blocks used in the TETRAD model. The thickness of the contaminated zone (0.5 m) was based on guidance in the National Council on Radiation Protection (NCRP) Report Number 123, *Screening Models for Releases of Radionuclides* (NCRP 1996).

The subsurface environment beneath the INL Site is composed of basalt flows separated by sedimentary interbeds. The basalt flows are oftentimes fractured, allowing water to move freely in the vertical direction. The Track 2 methodology (DOE-ID 1994) recognized this feature of the system and assumed water transport time through the fractured basalt is relatively instantaneous. Water travel time through the entire unsaturated zone is ultimately controlled by the presence of sedimentary interbeds. Therefore, only transport through sedimentary interbeds was considered when computing contaminant transport in the unsaturated zone. The total thickness of sedimentary interbeds was obtained from the geologic model of INTEC and represents the total interbed thickness below CPP-31 (17.6 m). Most of the contamination at INTEC was derived from leaky pipes at CPP-31; therefore, the sedimentary interbeds present below this facility would be most relevant in terms of estimating contaminant transport in the unsaturated zone.

Infiltration of precipitation through the alluvium was estimated to be 18 cm/yr across the INTEC site. This value is substantially greater than the Track 2 default value of 10 cm/yr (DOE-ID 1994) because much of INTEC is unvegetated gravely alluvium. Additional anthropogenic water from leaky pipes was estimated to increase the infiltration through surface alluvium from 18 cm/yr to 40 cm/yr.

Water fluxes through sedimentary interbeds at INTEC are influenced by the presence of the Big Lost River and the INTEC percolation ponds. Annual average water fluxes through interbeds in the north end of INTEC (near CPP-31) were estimated to be ~2 m/yr. The value of 2 m/yr was used in the GWSCREEN simulation to estimate water travel time through the interbeds. The GWSCREEN code only allows input of a single water flux. Therefore, a water flux of 2 m/yr was input and source thickness was adjusted so that leaching from the alluvium would occur at a rate equivalent to 40 cm/yr infiltration. The leach rate constant is given by

$$\lambda_L = \frac{I}{H\,\theta\left(1+\frac{K_d\rho}{\theta}\right)} \qquad \text{(A-9-1)}$$

where

I = assumed infiltration rate (0.18 m yr^{-1})

H = assumed waste thickness (0.5 m)

ρ = bulk density (g/cm^3)

K_d = sorption coefficient (g/cm^3)

θ = moisture content (m^3/m^3).

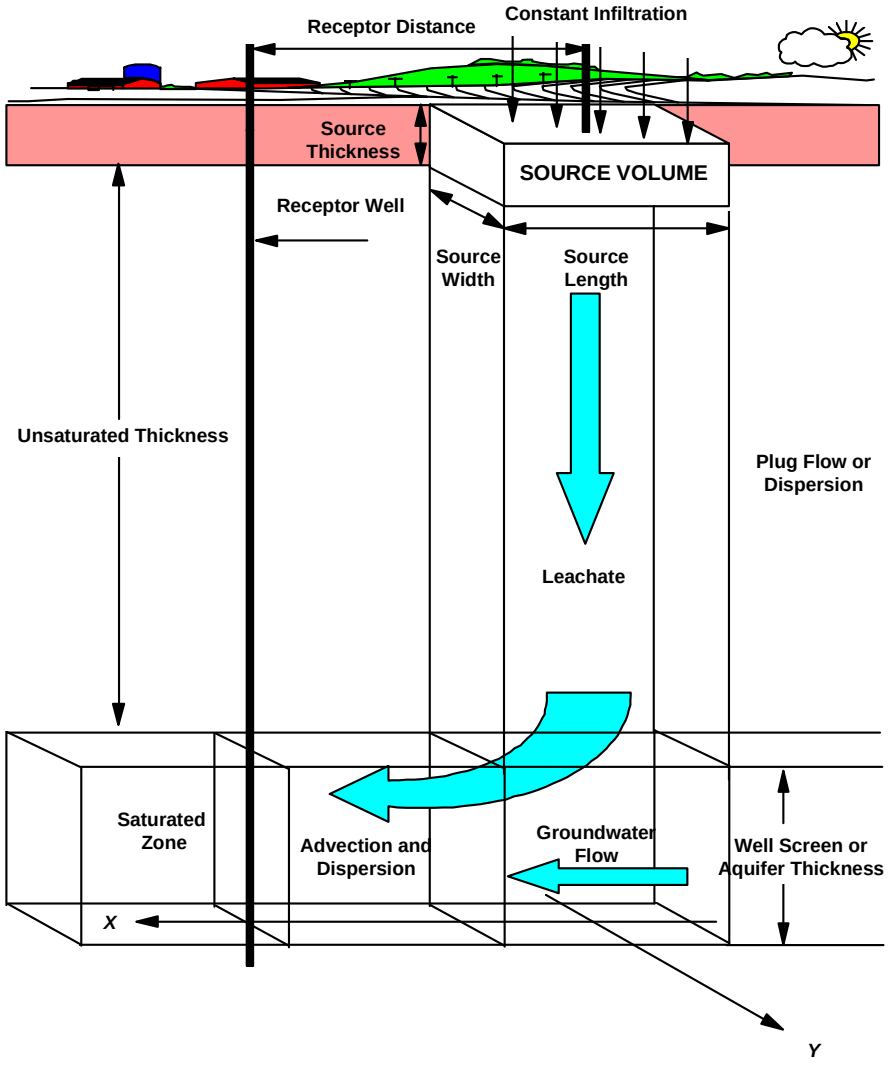

Figure A-9-1. Conceptual model for GWSCREEN.

The equivalent source thickness can be calculated by rearrangement of Equation 9-1.

$$H = \frac{I}{\lambda_L \, \theta \left(1 + \frac{K_d \rho}{\theta}\right)} \tag{A-9-2}$$

The moisture content in the sources was determined using the van Genuchten fitting parameters for high-permeability alluvium (α = 127 1/m. n = 1.1, K_{sat} = 4170, θ_{sat} = 0.42, θ_r = 0.0002). Using the van Genuchten parameters for high-permeability alluvium and the stated infiltration rates of 40 cm/yr for the alluvium and 2 m/yr for the interbeds resulted in moisture contents of 0.343 and 0.367 respectively. The leach rate constant for 40 cm/yr infiltration (assuming a K_d of zero) is

$$\lambda_L = \frac{40\,\text{cm/yr}}{0.5\,\text{m}\ \ 0.343} = 2.33\,\text{yr}^{-1} \tag{A-9-3}$$

The effective source thickness is then

$$H = \frac{2\,\text{m/yr}}{2.33\,\text{yr}^{-1}\,0.367} = 2.34\,\text{m} \qquad \text{(A-9-4)}$$

Dispersion was considered in the unsaturated zone because dispersion is a conservative assumption when contaminants with short half-lives relative to their transit times are considered. Contaminants entering the aquifer from the unsaturated zone mix with water in the aquifer over a depth defined by a typical well screen of 15 m (DOE-ID 1994). Concentrations are then evaluated at the downgradient edge of the source. This receptor is the point where the highest concentrations in the aquifer are computed.

The GWSCREEN model also considers transport of radioactive progeny. For simplicity, progeny are assumed to travel at the same rate as their parent. Under most circumstances, this assumption leads to conservative dose estimates at the receptor point. However, when considering the transport of a short-lived immobile parent that has a long-lived mobile progeny, results can be distorted and, in many cases, not conservative. This situation occurs for the Pu-241⇒Am-241⇒Np-237 and Pu-238⇒U-234 decay chains. In general, the short-lived immobile parent nuclide never leaves the waste zone and instead decays to its more mobile long-lived progeny. The sorption characteristics of the progeny then determine the overall transit time of the decay chain along with accompanying radiation dose. For conservatism, the entire activity of the short-lived immobile parent is converted to the equivalent mobile progeny activity by:

$$A_{Prog} = A_{Parent}\,\frac{T_{parent}}{T_{Prog}} \qquad \text{(A-9-5)}$$

where

A_{Prog} = equivalent activity of the long-lived mobile progeny (Ci)
A_{Parent} = original activity of the short-lived immobile parent (Ci)
T_{Prog} = half-life of the long-lived mobile progeny (years)
T_{Parent} = half-life of the short-lived immobile parent (years).

The receptor scenario assumes the person drinks 2 L of water per day for 365 days per year. Ingestion doses are computed using dose conversion factors published in EPA (1988) and include contributions from all progeny.

The screening criterion for radionuclides was set at 0.4 mrem/yr and was based on 1/10th the allowable drinking water dose for beta-gamma-emitting radionuclides of 4 mrem/yr as stated in 40 CFR 141. This was the same screening criterion that was applied in the Idaho CERCLA Disposal Facility (ICDF) Performance Assessment (DOE-ID 2003c). For metals, maximum groundwater concentrations were compared with their corresponding maximum contaminant limits (Snake River Plain Aquifer MCLs). Uranium was addressed both as a radionuclide and a metal.

Input data for the GWSCREEN screening simulation (Figure A-9-1) were primarily obtained from the Track 2 guidance document (DOE-ID 1994) and modified as noted. The receptor well is placed on the downgradient edge of the source. Note that the receptor distance is measured from the center of the source. The conceptual model assumes no presence of engineered barriers or other devices that would limit infiltration and reduce contaminant leaching. The waste is then assumed to be exposed to infiltrating water, and contaminants are leached from the waste and move into the subsurface.

Table A-9-1 Parameter values for the GWSCREEN screening analysis.

Parameter	Value	Reference
Length parallel to groundwater flow	100 m	TETRAD large-scale vadose zone model grid cell size
Width perpendicular to groundwater flow	100 m	TETRAD large-scale vadose zone model grid cell size
Infiltration through alluvium	0.40 m/yr	This study
Thickness of source	0.5 m	Based on default groundwater scenario in NCRP (1996)
Water-filled porosity – source	0.343	This study (high-permeability alluvium and 40 cm/yr infiltration
Water-filled porosity – unsaturated zone	0.4438	This study (high-permeability interbed and 2 m/yr infiltration)
Unsaturated interbed thickness (transport time through basalt assumed to be instantaneous)	17.6 m	Interbed thickness below CPP-31
Bulk density-source	1.5 g/cm^3	DOE-ID (1994)
Bulk density-unsaturated zone	1.9 g/cm^3	DOE-ID (1994)
Bulk density-saturated zone	1.9 g/cm^3	DOE-ID (1994)
Well screen thickness[a]	15 m	DOE-ID (1994)
Receptor distance parallel to groundwater flow (measured from center of source)	50 m	Based on guidance in DOE-ID (1994)
Receptor distance perpendicular to groundwater flow (measured from center of source)	0 m	Based on guidance in DOE-ID (1994)
Water ingestion rates for receptor	2 L/d	DOE-ID (1994)
Exposure frequency	365 d/yr	DOE-ID (1994)
Darcy velocity in aquifer	21.9 m/yr	Fate and transport modeling design of the ICDF landfill cap (DOE-ID 2003d; EDF-ER-275)
Longitudinal dispersivity	9 m	DOE-ID (1994)
Transverse dispersivity	4 m	DOE-ID (1994)
Aquifer porosity	0.03	DOE-ID (2003d)
a. A vertically averaged solution is used per Track 2 guidance (DOE-ID 1994). Thickness of the vertical section is taken to be the well screen thickness.		

Nuclide-specific data are reported in Table A-9-2. The primary source of sorption coefficient data was DOE-ID (1994) (the Track 2 screening process). If a value for a given nuclide did not exist in DOE-ID (1994), then other sources were consulted, including Sheppard and Thibault (1990), NCRP (1996), and DOE-ID (1997). The sorption coefficients or K_d values were assumed to be applicable to sedimentary rocks and materials that make up the surface alluvium and interbeds. Sorption coefficients in fractured basalt, which makes up most of the aquifer, tend to be lower than in sedimentary materials because surface area of available sorption sites are lacking. The ratio of the aquifer basalt-to-soil K_d value was estimated in the INTEC RI/BRA (DOE-ID 1997) to be 0.04. The ratio was multiplied by all sediment K_d values to obtain the aquifer K_d values used in the GWSCREEN simulation. Radionuclide solubility was assumed to be infinite in all cases. The Darcy velocity in the aquifer was taken from the screening analysis for the ICDF PA (DOE-ID 2003c).

A-9.1.1 Results of GWSCREEN Analysis

Screening results are given in Table A-9-2 where the initial 22 radionuclides and their daughter products are listed in the first column. The last column indicates the 14 nuclides that were removed from further consideration. The last column also indicates the 8 remaining radionuclides that were carried forward based on the 0.4-mrem criteria. These remaining nuclides include H-3, I-129, Np-237, Pu-239, Pu-240, Sr-90, Tc-99, and U-234.

Uranium isotopes were compared with the Snake River Plain Aquifer MCL of 30 µg/L (Table A-9-3). Each uranium isotope represents a different uranium mass because each isotope has a different half-life. Therefore, the 30-µg/L limit was converted to an equivalent activity concentration for each uranium isotope and compared with the maximum activity concentration estimated by GWSCREEN for that isotope. The sum of the ratio of the maximum uranium isotope concentration to the isotope-specific Snake River Plain Aquifer MCL activity concentration provides a measure of the total uranium concentration in groundwater. If the aforementioned ratio is less than one, then the total uranium mass is less than 30 µg/L. In this screening exercise, none of the uranium isotope mass concentrations exceeded the Snake River Plain Aquifer MCL and the total uranium mass concentration was less than the Snake River Plain Aquifer MCL.

Evaluation of metals was limited to mercury, arsenic, chromium, and nitrate. Water solubilities were obtained from Perry et al. (1984), except for nitrate, which assumed an infinite solubility. All nonradionuclide concentrations were less than their respective Snake River Plain Aquifer MCLs except nitrate, which had a maximum concentration about nine times the Snake River Plain Aquifer MCL of 10 mg/L. The results of the nonradionuclide screening are provided in Table A-9-4.

The screening analysis used the Track 2 guidance K_d values (DOE-ID 1994) and was performed prior to the estimation of the groundwater K_d values used for the RI/BRA full modeling process. The Track 2 K_d values are generally very conservative, but several RI/BRA K_d values were smaller than those used in the screening analysis. These contaminants included: Am-241, Arsenic, C-14, Chromium, Cs-137, Np-237, Sr-90 and U-235. The RI/BRA analysis evaluated the risk from Np-237, Sr-90 and U-235; and the effect of a less conservative K_d was considered. The remaining contaminants with screening K_d values larger than the RI/BRA values all had screening concentrations several orders of magnitude lower than the SRPA MCL and would not pose a risk to the SRPA, if the RI/BRA values were used in the screening analysis.

Table A-9-2 Results of radionuclide screening (blue color denotes the parent contaminants are retained for the full modeling process)

Radionuclide Progeny[a]	Mass	Half-Life (Years)	Activity (Ci)	Ingestion DCF (rem/Ci)	K_d (mL/g)	Dose (mrem)	Is Dose < 0.4 (mrem)?
Am-241 (Np-237)	237	2.14E+06	4.10E-04	4.44E+06	8	1.4E-01	
U-233	233	1.59E+05		2.89E+05	6	7.4E-06	
Th-229	229	7.43E+03		4.03E+06	100	4.1E-08	
TOTAL						1.4E-01	Yes
C-14	14	5,730	2.81E-05	2,086.8	5	8.3E-06	Yes
Co-60	60	5.27E+00	1.96E+01	2.69E+04	10	5.6E-04	Yes
Cs-137	137	3.02E+01	1.91E+04	5.00E+04	500	1.9E-15	Yes
H-3	3	1.23E+01	9.71E+00	6.40E+01	0	1.6E+00	NO
I-129	129	1.57E+07	1.26E-03	2.76E+05	0	1.1E+00	NO
Np-237	237	2.14E+06	2.72E-02	4.44E+06	8	9.6E+00	
U-233	233	1.59E+05		2.89E+05	6	4.9E-04	
Th-229	229	7.43E+03		4.03E+06	100	2.7E-06	
TOTAL						9.6E+00	NO
Pu-236 (U-232)	232	7.20E+01	2.13E-05	1.31E+06	6	1.4E-03	
Th-228	228	1.91E+00		8.08E+05	100	5.2E-05	
TOTAL						1.4E-03	Yes
Pu-238 (U-234)	234	2.45E+05	6.71E-03	2.83E+05	6	2.1E-01	
Th-230	230	7.54E+04		5.48E+05	100	2.4E-05	
Ra-226	226	1.60E+03		1.33E+06	100	1.1E-06	
Pb-210	210	2.20E+01		7.27E+06	100	3.6E-06	
TOTAL						2.1E-01	Yes
Pu-239	239	2.41E+04	6.94E+00	3.54E+06	22	9.9E+02	
U-235	235	7.04E+08		2.67E+05	6	7.0E-05	
Pa-231	231	3.28E+04		1.06E+07	550	1.3E-07	
Ac-227	227	2.18E+01		1.48E+07	450	1.8E-07	
TOTAL						9.9E+02	NO
Pu-240	240	6.57E+03	1.07E+00	3.54E+06	22	1.5E+02	
U-236	236	2.34E+07		2.69E+05	6	3.2E-04	

Radionuclide Progeny[a]	Mass	Half-Life (Years)	Activity (Ci)	Ingestion DCF (rem/Ci)	K_d (mL/g)	Dose (mrem)	Is Dose < 0.4 (mrem)?
Th-232	232	1.41E+10		2.73E+06	100	2.0E-12	
Ra-228	228	5.75E+00		1.44E+06	100	8.0E-13	
Th-228	228	1.91E+00		8.08E+05	100	4.9E-13	
TOTAL						1.5E+02	NO
Pu-241 (Np-237)	241	2.14E+06	4.88E-04	4.44E+06	8	1.7E-01	
U-233	233	1.59E+05		2.89E+05	6	8.9E-06	
Th-229	229	7.43E+03		4.03E+06	100	4.9E-08	
TOTAL						1.7E-01	Yes
Pu-242	242	3.76E+05	1.73E-04	3.36E+06	22	2.4E-08	
U-238	238	4.47E+09		2.70E+05	6	2.5E-10	
U-234	234	2.45E+05		2.83E+05	6	1.4E-13	
Th-230	230	7.54E+04		5.48E+05	100	2.0E-17	
Ra-226	226	1.60E+03		1.33E+06	100	1.5E-18	
Pb-210	210	2.20E+01		7.27E+06	100	6.7E-18	
TOTAL						2.5E-08	Yes
Pu-244	244	8.26E+07	1.80E-11	4.03E+08	100	4.4E-10	
Pu-240	240	6.57E+03		3.54E+06	22	4.0E-10	
U-236	236	2.34E+07		2.69E+05	6	1.9E-15	
Th-232	232	1.41E+10		2.73E+06	100	3.6E-23	
Ra-228	228	5.75E+00		1.44E+06	100	1.5E-23	
Th-228	228	1.91E+00		8.08E+05	100	9.6E-24	
TOTAL						8.4E-10	Yes
Sr-90	90	2.86E+01	1.81E+04	1.42E+05	12	3.9E+03	NO
Tc-99	99	2.13E+05	3.56E+00	1.46E+03	0.2	7.9E+00	NO
U-232	232	7.20E+01	2.78E-05	1.31E+06	6	1.8E-03	
Th-228	228	1.91E+00		8.08E+05	100	6.8E-05	
TOTAL						1.9E-03	Yes
U-233	233	1.59E+05	2.61E-06	2.89E+05	6	8.4E-05	
Th-229	228	5.75E+00		4.03E+06	100	2.4E-05	

Radionuclide Progeny[a]	Mass	Half-Life (Years)	Activity (Ci)	Ingestion DCF (rem/Ci)	K_d (mL/g)	Dose (mrem)	Is Dose < 0.4 (mrem)?
TOTAL						1.1E-04	Yes
U-234	234	2.44E+05	4.36E-02	2.83E+05	6	1.4E+00	
Th-230	230	7.54E+04		5.48E+05	100	1.6E-04	
Ra-226	226	1.60E+03		1.33E+06	100	6.9E-06	
Pb-210	210	2.20E+01		7.27E+06	100	2.3E-05	
TOTAL						1.4E+00	NO
U-235	235	7.04E+08	6.04E-03	2.67E+05	6	1.8E-01	
Pa-231	231	3.28E+04		1.06E+07	550	1.9E-04	
Ac-227	227	2.18E+01		1.48E+07	450	2.2E-04	
TOTAL						1.8E-01	Yes
U-236	236	2.34E+07	4.47E-03	2.69E+05	6	1.3E-01	
Th-232	232	1.41E+10		2.73E+06	100	4.6E-10	
Ra-228	228	5.75E+00		1.44E+06	100	1.8E-10	
Th-228	228	1.91E+00		8.08E+05	100	1.1E-10	
TOTAL						1.3E-01	Yes
U-238	238	4.47E+09	6.33E-04	2.70E+05	6	1.7E-02	
U-234	234	2.45E+05		2.83E+05	6	5.5E-06	
Th-230	230	7.54E+04		5.48E+05	100	3.2E-10	
Ra-226	226	1.60E+03		1.33E+06	100	9.4E-12	
Pb-210	210	2.20E+01		7.27E+06	100	2.7E-11	
TOTAL						1.7E-02	Yes

a. Progeny are left justified in this column. Radionuclides in parentheses indicate the progeny that is simulated. The activity inventory represents that of the parent converted to equivalent progeny.

Table A-9-3 Uranium isotope mass concentrations and comparison to the Snake River Plain Aquifer MCL of 30 µg/L.

Uranium Isotope	Specific Activity (Ci/g)	Equivalent SRPA MCL Activity Concentration (pCi/L)	Maximum Concentration (pCi/L)	Ratio to SRPA MCL
U-232	2.24E+01	6.72E+08	1.9E-03	2.81E-12
U-233	9.64E-03	2.89E+05	4.3E-04	1.48E-09
U-234	6.23E-03	1.87E+05	7.1E+00	3.82E-05
U-235	1.92E-06	5.77E+01	9.9E-01	1.72E-02
U-236	6.51E-05	1.95E+03	7.3E-01	3.75E-04
U-238	3.33E-07	9.99E+00	1.0E-01	1.04E-02
TOTAL				2.80E-02

Table A-9-4 Results of nonradionuclide screening.

Non-radionuclide	Mass	Inventory (mg)	SRPA MCL (mg/L)	K_d (mL/g)	Water Solubility (mg/L)	Peak Concentration (mg/L)	Ratio to SRPA MCL
Hg	2.006E+02	7.164E+07	2.00E-03	100	7	7.30E-04	3.65E-01
Cr	5.200E+01	1.309E+07	1.00E-01	30	1,740,000	4.43E-04	4.43E-03
As	7.492E+01	4.315E+03	5.00E-03	50	658,000	8.78E-08	1.76E-05
NO_3	6.200E+01	2.116E+10	1.00E+01	0	∞	9.23E+01	9.23E+00

A-9.2 Contaminants of Potential Concern Source Terms

The results of the screening analysis identified 10 COPCs which were simulated with the vadose zone and aquifer models. The simulated radionuclide COPCs were the following: H-3, I-129, Np-237, Pu-239, Pu-240, Sr-90, Tc-99, and U-234. The nonradionuclides were mercury and nitrate. The simulations included the following contaminant sources: (1) the known OU 3-14 releases, (2) the known OU 3-13 liquid releases, (3) the OU 3-13 soil sources, (4) the CPP-3 injection well releases, and (5) the former percolation pond releases. The source term placement within the model is the same as that presented in Section A-5.1.4.1.

The contaminants originating at RTC were not included in the OU 3-14 analysis because the current aquifer model predicts those contaminants to remain mostly west of the INTEC plume. The two plumes may merge far south and west of the INTEC, but the contaminant concentrations in the areas where the two plumes may intersect are very dilute. The OU 3-14 release sources are summarized in Section A-9.2.1. The OU 3-13 soil contamination sources are presented in Section A-9.2.2, and the service waste sources (CPP-3 injection well and former percolation ponds) are presented in Section A-9.2.3. These source inventories are summarized in Table A-9-5.

Table A-9-5 COPC source term summary.

COPC	OU 3-14 Releases (Ci or kg)	Injection Well (Ci or kg)	Former Percolation Ponds (Ci or kg)	OU 3-13 Contaminated Soil Sites (Ci or kg)	OU 3-13 Liquid Releases (Ci)	Total (Ci or kg)
H-3	9.71	2.01e+4	9.99e+2	0.	378.1	2.15e+4
I-129	1.26e-3	0.86	8.2e-2	3.89e-2	0.	.982
Np-237	2.72e-2	1.07	0.	1.33e-1	0.	1.23
Pu-239	6.94	1.35e-2	1.14e-3	1.05e+0	0.	8.01
Pu-240	1.07	6.77e-3	5.71e-4	1.18e-1	0.	1.19
Sr-90	1.81e+4	2.43e+1	2.95e-1	9.18e+2	308.8	1.94e+4
Tc-99	3.56	1.19e+1	1.13e+0	9.30e-2	0.	16.7
U-234	0.138[a]	1.35e-1	4.03e-2	1.40e-1	0.	.410
Mercury	72.4	4.00e+2	0.	5.85e+2	0.	1.06e+3
Nitrate	2.12e+4	2.83e+6	1.31e+6	0.	0.	4.16e+6

a. Early estimate of U-234 source term. The estimate for U-234 developed in Section 5 of the main document was smaller, but the model was not rerun with the latest value because the source term was conservatively larger.

A-9.2.1 Release Estimates for OU 3-14 Sites

Based on process knowledge, some of the release estimates used for the OU 3-13 RI/FS were determined to be inaccurate. Because of their importance, the release times, concentrations, and volumes were revised based on an in-depth analysis of INTEC operations. In some cases (e.g., CPP-31), the total volumes were increased; others were decreased. A complete discussion of the revision process and rationale can be found in Section 5 of the main document. Each of the contaminant sources contained in Table A-9-6 were incorporated into the model as a liquid release during the estimated release period.

Table A-9-6 OU 3-14 liquid releases.

Site	First Day	Last Day	Liquid Volume (gal)	H-3 (Ci)	I-129 (Ci)	Np-237 (Ci)	Pu-239 (Ci)	Pu-240 (Ci)	Sr-90 (Ci)	Tc-99 (Ci)	U-234 (Ci)	Nitrate (kg)	Mercury (kg)
CPP-31	11/1/72	11/7/72	18,600	2.34E+0	2.51E-4	2.51E-2	4.34E+0	1.00E+0	1.59E+4	3.17E+00	4.34E-2	19,100	70.1
CPP-28	2/1/74	4/30/74	230.	5.59E-1	1.52E-4	5.80E-6	2.97E-2	1.04E-2	6.62E+2	1.10E-1	8.28E-6	130	0.518
CPP-79 deep1967	1/1/67	1/1/67	120.	1.58E+0	1.07E-4	3.67E-4	7.33E-1	6.77E-3	2.62E+2	4.51E-2	1.49E-5	114	0.092
CPP-79 deep1973	1/1/73	1/2/73	280.	3.68E+0	2.50E-4	8.55E-4	1.71E+0	1.58E-2	6.12E+2	1.05E-1	3.49E-5	266	0.214
CPP-27/33 1964 scrub solution	1/1/64	12/31/64	180.	4.00E-1	1.10E-4	2.99E-4	4.08E-2	1.09E-2	2.40E+2	4.00E-2	3.50E-5	0	0.478
CPP-27/33 1966-1967 scrub solution	1/1/66	12/31/67	360.	8.00E-1	2.20E-4	5.99E-4	8.17E-2	2.18E-2	4.80E+2	8.00E-2	7.00E-5	0	0.957
CPP-27/33 1964-1974 decon solution	1/1/64	12/31/73	500.	0	0	0	0	0	0	0	0	1,100	
CPP-15	3/1/74	3/4/74	2,000.	1.20E-4	3.00E-6	2.14E-7	5.45E-5	8.39E-6	1.50E-1	2.40E-5	1.67E-2[a]	1.2	
CPP-16	1/1/76	1/7/76	150.	1.10E-3	9.30E-8	1.15E-6	2.94E-4	4.53E-5	6.10E-1	1.30E-4	3.34E-2[a]	7.9	
CPP-20	1/1/58	12/31/77	100.	3.00E-5	2.00E-9	1.14E-8	2.91E-6	4.48E-7	8.00E-3	1.00E-6	0.0E+0[a]	0.23	
CPP-79 (shallow)	7/15/86	7/15/86	2,530.00	0.18	1.40E-4	1.85E-6	4.72E-4	7.27E-5	1.3	2.60E-4	3.52E-8[a]	77	0.
CPP-24	2/1/54	2/1/54	1.00	1.30E-2	6.70E-7	7.12E-12	1.82E-9	2.80E-10	6.00E-6	6.70E-6	1.29E-5[a]	0.023	0.
CPP-25	8/1/60	8/1/60	10.00	2.00E-4	8.10E-8	4.27E-6	1.09E-3	1.67E-4	2.30E-1	4.90E-5	6.95E-5[a]	7	0.
CPP-26	5/1/64	5/1/64	2.00	2.00E-2	1.20E-6	1.08E-5	2.76E-3	4.25E-4	7.6	1.10E-3	6.86E-7[a]	2.6	0.
CPP-30	6/1/76	6/1/76	0.0026	1.50E-6	1.60E-9	9.97E-9	2.54E-6	3.92E-7	7.00E-3	1.10E-6	4.29E-10[a]	0.0015	0.
CPP-32E	12/1/76	12/1/76	0.0008	2.00E-6	4.00E-10	2.85E-9	7.27E-7	1.12E-7	2.00E-3	3.00E-7	2.57E-4[a]	0.0003	0.
CPP-32W	12/1/76	12/1/76	1.00	1.96E-6	5.32E-10	3.45E-9	8.8E-7	1.35E-7	2.32E-3	3.87E-7	6.52E-4[a]	0.00007	0.
CPP-58E 1976	9/1/76	9/15/76	2,500	6.80E-3	1.60E-5	3.70E-10	9.45E-8	1.45E-8	9.40E-5	1.60E-4	1.72E-7[a]	176	0.
CPP-58W	8/1/54	8/1/54	100.00	3.60E-2	3.60E-6	5.13E-11	1.31E-8	2.01E-9	3.60E-5	3.60E-5	2.08E-7[a]	7	0.

a. Early estimate of U-234 source term. The estimate for U-234 developed in Section 5 of the main document was smaller, but the model was not rerun with the latest value because the source term was conservatively larger.

A-9.2.2 Remaining OU 3-13 Sites

Sites CPP-02 and CPP-80 are OU 3-13 liquid release sites. The source estimates for these sites were taken from the OU 3-13 RI/FS and are presented in Table A-9-7. These estimated releases were not revisited during the analysis presented in Section 5 of the main document and may have been overestimated in the OU 3-13 RI/FS. Site CPP-87/89 is a Group 2 site (under Building CPP-649). It was originally identified in the OU 3-14 RI/FS Work Plan (DOE-ID 2004a) as a new site in CPP-58 but has since been more appropriately identified as an OU 3-13 Group 2 site. The source term is developed in Section 5 of the main document (under CPP-58).

Table A-9-7 Remaining OU 3-13 Sources.

Site	First Day	Last Day	Liquid Volume (gal)	H-3 (Ci)	I-129 (Ci)	Np-237 (Ci)	Pu-239 (Ci)	Pu-240 (Ci)	Sr-90 (Ci)	Tc-99 (Ci)	U-234 (Ci)	Nitrate (kg)	Mercury (kg)
CPP-02	1/1/58	12/31/66	4.78E+7	378.1	0.	0.	0.	0.	3.38E+1	0.	0.	0.	0.
CPP-80	1/1/83	12/31/89	1.51E+3	0.	0.	0.	0.	0.	2.75E+2	0.	0.	0.	0.
CPP-87/89 1975	10/1/75	10/14/75	2.50E+3	9.00E-02	9.00E-6	5.84E-10	1.49E-7	2.29E-8	3.40E-4	9.00E-5	6.00E-7[a]	176	0.

a. Early estimate of U-234 source term. The estimate for U-234 developed in Section 5 of the main document was smaller, but the model was not rerun with the latest value because the source term was conservatively larger.

Estimated inventories for the contaminated OU 3-13 soil sites were also taken from the OU 3-13 RI/FS (DOE-ID 1997). These are represented by worst-case scenarios based on measured soil concentrations and site soil volumes. The contaminated soil volume was assumed to be a rectangular box encompassing the surrounding clean soil borings and extending from land surface to the basalt. The contaminant concentration typically assigned to the entire volume corresponded to the maximum value of all samples within each rectangle. As a result, the soil volume was probably overestimated as was the radionuclide inventory. In the model, these sites were incorporated over a 1-day period (March 29, 1996), corresponding to the average date when the samples were collected.

Site CPP-37B is an old gravel pit that received mainly construction debris before it was backfilled. Before 1982, it received waters released from the sludge dewatering pit of the old Sewage Treatment Plant, but the volume is believed to be low (DOE-ID 2004d). In 1991, 26 soil samples were collected from four boreholes approximately every 5 ft to basalt, plus one sample in an interbed at 109 ft deep. Samples were analyzed for inorganics, volatile organic compounds, semivolatile organic compounds, pesticides, herbicides, polychlorinated biphenyls, and radionuclides.

A table of unvalidated data in a draft report (Golder Associates 1992) indicates that 26 samples were analyzed for I-129, 25 of which were nondetect. Only one sample (20 ft deep) had a positive detect for I-129 (1.57 ± 0.82 pCi/g), and it is assumed from reviewing all radionuclide data that the counting error was reported at 2 sigma. From this one sample, the OU 3-13 RI/BRA very conservatively assumed that the entire area of the gravel pit down to bedrock had this concentration of I-129. This calculates to be 3.89×10^{-2} Ci of I-129, which is over 30 times more I-129 than from all of the tank farm sources combined (1.27×10^{-3} Ci). Given that I-129 is highly mobile, was nondetect in all of the 2004 tank farm alluvium samples, and is much more prevalent in tank farm sources (including CPP-31 and CPP-79 [deep]) than CPP-37B sources, the OU 3-13 RI/BRA estimate of the I-129 source term for CPP-37B is too conservative for use in the INTEC model.

Site CPP-37B is a Group 3 (Other Surface Soils) site. The OU 3-13 ROD (DOE-ID 1999) states that modeling and sampling of the site indicated the site is not a significant contributor to groundwater risk or surface exposure risk. No OU 3-13 remediation goals were exceeded (DOE-ID 2004d), including Cs-137, which had a maximum value of 4.2 ± 0.15 pCi/g and Sr-90, which had a maximum concentration of 4.31 ± 0.33 pCi/g. The lack of Sr-90 and Cs-137 contamination also indicates that I-129 should not be a COC for this site.

Site CPP-37B was sampled for I-129 in September of 2005 during ongoing OU 3-13 Group-3 work. There were 11 samples taken and one duplicate. Ten samples were non-detect and 2 were flagged UJ (false positive). The OU 3-13 Group-3 work concluded that the site will not result in unacceptable risk to human health or the environment and that the site will not require further action (personal communication with Dean Shanklin). The Site CPP-37B I-129 was not included as a source term in the revised INTEC model.

At Site CPP-89, the plutonium was reported as total Pu-239/240 as a combined value. This value was used as the Pu-239 source and also for the Pu-240 source, essentially doubling the inventory. Table A-9-8 summarizes the OU 3-13 soil site sources used in the OU 3-14 baseline risk assessment.

Table A-9-8 OU 3-13 contaminated soil sites.

Site	H-3 (Ci)	I-129 (Ci)	Np-237 (Ci)	Pu-239 (Ci)	Pu-240 (Ci)	Sr-90 (Ci)	Tc-99 (Ci)	U-234 (Ci)	Nitrate (kg)	Mercury (kg)
CPP-89	0.	0.	0.	1.18e-1	1.18e-1	9.78e+1	0.	4.95E-2	0.	1.08E+2
CPP-35	0.	0.	0.	9.98e-4	0.	4.46e+0	0.	0.	0.	9.96e+0
CPP-36/91	0.	0.	0.	2.64e-1	0.	5.38e+1	0.	2.29e-3	0.	1.36e+1
CPP-01/04/05	0.	0.	0.	5.88e-2	0.	2.38e+1	0.	0.	0.	0.
CPP-08/09	0.	0.	0.	0.	0.	4.98e-1	0.	0.	0.	0.
CPP-10	0.	0.	0.	0.	0.	2.83e-2	0.	0.	0.	0.
CPP-11	0.	0.	2.57e-4	0.	0.	2.25e-2	0.	2.06e-3	0.	0.
CPP-03	0.	0.	0.	0.	0.	5.59e-1	0.	0.	0.	0.
CPP-17A	0.	0.	0.	0.	0.	7.81e-3	0.	0.	0.	0.
CPP-37A	0.	0.	1.12e-2	0.	0.	8.62e-3	0.	0.	0.	1.08e+1
CPP-37B	0.	0.	6.53e-2	0.	0.	3.58e-1	0.	0.	0.	0.
CPP-14	0.	0.	4.55e-2	0.	0.	7.17e-3	0.	5.02e-2	0.	3.03e+0
CPP-34[a]	0.	0.	1.05e-2	0.	0.	1.88e+2	0.	3.61e-2	0.	0.
CPP-13	0.	0.	0.	0.	0.	5.69e+0	3.68e-3	0.	0.	3.81e-1
CPP-06	0.	0.	0.	0.	0.	3.37e-3	0.	0.	0.	0.
CPP-19	0.	0.	0.	6.13e-1	0.	5.43e+2	0.	0.	0.	6.52e-1
CPP-22	0.	0.	0.	0.	0.	1.38e-1	8.93e-2	0.	0.	0.
CPP-90	0.	0.	0.	0.	0.	6.95e-2	0.	0.	0.	1.07e+1
CPP-93	0.	0.	0.	0.	0.	0.	0.	0.	0.	4.28e+2

a. Site CPP-34 has been remediated but was included in the model.

A-9.2.3 Service Waste

The CPP-3 injection well and former INTEC percolation ponds were used to receive process water and evaporator condensate created during liquid waste calcination. Evaporator condensate is also known as "service waste." The service waste volume and concentrations were taken directly from the OU 3-13 RI/BRA with the exception of the inventories for I-129, Tc-99, and nitrate.

The I-129 discharged into the injection well was taken from the OU 3-13 Group 5 Monitoring Report and Decision Summary (DOE-ID 2004c). The Monitoring Report and Decision Summary reevaluated the inventory of I-129 discharged into the injection well, resulting in a reduction from 1.39 Ci to 0.86 Ci.

Tc-99 concentrations discharged in the service waste were assumed to be equal to the ratio of Tc-99 to I-129 concentrations in the aquifer (DOE-ID 2002) near the CFA in 2001. The current aquifer concentration ratio far south of the INTEC should be representative of the disposal ratio if the two radionuclides are transported identically. Both Tc-99 and I-129 are long-lived and mobile contaminants. The 2001 average aquifer concentration ratio of Tc-99 to I-129 was 13.8 to 1 in wells LF3-10, LF3-08, LF2-09, LF2-08, LF2-11, and CFA-1. This ratio results in a Tc-99 inventory of 12.6 Ci in the service waste. Using this method of estimating, the Tc-99 inventory has limitations because the sorption chemistry and volatility differ between the two radionuclides. However, records of Tc-99 discharges were not kept and significant amounts of Tc-99 were released with the service waste.

The nitrate discharges in the service waste were assumed to be equal to the reported 1981 (Honkus 1982) measured concentrations. That year was chosen because it represents a typical operational year at INTEC and good records of service waste contents were available. The report indicated the average service waste nitrate concentration was 16 µg/mL (as N), which is about 71 mg/L as NO_3-.

The OU 3-13 RI/BRA model applied two average disposal rates to represent the service waste ponds to account for reduced fluxes during the early 1990s. The first rate was taken from disposal records for the period 1984-1990 and the second rate was for the period 1991-1995. The reduction in contaminant flux occurring in the early 1990s occurred as a result of the installation of the Liquid Effluent Treatment and Disposal facility (LET&D), which became operational in January 1993. The LET&D facility removed almost all of the contaminants from the service waste stream. The OU 3-14 model used a single average service waste source term for the period 1984-1993. After 1993, the simulated percolation ponds only received clean water. The service waste source term is summarized in Table A-9-9.

Table A-9-9 Service waste source terms.

COPC	First Day	Last Day	Liquid Volume	H-3 (Ci)	I-129 (Ci)	Np-237 (Ci)	Pu-239 (Ci)	Pu-240 (Ci)	Sr-90 (Ci)	Tc-99 (Ci)	U-234 (Ci)	NO_3- (kg)	Hg (kg)
Injection well (Ci or kg)	12/1/53	3/31/84	Variable	2.01e+4	0.86	1.07	1.35e-2	6.77e-3	2.43e+1	1.19e+1	1.35e-1	2.83e+6	4.00e+2
Percolation pond (Ci or kg)	4/1/84	12/31/93	1.54e+6 (gal/day)	9.99e+2	8.2e-2	0.	1.14e-3	5.71e-4	2.95e-1	1.13e+0	2.15e-2	1.31e+6	0.

A-9.3 Groundwater Simulation Results

Simulation results for the transport of the 10 COPCs are presented in Sections A-9.3.1- A-9.3.9. The transport parameters, federal drinking water standard, slope factor, and background concentration for each COPC is given in Table A-9-10. The constant background concentration was added to the simulation results during the postprocessing. Simulation results are presented first for the vadose zone and then for the aquifer. The overall summary is presented in Section A-9.3.10.

The simulation results are presented in a consistent format for each COPC. The vadose zone simulation results includes the following information: (1) horizontal contour plots of vadose zone concentration at four time periods, (2) vertical contour plots of vadose concentrations at four time periods, (3) time history plot of peak vadose zone concentration, and (4) time history plot of contaminant mass or contaminant activity flux into the aquifer. The aquifer simulation results include the following information: (1) horizontal concentration plots at four time periods and (2) time history plots of peak aquifer concentration. The Sr-90 simulation results are presented in Appendix J along with the geochemical model development. The contaminant concentrations were obtained through simulation in three-dimensions. To present the concentration contours shown in the following sections, these data were reduced by using the maximum concentration at any depth at each horizontal grid block location for the horizontal contour plots. Likewise, the vertical contour plots were created by using the maximum concentration at each vertical grid block location.

This data reduction scheme essentially compresses the contaminant plume in the vertical direction for the horizontal plots and compresses the contaminant plume in the east/west direction for the vertical plots. The vadose zone contour intervals are presented for each order of magnitude above and below the Snake River Plain Aquifer MCL, with the range spanning 10^{-1} * Snake River Plain Aquifer MCL to 10^{1} * Snake River Plain Aquifer MCL. The concentration isopleths below, equal to, and above the Snake River Plain Aquifer MCL are denoted by thin black lines, a thick red line, and thin red lines, respectively. The background concentrations for Orr et al. (1991) for each COPC were added to the vadose zone and aquifer simulations results. The aquifer contour intervals include a 10^{-2} * Snake River Plain Aquifer MCL isopleth, which is denoted by a thin dashed black line.

Table A-9-10 Contaminants of potential concern summary.

COPC	Half-Life (years)	Vadose Zone Alluvium K_d (mL/g)	Vadose Zone Interbed K_d (mL/g)	Vadose Zone Basalt K_d (mL/g)	Aquifer Interbed K_d (mL/g)	Aquifer Basalt K_d (mL/g)	SRPA MCL (pCi/L or mg/L)	Slope Factor (1/pCi)	Background Concentration (pCi/L or mg/L)
H-3	1.23e+1	0.	0.	0.	0.	0.	20,000.	5.07e-14	100.
I-129	1.57e+7	1.5	0.7	0.	0.7	0.	1.	1.48e-10	0.05
Np-237	2.14e+6	2.	2.	0.	2.	0.	15.	6.18e-11	0.
Pu-239	2.41e+4	1,000.	1,000.	0.	1,000.	0.	15.	1.35e-10	0.
Pu-240	6.57e+3	1,000.	1,000.	0.	1,000.	0.	15.	1.35e-10	0.
Sr-90	2.86e+1	Variable[a]	50.[b]	0.	1.34	0.038	8.	5.59e-11	0.1
Tc-99	2.13e+5	0.	0.	0.	0.	0.	900.	2.75e-12	0.
U-234	2.44e+5	1.6	1.6	0.	1.6	0.	0.03 (mg/L)	7.07e-11	0.000002 (mg/L)[c]
Mercury	none	118	156	0.	156	0.	0.002	3.0e-4	0.0001
Nitrate	none	0.1	0.1	0.	0.1	0.	10.	None	1.5
a. The geochemical model presented in Appendix J was used to estimate initial Sr-90 transport and residual K_d.									
b. The interbed Sr-90 K_d value prensented in Appendix D was revised in Appendix J.									
c. Total uranium background concentrations were taken from Roback et al., (2001).									

A-9.3.1 H-3

The sources of tritium in the vadose zone, listed in order of decreasing magnitude, are (1) service waste ponds at 999 Ci, (2) CPP-3 injection well failure at 708 Ci, (3) CPP-02 site at 378 Ci, and (4) the tank farm sources at 9.7 Ci. The tritium released directly into the aquifer through the injection well was 1.94e+4 Ci, which is orders of magnitude greater than that released in the tank farm.

A-9.3.1.1 Vadose Zone H-3 Simulation Results

Figures A-9-2 and A-9-3 illustrate the horizontal and vertical distribution of tritium in the vadose zone at four time periods: 1979, 2005, 2049, and 2095. The concentration isopleths are presented in Figures A-9-2 and A-9-3. Figure A-9-4 presents the peak vadose zone concentrations through time (excluding the tank farm submodel area), and Figure A-9-5 illustrates the tritium activity flux into the aquifer.

Tritium concentrations drop quickly in the vadose zone because it is nonsorbing and because it has a short (12.3-year) half-life. The vadose zone concentrations are highest in central and southern INTEC as a result of the CPP-3 injection well failure and the service waste ponds. The highest tritium concentration occurred in 1965 as a result of the CPP-02 site, which is the former french drain located in southern INTEC. The injection well failure results in a large initial arrival in the aquifer during the early 1970s, and the percolation pond operation results in a later and smaller arrival during the 1980s to early 1990s. The simulated tritium concentrations in the northern shallow perched water were similar in magnitude to the observed concentrations. However, simulated tritium concentration in the northern deep perched water were lower than observed in well MW-18 and USGS-50.

A-9.3.1.2 Aquifer H-3 Simulation Results

Figure A-9-6 illustrates the horizontal distribution of aquifer tritium at four time periods: 1979, 2005, 2049, and 2095. Figure A-9-7 presents the peak aquifer concentrations through time.

The highest aquifer concentrations were the result of the CPP-3 injection well operation. The peak aquifer tritium concentration was 4.02e+6 pCi/L in 1965. The simulated tritium concentrations exceeded the Snake River Plain Aquifer MCL from 1954 to 2001. The current location of the highest tritium concentrations are near the CFA. The tritium contamination currently beneath INTEC is most likely from tritium discharged to the percolation ponds and other vadose sources. These sources are now entering the aquifer.

Figure A-9-2. H-3 horizontal vadose zone concentrations (pCi/L) (SRPA MCL = thick red line, 10*SRPA MCL = thin red line, SRPA MCL/10 = thin black line).

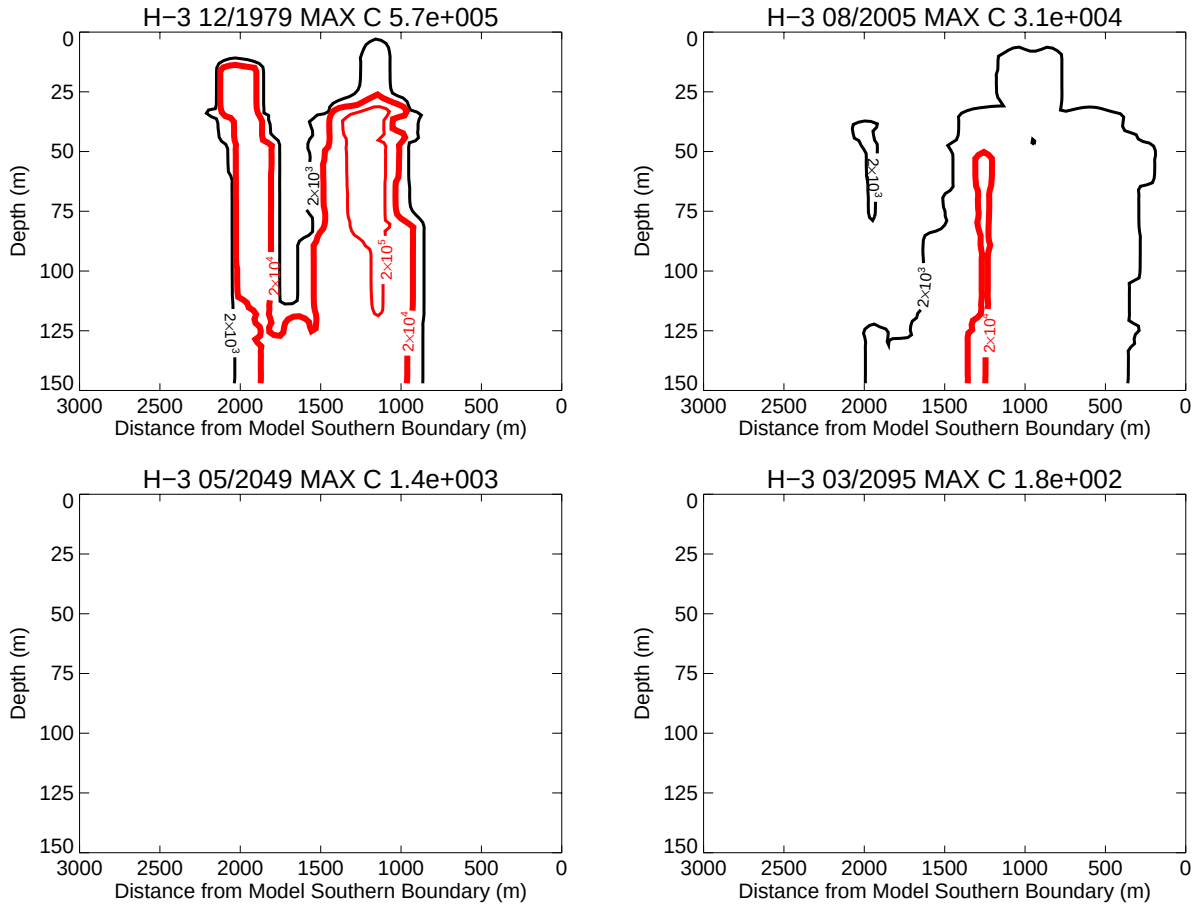

Figure A-9-3. H-3 vertical vadose zone concentrations (pCi/L) (SRPA MCL = thick red line, 10*SRPA MCL = thin red line, SRPA MCL/10 = thin black line).

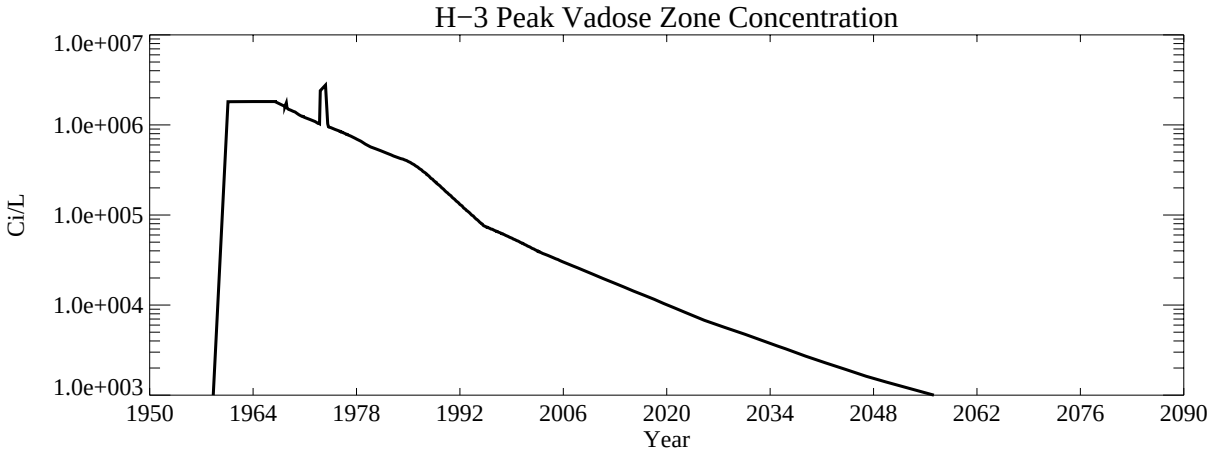

Figure A-9-4. H-3 peak vadose zone concentrations excluding tank farm submodel area (pCi/L) (SRPA MCL = blue, model predicted = black line).

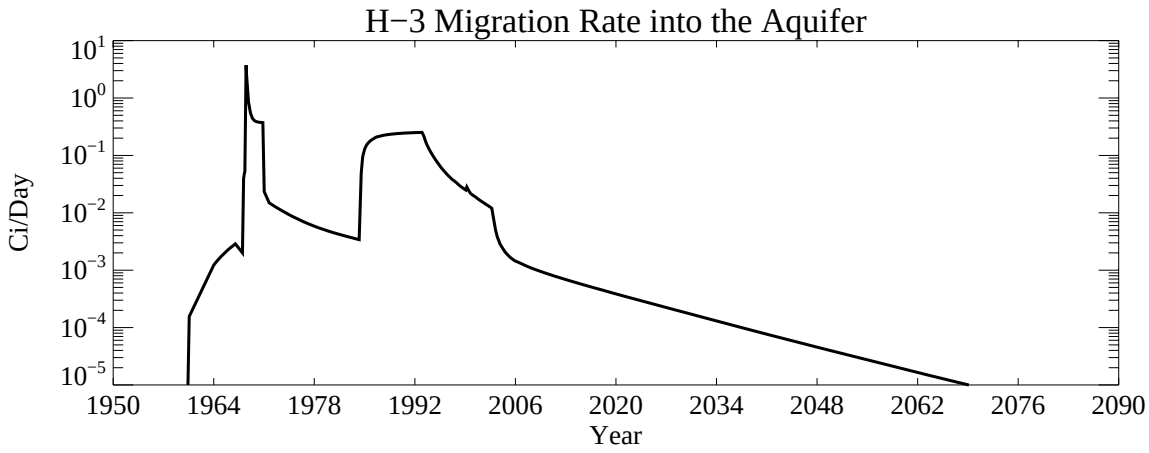

Figure A-9-5. H-3 peak activity flux into the aquifer (Ci/day).

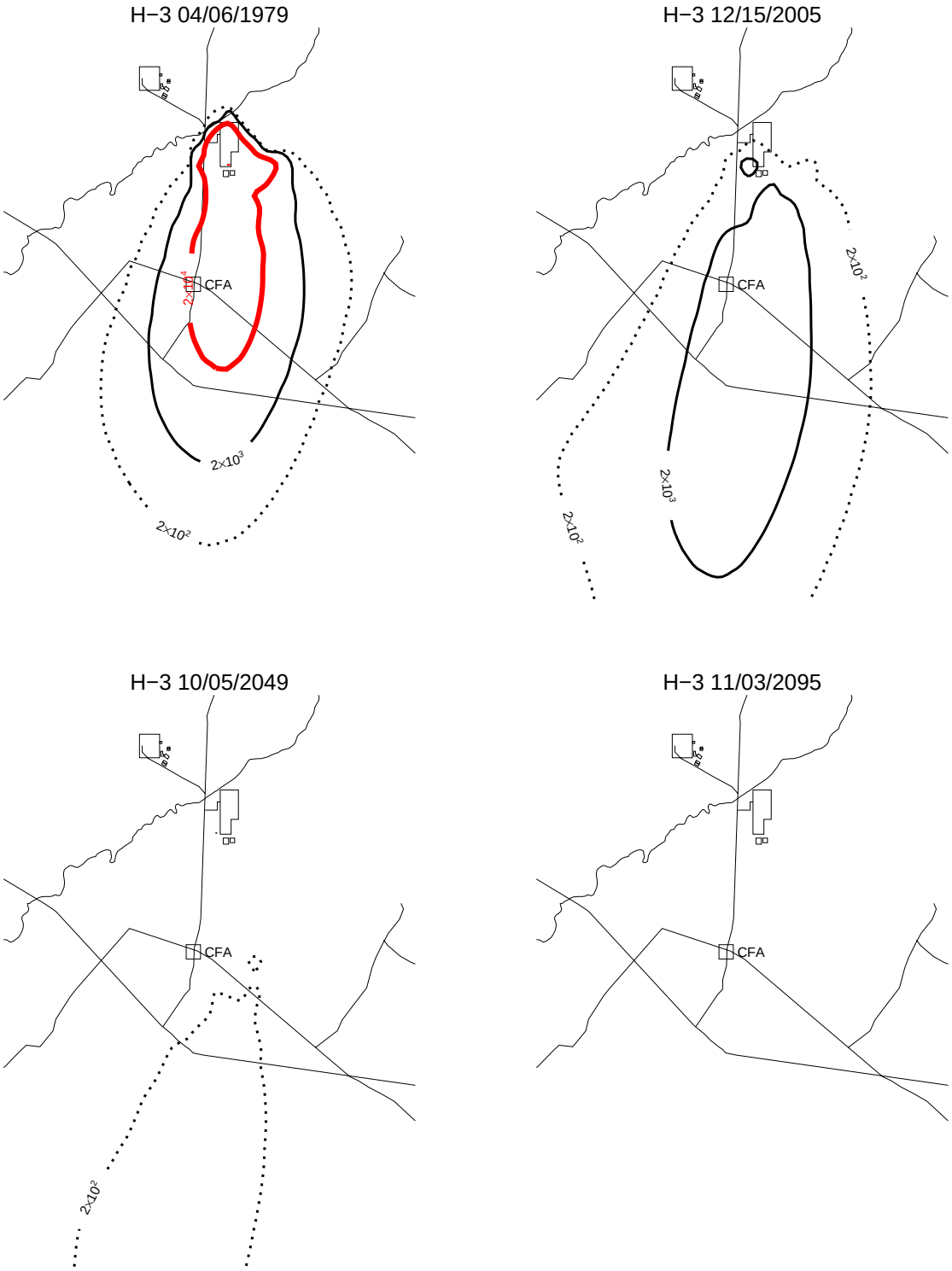

Figure A-9-6. H-3 horizontal aquifer concentrations (pCi/L) (SRPA MCL = thick red line, 10*SRPA MCL = thin red line, SRPA MCL/10 = thin black line, SRPA MCL/100 = thin black dashed line).

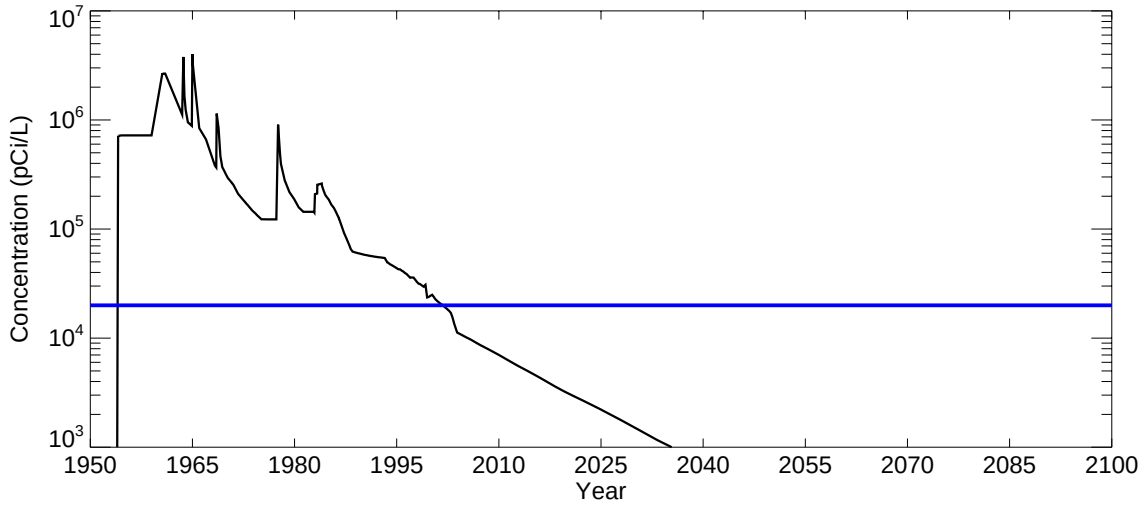

Figure A-9-7. H-3 peak aquifer concentrations (pCi/L) (SRPA MCL = blue line, model predicted = black line).

A-9.3.2 I-129

The sources of I-129 in the vadose zone, listed in order of decreasing magnitude, are (1) CPP-3 injection well failure at 0.08 Ci, (2) service waste ponds at 0.082 Ci, (3) OU 3-13 soil sources at 0.039 Ci, and (4) the tank farm sources at 0.00126 Ci. The I-129 released directly to the aquifer from the injection well was 0.78 Ci.

A-9.3.2.1 Vadose Zone I-129 Simulation Results

Figures A-9-8 and A-9-9 illustrate the horizontal and vertical location of the vadose zone I-129 at four time periods: 1979, 2005, 2049, and 2095. Figure A-9-10 presents the peak vadose zone concentrations through time (excluding the tank farm submodel area), and Figure A-9-11 illustrates the I-129 peak activity flux into the aquifer.

Like tritium, the majority of the I-129 originates from the service waste discharged into the CPP-3 injection well and the service waste ponds. The simulated I-129 is widespread in the central INTEC deep vadose zone water during the injection well failure period and widespread in the southern vadose zone during the percolation pond operation. The peak simulated vadose zone concentration (excluding the tank farm submodel area) was 30 pCi/L in 1971.

A-9.3.2.2 Aquifer I-129 Simulation Results

Figure A-9-12 illustrates the horizontal distribution of I-129 in the aquifer in 1979, 2005, 2049, and 2095. Figure A-9-13 presents the peak aquifer concentrations through time. Like tritium, the highest simulated aquifer I-129 concentrations were the result of the CPP-3 injection well operation. The peak aquifer I-129 concentration was predicted to be 22.6 pCi/L and occurred in 1970 from the service waste disposed of in the CPP-3 injection well.

The I-129 concentrations were predicted to exceed the Snake River Plain Aquifer MCL from 1954 to 2080. The peak simulated concentration in the year 2095 was 0.9 pCi/L. The current simulated location of the highest I-129 concentrations are near the CFA, and the source is from I-129 discharged into the CPP-3 injection well and former percolation ponds. The general trend of the model is to overpredict aquifer I-129 concentrations. The highest three measured concentrations reported in the 2004 Group 5 monitoring report

(DOE-ID 2006) were 0.772, 0.615, and 0.608 pCi/L in wells USGS-47, USGS-57, and LF3-08, respectively. The model predicts concentrations near LF3-9 to be 0.9 pCi/L, but also predicts concentrations at LF2-11 (located approximately 1,200 m northeast of LF3-9) to be near 4 pCi/L in 2005. The most recent measured concentration was in well LF2-11 and was 0.98 pCi/L in 2001. The model could be overpredicting current maximum concentrations by approximately factor of four.

Figure A-9-8. I-129 horizontal vadose zone concentrations (pCi/L) (SRPA MCL = thick red line, 10*SRPA MCL = thin red line, SRPA MCL/10 = thin black line).

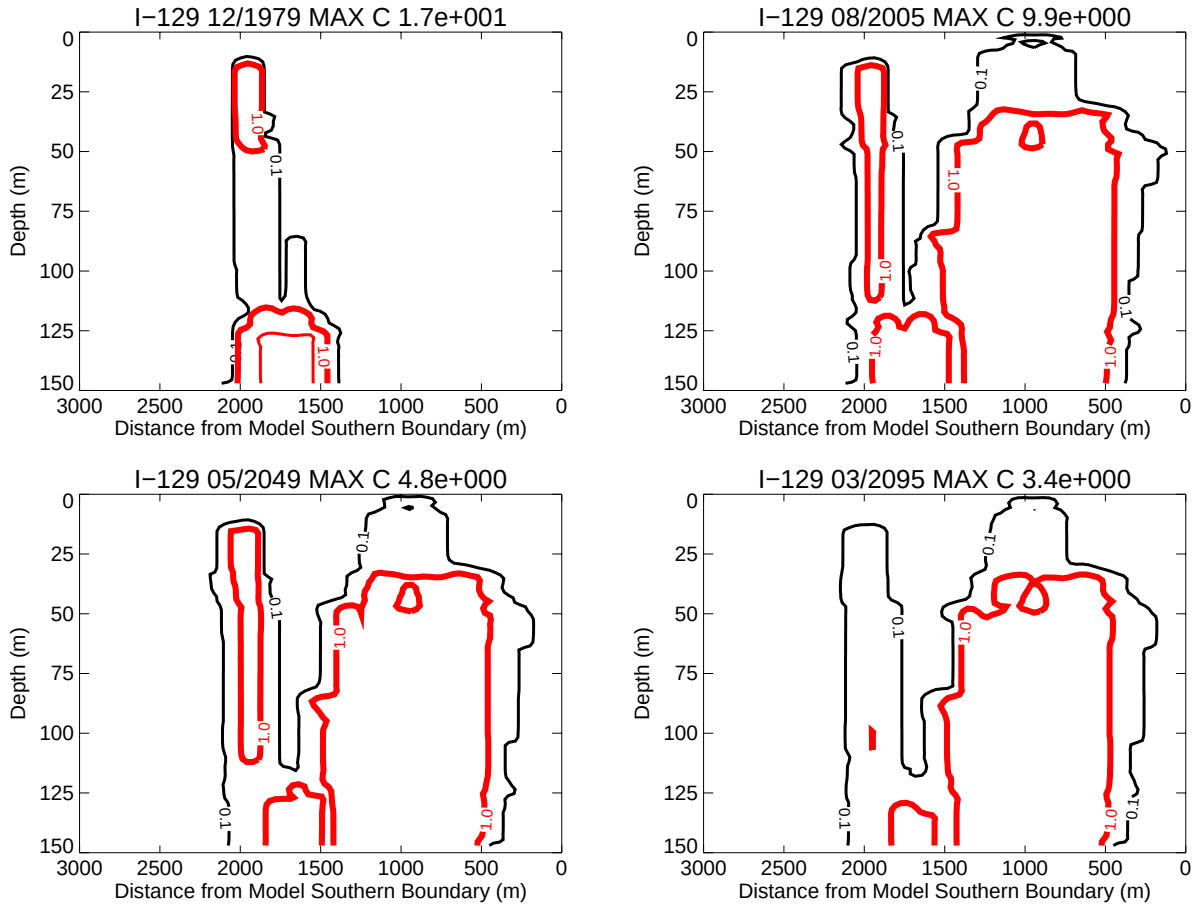

Figure A-9-9. I-129 vertical vadose zone concentrations (pCi/L) (SRPA MCL = thick red line, 10*SRPA MCL = thin red line, SRPA MCL/10 = thin black line).

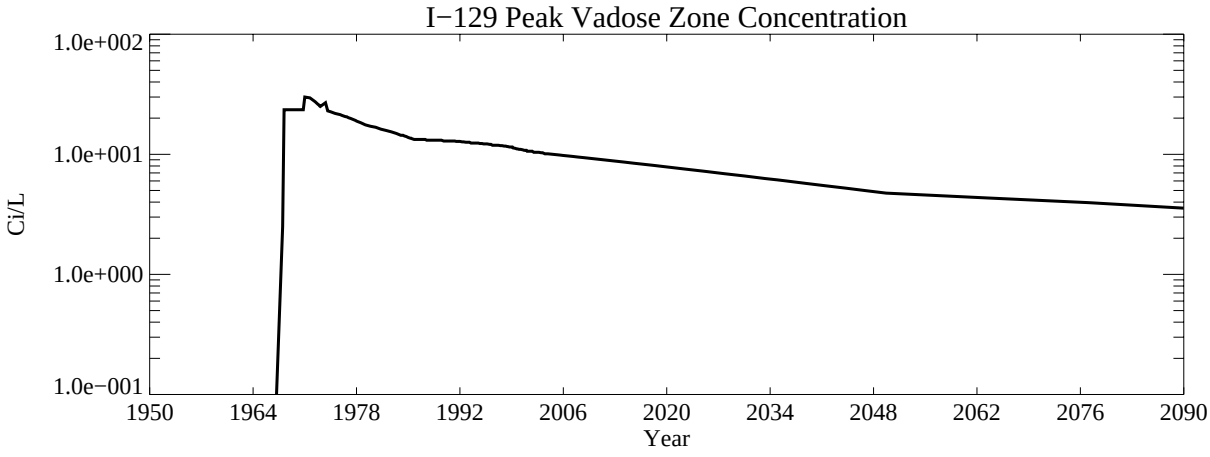

Figure A-9-10. I-129 peak vadose zone concentrations excluding tank farm submodel area (pCi/L).

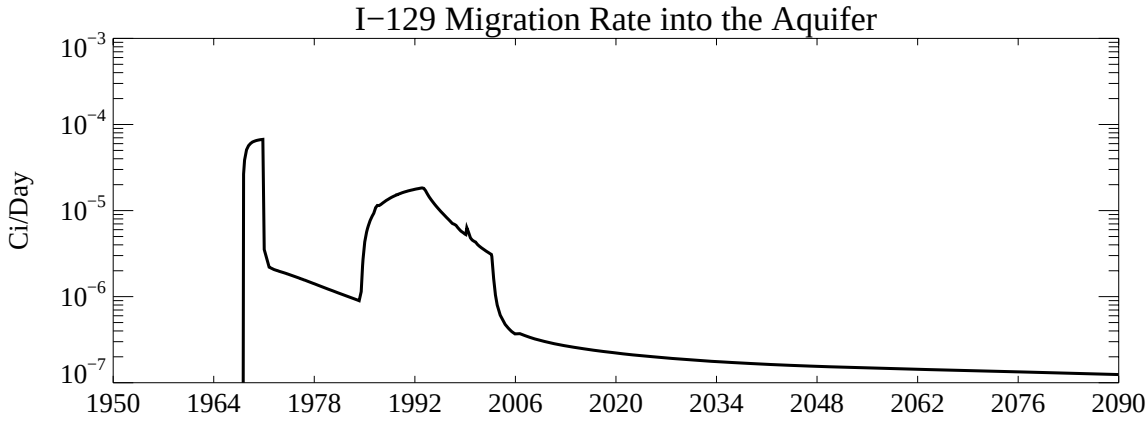

Figure A-9-11. I-129 peak activity flux into the aquifer (Ci/day).

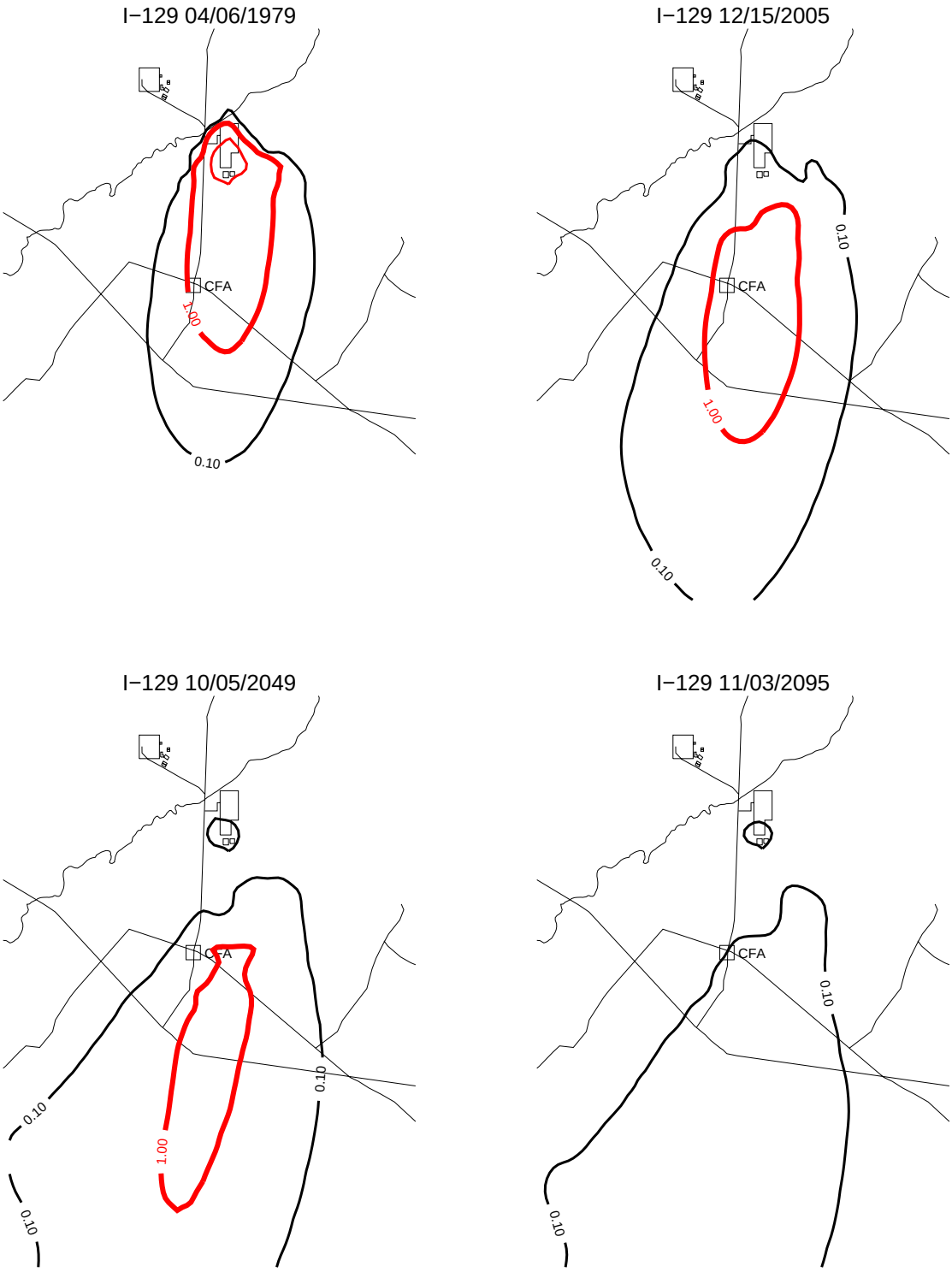

Figure A-9-12. I-129 horizontal aquifer concentrations (pCi/L) (SRPA MCL = thick red line, 10*SRPA MCL = thin red line, SRPA MCL/10 = thin black line, SRPA MCL/100 = thin black dashed line).

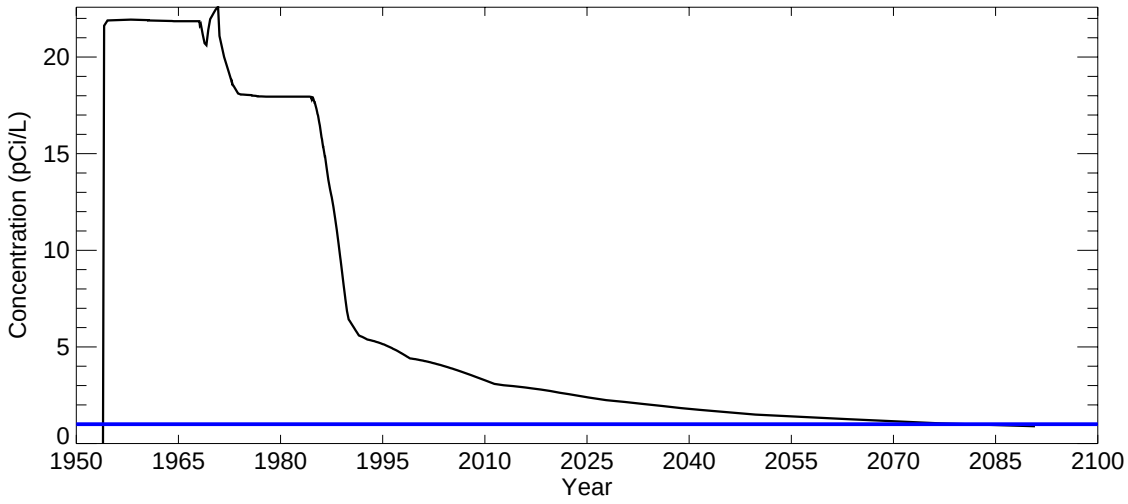

Figure A-9-13. I-129 peak aquifer concentrations (pCi/L) (SRPA MCL = blue line, model predicted = black line).

A-9.3.3 Np-237

The sources of Np-237 in the vadose zone, listed in order of decreasing magnitude, are (1) the OU 3-13 soil sites at 0.133 Ci, (2) CPP-3 injection well failure at 0.093 Ci, and (3) the tank farm sources at 0.027 Ci. The amount of Np-237 released directly into the aquifer from the injection well was 0.93 Ci.

A-9.3.3.1 Vadose Zone Np-237 Simulation Results

Figures A-9-14 and A-9-15 illustrate the horizontal and vertical distribution of vadose zone Np-237 in 1979, 2005, 2049, and 2095. Figure A-9-16 presents the peak vadose zone concentrations through time (excluding the tank farm submodel area), and Figure A-9-17 illustrates the Np-237 activity flux into the aquifer.

The simulated peak concentration (excluding the tank farm submodel area) was 6.00e+3 pCi/L in 1990 and corresponds to the near-surface soils at Sites 37A and 37B, which contributed a combined total of 0.0765 Ci. These sites were placed in the model in 1990 and may have been conservatively overestimated. The location of the CPP-37A and CPP-37B sites east of the tank farm and the neptunium K_d (2.0 mL/g) result in vadose zone concentrations persisting because of a lower infiltration rate in this area and retardation.

Site CPP-37B was sampled for Np-237 in fall 2005 during ongoing OU 3-13 Group-3 work. There were 11 samples taken and one duplicate. Nine samples and the duplicate were non-detect. Two samples were flagged J (an estimated quantity) and the soil concentration for these two samples was 0.3 +/- 0.1pCi/g. These results were received after the Np-237 modeling was completed for OU 3-14. Using the conservative OU 3-13 estimate in the model for this site resulted in a predicted future concentration that was always below MCLs. No attempt was made to decrease the Np-237 source term based on the new data or rerun the model, because the conservative estimate did not result in an unacceptable predicted future aquifer concentration.

A-9.3.3.2 Aquifer Np-237 Simulation Results

Figure A-9-18 illustrates the horizontal distribution in the aquifer Np-237 in 1979, 2005, 2049, and 2095. Figure A-9-19 presents the peak aquifer concentrations through time. The peak aquifer Np-237 concentration was 27.1 pCi/L in 1971 and originated from the CPP-3 injection well. Np-237 exceeded the Snake River Plain Aquifer MCL concentration from 1954 through 1987.

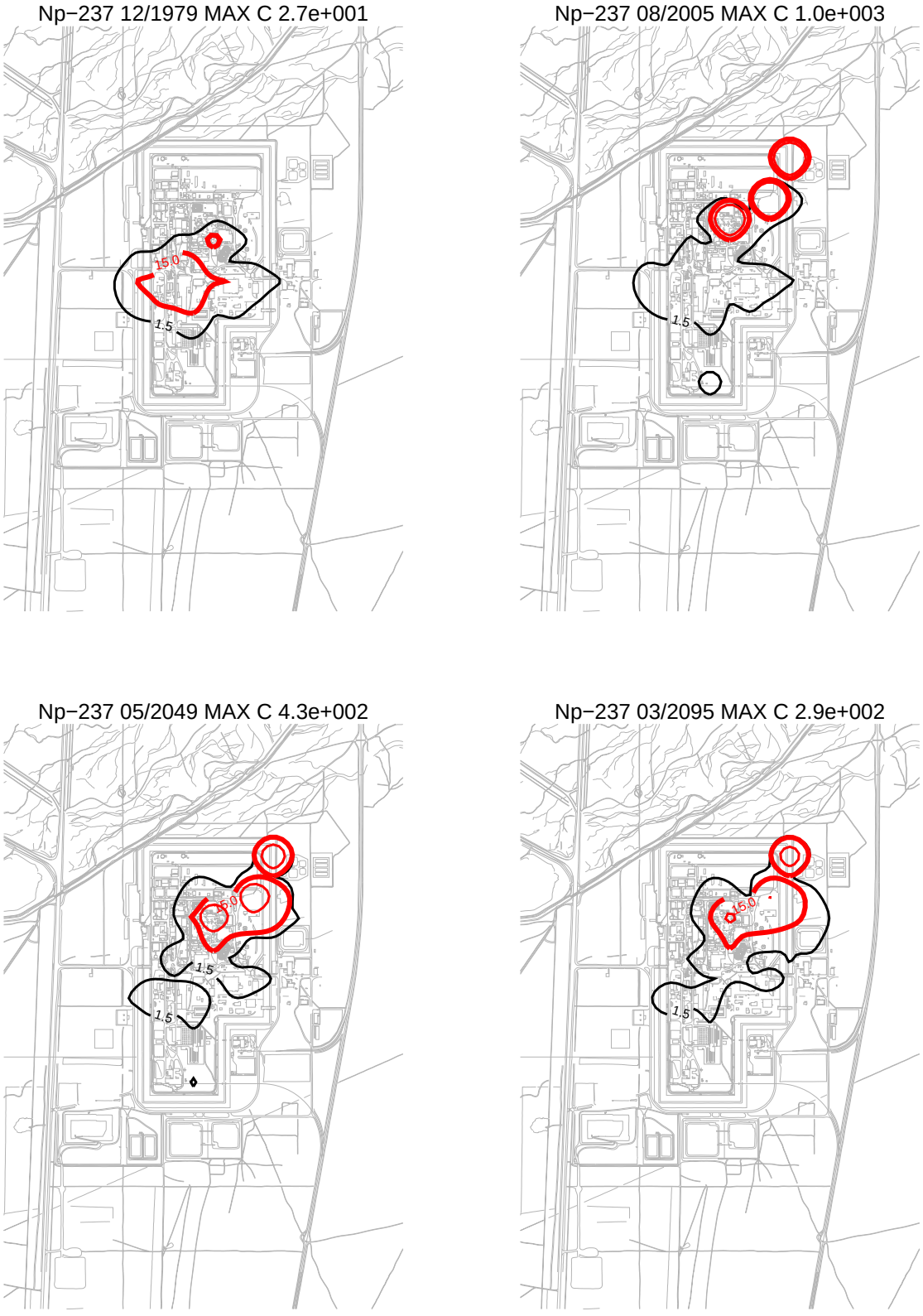

Figure A-9-14. Np-237 horizontal vadose zone concentrations (pCi/L) (SRPA MCL = thick red line, 10*SRPA MCL = thin red line, SRPA MCL/10 = thin black line).

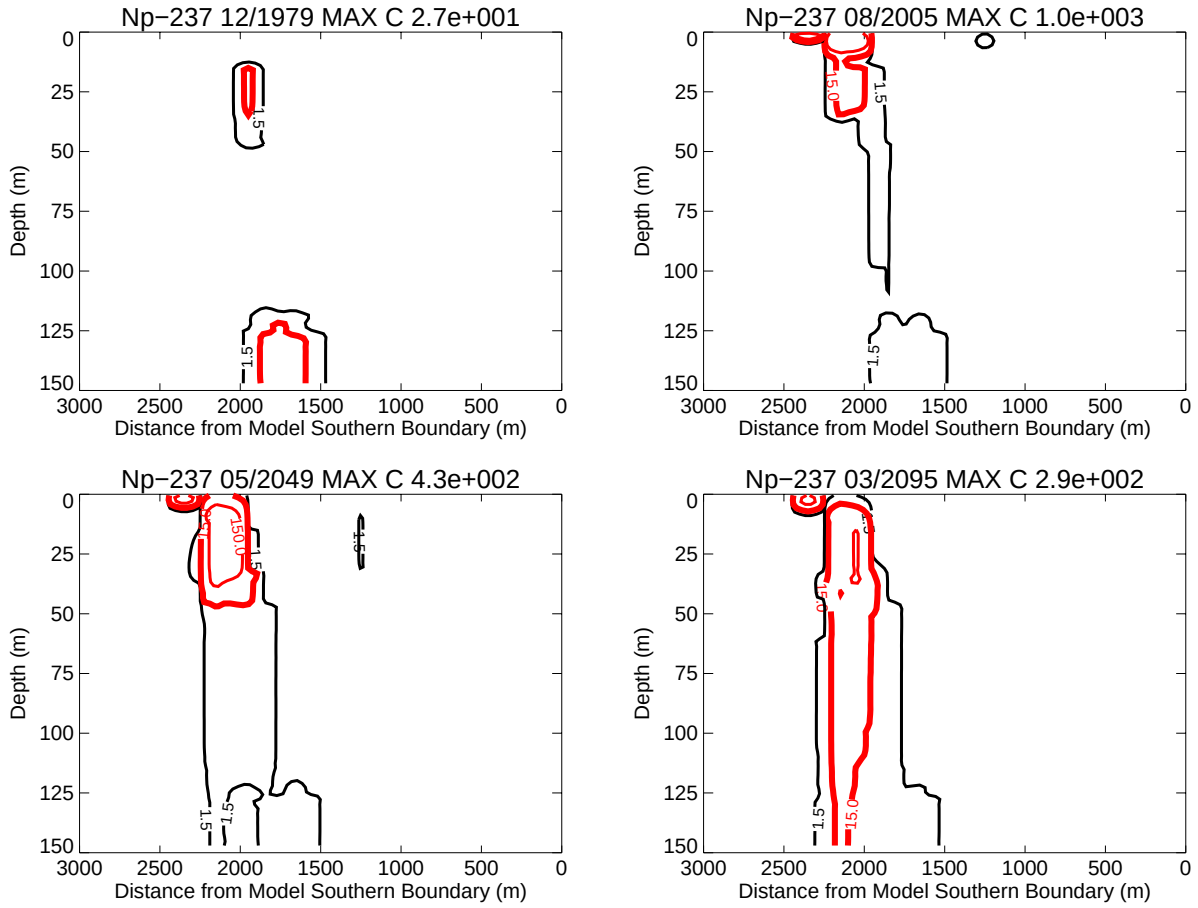

Figure A-9-15. Np-237 vertical vadose zone concentrations (pCi/L) (SRPA MCL = thick red line, 10*SRPA MCL = thin red line, SRPA MCL/10 = thin black line).

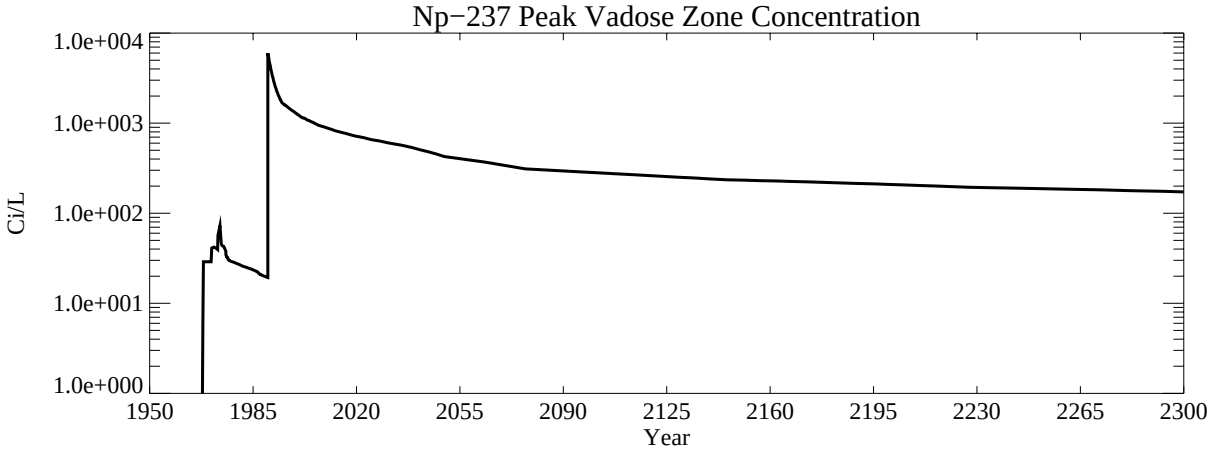

Figure A-9-16. Np-237 peak vadose zone concentrations excluding tank farm submodel area (pCi/L).

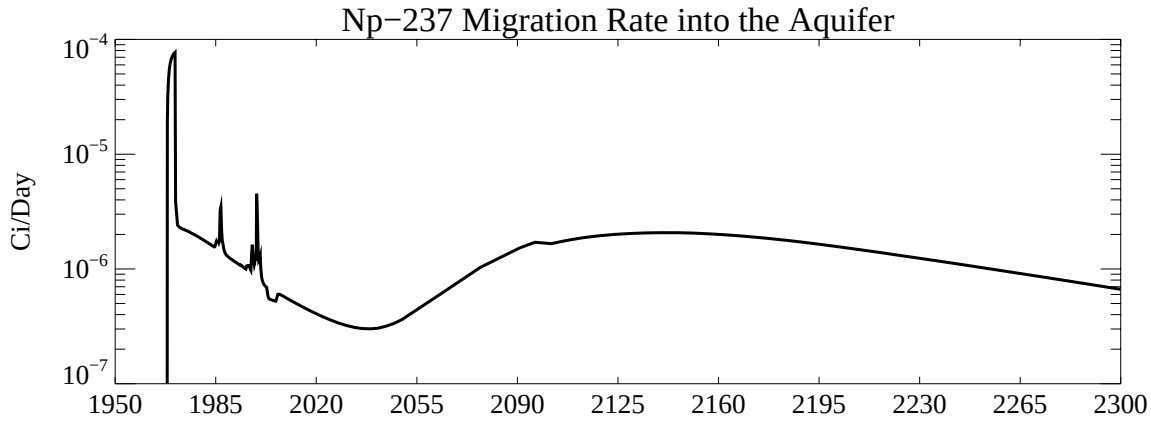

Figure A-9-17. Np-237 activity flux into the aquifer (Ci/day).

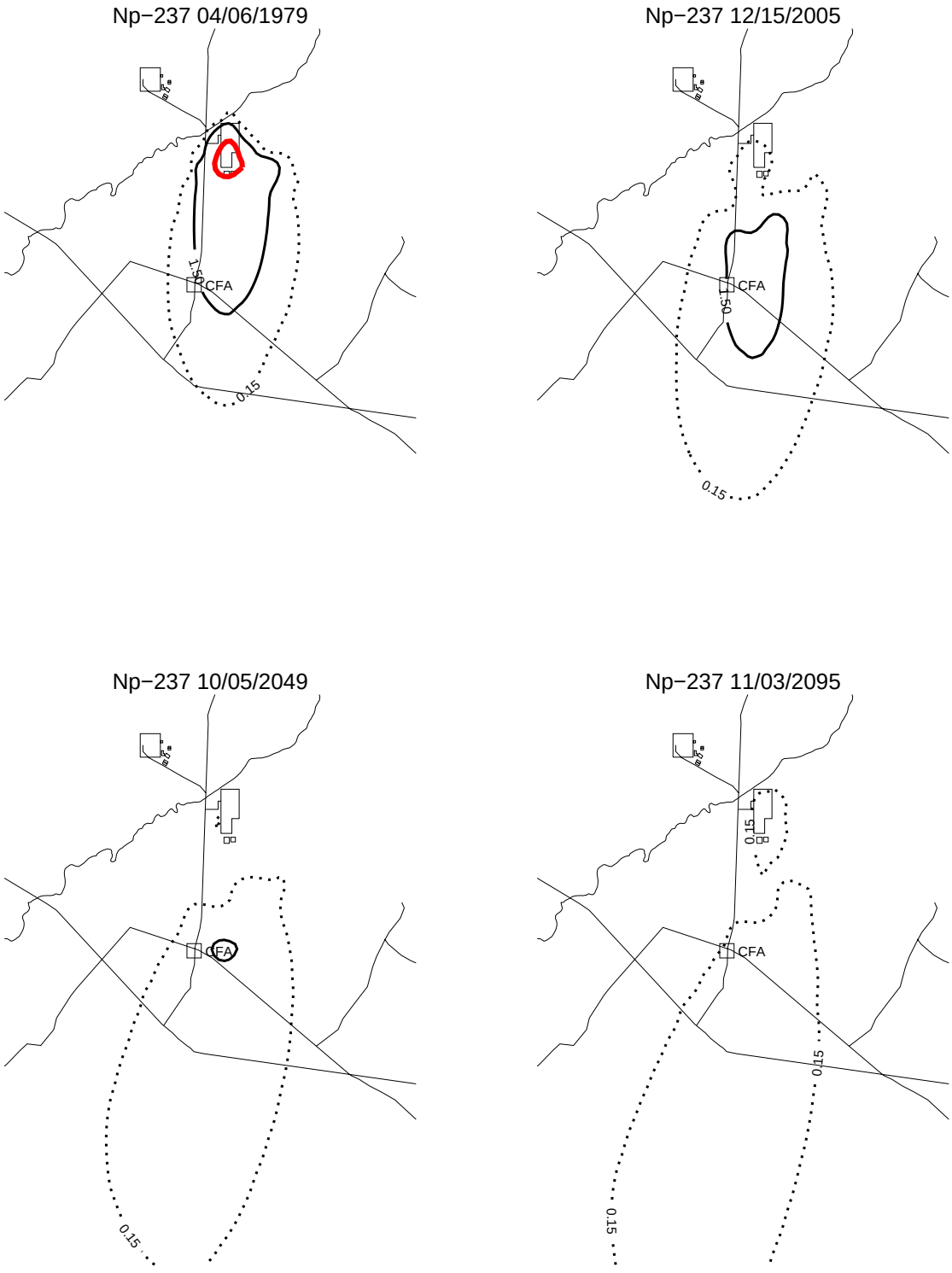

Figure A-9-18. Np-237 horizontal aquifer concentrations (pCi/L) (SRPA MCL = thick red line, 10*SRPA MCL = thin red line, SRPA MCL/10 = thin black line, SRPA MCL/100 = thin black dashed line).

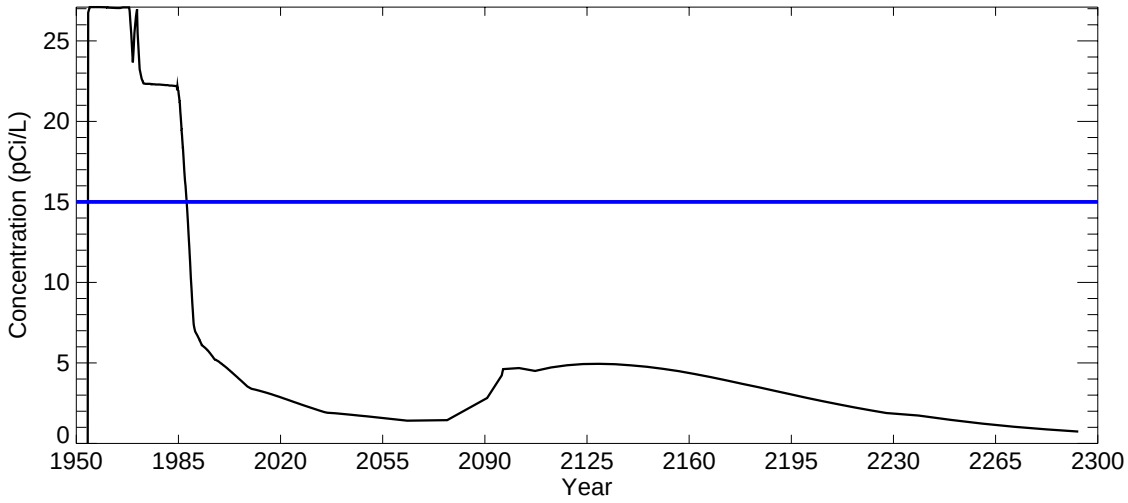

Figure A-9-19. Np-237 peak aquifer concentrations (pCi/L) (SRPA MCL = blue line, model predicted = black line).

A-9.3.4 Pu-239

The sources of Pu-239 in the vadose zone, listed in order of decreasing magnitude, are (1) the tank farm sources at 6.94 Ci, (2) the OU 3-13 soil sites at 1.05 Ci, (3) CPP-3 injection well failure at 0.011 Ci, and (4) the former percolation ponds at 0.0011 Ci. The amount of Pu-239 released directly to the aquifer from the injection well was 0.0124 Ci.

A-9.3.4.1 Vadose Zone Pu-239 Simulation Results

Figures A-9-20 and A-9-21 illustrate the horizontal and vertical distribution of the vadose zone Pu-239 at four time periods: 1979, 2005, 2049, and 2095. Figure A-9-22 presents the peak vadose zone concentrations through time (excluding the tank farm submodel area). Figure A-9-23 presents Pu-239 activity flux to the aquifer and illustrates only a small fraction of the tank farm Pu-239 reaches the aquifer because of the large retardation factor and radioactive decay.

The tank farm sources account for most of the Pu-239 released into the vadose zone. The peak simulated vadose zone concentration (excluding the tank farm submodel area) was 53.8 pCi/L in 1973 and corresponds to the CPP-31, and CPP-79 deep sites. The 1,000 (mL/g) K_d allows the Pu-239 to act as a nearly continuous leaching source during the simulation. This can be seen in the activity flux rate (Figure A-9-23).

A-9.3.4.2 Aquifer Pu-239 Simulation Results

The Pu-239 aquifer model was only run to evaluate effect of the injection well Pu-239 on aquifer water quality. Figures A-9-22 and A-9-23 indicate that the peak vadose zone concentrations will fall below the Snake River Plain Aquifer MCL before the peak Pu-239 arrives in the aquifer. The Tc-99 and Sr-90 simulations indicate an activity flux to the aquifer resulting from the tank farm sources of nearly 10^{-5} Ci/day is needed to bring aquifer concentrations near 10 pCi/L. The peak Pu-239 activity flux is always less than 10^{-8} Ci/day. The peak simulated aquifer concentration was 0.0334 pCi/L in 1960 and is the result of the CPP-3 injection well operation. Concentration contour plots are not provided because the Pu-239 concentrations were always predicted to be nearly two orders of magnitude lower than the Snake River Plain Aquifer MCL of 15 pCi/L during the simulation. Figure A-9-24 presents the peak aquifer concentrations resulting from the CPP-3 injection well through time averaged over a 15-m well screen.

The simulated Pu-239 occurring in the aquifer was only the result of direct injection into the CPP-3 disposal well, because the large interbed and alluvium plutonium K_d (1,000 mL/g) prevents significant amounts of Pu-239 originating from the tank farm sources from reaching the aquifer during the simulation period. The OU 3-14 groundwater pathway analysis did not predict an unacceptable aquifer risk from plutonium because it used a realistic plutonium K_d for the alluvium and interbed sediments (see Appendix D) and the isotope-specific half-life. This is in contrast to the OU 3-13 analysis, which predicted a groundwater risk, because it used the very conservative Track 2 guidance K_d of 22 mL/g (DOE-ID 1994) and used the longer Pu-241 half-life for all the plutonium isotopes. The better assessment results in more realistic risk analysis and leads to a conclusion of aquifer concentrations never exceeding the Snake River Plain Aquifer MCL.

The aquifer risk from a mobile fraction can be estimated from the Tc-99 simulation because both are be long-lived and mobile. Appendix D provides an estimate of 1 to 2.5% for the total mobile fraction in SDA sediment from column experiments. The Tc-99 simulation provided a maximum aquifer concentration of 10.8 pCi/L in 2095 from a total 4.78 Ci shallow vadose zone source (3.56 Ci from the tank farm, 1.13 Ci from the percolation ponds, 0.093 from the OU 3-13 sources). Using the upper bound for the mobile fraction (2.5%) and a total shallow vadose zone source of 9.18 Ci (8.01 Ci from the tank farm, 0.0017 Ci from the percolation ponds, 1.17 Ci from the OU 3-13 soils sites), the maximum aquifer concentration would be 0.52 pCi/L from 0.23 total mobile curies of plutonium. This is far below the 15 pCi/L Snake River Plain Aquifer MCL concentration.

Figure A-9-20. Pu-239 horizontal vadose zone concentrations (pCi/L) (SRPA MCL = thick red line, 10*SRPA MCL = thin red line, SRPA MCL/10 = thin black line).

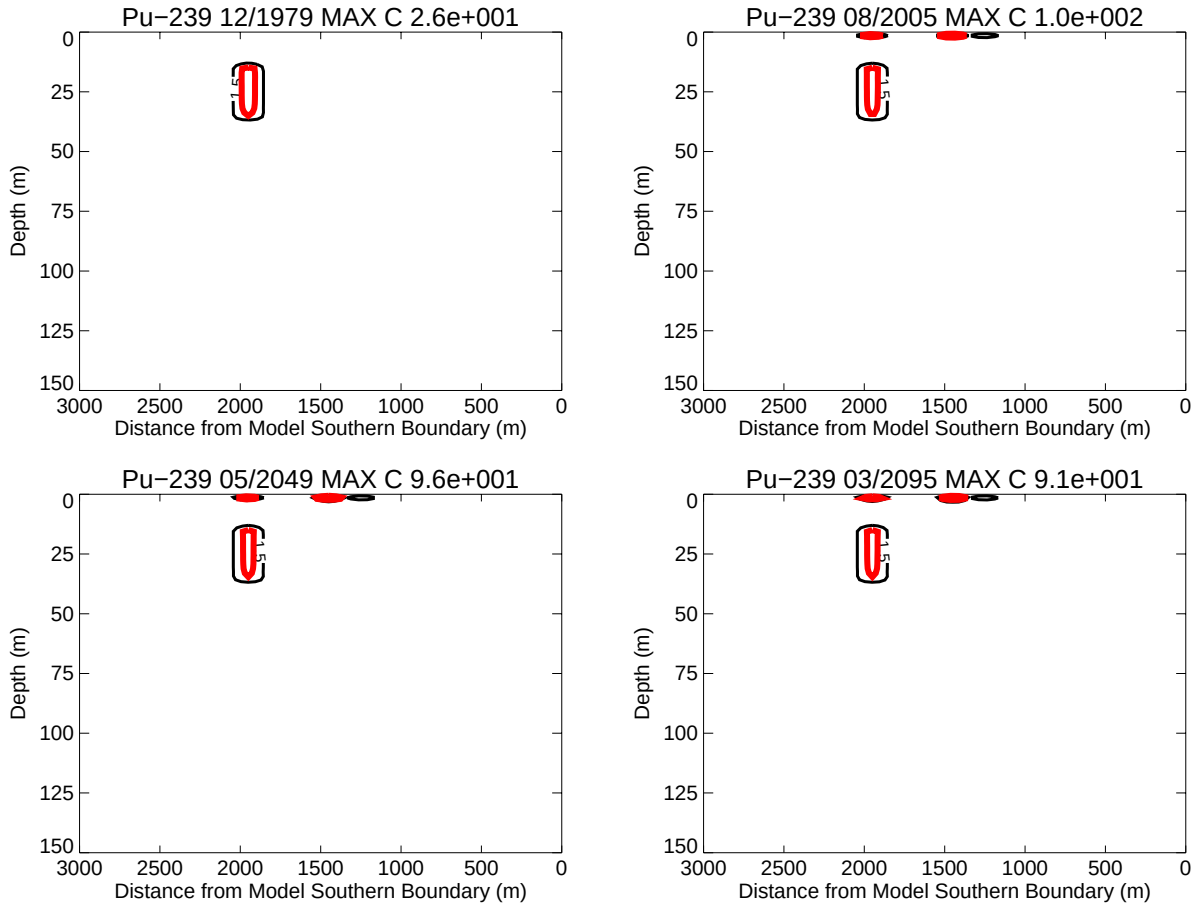

Figure A-9-21. Pu-239 vertical vadose zone concentrations (pCi/L) (SRPA MCL = thick red line, 10*SRPA MCL = thin red line, SRPA MCL/10 = thin black line).

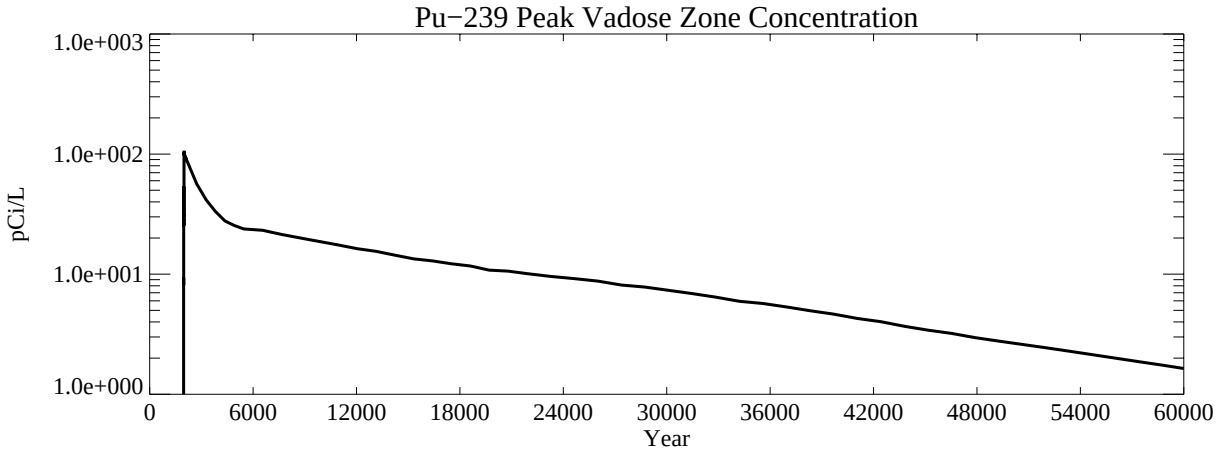

Figure A-9-22. Pu-239 peak vadose zone concentrations excluding tank farm submodel area (pCi/L).

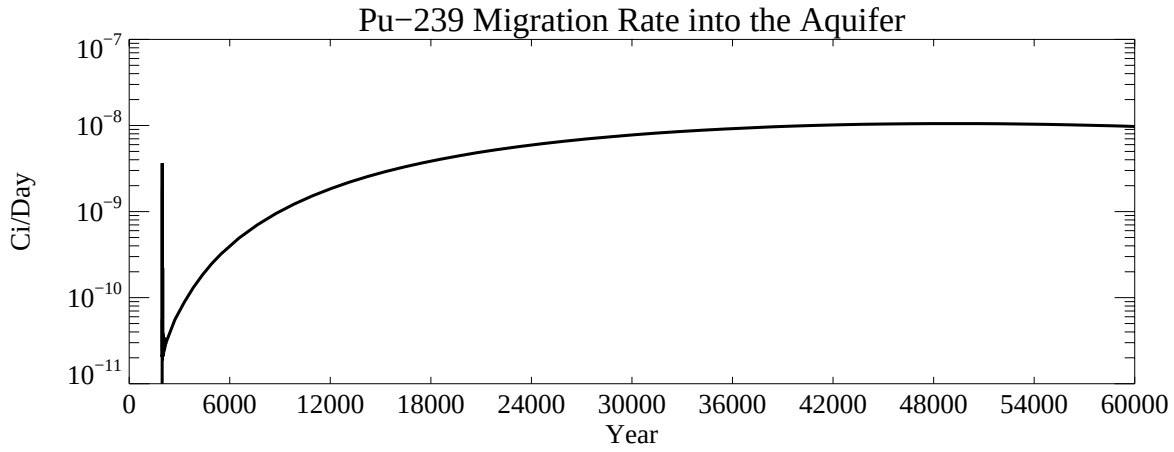

Figure A-9-23. Pu-239 activity flux into the aquifer (Ci/day).

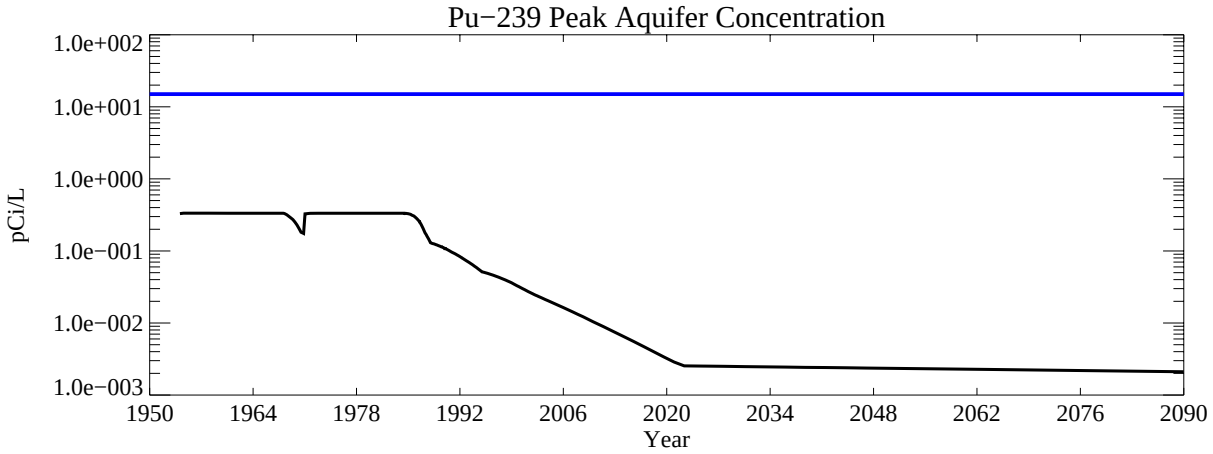

Figure A-9-24. Pu-239 peak aquifer concentrations (pCi/L) (SRPA MCL = blue line, model predicted = black line).

A-9.3.5 Pu-240

The sources of Pu-240 in the vadose zone, listed in order of decreasing magnitude, are (1) the tank farm sources at 1.07 Ci, (2) the OU 3-13 soil sites at 0.12 Ci, (3) CPP-3 injection well failure at 0.0005 Ci, and (4) the former percolation ponds at 0.0006 Ci. The amount of Pu-240 released directly into the aquifer from the injection well was 0.0063 Ci.

A-9.3.5.1 Vadose Zone Pu-240 Simulation Results

Figures A-9-25 and A-9-26 illustrate the horizontal and vertical distribution of the vadose zone Pu-240 at four time periods: 1979, 2005, 2049, and 2095. Figure A-9-27 presents the peak vadose zone concentrations through time. The tank farm sources (e.g., primarily CPP-31) account for most of the Pu-240. The alluvium and interbed retardation factors result in nearly all of the Pu-240 remaining in the alluvium with little Pu-240 transported to the aquifer. The peak vadose zone Pu-240 concentration (excluding the submodel area) was predicted to be 19.4 pCi/L in 1990. The large K_d allows the Pu-240 to behave as a continuous leaching source.

A-9.3.5.2 Aquifer Pu-240 Simulation Results

Like the Pu-239 simulation, the Pu-240 aquifer model was only run to evaluate the effect of the injection well Pu-240 on aquifer water quality. Figures A-9-27 and A-9-28 indicate that the peak vadose zone concentrations will fall below the Snake River Plain Aquifer MCL before the peak Pu-240 arrives in the aquifer. The Tc-99 and Sr-90 simulations indicate an activity flux to the aquifer resulting from the tank farm sources of nearly 10^{-5} Ci/day is needed to bring aquifer concentrations near 10 pCi/L. The peak Pu-240 activity flux is always less than 10^{-10} Ci/day after the failed injection well flux. The peak simulated aquifer Pu-240 concentration was 0.167 pCi/L in 1960 and is the result of the CPP-3 injection well. Concentration contour plots and concentration time history plots are not provided because the Pu-240 concentrations were always much less than the Snake River Plain Aquifer MCL of 15 pCi/L. Figure A-9-29 presents the peak aquifer concentrations resulting from the CPP-3 injection well through time averaged over a 15-m well screen.

The simulated Pu-240 in the aquifer is the result of direct injection to the CPP-3 well. The plutonium K_d (1,000 mL/g) and radioactive decay prevents significant transport of Pu-240 to the aquifer.

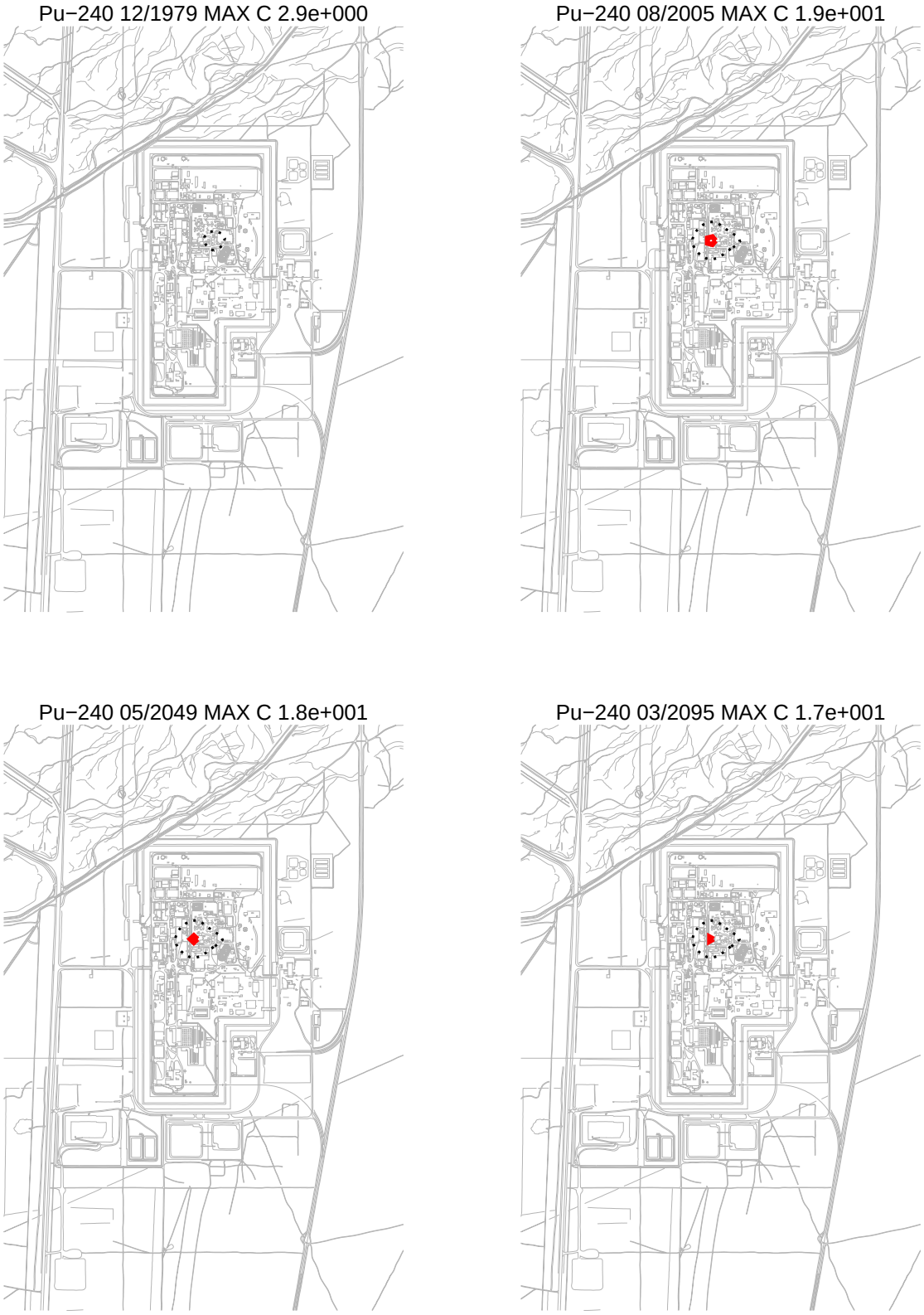

Figure A-9-25. Pu-240 horizontal vadose zone concentrations (pCi/L) (SRPA MCL = thick red line, 10*SRPA MCL = thin red line, SRPA MCL/10 = thin black line).

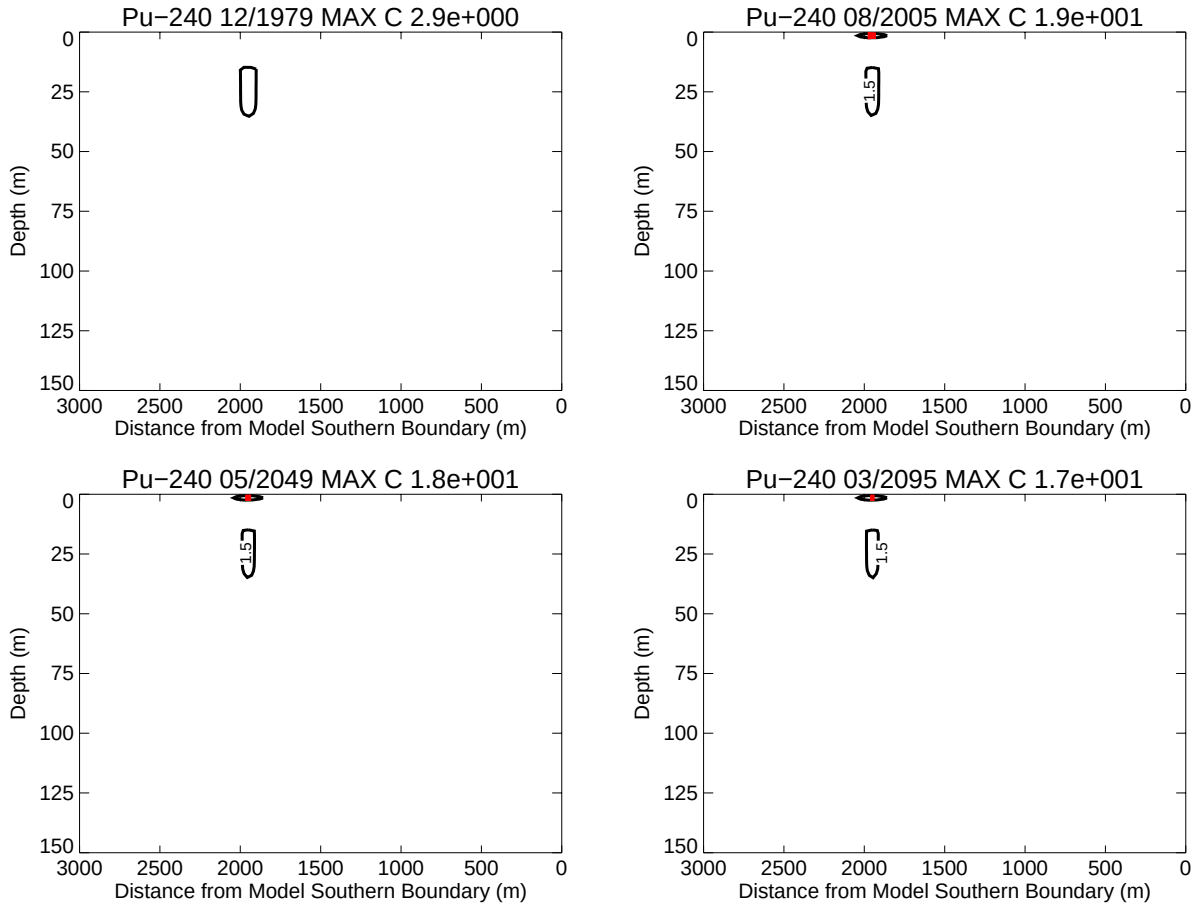

Figure A-9-26. Pu-240 vertical vadose zone concentrations (pCi/L) (SRPA MCL = thick red line, 10*SRPA MCL = thin red line, SRPA MCL/10 = thin black line).

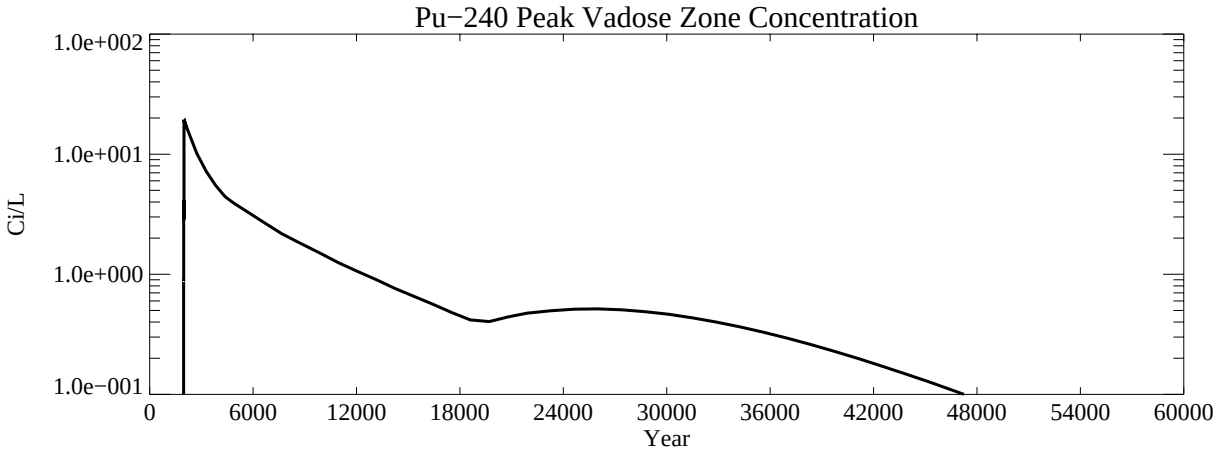

Figure A-9-27. Pu-240 peak vadose zone concentrations excluding tank farm submodel area (pCi/L).

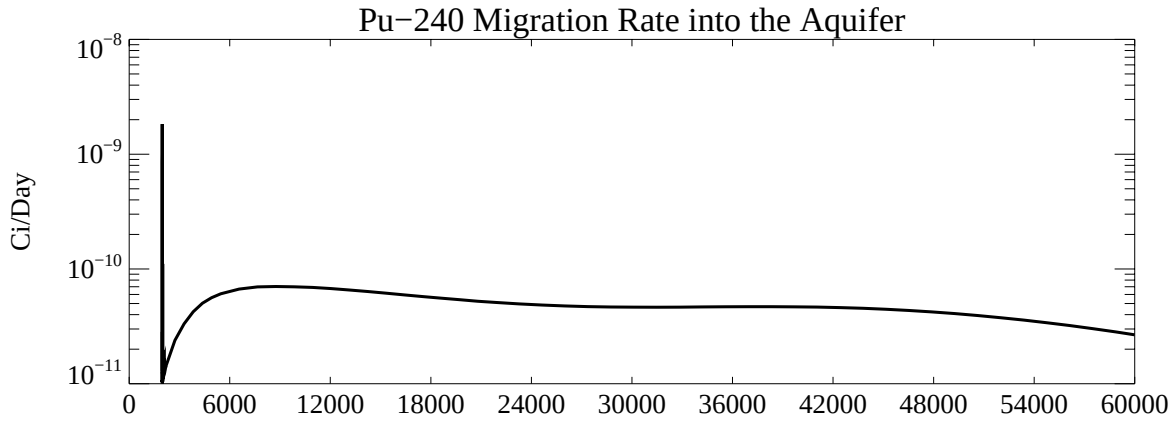

Figure A-9-28. Pu-240 activity flux into the aquifer (Ci/day).

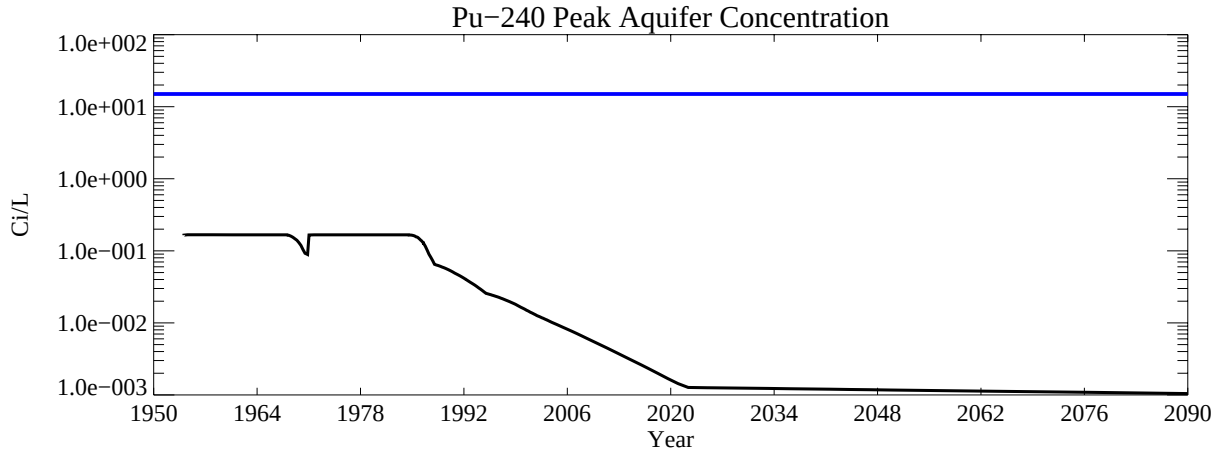

Figure A-9-29. Pu-240 peak aquifer concentrations (pCi/L) (SRPA MCL = blue line, model predicted = black line).

A-9.3.6 Tc-99

The sources of Tc-99 in the vadose zone, listed in order of decreasing magnitude, are (1) the tank farm at 3.56 Ci, (2) service waste ponds at 1.13 Ci, (3) CPP-3 injection well failure at 1.04 Ci, and (4) the OU 3-13 Group 4 soil sources at 0.1 Ci. The amount of Tc-99 released directly into the aquifer during the injection well failure was 10.9 Ci. Tc-99 is primarily produced as a fission product in nuclear fuel, and the naturally occurring background concentration should be zero. Tc-99 is long-lived and very mobile in the subsurface.

A-9.3.6.1 Vadose Zone Tc-99 Simulation Results

Figures A-9-30 and A-9-31 illustrate the horizontal and vertical distribution of Tc-99 in the vadose zone at four time periods: 1979, 2005, 2049, and 2095. The shallow vadose zone contamination located immediately northwest of the former percolation ponds is due to the CPP-22 OU 3-13 soil site (0.1 Ci), which was placed in the model in 1990. The CPP-22 site is a particulate air release south of CPP-603. Figure A-9-32 presents the peak vadose zone concentrations through time and Figure A-9-33 illustrates the Tc-99 peak activity flux into the aquifer.

Tc-99 from the tank farm releases has migrated deep into the vadose zone and has contaminated the aquifer beneath INTEC. The vast majority of the Tc-99 is from the tank farm sources in northern INTEC. However, the CPP-22 soil site located south of the CPP-603 building released 0.089 Ci, and high concentrations persist at this location because the infiltration rate is lower. The site straddles the southern INTEC fence line where the infiltration rate was 1 cm/year (outside the fence line). The Site CPP-22 source term was very conservatively overestimated and does not represent a realistic value for this site. The Site CPP-22 is a particulate air release south of Building CPP-603. The site covers a large area (13,900 m^2) and the soil contamination was assumed to be uniform across this area to a depth of 1.2 m at the maximum concentration measured.

The simulated Big Lost River had a large impact on Tc-99 peak activity flux into the aquifer. High recharge from high river flow in the simulations quickly drives Tc-99 residing in the deep vadose zone (i.e., 380-ft interbed) into the aquifer. The river recharge was estimated from losses during the period 1985-2004. The peak activity flux into the aquifer through time in Figure A-9-33 reflects the effect of the river. A hydrologic drought during the early 1990s resulted in reduced recharge and Tc-99 flux into the aquifer. The peak flow year for the Big Lost River recorded at Lincoln Boulevard bridge gauge was 1999 and this period is followed by the peak in Tc-99 concentration.

The peak simulated vadose zone Tc-99 concentration (excluding the tank farm submodel area) was 1.64e+5 pCi/L following the CPP-31 release.

A-9.3.6.2 Aquifer Tc-99 Simulation Results

Figure A-9-34 illustrates the horizontal distribution of aquifer Tc-99 at four time periods: 1979, 2005, 2049, and 2095. Figure A-9-35 presents the peak aquifer concentrations through time.

The peak simulated aquifer Tc-99 concentration was 935 pCi/L in 1999 and is the result of the tank farm Tc-99 residing deep in the vadose zone being quickly moved to the aquifer by the peak 1999 Big Lost River flow. The migration of Tc-99 through the vadose zone was greatly influenced by the simulated Big Lost River flows, and the highest Tc-99 concentrations in the aquifer from the tank farm releases occur immediately after the peak flow of the Big Lost River recorded at Lincoln Boulevard bridge gauge in 1999. The simulated concentrations declined following this peak flow primarily because a hydrologic drought began in 2000. However, simulated concentrations increased after 2005 because the model used the long-term average river flow after this date.

Currently, measured aquifer concentrations exceed the Snake River Plain Aquifer MCL in ICPP-MON-A-230 and aquifer well ICPP-2021. The concentration in Well ICPP-MON-A-230 are approximately an order of magnitude higher than the simulated highest aquifer concentrations. The recently drilled ICPP-2020 and -2021 wells confirm the ICPP-MON-A-230 well is not an anomaly, and a large area of the aquifer beneath INTEC is currently above the Snake River Plain Aquifer MCL. This suggests the vadose zone model may be overestimating vadose zone attenuation or underestimating the vadose zone Tc-99 sources.

The Tc-99 source term for Site CPP-31 has a greater uncertainty than the other radionuclides because the concentration was not measured during tank sampling but was estimated based upon fission yield. The accuracy of the Tc-99 inventory is likely only within a factor of two. Doubling the Tc-99 Site CPP-31 inventory would place the maximum simulated aquifer concentration (1999) near that currently measured in the aquifer. The simulated peak aquifer concentration in 2095 was approximately 10 pCi/L. This represents a factor of 100 decrease in concentration from simulated peak values. If the model trend is correct, concentrations should be nearly a factor of 10 below the Snake River Plain Aquifer MCL even if the inventory is increased by a factor of 10.

Figure A-9-30. Tc-99 horizontal vadose zone concentrations (pCi/L) (SRPA MCL = thick red line, 10*SRPA MCL = thin red line, SRPA MCL/10 = thin black line).

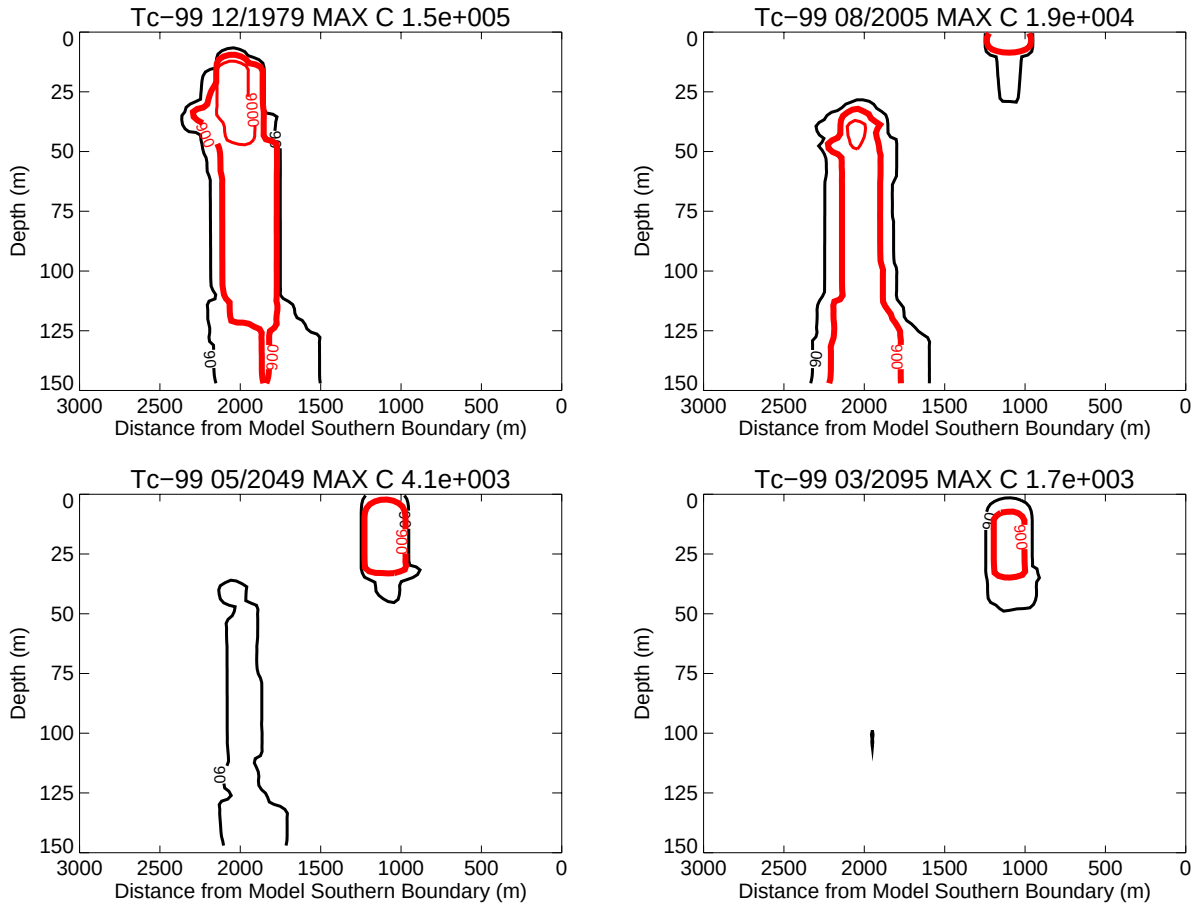

Figure A-9-31. Tc-99 vertical vadose zone concentrations (pCi/L) (SRPA MCL = thick red line, 10*SRPA MCL = thin red line, SRPA MCL/10 = thin black line).

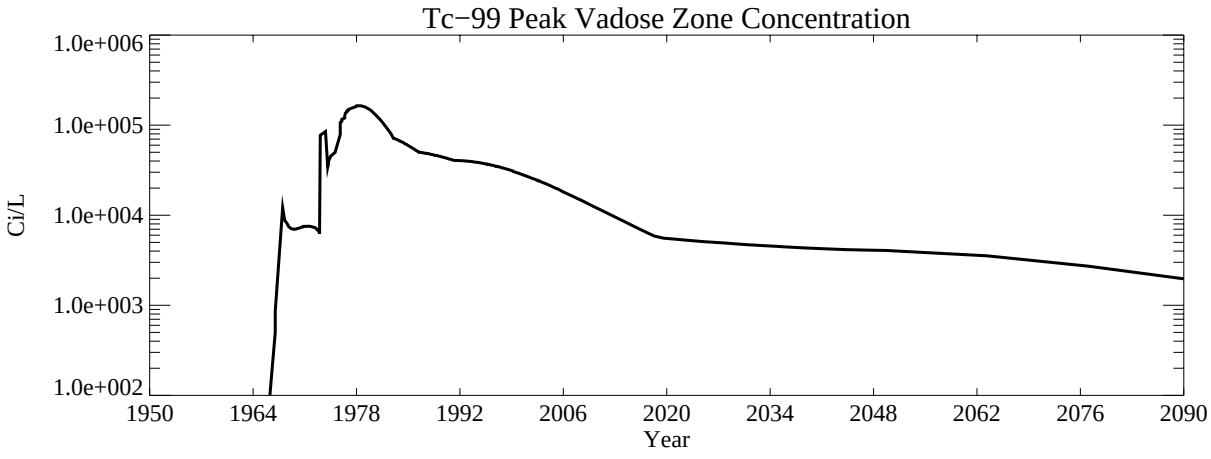

Figure A-9-32. Tc-99 peak vadose zone concentrations excluding tank farm submodel area (pCi/L).

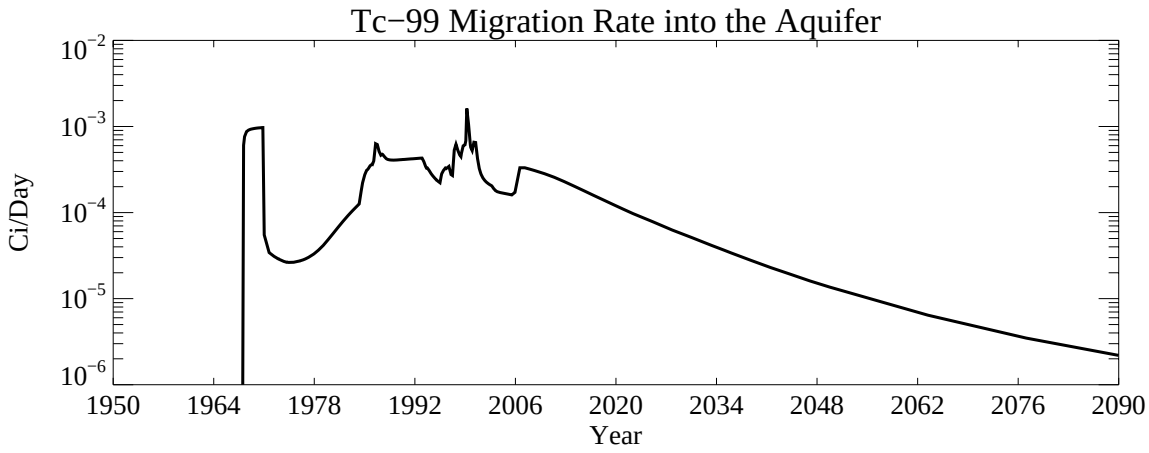

Figure A-9-33. Tc-99 activity flux into the aquifer (Ci/day).

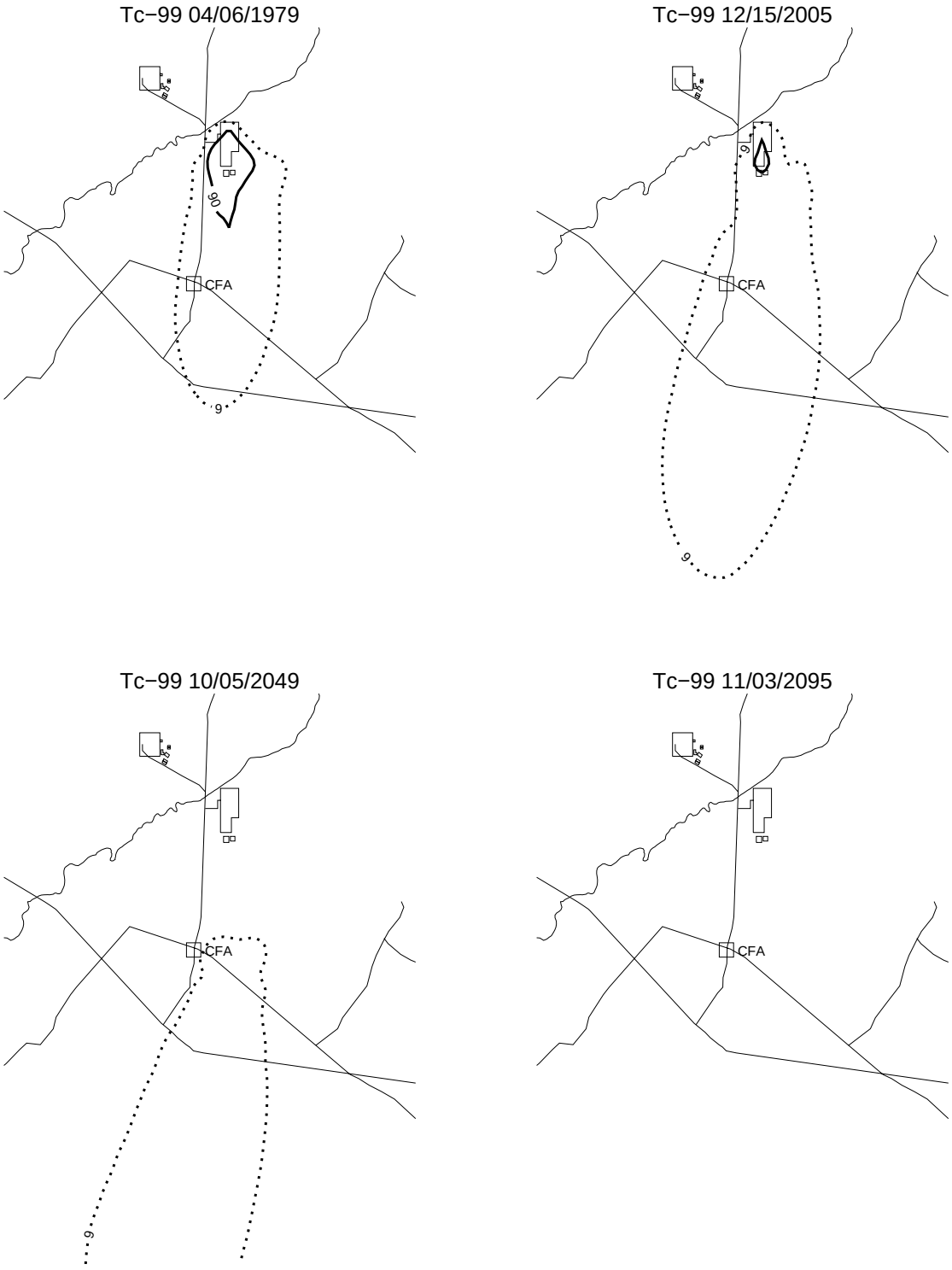

Figure A-9-34. Tc-99 horizontal aquifer concentrations (pCi/L) (SRPA MCL = thick red line, 10*SRPA MCL = thin red line, SRPA MCL/10 = thin black line, SRPA MCL/100 = thin black dashed line).

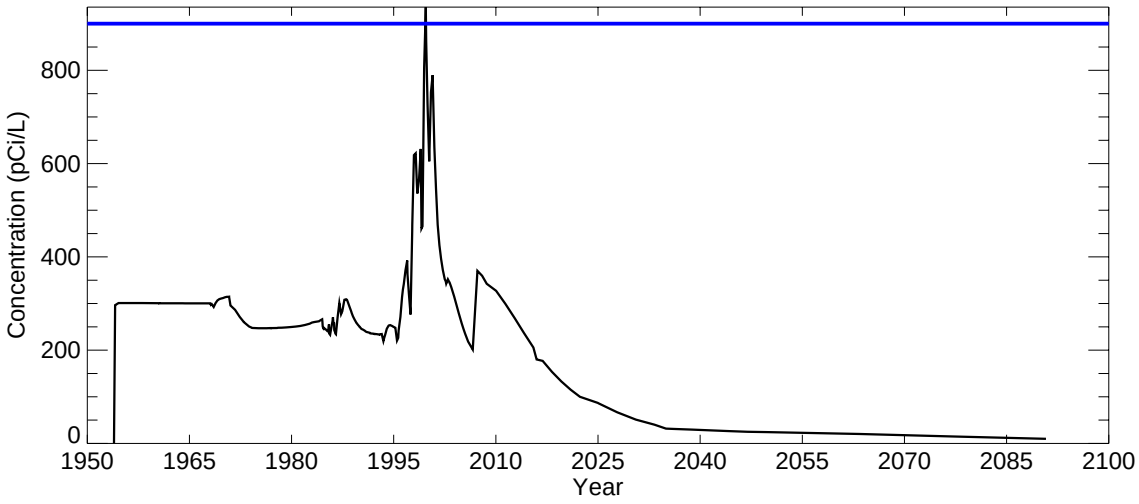

Figure A-9-35. Tc-99 peak aquifer concentrations (pCi/L) (SRPA MCL = blue line, model predicted=black line).

A-9.3.7 U-234

The sources of U-234 in the vadose zone, listed in order of decreasing magnitude, are (1) OU 3-13 soil sites (0.14 Ci), (2) the tank farm at 0.095 Ci, (3) service waste ponds at 0.040 Ci, and (4) CPP-3 injection well failure at 0.011 Ci. The amount of U-234 released directly into the aquifer due to the injection well failure was 0.13 Ci. An early conservative estimate of the OU 3-14 U-234 source term was mistakenly used for the U-234 simulation. The estimate for U-234 developed in Section 5 of the main document was smaller. The model was not rerun with the smaller value because the source term was conservatively larger and the peak simulated U-234 aquifer concentration was several orders of magnitude below the Snake River Plain Aquifer MCL. The Snake River Plain Aquifer MCL for uranium is based on toxicity, and the simulated impact of U-234 to groundwater is being evaluated based on the Snake River Plain Aquifer MCL of 0.03 mg/L.

A-9.3.7.1 Vadose Zone U-234 Simulation Results

Figure A-9-36 presents the peak vadose zone concentrations (excluding the tank farm submodel area) through time and Figure A-9-37 illustrates the U-234 mass flux into the aquifer. Horizontal and vertical concentration plots are not presented because the peak concentrations were always nearly two orders of magnitude below the Snake River Plain Aquifer MCL of 0.03 mg/L.

The purpose of reprocessing spent nuclear fuel was to recover uranium. The process was very efficient and the amount of uranium entering the reprocessing waste stream was small compared to the other radionuclides. The peak vadose zone concentration (excluding the tank farm submodel area) was 8.27e-4 mg/L in 1990 and corresponds to near-surface OU 3-13 soil sources.

A-9.3.7.2 Aquifer U-234 Simulation Results

Figure A-9-38 presents the peak aquifer concentrations through time. The peak aquifer U-234 concentration was 5.36e-7 mg/L in 1958 and is the result of the CPP-3 injection well. Horizontal aquifer concentration contour plots are not presented because the simulated U-234 concentrations were always several orders of magnitude below the Snake River Plain Aquifer MCL.

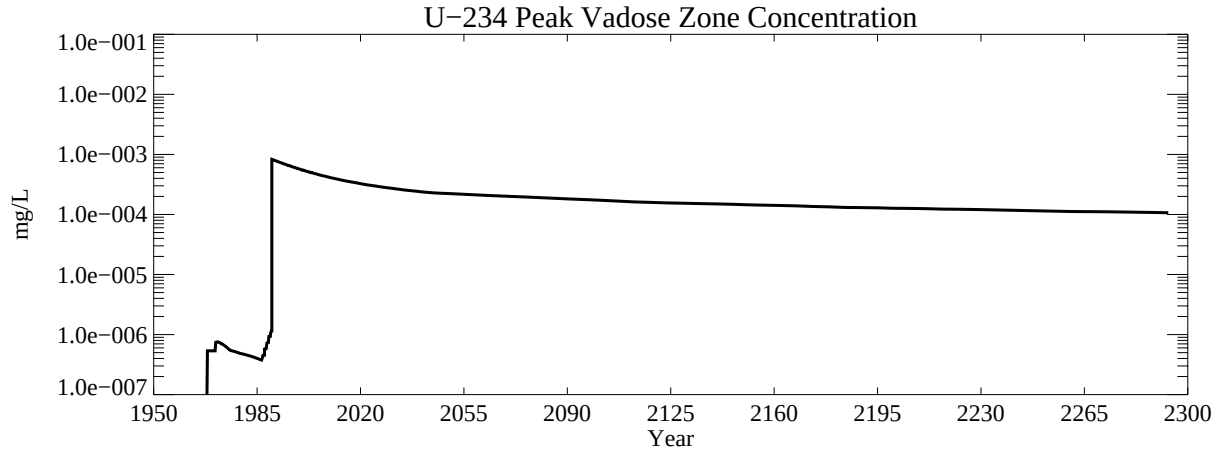

Figure A-9-36. U-234 peak vadose zone concentrations excluding tank farm submodel area (mg/L).

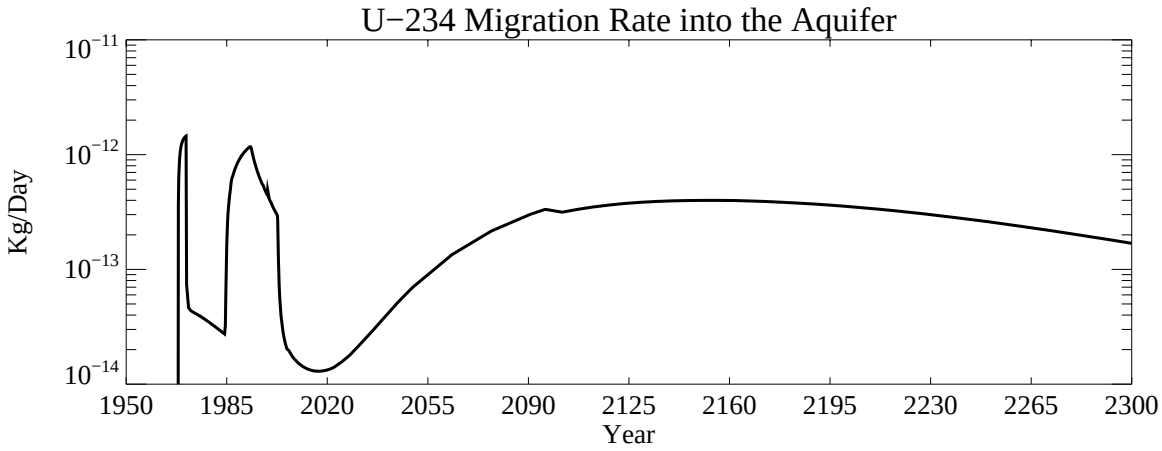

Figure A-9-37. U-234 mass flux into the aquifer (kg/day).

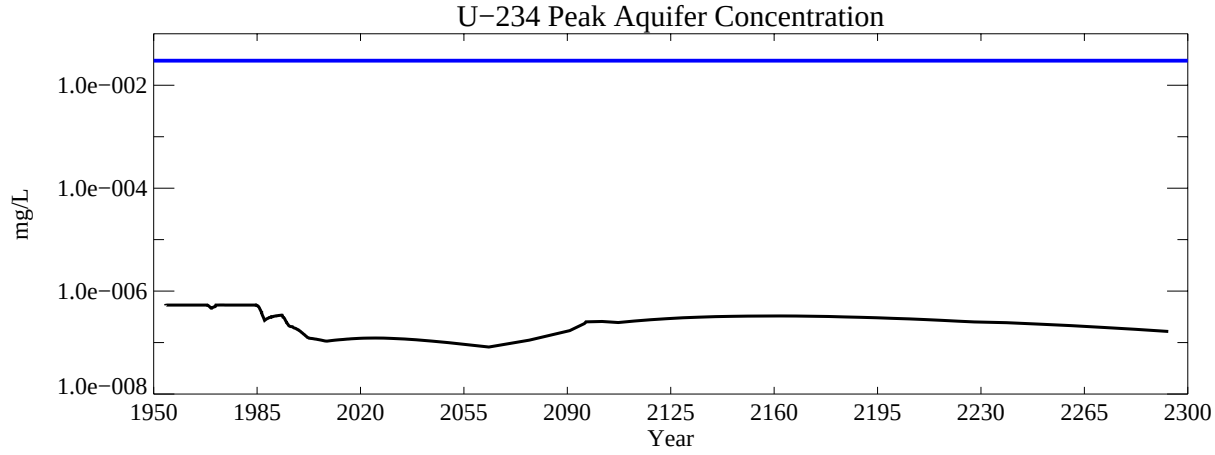

Figure A-9-38. U-234 peak aquifer concentrations (mg/L) (SRPA MCL = blue line, model predicted = black line).

A-9.3.8 Mercury

The sources of mercury in the vadose zone, listed in order of decreasing magnitude, are (1) the OU 3-13 soil sources at 585 kg, (2) the tank farm sources at 72.4 kg, (3) the failed CPP-3 injection well at 32.1 kg. The amount of mercury released directly to the aquifer due to the injection well failure was 368 kg.

A-9.3.8.1 Vadose Zone Mercury Simulation Results

Figures A-9-39 and A-9-40 illustrate the horizontal and vertical distribution of the vadose zone mercury at four time periods: 1979, 2005, 2049, and 2095. Figure A-9-41 presents the peak vadose zone concentrations through time and Figure A-9-42 illustrates the mercury mass arrival in the aquifer.

The peak vadose zone mercury concentration was 0.61 mg/L in 1990 and this date coincided with the start of OU 3-13 soil sources. A large amount of mercury was released to the INTEC vadose zone from the simulated tank farm releases and from the CPP-3 injection well failure. However, the sediment K_d (118 and 156 mL/g for the alluvium and interbed) results in the mercury moving very slowly through the vadose zone and allows the mercury to act as a continuous leaching source. The vast majority of the tank farm and OU 3-13 soil site mercury remains in the alluvium. The peak vadose zone concentrations are predicted to remain above the Snake River Plain Aquifer MCL through the end of the simulation period.

A-9.3.8.2 Aquifer Mercury Simulation Results

Figure A-9-43 illustrates the horizontal distribution the aquifer mercury at four time periods: 1979, 2005, 2049, and 2095. The peak aquifer concentration through time is presented in Figure A-9-44. The peak aquifer concentration was 9.67e-3 mg/L in 1981 and coincided with closing the CPP-3 injection well. Mercury concentrations were predicted to exceed the Snake River Plain Aquifer MCL from 1954 through 1993. The large alluvium and interbed K_d (118 and 156 mL/g) resulted in the mercury moving very slowly through the vadose zone. The peak aquifer concentration as a result of the vadose zone sources was 0.00016 mg/L in the year 3049.

Figure A-9-39. Mercury horizontal vadose zone concentrations (mg/L) (SRPA MCL = thick red line, 10*SRPA MCL = thin red line, SRPA MCL/10 = thin black line).

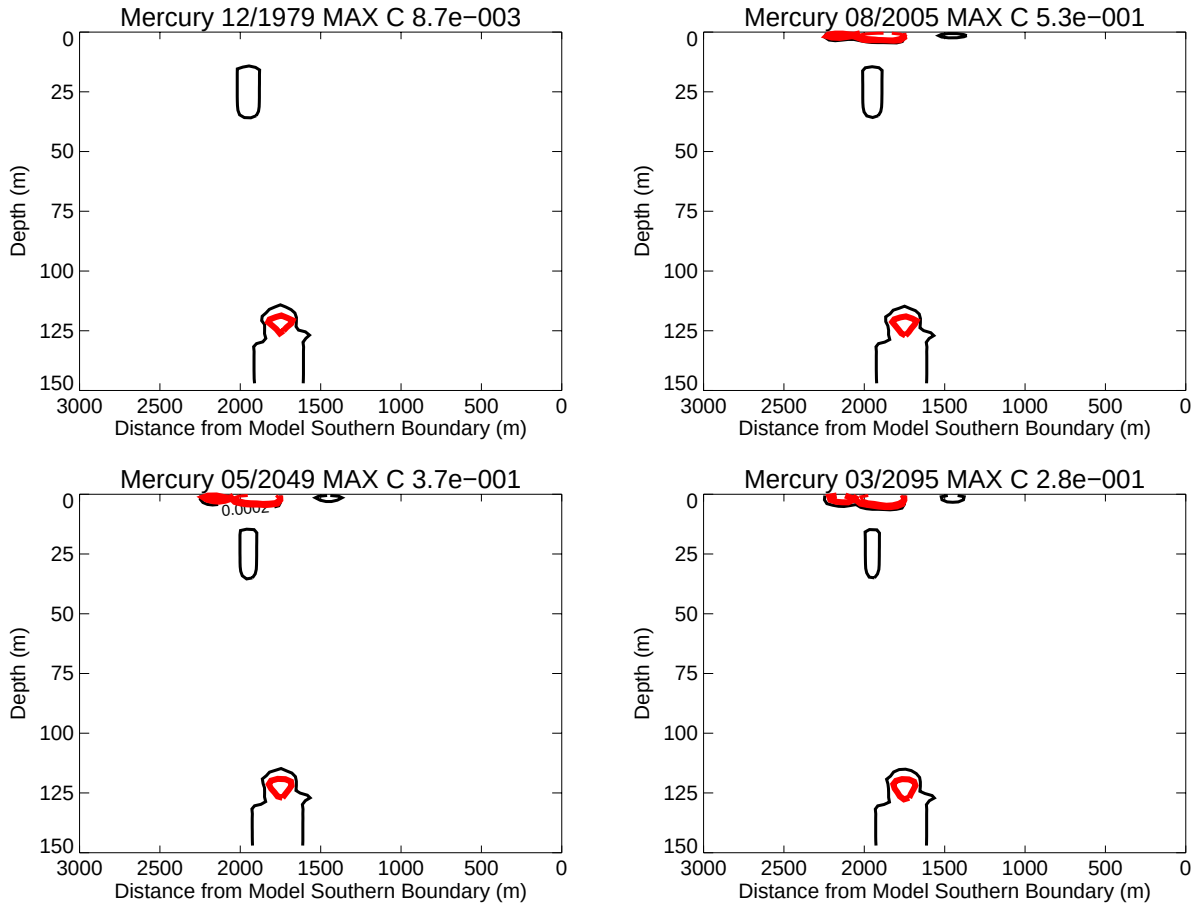

Figure A-9-40. Mercury vertical vadose zone concentrations (mg/L) (SRPA MCL = thick red line, 10*SRPA MCL = thin red line, SRPA MCL/10 = thin black line).

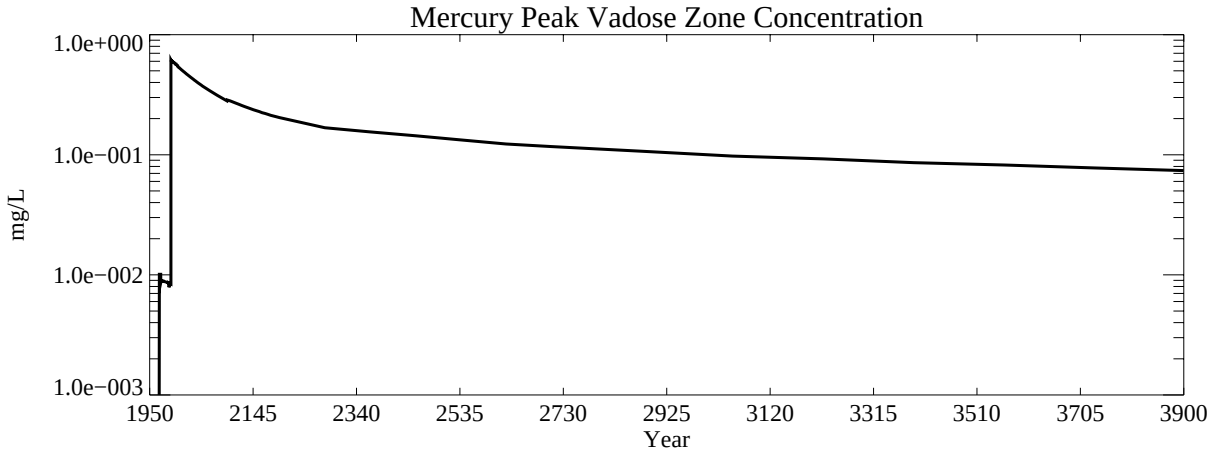

Figure A-9-41. Mercury peak vadose zone concentrations excluding tank farm submodel area (mg/L).

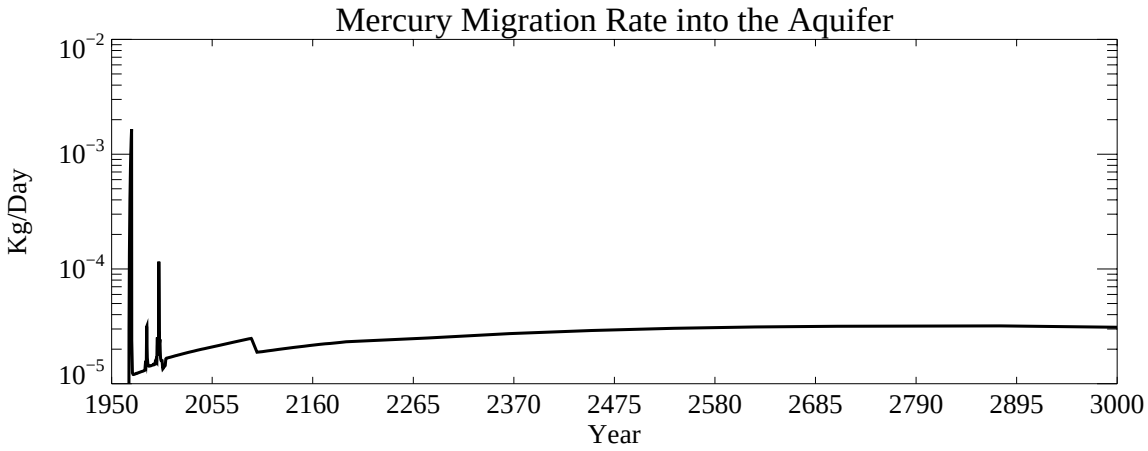

Figure A-9-42. Mercury mass flux into the aquifer (kg/day).

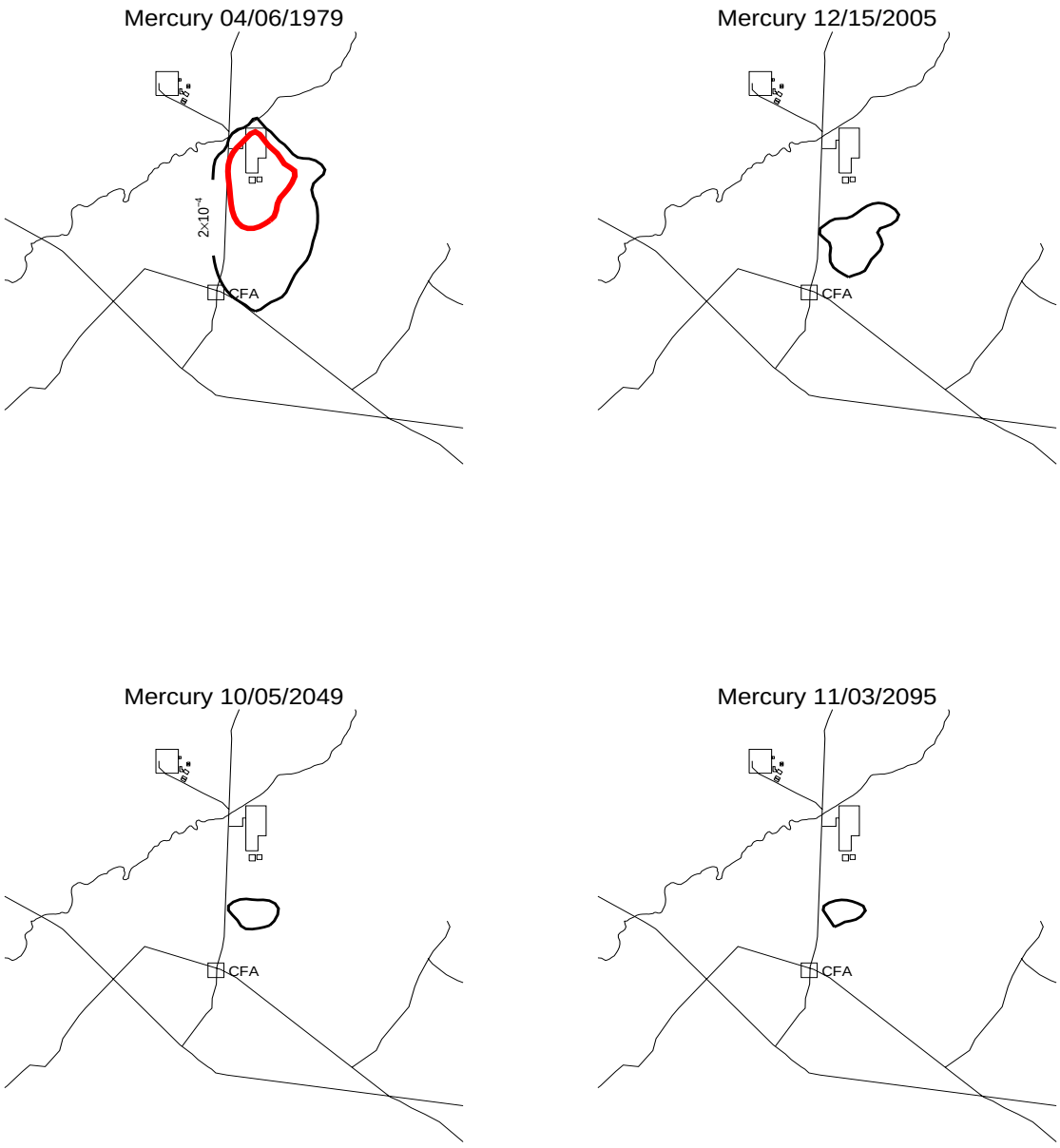

Figure A-9-43. Mercury horizontal aquifer concentrations (mg/L) (SRPA MCL = thick red line, 10*SRPA MCL = thin red line, SRPA MCL/10 = thin black line, SRPA MCL/100 = thin black dashed line).

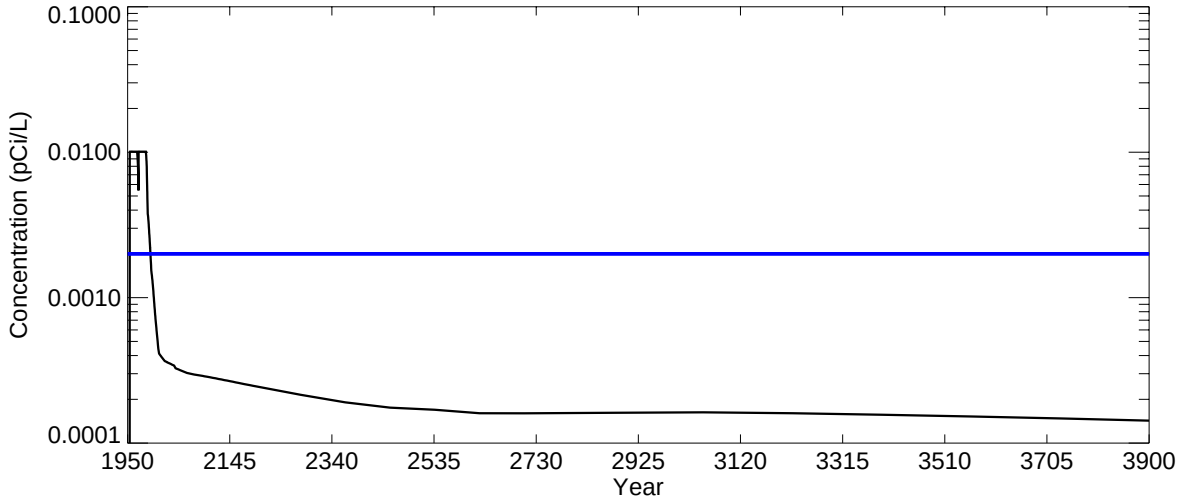

Figure A-9-44. Mercury peak aquifer concentrations (mg/L) (SRPA MCL = blue line, model predicted = black line).

A-9.3.9 Nitrate

The sources of nitrate in the vadose zone, listed in order of decreasing magnitude, are (1) service waste ponds at 1.3e+6 kg, (2) CPP-3 injection well failure at 2.2e+5 kg, and (3) the tank farm sources at 2.1e+4 kg. The nitrate released directly to the aquifer from the injection well was 2.6e+6 kg.

A-9.3.9.1 Vadose Zone Nitrate Simulation Results

Figures A-9-45 and A-9-46 illustrate the horizontal and vertical distribution of the vadose zone nitrate at four time periods: 1979, 2005, 2049, and 2095. Figure A-9-47 presents the peak vadose zone concentrations through, time and Figure A-9-48 illustrates the nitrate mass arrival in the aquifer.

The spent nuclear fuel reprocessed at the INTEC was dissolved in nitric or hydrofluric acid during the uranium recovery process, resulting in large amounts of nitrate discharged in the liquid waste. Nitrate is an anion and is very mobile in the subsurface. Nitrate is also ubiquitous in most groundwaters, and the background concentration in the Snake River Plain Aquifer is approximately 1.5 mg/L (Orr et al. 1991). The peak vadose zone concentration was 6.76e+2 mg/L after the 1972 CPP-31 release.

A-9.3.9.2 Aquifer Nitrate Simulation Results

Figure A-9-49 illustrates the horizontal distribution of nitrate in the aquifer at four time periods: 1979, 2005, 2049, and 2095. Figure A-9-50 presents the peak aquifer concentrations through time.

The peak aquifer nitrate concentration was 18.2 mg/L as N in 1993. A large amount of nitrate was present in both the injection well and service waste pond disposal water. The peak concentration corresponds to the combined input of both these sources to the aquifer. Nitrate was predicted to remain above the Snake River Plain Aquifer MCL from 1954 through 1998.

Figure A-9-45. Nitrate horizontal vadose zone concentrations (mg/L as N) (SRPA MCL = thick red line, 10*SRPA MCL = thin red line, SRPA MCL/10 = thin black line).

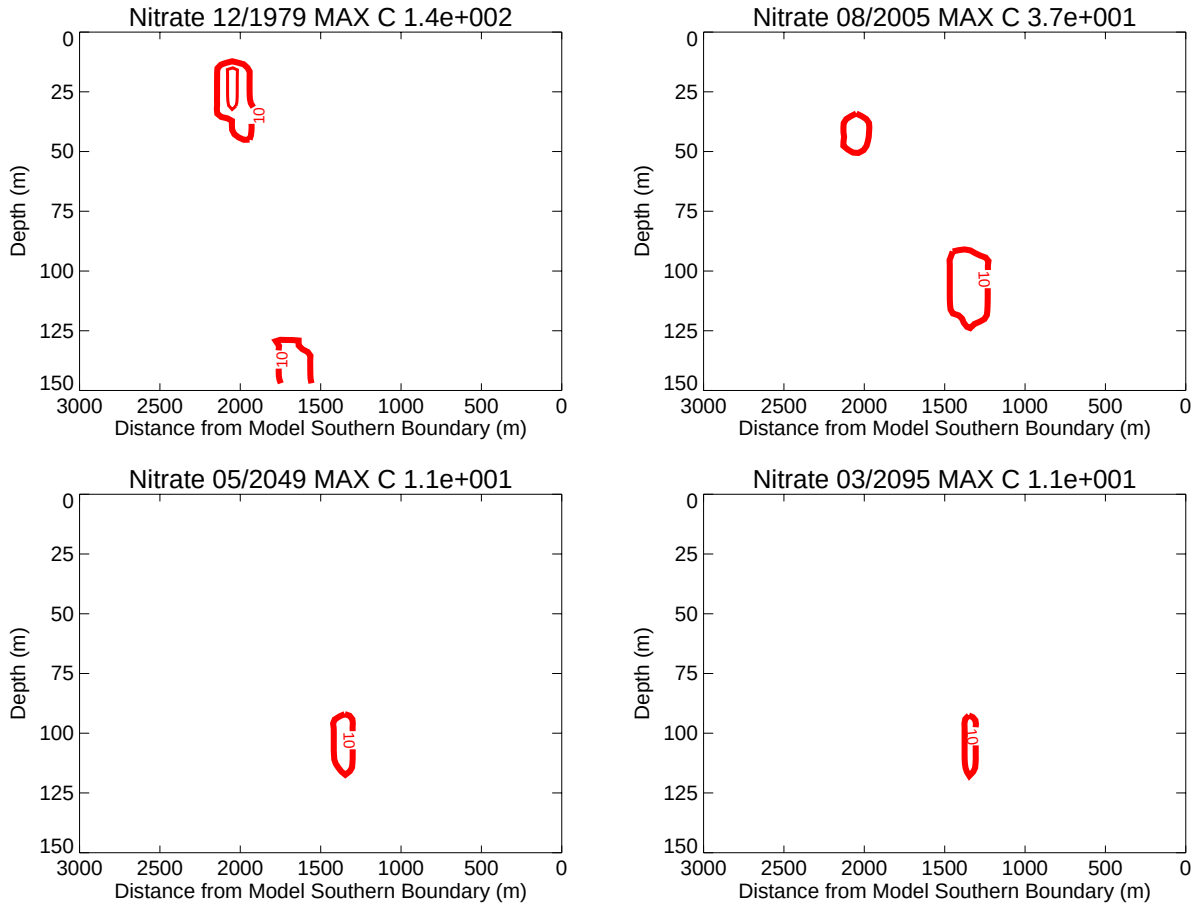

Figure A-9-46. Nitrate vertical vadose zone concentrations (mg/L as N) (SRPA MCL = thick red line, 10*SRPA MCL = thin red line, SRPA MCL/10 = dotted line).

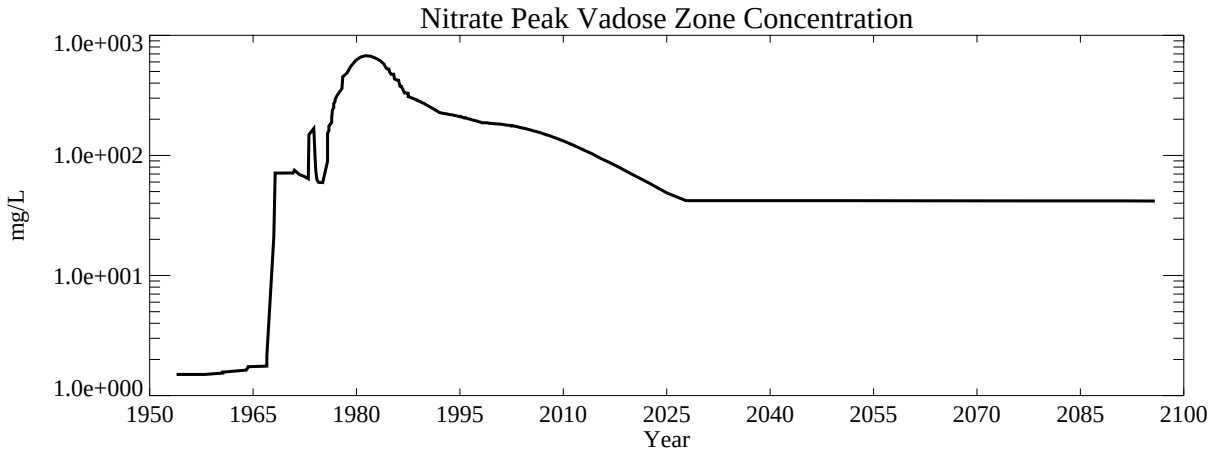

Figure A-9-47. Nitrate peak vadose zone concentrations excluding tank farm submodel area (mg/L as N).

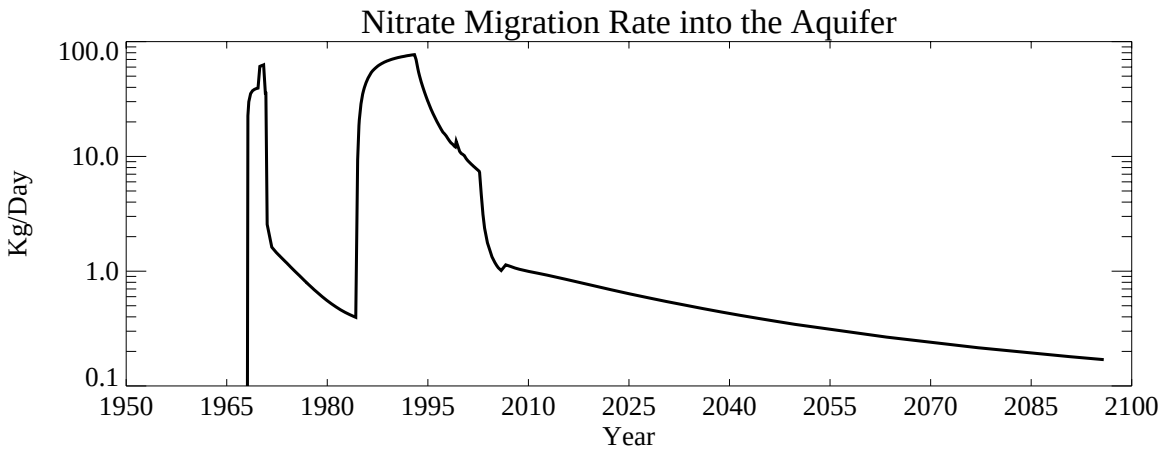

Figure A-9-48. Nitrate aquifer mass concentration history (kg/day as N).

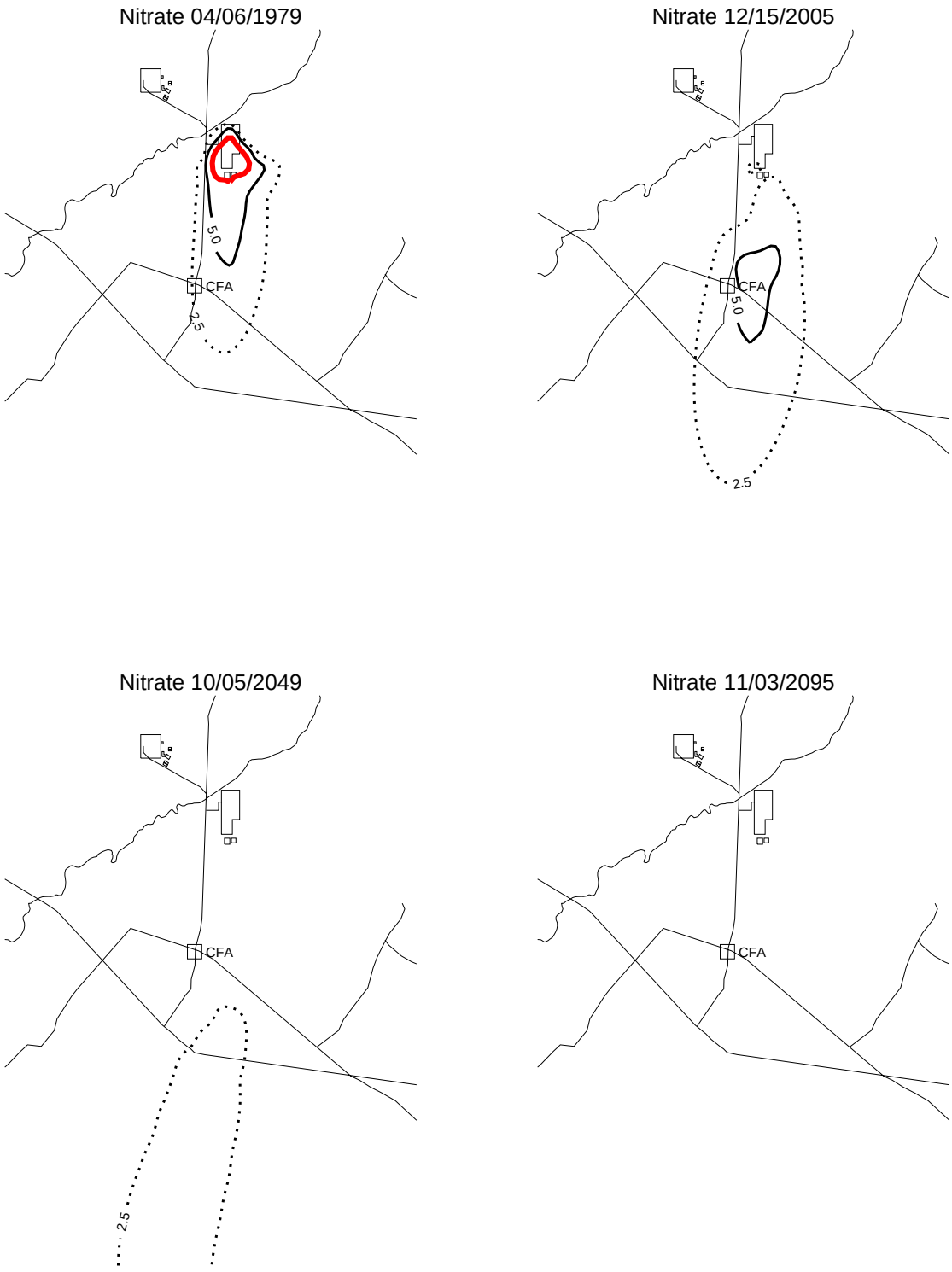

Figure A-9-49. Nitrate horizontal aquifer concentrations (mg/L as N) (SRPA MCL = thick red line, 10*SRPA MCL = thin red line, SRPA MCL/2 = thin black line, SRPA MCL/4 = thin black dashed line).

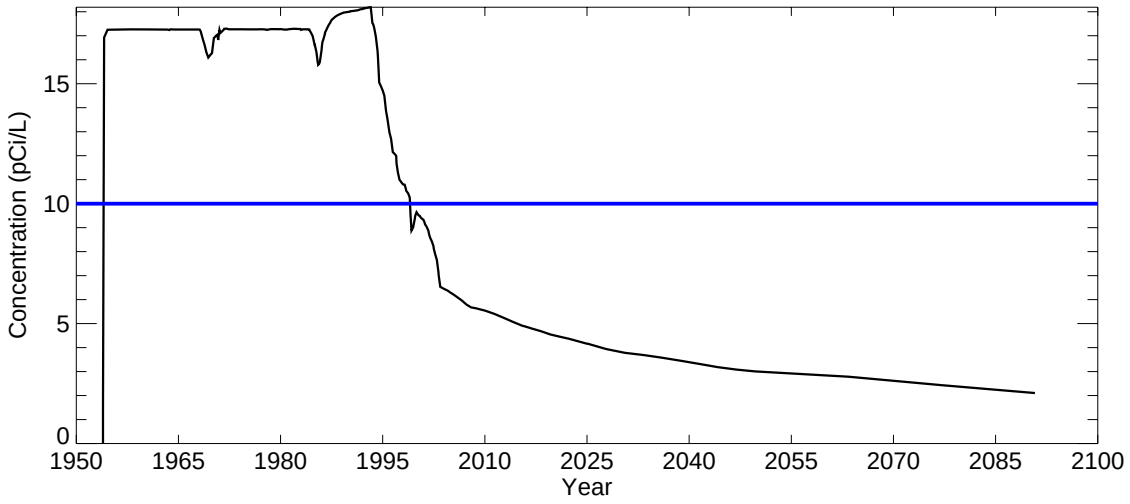

Figure A-9-50. Nitrate peak aquifer concentrations (mg/L as N) (SRPA MCL = blue line, model predicted = black line).

A-9.3.10 Groundwater Pathway Simulation Results Summary

The transport of 10 COPCs originating from the INTEC contaminated soil, CPP-3 injection well, and service waste ponds was simulated from land surface to the Snake River Plain Aquifer. The simulations also included contributing sources from the nontank farm OU 3-13 contamination sites. The simulation results are summarized for the vadose zone and aquifer in Sections A-9.3.10.1 and A-9.3.10.2, respectively. The Sr-90 simulation results are disscussed in Appendix J.

A-9.3.10.1 Vadose Zone Results

Table A-9-11 contains the simulated peak concentrations in the vadose zone model and includes the Snake River Plain Aquifer MCL, year of the peak concentration, peak concentration, peak concentration in 2005, peak concentration in 2095, and the year peak concentrations fall below the Snake River Plain Aquifer MCL. All the contaminants in the vadose zone except U-234 exceeded the Snake River Plain Aquifer MCL within the vadose zone at some time during the simulations. Only tritium and U-234 in the vadose zone were below the Snake River Plain Aquifer MCL before the year 2095. The timeframes over which vadose concentrations exceed the MCL are presented for reference only. The time when vadose zone concentrations fall below the Snake River Plain MCL provides an extremely conservative estimate of when the vadose zone pore water could not adversely impact the Snake River Plain Aquifer under any circumstance (i.e., fast flow paths and leaky well bores, etc.). Dispersion, dilution, adsorption, and radioactive decay within the vadose zone will result in aquifer concentrations being much less than those in the vadose zone.

Table A-9-11 Vadose zone simulation results.

COPC	SRPA MCL (pCi/L or mg/L)	Year of Simulated Peak	Peak Simulated Vadose Zone Concentration (pCi/L or mg/L)	Peak Simulated Vadose Zone Concentration in 2005 (pCi/L or mg/L)	Maximum Simulated Vadose Zone Concentration in 2095 (pCi/L or mg/L)	Year Below SRPA MCL in the Vadose Zone
H-3	20,000	1965	1.82e+6	3.13e+4	1.82e+2	2011
I-129	1	1971	3.00e+1	9.86e+0	3.37e+0	>2095[a]
Np-237	15	1990	6.00e+3	1.01e+3	2.88e+2	>2300[a]
Pu-239	15	1973	5.38e+1	1.01e+2	9.12e+1	14226
Pu-240	15	1990	1.94e+1	1.91e+1	1.71e+1	2287
Sr-90	8	1977	1.99e+9	1.94e+7	3.07e+4	>2300[a]
Tc-99	900	1982	1.64e+5	1.91e+4	1.68e+3	>2095[a]
U-234	0.03 (mg/L)	1990	8.27e-4	4.65e-4	1.47e-4	>2300[a]
Mercury	0.002	1990	6.14e-1	5.31e-1	2.81e-1	>4580[a]
Nitrate	10	1981	6.76e+2	1.61e+2	4.14e+1	>2095[a]
a. Concentration remained above Snake River Plain Aquifer MCL at simulation end time.						

A-9.3.10.2 Aquifer Results

Table A-9-12 contains the simulated peak concentrations in the aquifer model and includes the Snake River Plain Aquifer MCL, year of the peak concentration, peak concentration, peak concentration in 2005, peak concentration in 2095 and the year concentrations fall below the Snake River Plain Aquifer MCL.

Tritium, I-129, Np-237, Sr-90, Tc-99, mercury, and nitrate were predicted to exceed the groundwater Snake River Plain Aquifer MCL during the simulation time periods. However, only Sr-90 was predicted to exceed the Snake River Plain Aquifer MCL in the year 2095. The contaminants exceeding the Snake River Plain Aquifer MCL are summarized below:

- Tritium was predicted to exceed the Snake River Plain Aquifer MCL from 1954 through 2001. The primary source of aquifer contamination was the CPP-3 injection well prior to1984 and the service waste ponds after 1984. Radioactive decay, dispersion, and dilution reduce the tritium concentrations below the Snake River Plain Aquifer MCL by 2006. This is consistent with observed tritium concentrations in the aquifer monitoring wells.

- I-129 was predicted to exceed the Snake River Plain Aquifer MCL from 1954 through 2080. The primary source of aquifer contamination was the CPP-3 injection well and the service waste ponds. Dispersion and dilution reduced the I-129 concentrations below the Snake River Plain Aquifer MCL in the year 2088. Radioactive decay is negligible because the I-129 half-life is 1.57e+7 years. The simulated I-129 concentrations were consistent with the observed I-129 concentrations in the aquifer.

- Np-237 was predicted to exceed the Snake River Plain Aquifer MCL from 1954 through 1987. The

primary source of aquifer contamination was the injection well.

- Sr-90 was predicted to exceed the Snake River Plain Aquifer MCL from 1958 through 2128. The Sr-90 aquifer simulations are discussed in Appendix J.

- Tc-99 was predicted to exceed the Snake River Plain Aquifer MCL in 1999. The Tc-99 only briefly exceeded the Snake River Plain Aquifer MCL following the peak Big Lost River flow. This is the result of the tank farm Tc-99 residing deep in the vadose zone being quickly moved to the aquifer by the peak Big Lost River flow. Current aquifer concentrations exceed the Snake River Plain Aquifer MCL in the ICPP-MON-A-230 well and are approximately an order of magnitude higher than the simulated current highest aquifer concentrations. The recently drilled ICPP-2020 and -2021 wells confirm the ICPP-MON-A-230 well is not an anomaly, and a large area of the aquifer beneath INTEC is currently above the Snake River Plain Aquifer MCL. This suggests the vadose zone model may be overestimating vadose zone attenuation or underestimating the vadose zone Tc-99 sources. The Tc-99 source term for site CPP-31 has a greater uncertainty than the other radionuclides because the concentration was not measured during tank sampling but was estimated based upon fission yield. The accuracy of the Tc-99 inventory is likely only within a factor of two. Doubling the Tc-99 Site CPP-31 inventory would place the maximum simulated aquifer concentration (1999) near that currently measured in the aquifer. The simulated peak aquifer concentration in 2095 was approximately 10 pCi/L. This represents a factor of 100 decrease in concentration from simulated peak values. If the model trend is correct, concentrations should be nearly a factor of 10 below the Snake River Plain Aquifer MCL even if the inventory is increased by a factor of 10.

- Mercury was predicted to exceed the Snake River Plain Aquifer MCL from 1954 through 1993. The primary source of aquifer contamination was the CPP-3 injection well. Dispersion and dilution reduced aquifer concentrations below the Snake River Plain Aquifer MCL by the year 1994.

- Nitrate was predicted to exceed the Snake River Plain Aquifer MCL from 1954 through 1998. The primary source of aquifer contamination was initially the CPP-3 injection well and later the service waste ponds. The model predicts dispersion and dilution will reduce aquifer concentrations below the Snake River Plain Aquifer MCL by the year 1999. The simulated nitrate concentrations were consistent with the observed nitrate concentrations in the aquifer.

Table A-9-12 Aquifer simulation results.

COPC	SRPA MCL (pCi/L or mg/L)	Year of Simulated Peak	Peak Simulated Concentration (pCi/L or mg/L)	Maximum Simulated Concentration in 2005 (pCi/L or mg/L)	Peak Simulated Concentration in 2095 (pCi/L or mg/L)	Year Below SRPA MCL
H-3	20,000	1965	4.02e+6	9.97e+4	1.23e+2	2001
I-129	1	1970	2.26e+1	3.85e+0	9.00e-1	2080
Np-237	15	1965	2.71e+1	4.06e+0	4.22e+0	1987
Pu-239	15	1960	3.34e-1	1.72e-2	2.07e-3	Always
Pu-240	15	1960	1.67e-1	8.61e-3	1.03e-3	Always
Sr-90	8	1965	5.76e+3	4.08e+1	1.81e+1	2128
Tc-99	900	1999	9.35e+2	2.35e+2	9.84e+0	1999
U-234	0.03 (mg/L)	1958	5.36e-7	1.15e-7	2.34e-7	Always
Mercury	0.002	1981	9.67e-3	5.86e-4	1.30e-4	1993
Nitrate	10	1993	1.82e+1	6.20e+0	2.10e+0	1998

A-10 ASSESSMENT OF MODEL LIMITATIONS

The models used in this analysis are simplified representations of the vadose zone and aquifer. Mismatches between measured data and predictions arise as a result of simplified parameterization and uncertainty in input parameters. The sensitivity and uncertainty in predictions are quantified and bounded in the following sections. The model sensitivity was assessed by determining the potential range of model output given natural variability in the input parameters. This is done and to determine whether the possible range of each parameter value can result in significant variation in model predictions. The model sensitivity to parametric variability is presented in Section A-10.1.

Predictive sensitivity can be quantified using Monte Carlo simulation given the probability density of each parameter and given the joint density between parameters. In Monte Carlo simulation, repeated random sampling from each probability distribution is used in forward simulations, and the resultant of many such simulations is a distribution of possible model predictions. In these simulations, there are insufficient data from which to determine the probability density (and joint density) functions for each parameter (or each combination of parameters). As a result, model parametric uncertainty is qualitatively evaluated based on the behavior of selected sensitivities.

Each predictive simulation is subject to both parametric uncertainty and conceptual uncertainty. The conceptual uncertainty is in addition to the parametric variability captured in the sensitivity analysis. This uncertainty arises through the development of the conceptual model of flow and transport because complex processes may be oversimplified or poorly understood. It is introduced as the contaminant source releases are estimated and is compounded as transport parameters and boundary conditions are assigned. The relative impact of these sources of uncertainty is qualitatively discussed in Section A-10.2.

A-10.1 Model Sensitivity Analysis

Model sensitivity, or the relationship between information being input and output, is presented in this section for a select set of model inputs. This sensitivity analysis can be used to focus the uncertainty analysis, i.e., only those model inputs resulting in large deviations in model output require discussion in the model uncertainty analysis. The model calibration process reduces the initial uncertainty by seeking to obtain a match between observed and predicted conditions. The subsurface underlying INTEC is complex, the boundary conditions are variable, and the data are not always located optimally in both space and time. As a combined result, there is a resultant mismatch between model predictions and observed data. The “uncertain” parameters are included here as the basis of the model sensitivity/uncertainty analysis. Seven model parameters or design features were identified as having a potentially large impact on model predictions during the model calibration work. The sensitive parameters are (1) the interbed structure and permeability, (2) assumed recharge from precipitation, (3) existence of fast flow paths allowing Tc-99 to reach the aquifer at the ICPP-MON-A-230 well, (4) the Tc-99 service waste source, (6) the horizontal discretization used in the model, and (7) strontium sorption and dispersion. The sensitivity investigation presented in this section focused on Tc-99. The Sr-90 model sensitivity hydrological inputs is presented with the geochemical modeling in Appendix J. The simulations testing the sensitivity to these parameters are listed in Table A-10-1, and the results are summarized in Section A-10.1.6.

Table A-10-1 Sensitivity analysis simulations.

Sensitivity Simulation	Section	Parameter values
Interbed thickness and permeability	A-10.1.1.1	Highest conductance for Tc-99
	A-10.1.1.2	Lowest conductance for Tc-99
Alluvium recharge rate	A-10.1.2.1	3 cm/year tank farm recharge for Tc-99
	A-10.1.2.2	39 cm/year tank farm recharge for Tc-99
	A-10.1.2.3	Maximum possible recharge focused on the northern INTEC
Tc-99 preferential flow path between the 380-ft interbed and aquifer near the location of ICPP-MON-A-230	A-10.1.3.1	10 gal/min preferential flow path from 380 ft interbed
Tc-99 service waste inventory	A-10.1.4.1	Estimate from 25.1 Tc-99/I-129 ratio
Horizontal grid discretization	A-10.1.5.1	50- x 50-m horizontal grid for Tc-99

The base case simulations for the sensitivity analysis correspond to the Tc-99 calibration results discussed in Section A-7.3.1. Comparisons to the base case (calibration run) are presented by plotting the sensitivity run and base case values for peak concentrations (vadose zone and aquifer) and mass flux rates into the aquifer.

A-10.1.1 Interbed Thickness and Permeability

The contrast between basalt and sediment hydraulic and transport properties is large and their structural distribution is highly variable. Structural variability can change primary flow paths, allowing contaminants to bypass interbeds or to flow through sediment regions with higher permeability.

Spatial stochastic simulation based on variogram models for high- and low-permeability alluvium, interbed, and basalt were used to generate the structure used in the calibration and base case simulations. This process generates many realizations, each honoring the underlying statistical parameters. The calibration and baseline risk assessment simulations used the most probable (or average) structure as the basis of the predictions. To test the sensitivity of these structures, a highest conductance structure (i.e., minimum interbed thickness and maximum interbed permeability) and a lowest conductance structure (i.e., maximum interbed thickness and minimum interbed permeability) were selected from the realizations. The most conductive structure defined 10% of the subsurface as interbed with 5% being low-permeability interbed. The least conductive structure defined 15% of subsurface as interbed with 10% being low-permeability interbed. The model calibration simulation and base case sensitivity simulation had 14% as interbed with 8% being low-permeability interbed.

The highest conductance simulations resulted in fewer areas of high saturation and much less perched water beneath the Big Lost River than was predicted in the base case. The lowest conductance simulations resulted in more areas of high saturation but did not significantly increase the areal extent of the perched water beneath the Big Lost River from the base case. However, the location of the perched water was slightly different from the base case. Figures A-10-1 and A-10-2 illustrate the horizontal extent of perched water in the INTEC subsurface for the highest and lowest conductance simulations, respectively. These figures can be compared to the base case perched water locations contained in Figure A-7-1.

These structures were used as the basis of Tc-99 transport simulations in combination with the base case inventories to evaluate transport sensitivity. The results of these two simulations are presented in Sections A-10.1.1.1 and A-10.1.2.

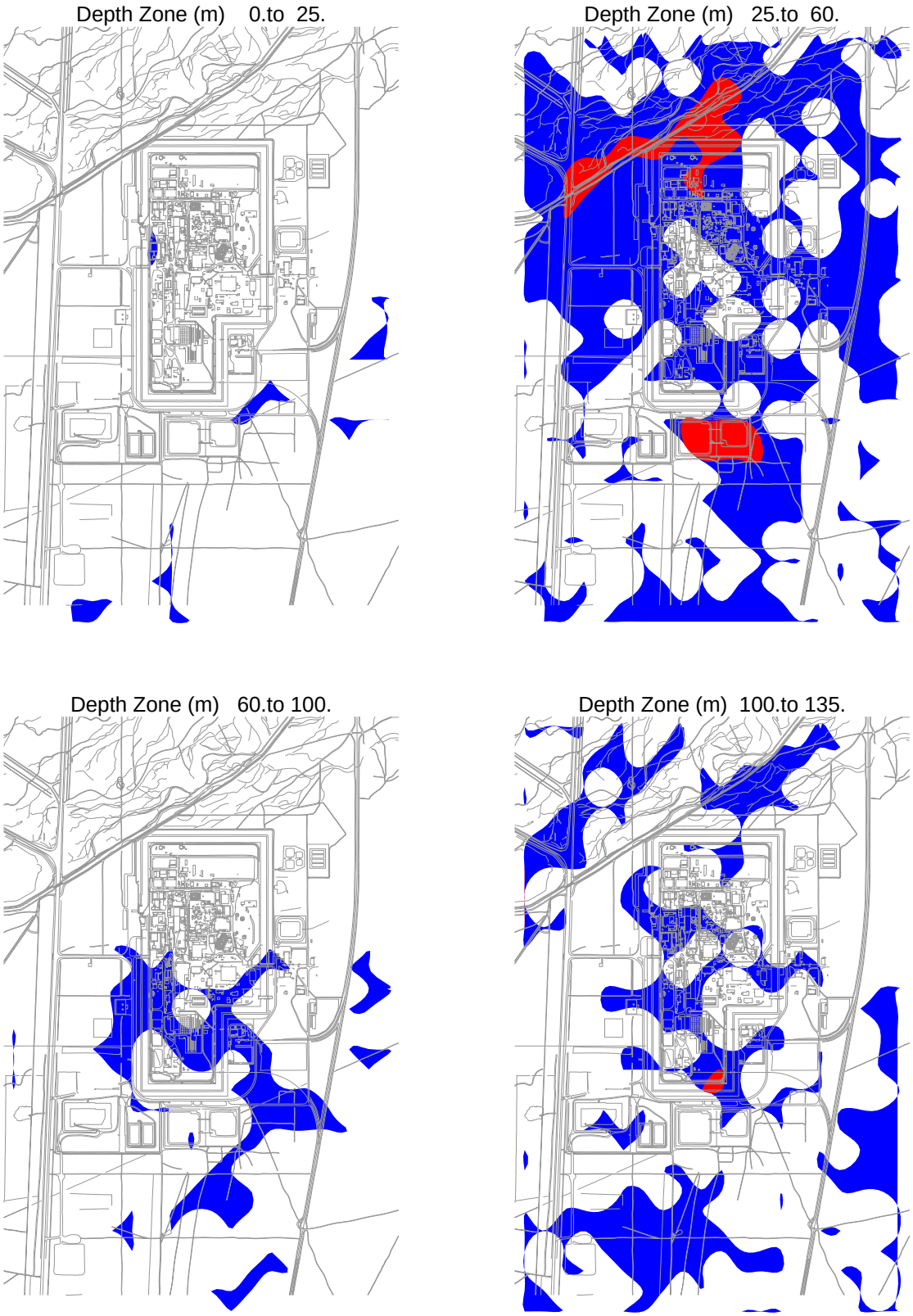

Figure A-10-1. Highest interbed conductance simulation horizontal extent of simulated perched water during peak Big Lost River flow (1999) (blue = 0.99 saturation, red = 1.0 saturation).

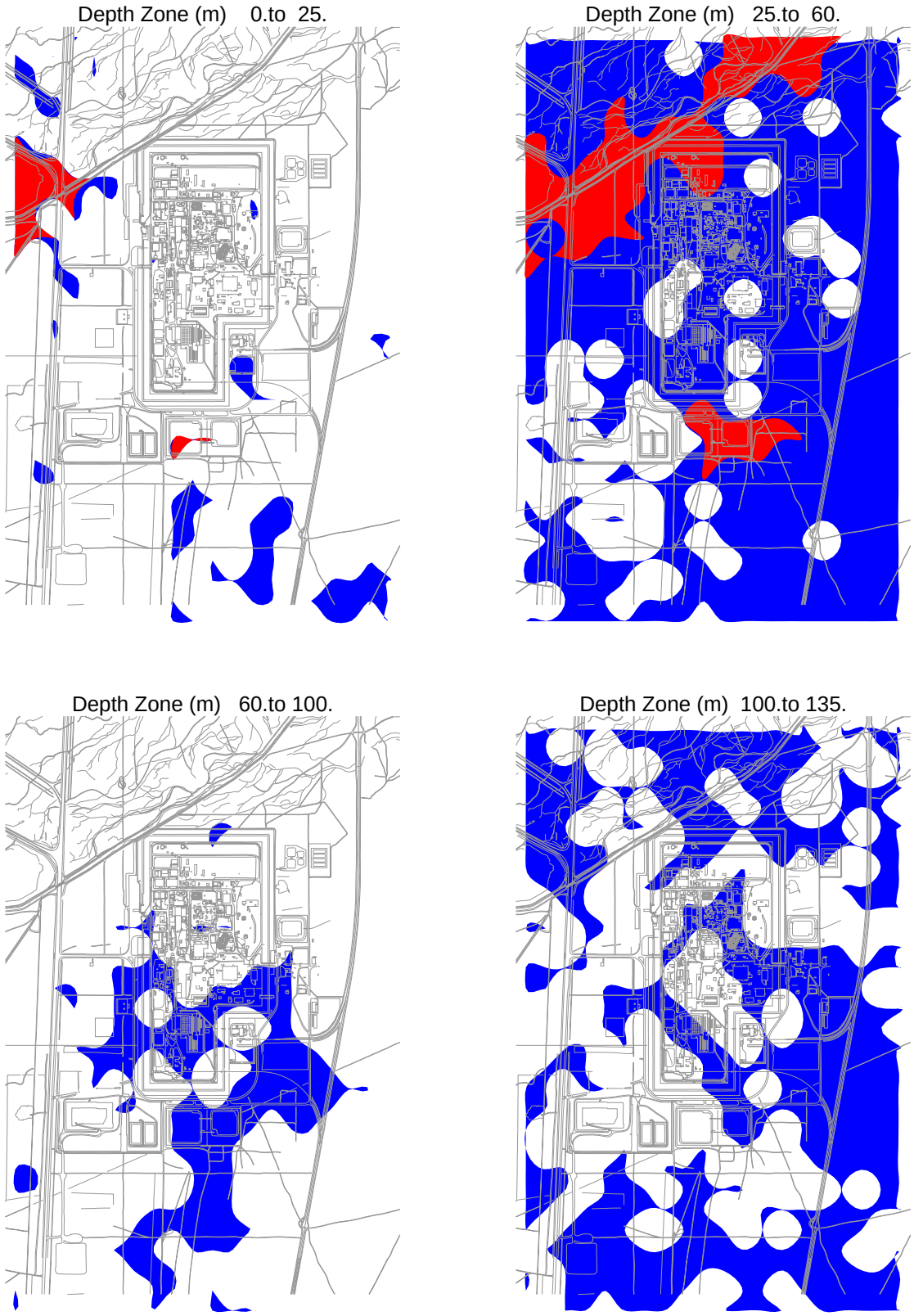

Figure A-10-2. Lowest interbed conductance simulation horizontal extent of simulated perched water during peak Big Lost River flow (1999) (blue = 0.99 saturation, red = 1.0 saturation).

A-10.1.1.1 Highest Interbed Conductance for Tc-99

The peak simulated concentration in the vadose zone for this case is 1.65e+5 pCi/L in 1978, which is after the CPP-31 release date. The peak concentration declined to 1.91e+4 pCi/L in 2005 and to 1.68e+3 pCi/L in 2095. Figures A-10-3 and A-10-4 illustrate the vertical and lateral extent of the simulated vadose zone concentrations. The shallow vadose zone contamination located immediately northwest of the former percolation ponds is due to the CPP-22 OU 3-13 soil site (0.1 Ci), which was placed in the model in 1990.

Figure A-10-5 illustrates the peak simulated vadose zone concentration through time and is the peak concentration anywhere within the vadose zone model domain. The peak vadose zone concentration falls below the MCL in approximately the year 2095. The Tc-99 activity flux into the aquifer is illustrated in Figure A-10-6 and is the total activity passing from the vadose zone model to the aquifer model. Four peak activity periods can be seen in Figure A-10-6. These are the result of the following: (1) the injection well failure during the late 1960s, (2) the service waste ponds during the early 1980s to the early 1990s, (3) the transient Big Lost River recharge during the late 1990s, and (4) the long-term average Big Lost River recharge following the recent hydrologic drought.

Figure A-10-6 indicates that the fluctuations caused by the historical Big Lost River flows are less than the base case because thinner and higher-permeability interbeds do not allow the Big Lost River water to move far enough laterally to reach the contaminated area beneath the tank farm. In addition to the effect of increased average interbed permeability, the surface slope of the 140-ft interbed was different in the maximum interbed realization of the vadose zone lithology. The dip towards the tank farm was less severe. The resultant transport through the vadose zone is controlled by the relatively constant anthropogenic and precipitation recharge. The Tc-99 concentration in key perched water wells is illustrated in Figure A-10-7. The overall agreement with the observed perched water concentration is similar to the base case.

Figure A-10-8 illustrates the horizontal aquifer concentrations and Figure A-10-9 illustrates peak aquifer concentrations through time. The peak concentration is taken from anywhere within the model domain and is at the CPP-3 injection screen during injection well operation or is at the water table for vadose zone sources percolating into the aquifer. Several distinct changes in peak groundwater concentration can be seen in Figure A-10-7. These are the result of the following: (1) service waste disposed in the CPP-3 injection well prior to 1968, (2) service waste entering the aquifer from the vadose zone during the well failure period, (3) service waste disposed of in the CPP-3 injection well after repairs in 1970, (4) service waste intermittently disposed of in the CPP-3 injection well after the service ponds began operating 1984, (5) service waste from the pond operation entering from the vadose zone after 1984, and (5) tank farm contamination entering from the vadose zone during high Big Lost River flow years in the late 1990s. Records of water volume and Tc-99 activity disposed of to the CPP-3 injection well after 1984 indicate widely varying contaminant concentrations in the well influent.

The abrupt increases in aquifer concentrations during peak Big Lost River flow years are not apparent in the minimum interbed thickness peak aquifer concentrations. This is because the Big Lost River does not spread laterally beneath the tank farm to the same extent as the base case. The peak simulated aquifer concentration in 2095 was 43 pCi/L and was four times higher than the base case. This is because the Big Lost River has less of an effect in quickly moving contaminants into the aquifer in the base case.

Figure A-10-3. Tc-99 horizontal vadose zone concentrations (pCi/L) for the highest conductance case (MCL = thick red, MCL/10 = thin black, MCL*10 = thin red).

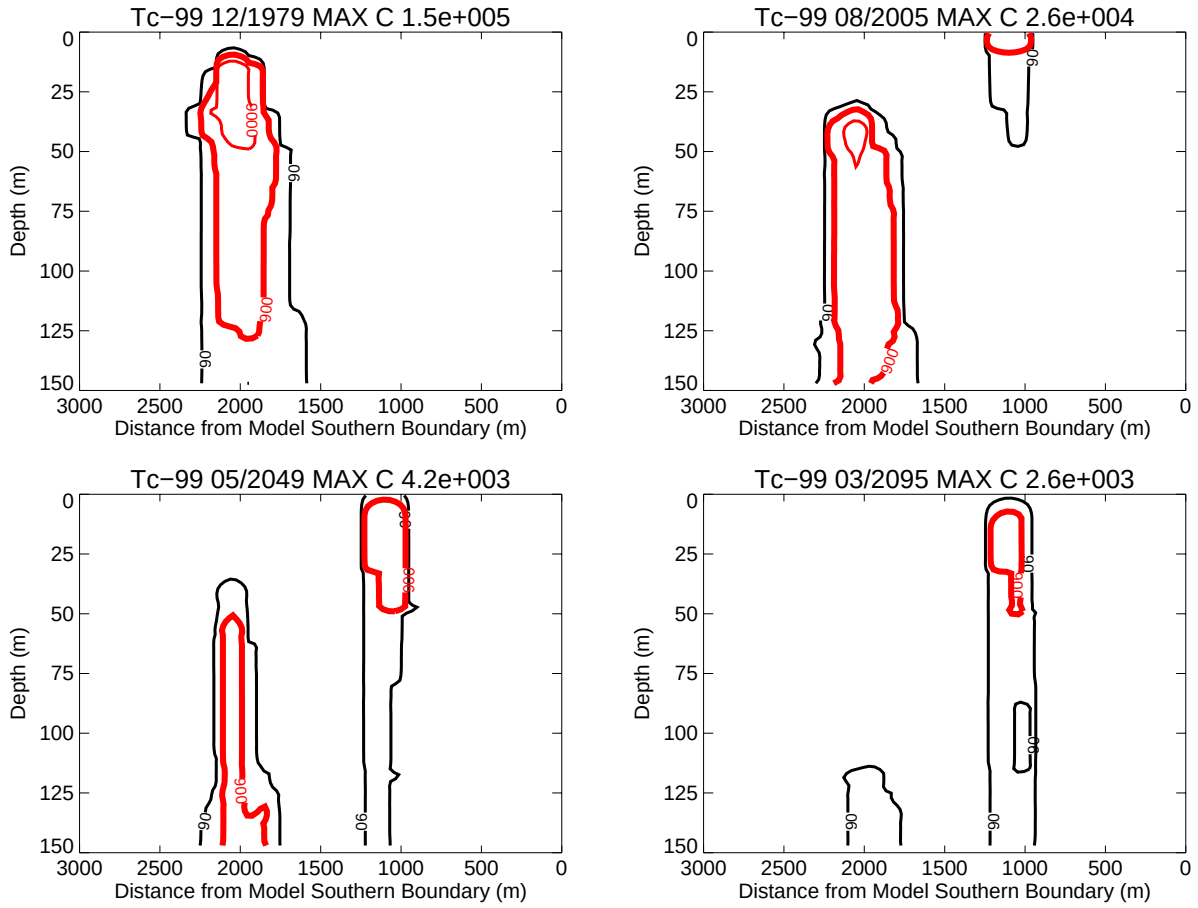

Figure A-10-4. Tc-99 vertical vadose zone concentrations (pCi/L) for the highest conductance case (MCL = thick red, MCL/10 = thin black, MCL*10 = thin red).

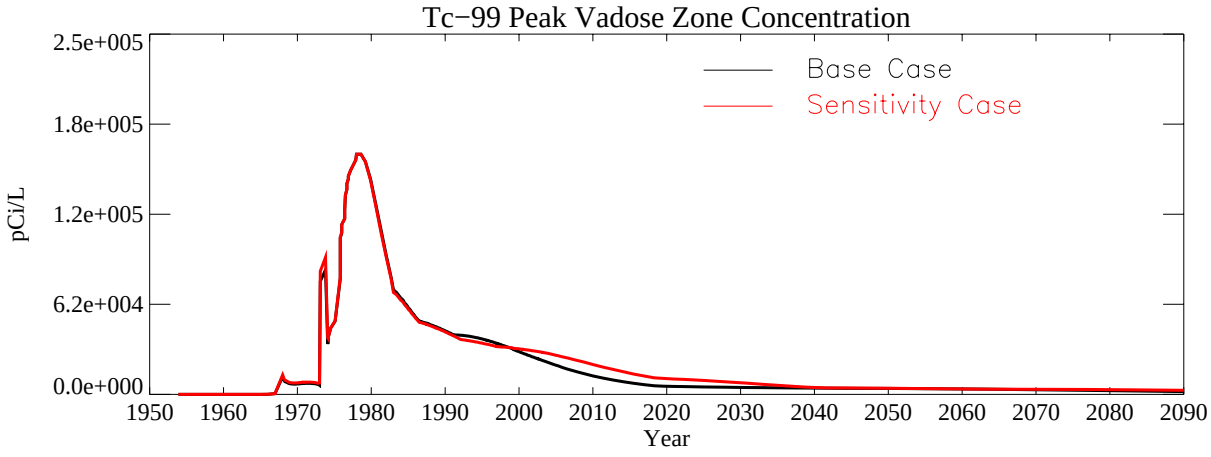

Figure A-10-5. Tc-99 peak vadose zone concentrations (excluding submodel area) (pCi/L) for the highest conductance case.

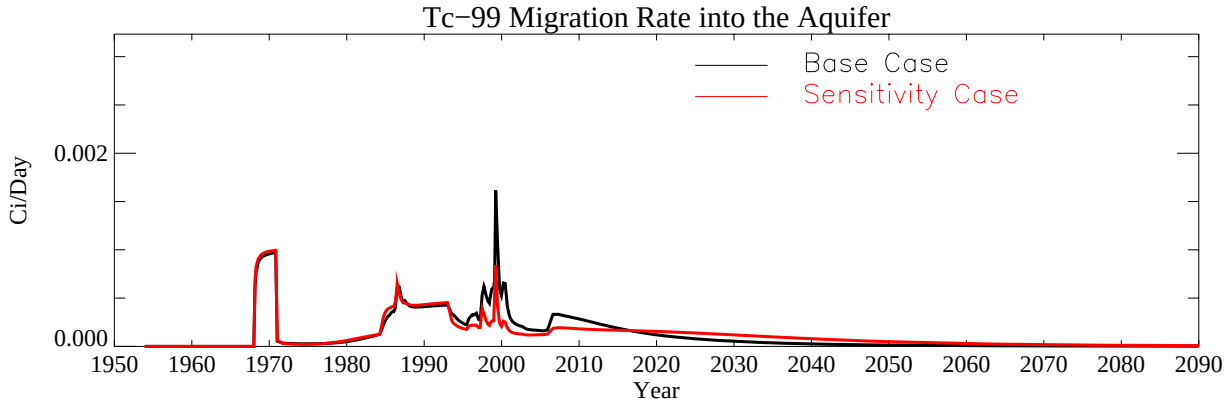

Figure A-10-6. Tc-99 flux into the aquifer (Ci/day) for the highest conductance case.

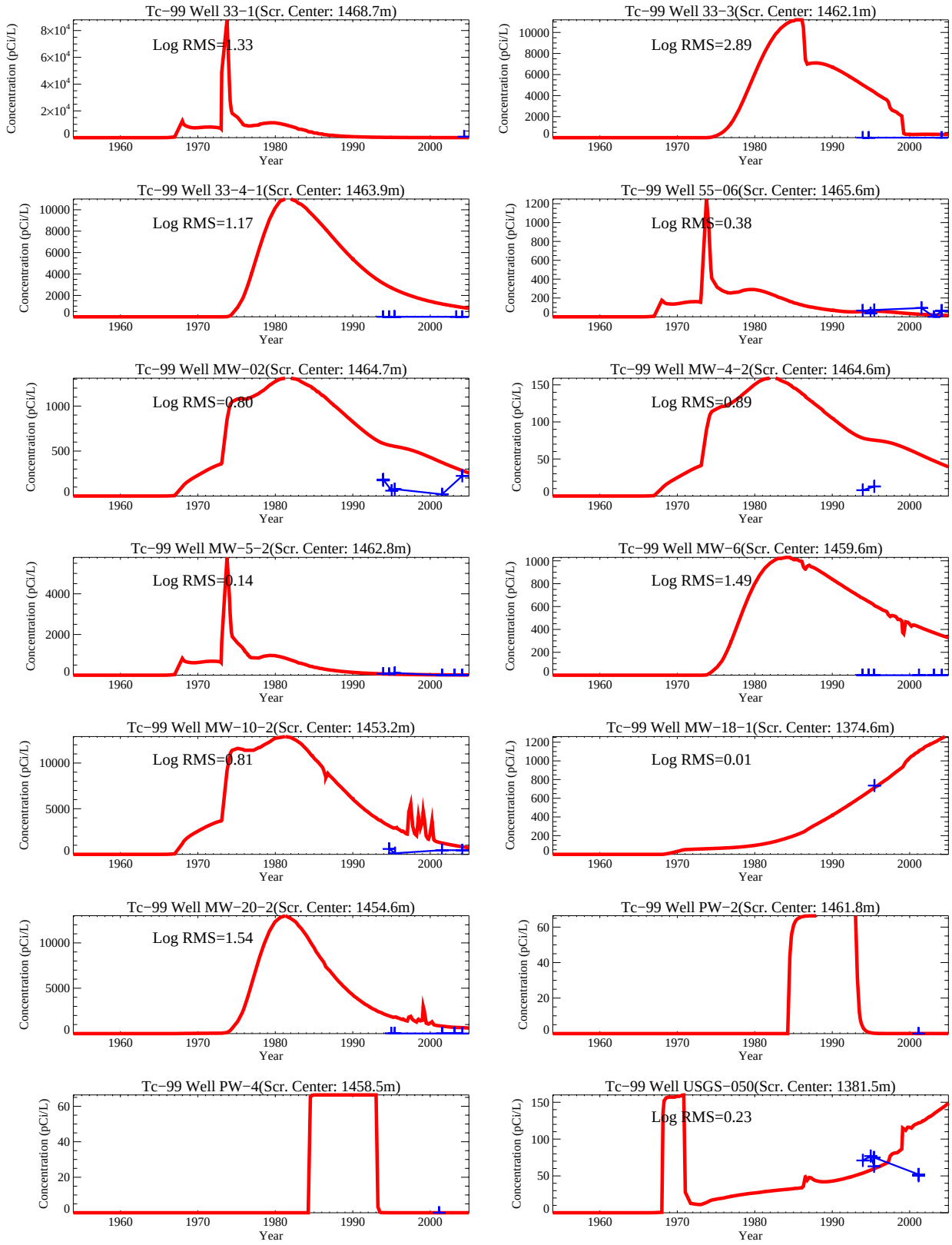

Figure A-10-7. Tc-99 concentration (pCi/L) in perched water wells for the highest conductance case (measured values = blue crosses, red = model at screen center).

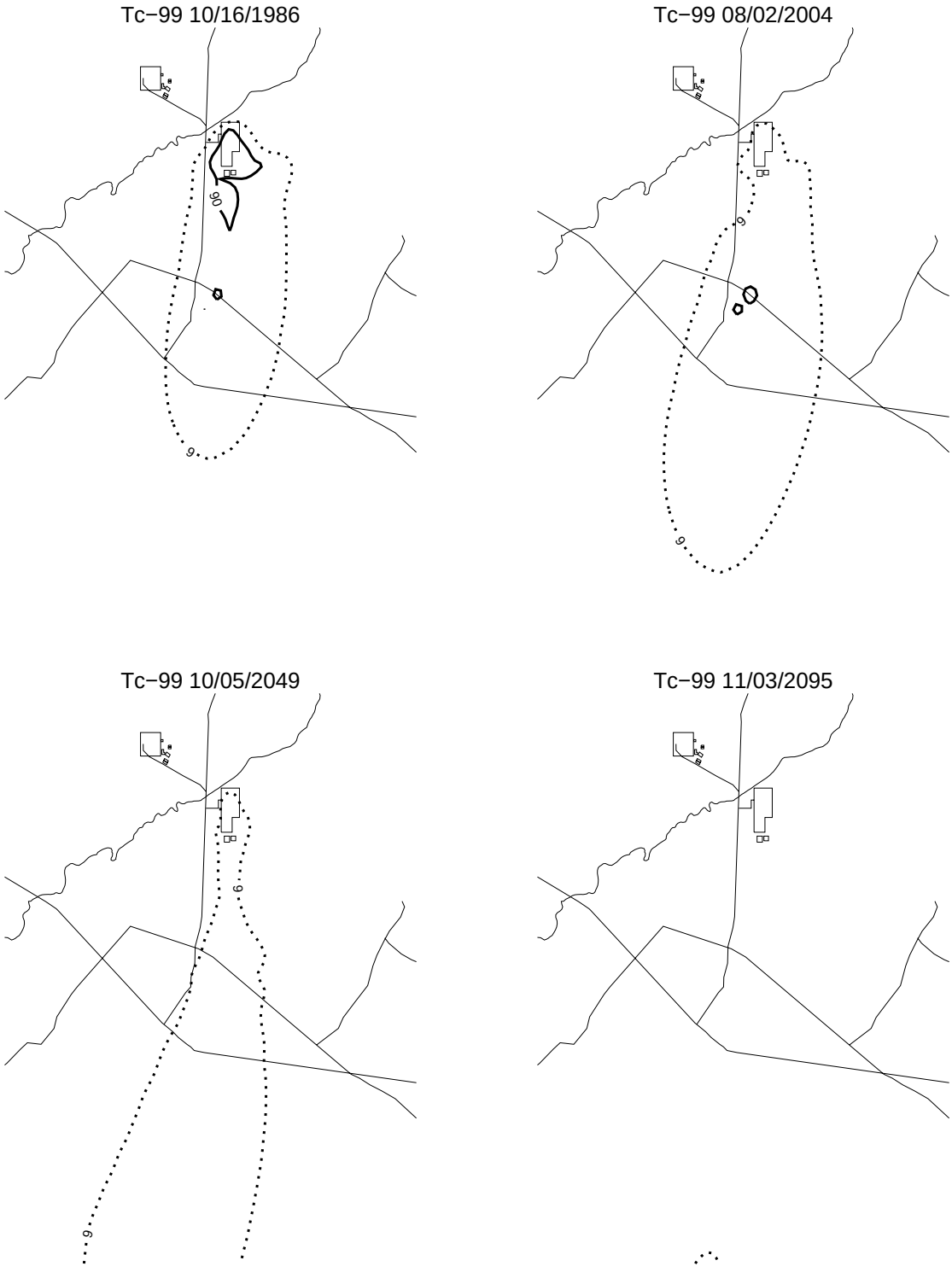

Figure A-10-8. Tc-99 aquifer concentrations (pCi/L) for the highest conductance case (MCL*10 = thin red, MCL = thick red, MCL/10 = thin black, MCL/100 = thin black dashed).

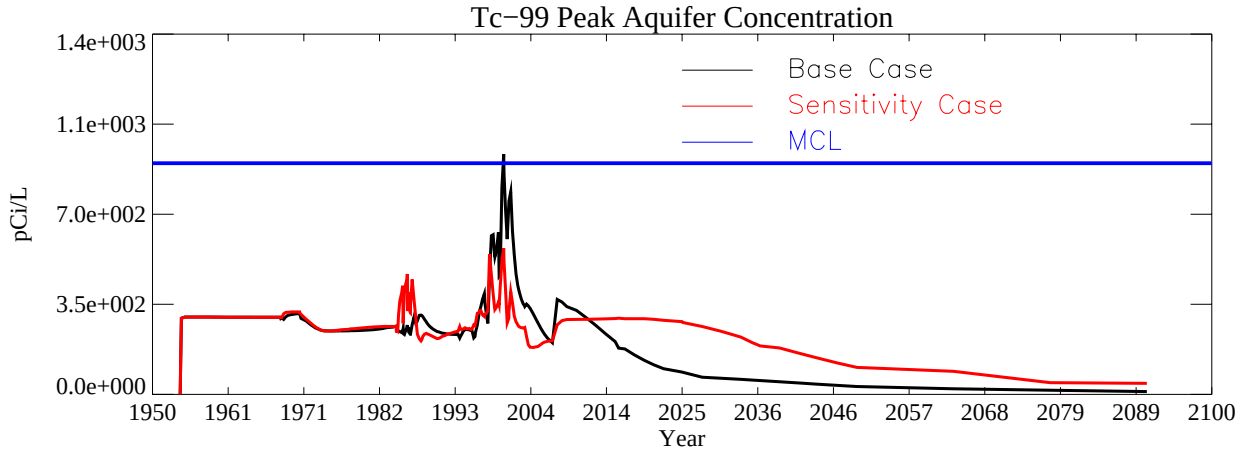

Figure A-10-9. Tc-99 peak aquifer concentrations (pCi/L) for the highest conductance case.

A-10.1.1.2 Lowest Interbed Conductance for Tc-99

The peak simulated concentration in the vadose zone for this case was 1.64e+5 pCi/L in 1972 and coincides with the CPP-31 release date. The simulated peak concentration declined to 2.71e+4 pCi/L in 2005 and to 2.56e+3 pCi/L in 2095. Figures A-10-10 and A-10-11 illustrate the vertical and lateral extent of the simulated vadose zone concentrations. The shallow vadose zone contamination located immediately northwest of the former percolation ponds is due to the CPP-22 OU 3-13 soil site (0.1 Ci), which was placed in the model in 1990.

Figure A-10-12 illustrates the peak vadose zone concentration through time. The Tc-99 activity flux into the aquifer is illustrated in Figure A-10-13 and indicates that the peak rate occurred during the CPP-3 injection well failure period. A second maximum occurred in the year 1999 following the peak flow year for the Big Lost River recorded at Lincoln Boulevard bridge gauge from the tank farm releases. As with the minimum interbed sensitivity simulation, the Big Lost River does not spread as far horizontally and does not increase activity arrival in the aquifer to the same extent as the base case. This was not expected and is because the maximum interbed simulation has a different slope for the 110-ft interbed and does not direct as much river water towards the tank farm. The Tc-99 concentration in key perched water wells is illustrated in Figure A-10-14.

The effect of decreasing the interbed permeability and increasing thickness was similar to that of the minimum thickness and maximum permeability because both sensitivity realizations of the vadose zone lithology decreased the dip of the 140-ft interbed towards the tank farm. The result was that the Big Lost River water did not move as far horizontally towards the tank farm as the base case and the mass flux into the aquifer after the Big Lost River's peak flow year recorded at Lincoln Boulevard bridge gauge in 1999 was less than the base case.

Figure A-10-15 illustrates the horizontal aquifer concentrations, and peak aquifer concentrations through time are given in Figure A-10-16. The maximum interbed sensitivity case decreased the peak aquifer concentrations at the water table from the peak Big Lost River flow year in 1999. During higher flow years the Big Lost River influence was less than the base case. This result is counter intuitive, but occurs because the increased interbed realization's 140 foot interbed did not slope towards the tank farm to the same extent as the base case. The peak aquifer concentration in the year 2095 was 45 pCi/L and was nearly four times the base case.

Figure A-10-10. Tc-99 horizontal vadose zone concentrations (pCi/L) for the lowest conductance case (MCL = thick red, MCL/10 = thin black, MCL*10 = thin red).

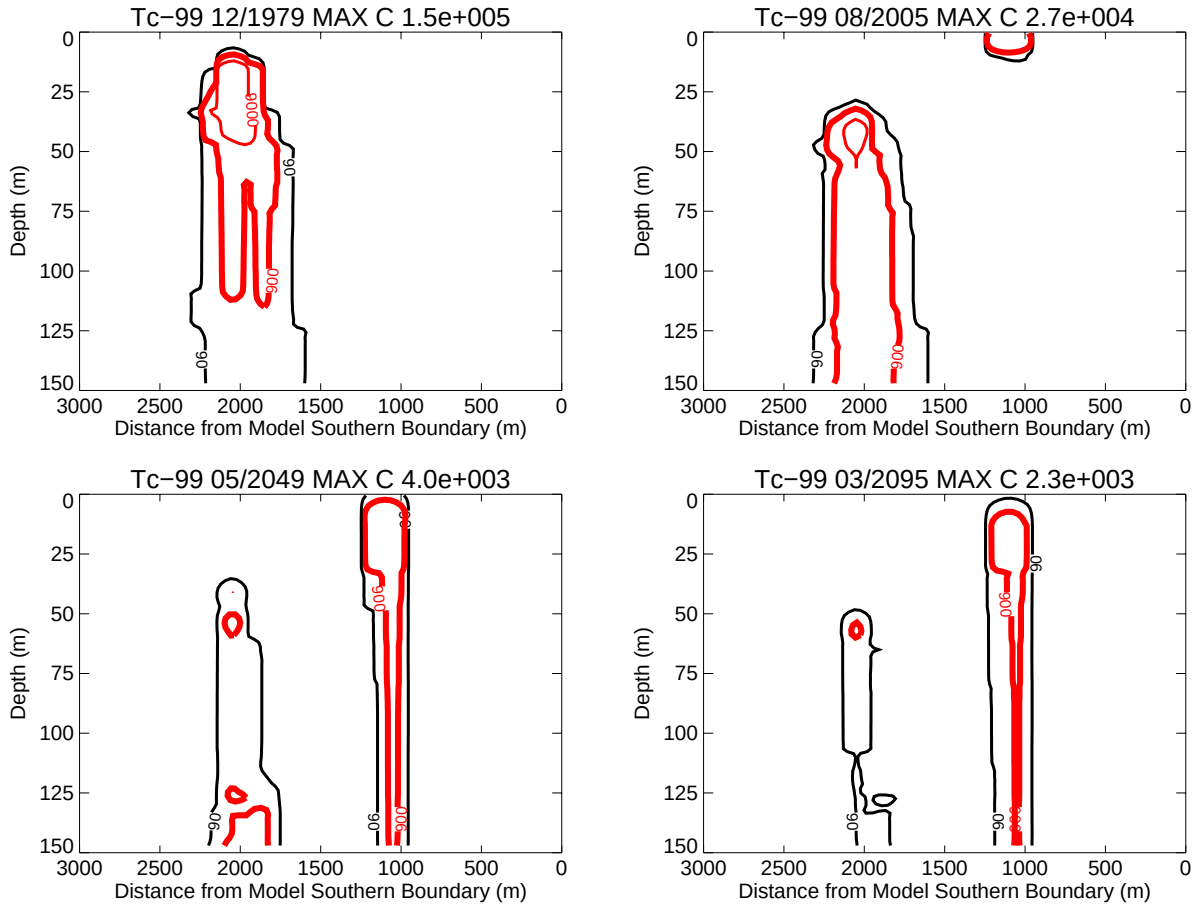

Figure A-10-11. Tc-99 vertical vadose zone concentrations (pCi/L) for the lowest conductance case (MCL = thick red, MCL/10 = thin black, MCL*10 = thin red).

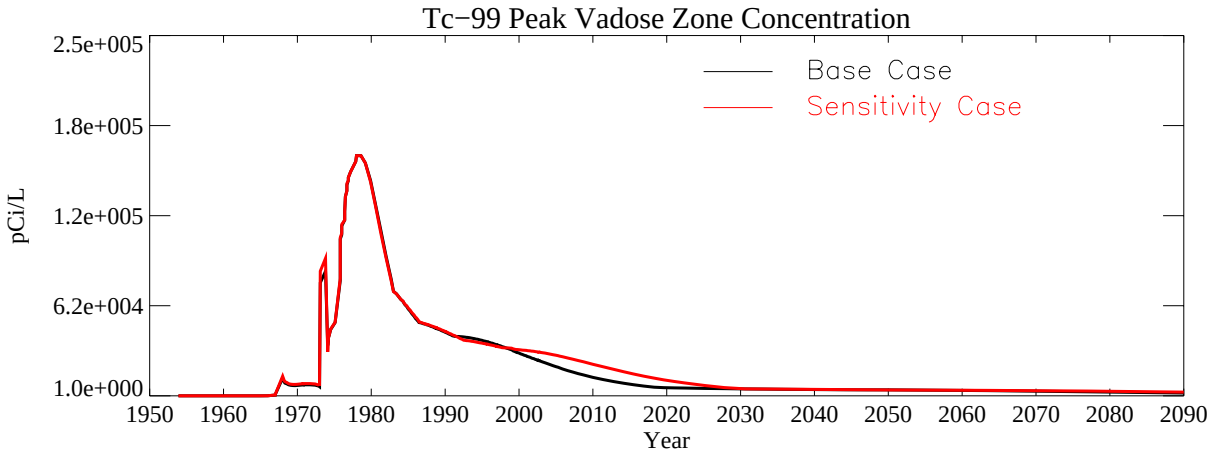

Figure A-10-12. Tc-99 peak vadose zone concentrations (excluding submodel area) (pCi/L) for the lowest conductance case.

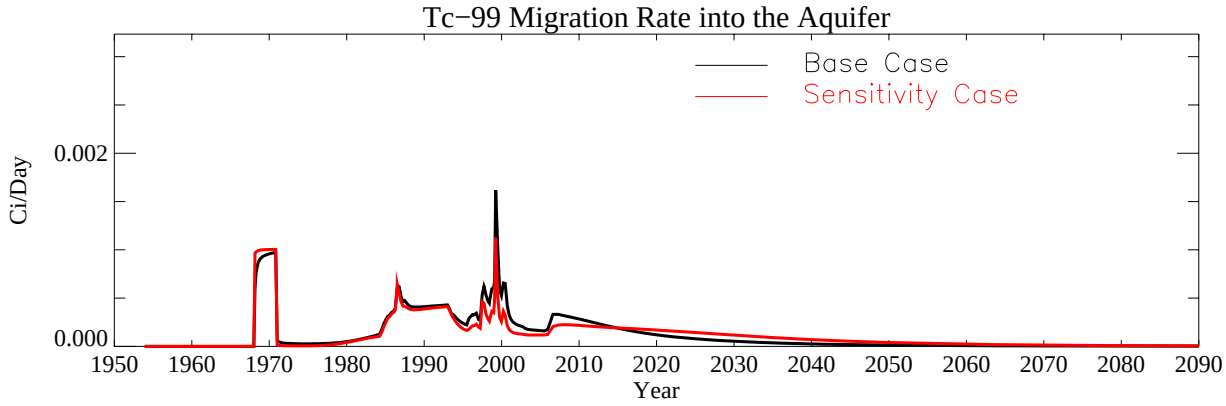

Figure A-10-13. Tc-99 flux into the aquifer (Ci/day) for the lowest conductance case.

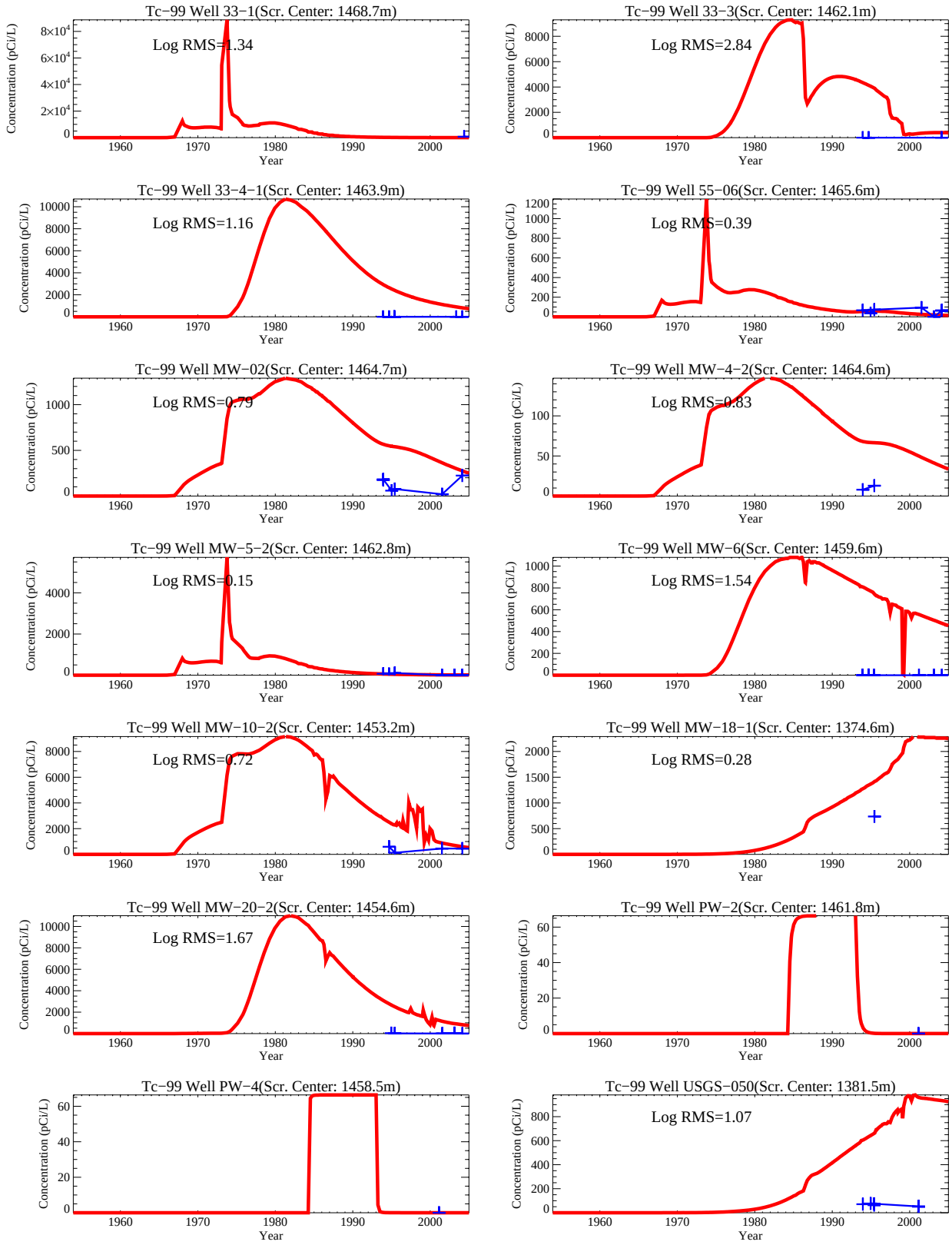

Figure A-10-14. Tc-99 concentrations (pCi/L) for the lowest conductance case (measured values = blue crosses, red = model at screen center).

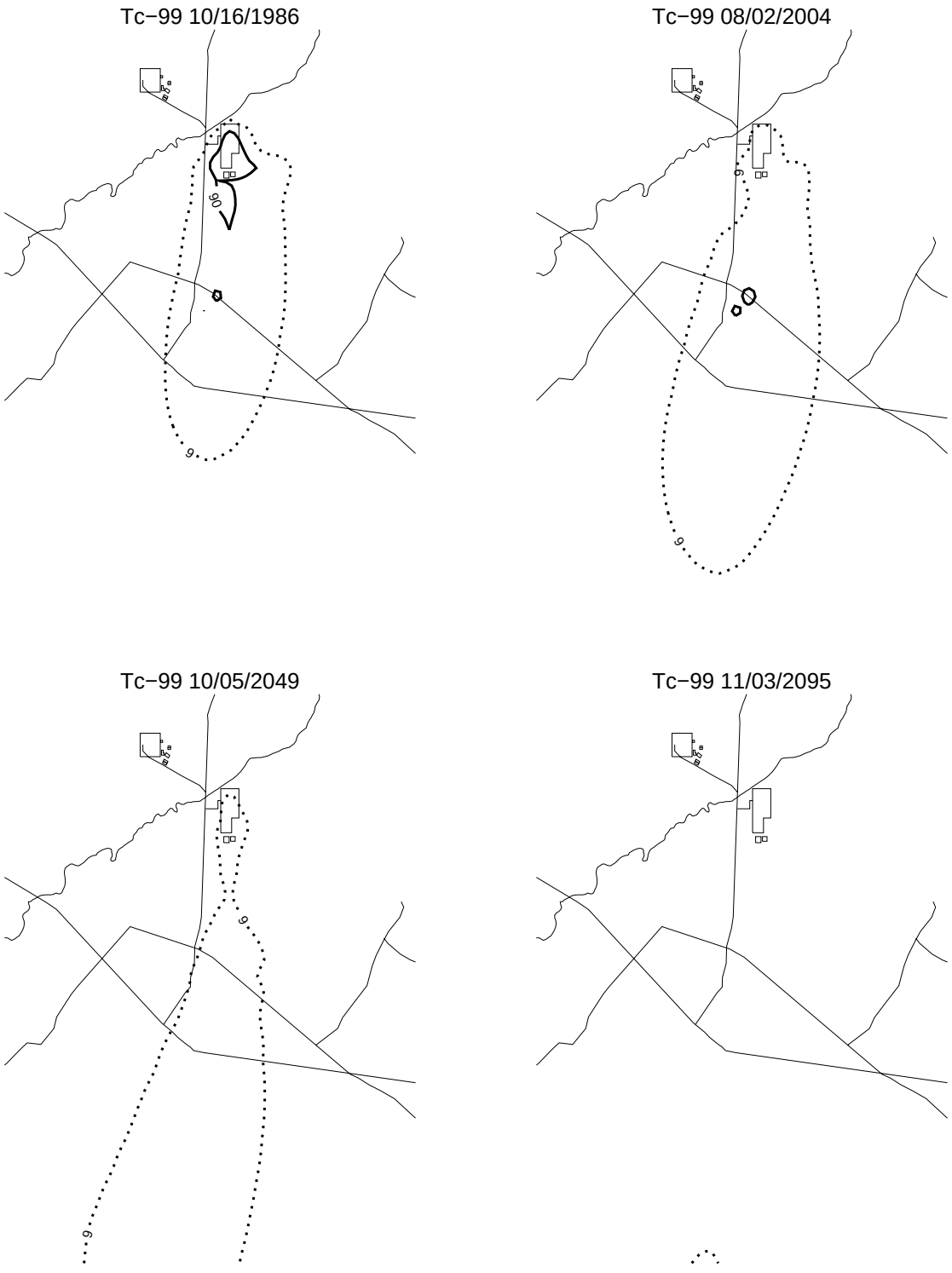

Figure A-10-15. Tc-99 aquifer concentrations (pCi/L) for the lowest conductance case (MCL*10 = thin red, MCL = thick red, MCL/10 = thin black, MCL/100 = thin black dashed).

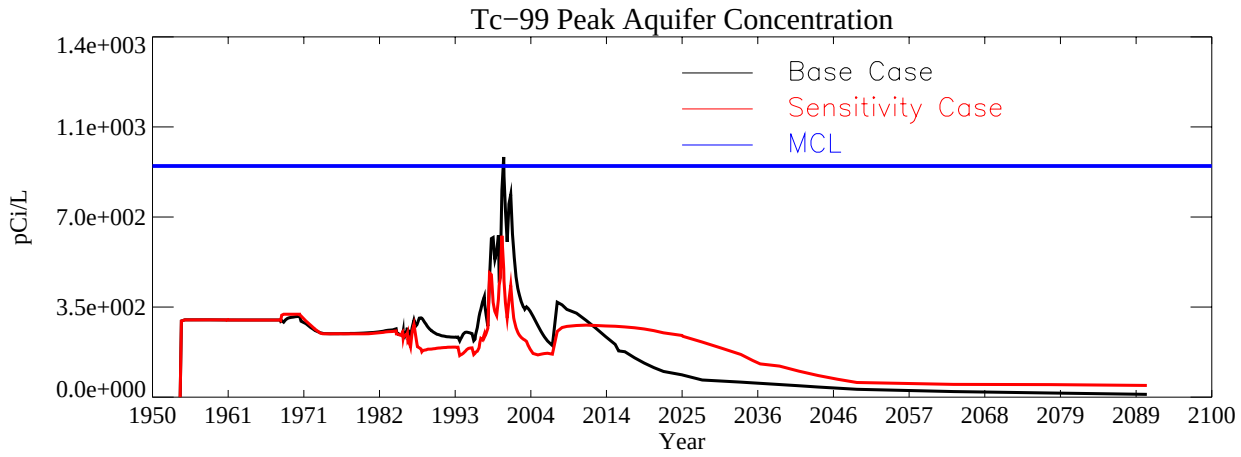

Figure A-10-16. Tc-99 peak aquifer concentrations (pCi/L) for the lowest conductance case.

A-10.1.2 Recharge Rate

Infiltrating water moving down through the contaminated soil mobilizes contaminants and eventually transports them to the aquifer. It is the primary mechanism by which tank farm sources contaminate the Snake River Plain Aquifer. In the base case simulations, the infiltration rate was spatially varying across the INTEC, with an average value, excluding the Big Lost River and former percolation ponds, of 29 cm/year being applied. This value included approximately 11 cm/year of anthropogenic water (i.e., lawn irrigation, steam vents, line leaks, etc.) and 18 cm/year of precipitation infiltration. The base case known recharge sources were applied at the known location (i.e., lawn irrigation areas or sanitary sewer systems [septic tanks] not using the central sewage treatment lagoon). The location of the water supply and fire suppression lines leaks are unknown, and the estimated recharge was uniformly distributed across the entire INTEC facility. The volumetric total of all anthropogenic water sources was approximately 9 M gal/year.

The base case simulated infiltration rate through the tank farm was limited to a precipitation infiltration rate of only 18 cm/year because the net infiltration through the tank farm was calculated through parameter estimation using tank farm soil moisture measurements taken during the spring of 1994 (see Appendix B). The resultant precipitation infiltration rate was determined to be spatially variable across the tank farm and ranged from 2.8 cm/year to 39 cm/year with an average value of 18 cm/year.

The model's sensitivity to the tank farm recharge rate and anthropogenic recharge rate outside the tank farm was investigated by applying a high and low value in place of the 18 cm/year through the tank farm and by using the maximum possible anthropogenic recharge rate outside the tank farm. The recharge sensitivity investigation included three simulations: (1) a low tank farm infiltration rate (3 cm/year) with base case anthropogenic recharge outside the tank farm, (2) a high tank farm infiltration rate (39 cm/year) with base case anthropogenic recharge, and (3) a maximum anthropogenic recharge rate estimated from the water production/ disposal imbalance (maximum of 52 M gal assuming all water is accurately metered and there are no losses to evaporation) with the base case tank farm recharge (18 cm/year).

The maximum anthropogenic recharge scenario represents the worst possible case for water infiltration to the northern perched water and assumes the following: (1) all unaccounted water goes into the ground, (2) the values from the 2004 water balance can be applied to any general time frame, and (3) all water infiltrates in northern INTEC around the high-density infrastructure area.

The maximum anthropogenic recharge rate was estimated from the water imbalance between water production and known final disposal. Recent monitoring of the INTEC water production and final use indicates

that approximately 10 to 11% of the water produced is unaccounted for. The total water usage in 2004 was approximately 495 M gal and 10.5% of this volume suggests an upper maximum of approximately 52 M gal could be discharged to the ground. However, this assumes all water meters are accurate and there are no losses to evaporation. The density of utilities at the INTEC also suggests that the discharge would be focused on northern INTEC in an area of approximately 49 acres surrounding the tank farm.

The maximum anthropogenic water recharge scenario was simulated by using the 2004 water imbalance recharge rate resulting from 52 M gal infiltrating across 49 acres (98 cm/year). This infiltration was in addition to the estimated recharge from infiltration of 18 cm/year (116 cm/year total). The simulated water was placed in the area surrounded by Palm Avenue, Hemlock Street, Ash Avenue, and the western INTEC security fence. The area beneath Building CPP-666 was also included. The area directly below the tank farm area was excluded and used the 18-cm/year precipitation recharge, because most utilities do not run through the tank farm and the high and low tank farm infiltration sensitivity simulations assessed the sensitivity of tank farm contaminant mobility to recharge rate. Sections A-10.1.2.1 and A-10.1.2.2 present the results of the low and high tank farm recharge rate sensitivity, respectively. Section A-10.1.2.3 presents the results of the maximum anthropogenic recharge rate sensitivity.

A-10.1.2.1 Tc-99 with 3-cm/year Tank Farm Recharge Rate

The peak simulated concentration in the vadose zone for this case was 1.01e+6 pCi/L in 1977 and occurs after the CPP-31 release date. The peak simulated concentration declined to 5.47e+4 pCi/L in 2005 and to 8.26e+3 pCi/L in 2095. Figures A-10-17 and A-10-18 present the vertical and lateral extent of the simulated vadose zone concentrations. The shallow vadose zone contamination located immediately northwest of the former percolation ponds is due to the CPP-22 OU 3-13 soil site (0.1 Ci), which was placed in the model in 1990.

Figure A-10-19 shows the peak vadose zone concentration through time and shows that the predicted peak vadose zone concentration remained above the MCL throughout the end of the simulation in 2095. Peak vadose zone concentrations are slightly higher than the base case. The Tc-99 activity flux into the aquifer is illustrated in Figure A-10-20 and shows that the peak Tc-99 flux into the aquifer during peak Big Lost River flow is less than the base case. This is because Tc-99 moves slower through the vadose zone and less Tc-99 resides in the 380-ft interbed during peak river flows. The Tc-99 concentration in key perched water wells is illustrated in Figure A-10-21.

Figure A-10-22 illustrates the horizontal aquifer concentrations, and the peak aquifer concentrations through time are given in Figure A-10-23. Peak aquifer concentrations resulting from the minimum recharge simulation are less than the base case, because the lower infiltration does place the bulk of the tank farm Tc-99 in the 380 ft interbed during peak Big Lost River flow (1999). The majority of the Tc-99 is higher in the vadose zone, where the influence of the river is less. The peak concentration in the year 2095 is 39 pCi/L, which is higher than the base case. This is because the lower infiltration rate results in a slower breakthrough to the aquifer. The base case Tc-99 concentrations have been declining for a longer period of time at the year 2095 than the 3-cm/year infiltration rate case.

Figure A-10-17. Tc-99 horizontal vadose zone concentrations (pCi/L) for the 3-cm/year tank farm recharge rate case (MCL = thick red, MCL/10 = thin black, MCL*10 = thin red).

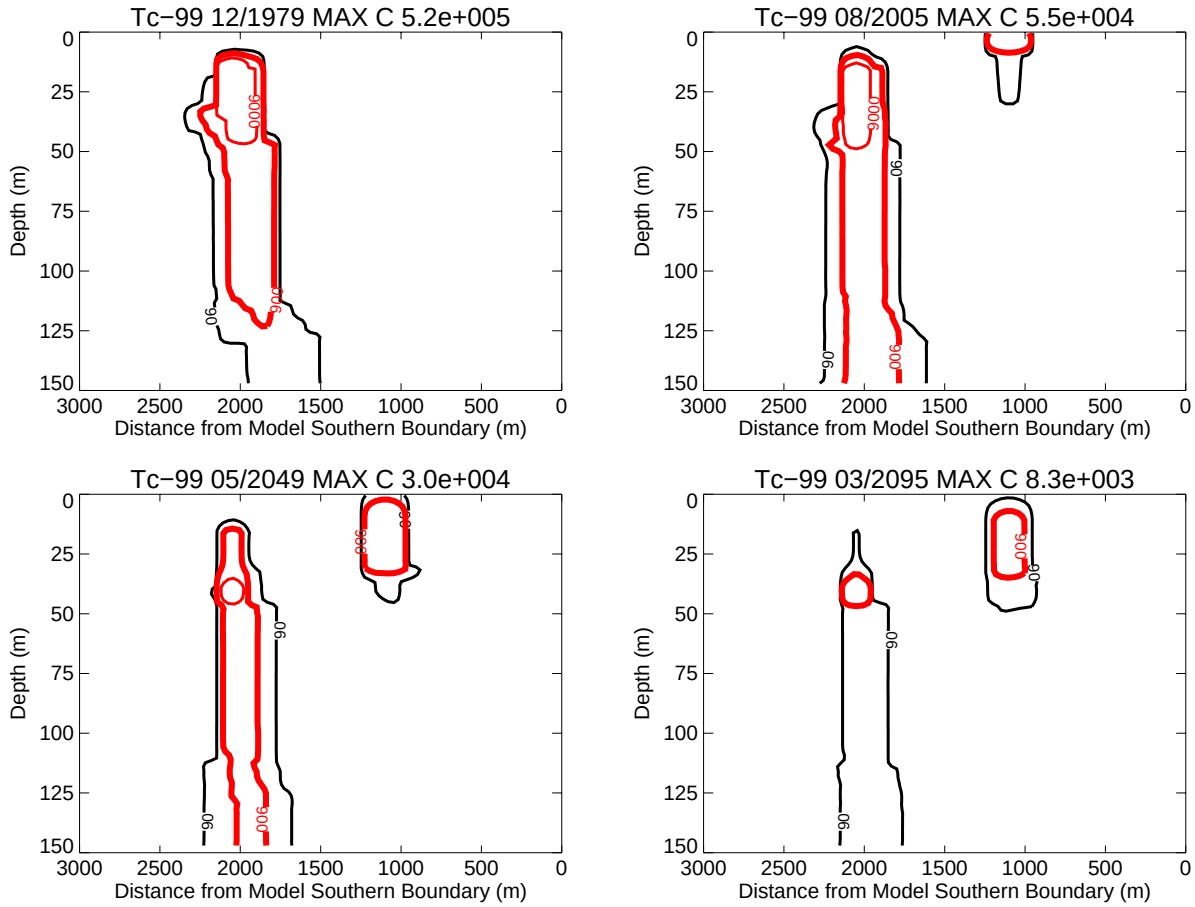

Figure A-10-18. Tc-99 vertical vadose zone concentrations (pCi/L) for the 3-cm/year tank farm recharge rate case (MCL = thick red, MCL/10 = thin black, MCL*10 = thin red).

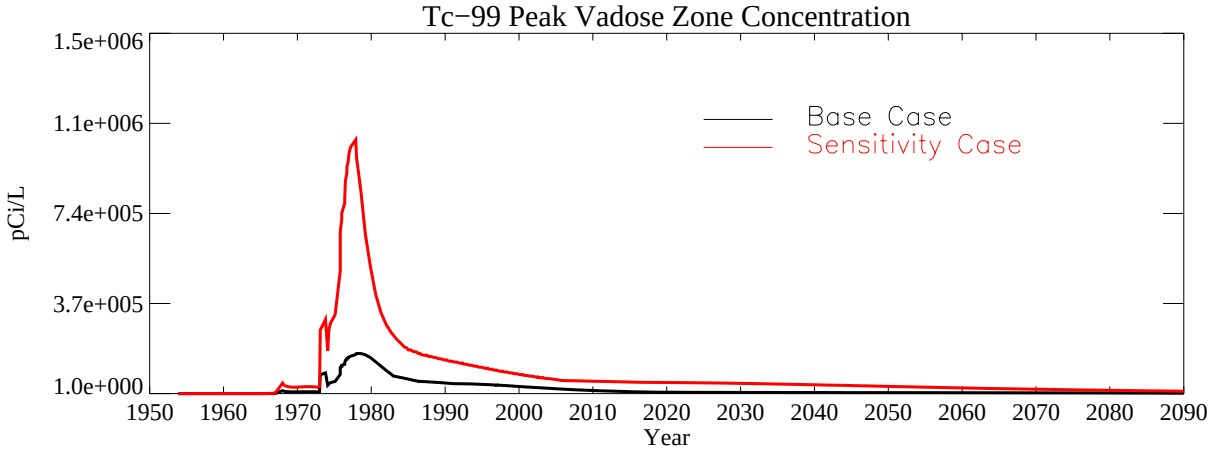

Figure A-10-19. Tc-99 peak vadose zone concentrations (pCi/L) (excluding submodel area) for the 3-cm/year tank farm recharge rate case.

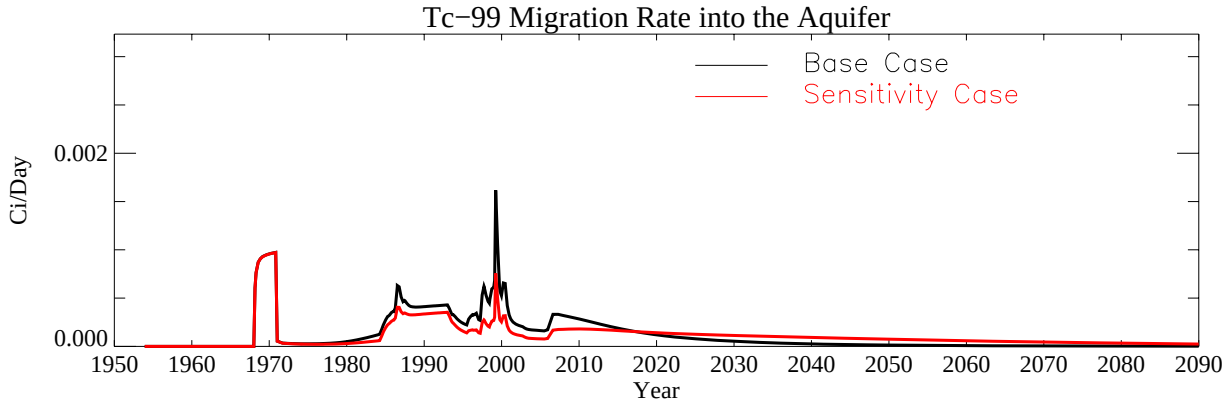

Figure A-10-20. Tc-99 flux into the aquifer (Ci/day) for the 3-cm/year tank farm recharge rate case.

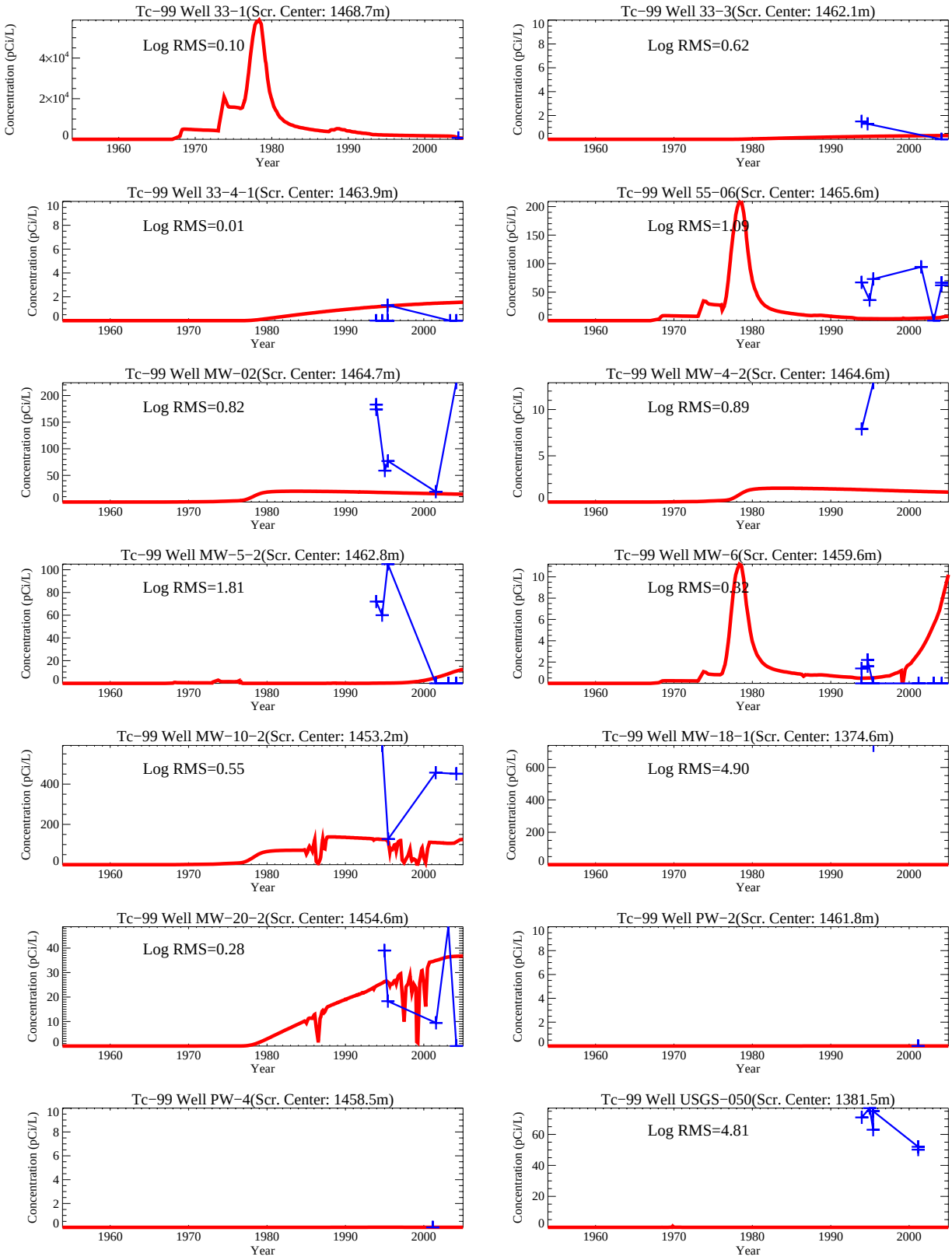

Figure A-10-21. Tc-99 concentration (pCi/L) in perched water wells for the 3-cm/year tank farm recharge rate case (measured values = blue crosses, red = model at screen center).

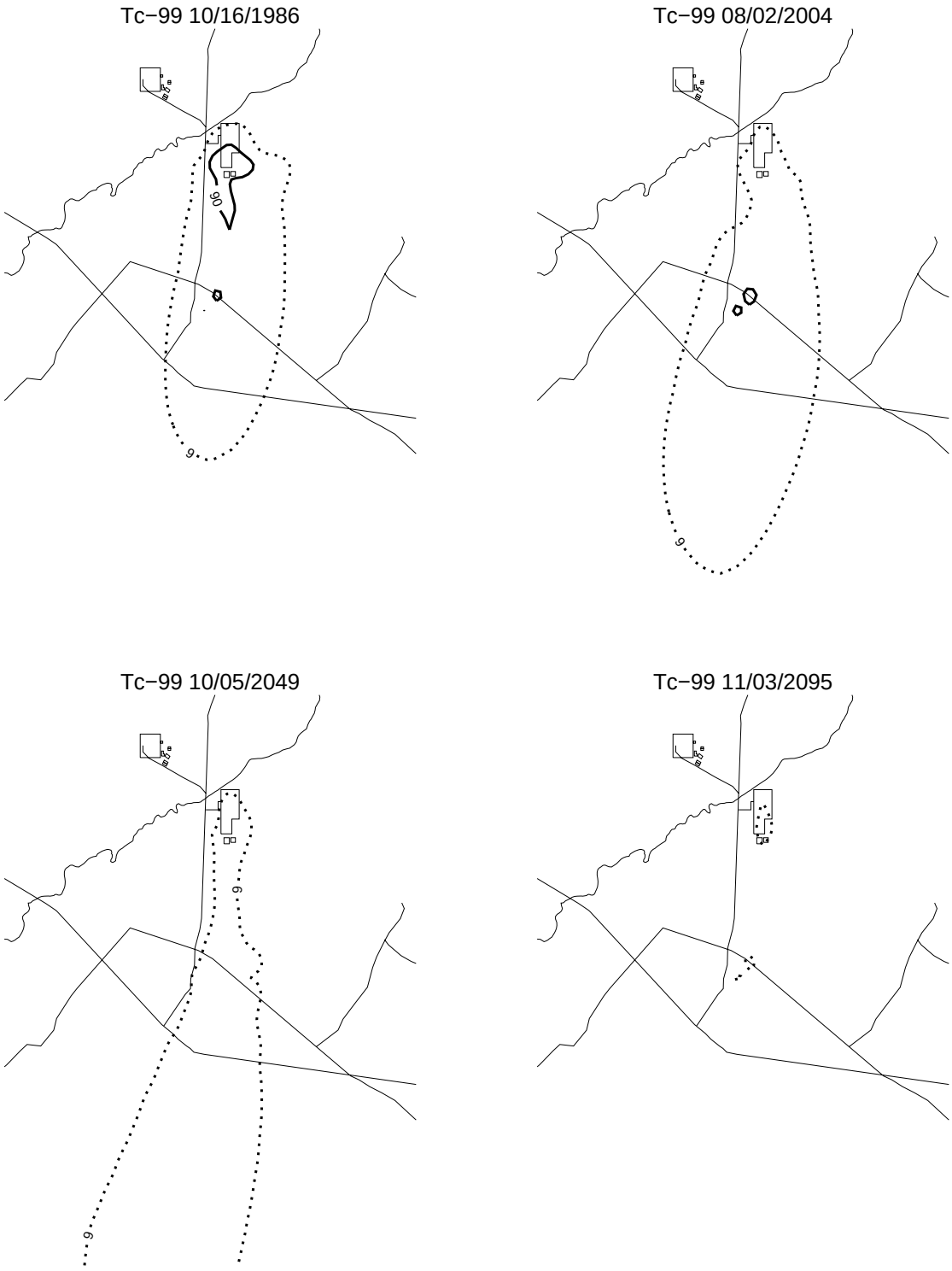

Figure A-10-22. Tc-99 aquifer concentrations (pCi/L) for the 3-cm/year tank farm recharge rate case (MCL*10 = thin red, MCL = thick red, MCL/10 = thin black, MCL/100 = thin black dashed).

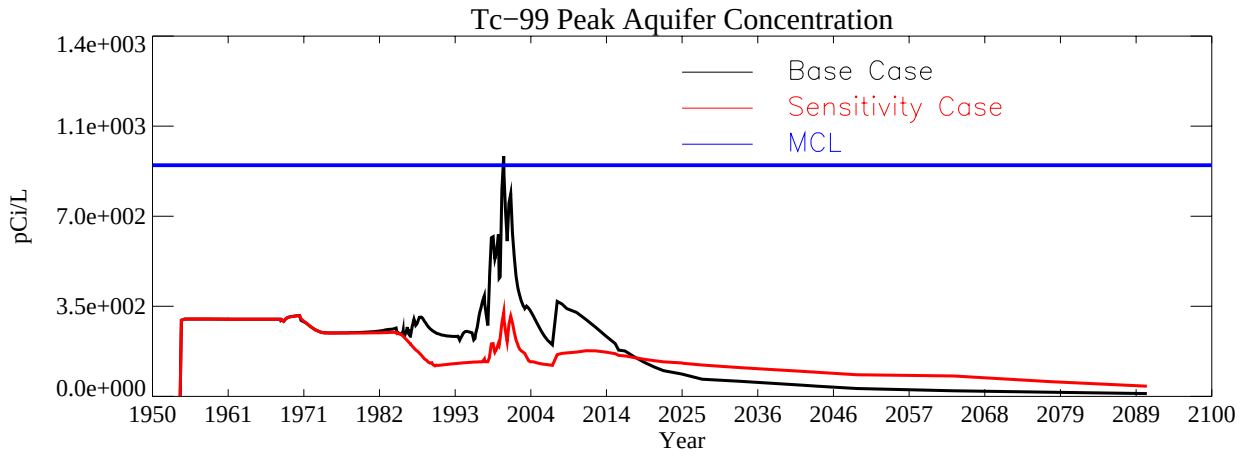

Figure A-10-23. Tc-99 peak aquifer concentration (pCi/L) for the 3-cm/year tank farm recharge rate case.

A-10.1.2.2 Tc-99 with 39-cm/year Tank Farm Recharge Rate

The peak simulated concentration in the vadose zone for this case was 1.49e+5 pCi/L in 1978 and is after the CPP-31 release date. The peak simulated concentration declined to 7.60e+3 pCi/L in 2005 and to 1.69e+3 pCi/L in 2095. Figures A-10-24 and A-10-25 illustrate the vertical and lateral extent of the simulated vadose zone concentrations. The shallow vadose zone contamination located immediately northwest of the former percolation ponds is due to the CPP-22 OU 3-13 soil site (0.1 Ci), which was placed in the model in 1990.

Figure A-10-26 illustrates the peak vadose zone concentration through time. The Tc-99 activity flux into the aquifer is illustrated in Figure A-10-27 and indicates that the tank farm Tc-99 is arriving slightly earlier than the base case. The Tc-99 concentration in key perched water wells is illustrated in Figure A-10-28.

The primary difference between the base case and the higher recharge sensitivity case is that the Tc-99 is transported through the vadose zone faster than the base case. This results in a slightly earlier breakthrough to the aquifer. However, breakthrough and aquifer concentrations were similar to the base case.

Figure A-10-29 illustrates the horizontal aquifer concentrations, and Figure A-10-30 illustrates peak aquifer concentrations through time. The peak aquifer concentration in the year 2095 was 10 pCi/L, which was similar to the base case.

Figure A-10-24. Tc-99 horizontal vadose zone concentrations (pCi/L) for the 39-cm/year tank farm recharge rate case (MCL = thick red, MCL/10 = thin black, MCL*10 = thin red).

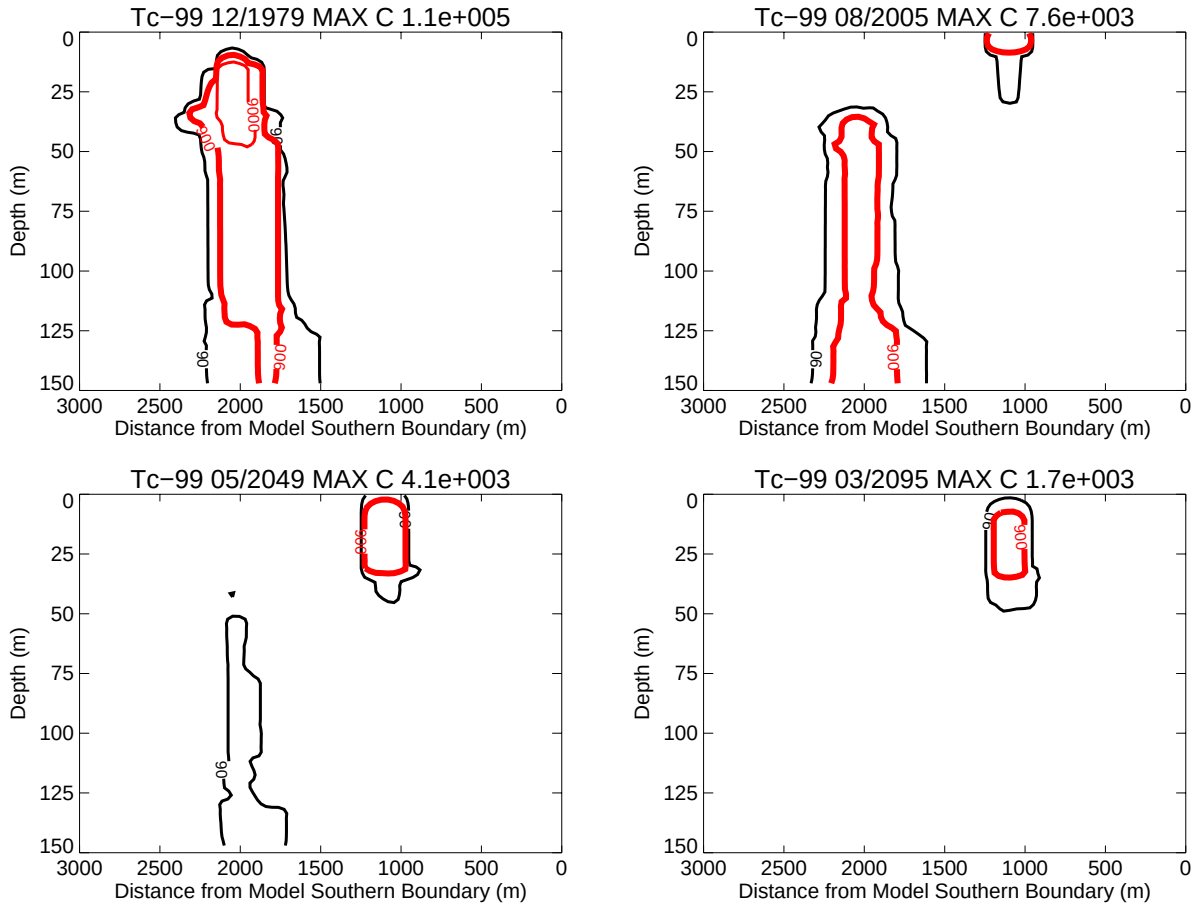

Figure A-10-25. Tc-99 vertical vadose zone concentrations (pCi/L) for the 39-cm/year tank farm recharge rate case (MCL = thick red, MCL/10 = thin black, MCL*10 = thin red).

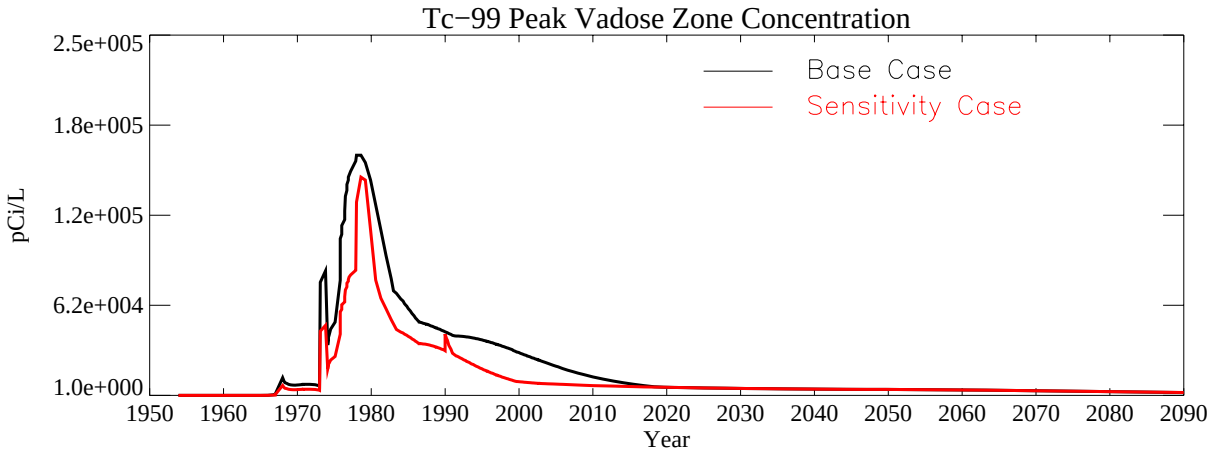

Figure A-10-26. Tc-99 peak vadose zone concentrations (excluding submodel area) (pCi/L) for the 39-cm/year tank farm recharge rate case.

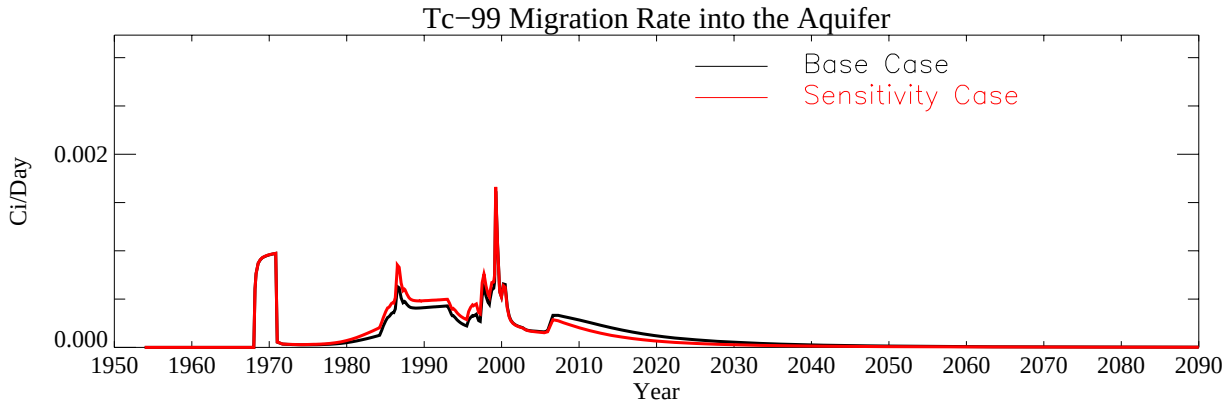

Figure A-10-27. Tc-99 flux into the aquifer (Ci/day) for the 39-cm/year tank farm recharge rate case.

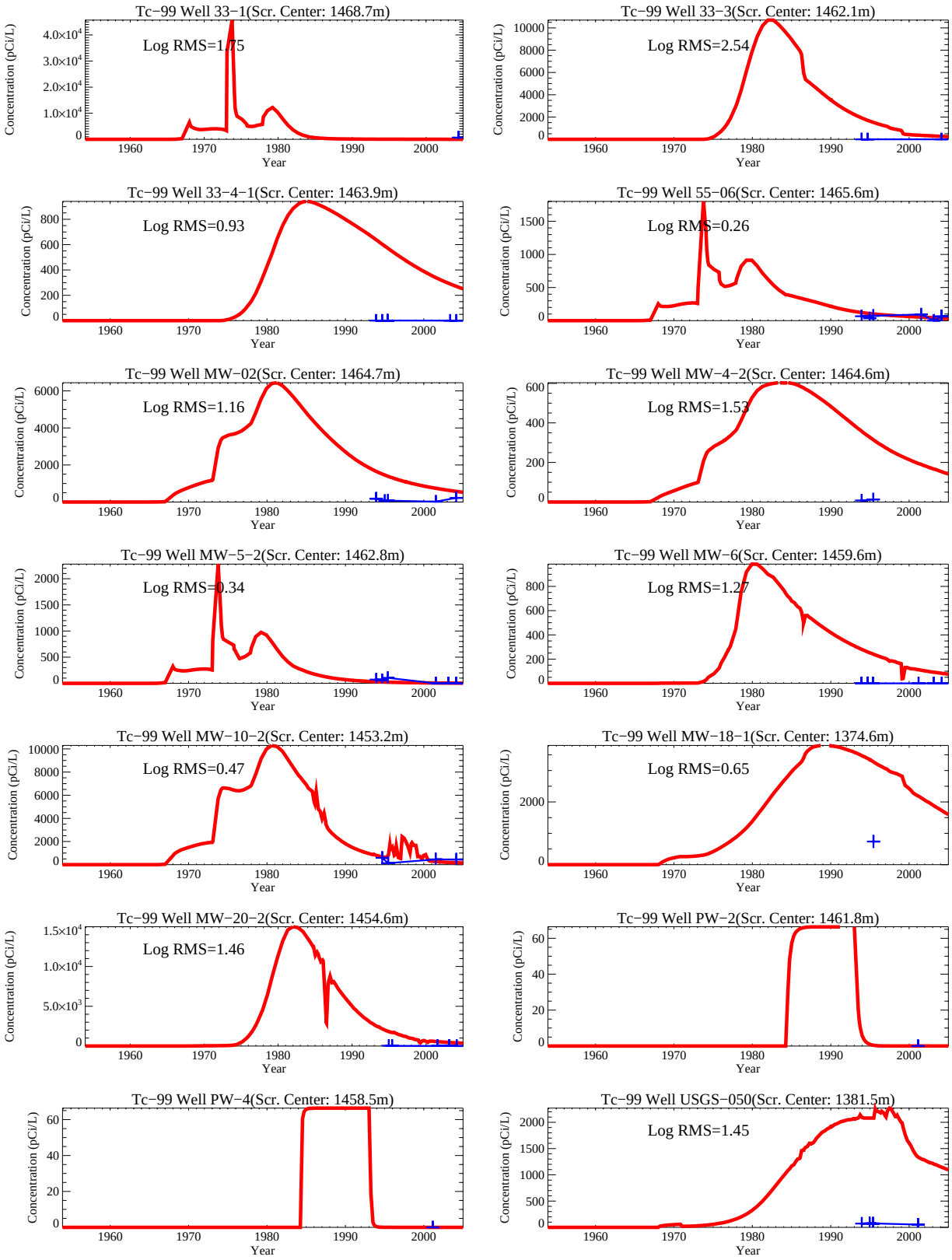

Figure A-10-28. Tc-99 concentration (pCi/L) in perched water wells for the 39-cm/year tank farm recharge rate case (measured values = blue crosses, red = model at screen center).

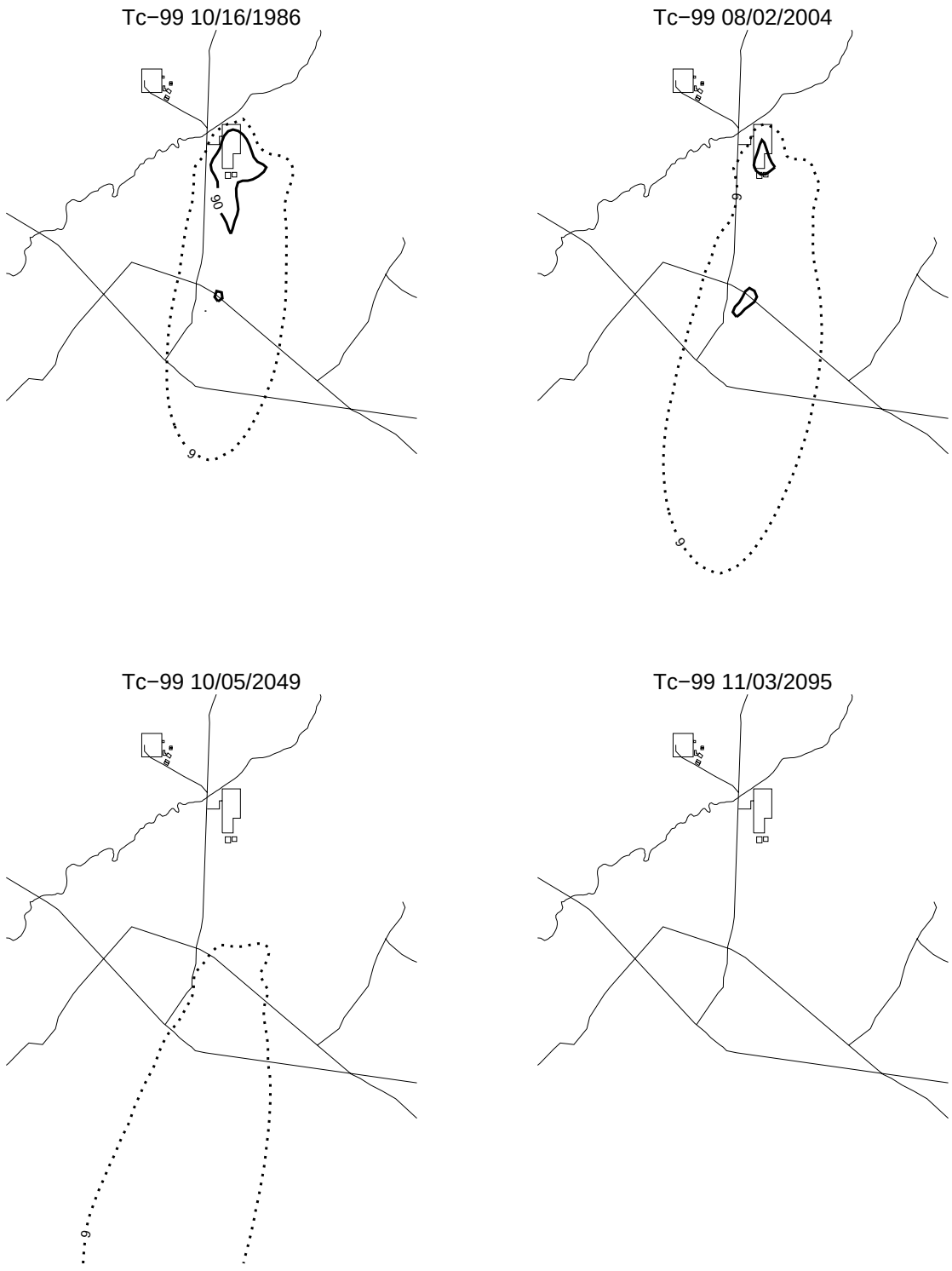

Figure A-10-29. Tc-99 aquifer concentrations (pCi/L) for the 39-cm/year tank farm recharge rate case (MCL*10 = thin red, MCL = thick red, MCL/10 = thin black, MCL/100 = thin black dashed).

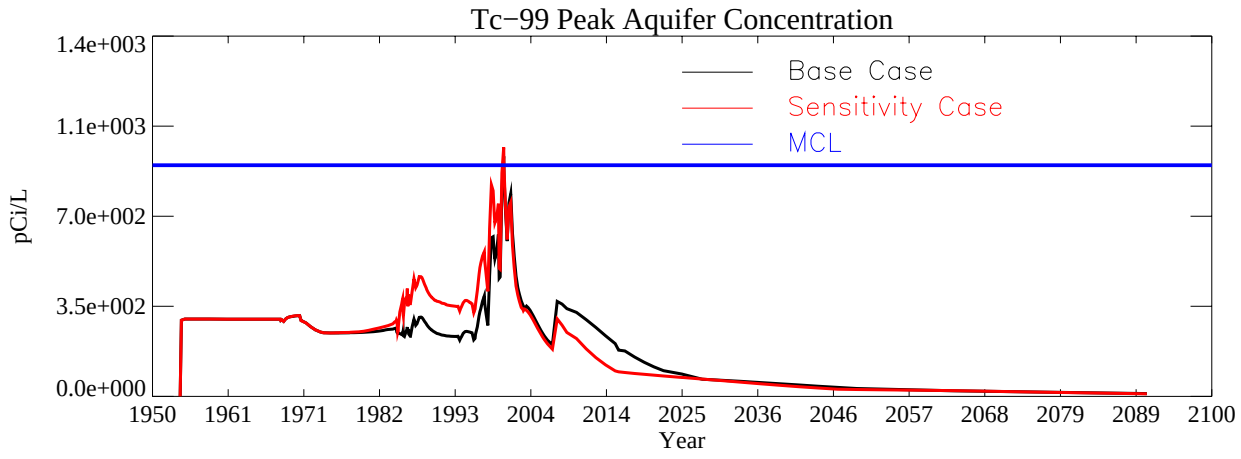

Figure A-10-30. Tc-99 peak aquifer concentration (pCi/L) for the 39-cm/year tank farm recharge rate case.

A-10.1.2.3 Tc-99 with Maximum Anthropogenic Recharge Rate

The peak simulated concentration in the vadose zone for this case was 3.34e+5 pCi/L in 1978 and occurs after the CPP-31 release date. The peak simulated concentration declined to 7.60e+3 pCi/L in 2005 and to 1.62e+3 pCi/L in 2095. Figures A-10-31 and A-10-32 present the vertical and lateral extent of the simulated vadose zone concentrations. The shallow vadose zone contamination located immediately northwest of the former percolation ponds is due to the CPP-22 OU 3-13 soil site (0.1 Ci), which was placed in the model in 1990.

Figure A-10-33 shows the peak vadose zone concentration through time. Peak vadose zone concentrations are much lower than the base case. The Tc-99 activity flux into the aquifer is illustrated in Figure A-10-34 and shows that the peak Tc-99 flux into the aquifer from the former percolation ponds and tank farm occurs much earlier than the base case. The Tc-99 concentration in key perched water wells is illustrated in Figure A-10-35.

Figure A-10-36 illustrates the horizontal aquifer concentrations, and the peak aquifer concentrations through time are given in Figure A-10-37. Peak aquifer concentrations resulting from the maximum recharge simulation are very similar to the base case, but less, and occurs earlier. The peak concentration in the year 2095 is 22 pCi/L, which is approximately two times the base case.

Figure A-10-31. Tc-99 horizontal vadose zone concentrations (pCi/L) for the maximum anthropogenic recharge rate case (MCL = thick red, MCL/10 = thin black, MCL*10 = thin red).

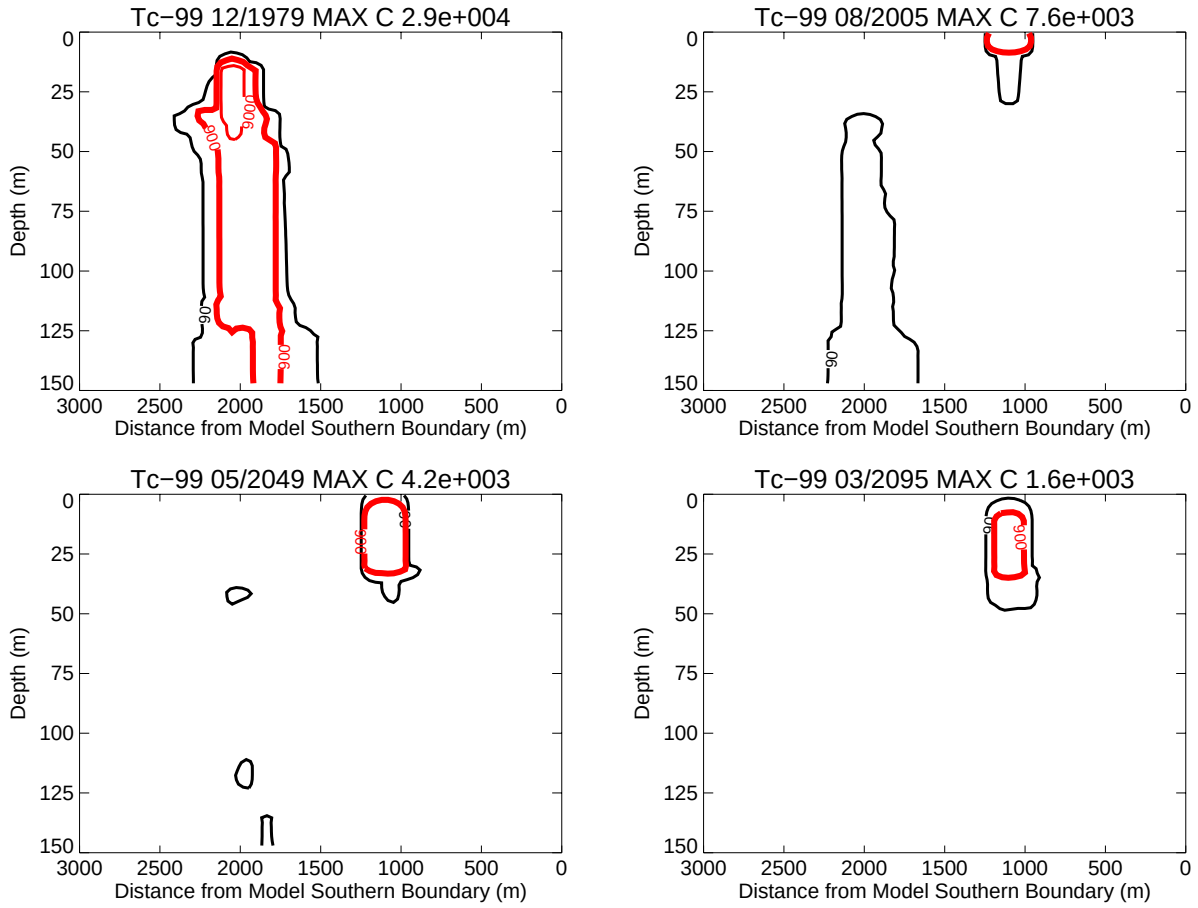

Figure A-10-32. Tc-99 vertical vadose zone concentrations (pCi/L) for the maximum anthropogenic recharge rate case (MCL = thick red, MCL/10 = thin black, MCL*10 = thin red).

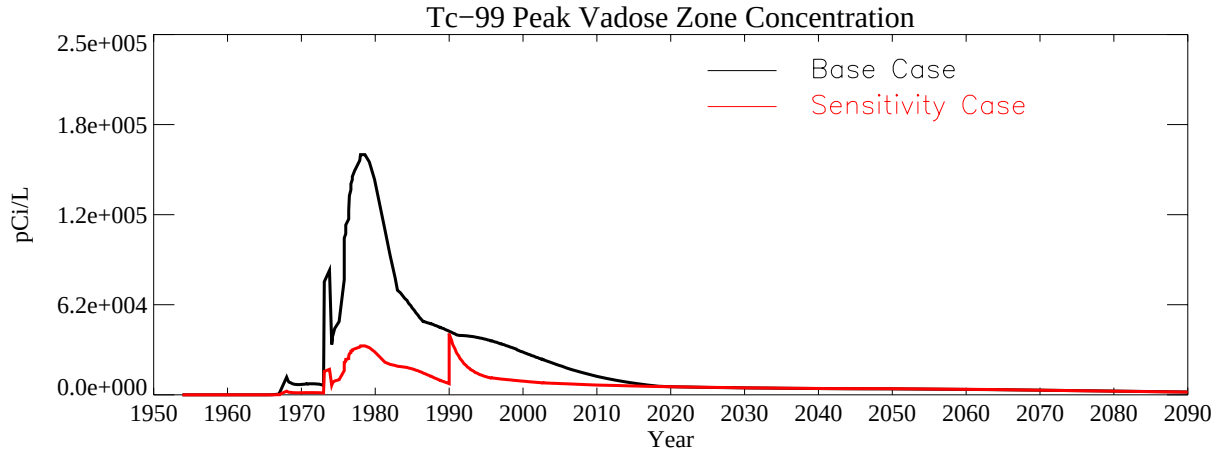

Figure A-10-33. Tc-99 peak vadose zone concentrations (excluding submodel area) (pCi/L) for the maximum anthropogenic recharge rate case.

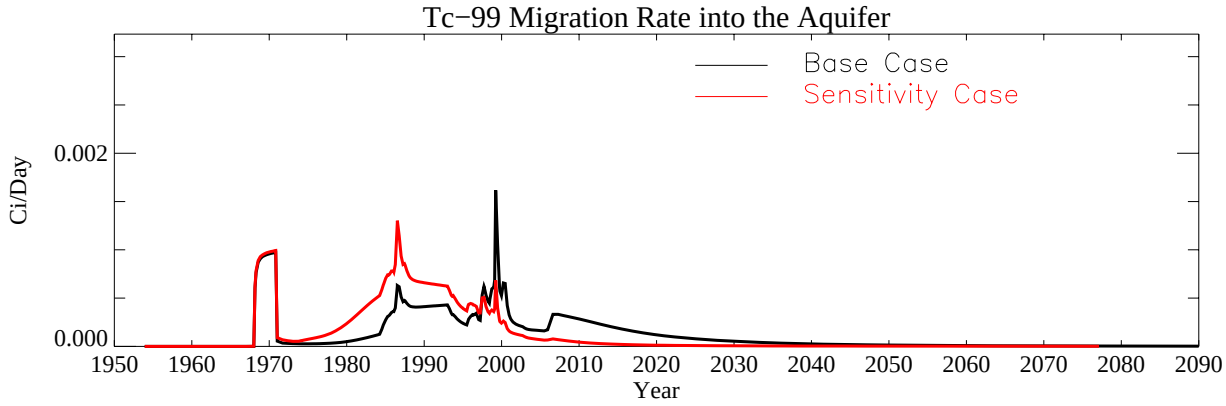

Figure A-10-34. Tc-99 flux into the aquifer (Ci/day) for maximum anthropogenic recharge rate case.

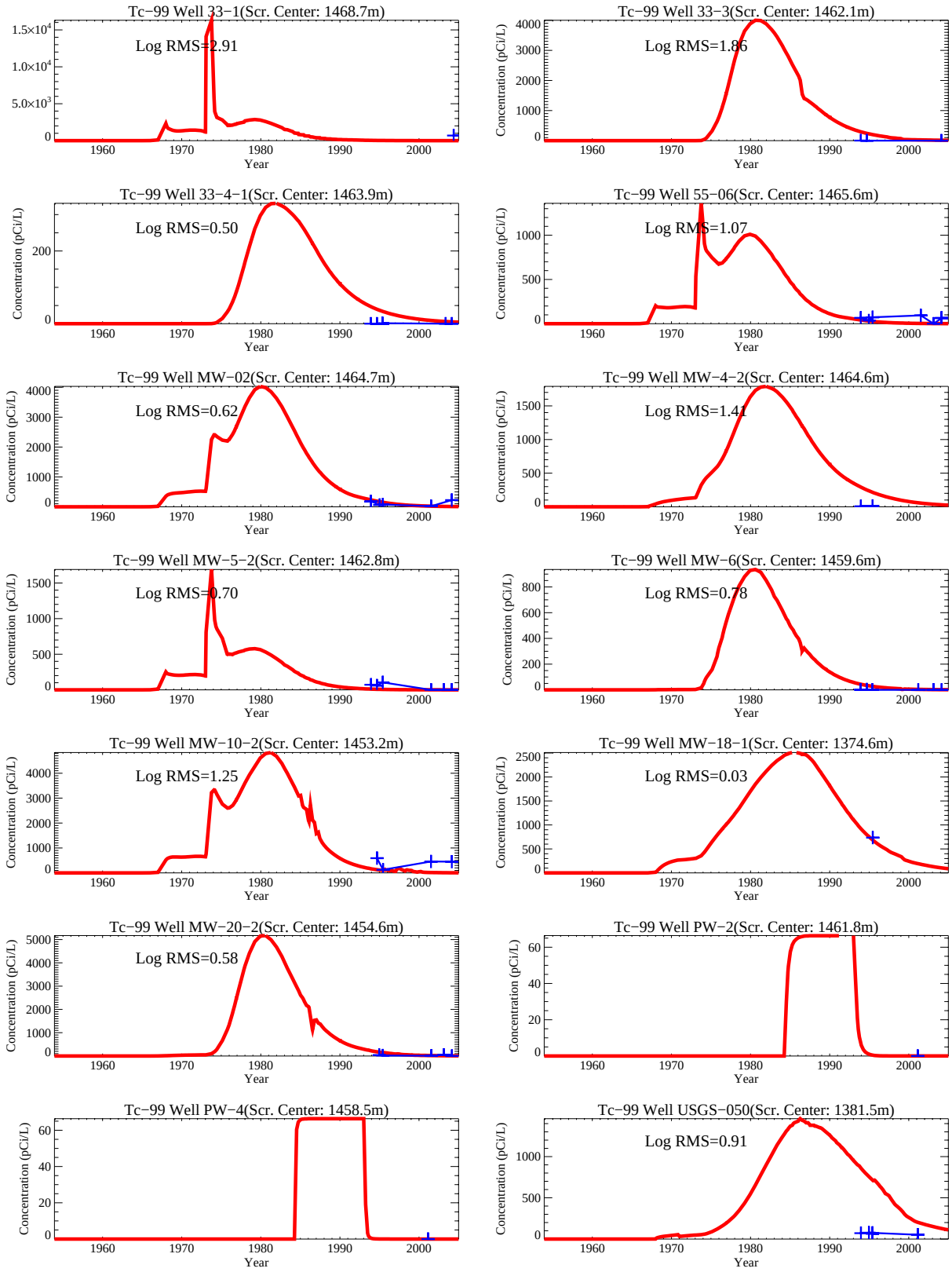

Figure A-10-35. Tc-99 concentration (pCi/L) in perched water wells for maximum anthropogenic recharge rate case (measured values = blue crosses, red = model at screen center).

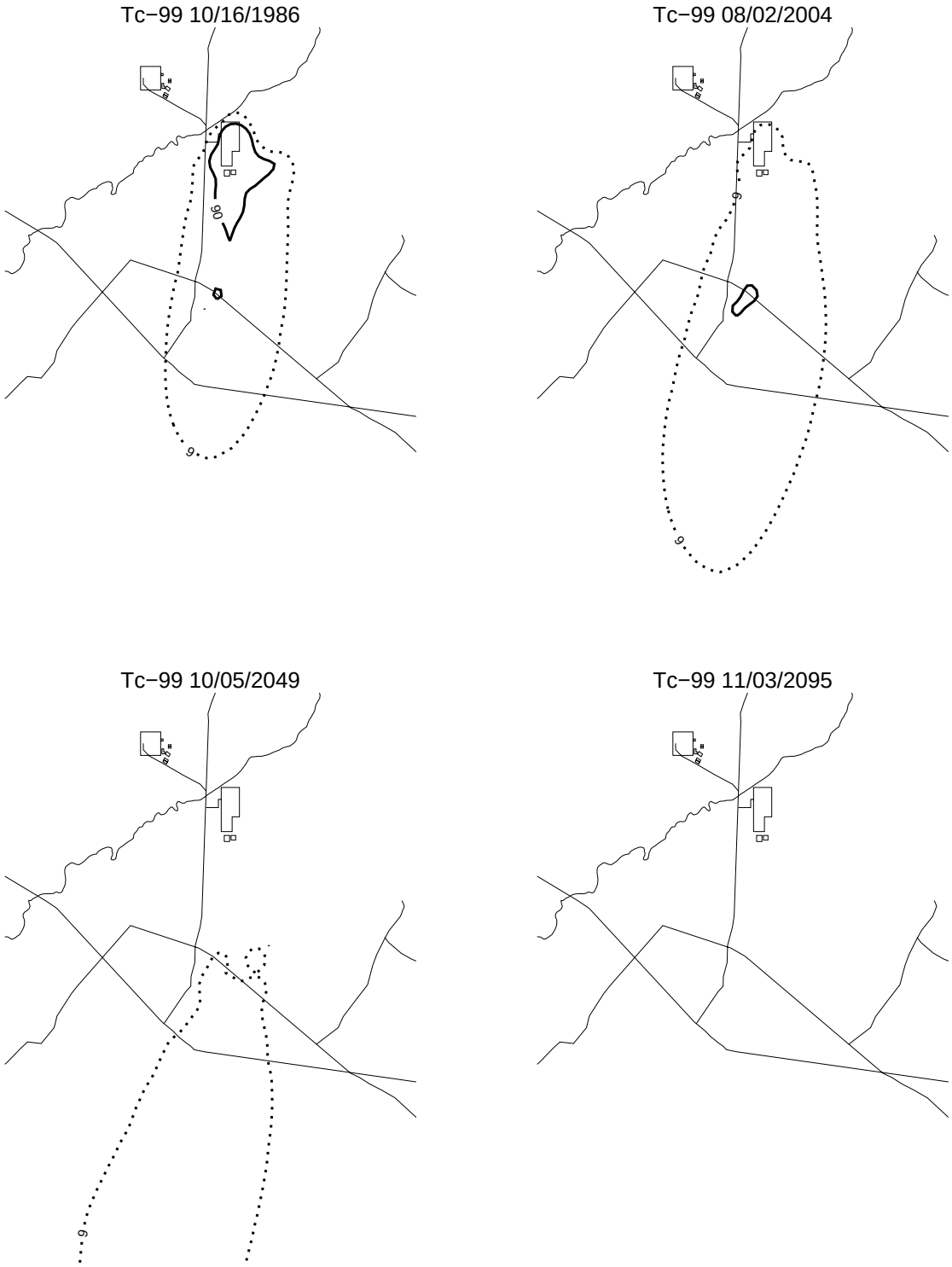

Figure A-10-36. Tc-99 aquifer concentrations (pCi/L) for the maximum anthropogenic rate case (MCL*10 = thin red, MCL = thick red, MCL/10 = thin black, MCL/100 = thin black dashed).

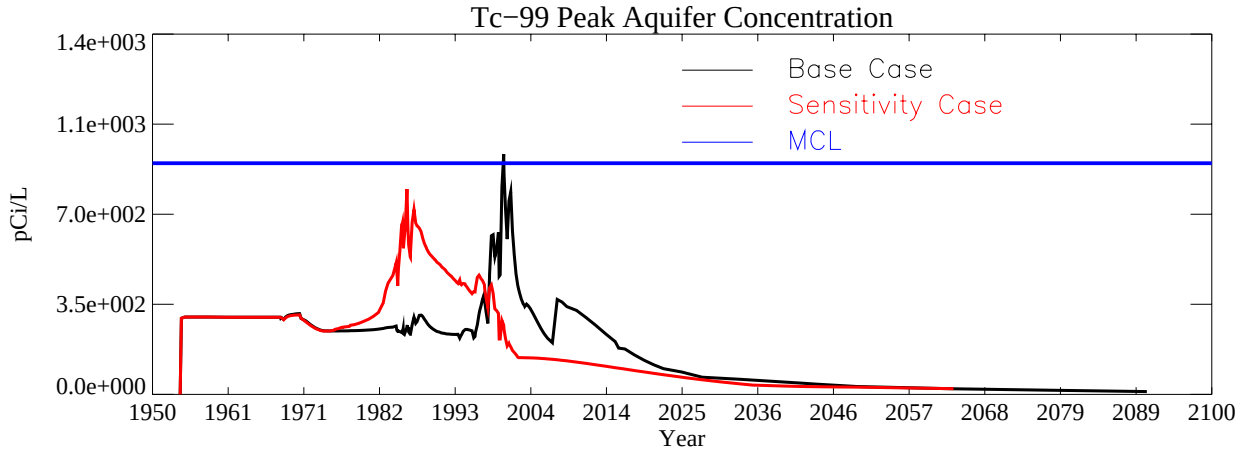

Figure A-10-37. Tc-99 peak aquifer concentration (pCi/L) for the maximum anthropogenic recharge rate case.

A-10.1.3 Tc-99 Preferential Flow Between the 380-ft Interbed and the ICPP-MON-A-230 Well

Routine sampling of the aquifer monitoring well ICPP-MON-230 2003 found Tc-99 concentrations at approximately twice the MCL. This was the first time that aquifer concentrations were found to exceed the MCL and prompted an investigation into the source of the Tc-99. The results of the Tc-99 investigation indicated that the source of the elevated Tc-99 in groundwater at well ICPP MON-A-230 was most likely attributable to historical liquid waste releases at the tank farm, in particular the Site CPP-31 release (ICP 2004).

The preponderance of evidence argues against the hypothesis that an improper annular seal at monitoring well ICPP-MON-A-230 could have allowed rapid downward migration of Tc-99 along the borehole to the aquifer. The 2005 Tc-99 results from new aquifer well ICPP-2021 (located 1500 feet away from MON-A-230) demonstrates that elevated Tc-99 concentrations are more widespread in the SRPA than previously believed. Moreover, the 2005 Tc-99 sampling results demonstrate that elevated Tc-99 concentrations are not present in the shallow perched water (TF-CH; 8.3 ±2.1 pCi/L) or deep perched water (TF-DP-L385; 7.8J ± 1.1 pCi/L) at the Tank Farm Well Set (DOE/ID, 2006). The low Tc-99 concentrations measured in the Tank Farm Well Set further bolsters the conclusion that the source of the elevated Tc-99 in the aquifer is not attributable to downward leakage of perched water at the boreholes of the Tank Farm Well Set. Rather, the most likely mechanism for transport of Tc-99 from contaminated tank farm soils to the aquifer is believed to be downward movement of contaminated water through the vadose zone to the water table, not short-circuiting down the borehole at well ICPP-MON-A-230.

The high aquifer concentrations of Tc-99 recently discovered in well ICPP-MON-A-230 could not be matched with the large-scale vadose zone model. The highest observed concentrations were approximately 3,000 pCi/L. The highest simulated concentrations were less than 1,000 pCi/L (see Section A-7.3.1). The high Tc-99 concentrations occurring in this well could be the result of a small-scale preferential flow path between the perched water near the 380-ft interbed beneath the tank farm and the aquifer near the ICPP-MON-A-230 well.

This hypothesis was investigated in the following manner: 1) the time history of the maximum Tc-99 concentration anywhere in the 380-ft interbed was used to define the preferential flow concentration, 2) a 10 gpm preferential pathway to the ICPP-MON-230 well location was placed in the aquifer model, and 3) the Tc-99 flux from the vadose zone into the aquifer model was uniformly reduced at all other blocks by the amount needed to maintain an unchanged total Tc-99 flux to the aquifer. This sensitivity simulation was only performed using the aquifer model and used the Tc-99 base case to define the Tc-99 flux.

The intent of this sensitivity simulation was to estimate the flow rate needed for a preferential flow path from the 380-ft interbed to the aquifer, which results in the observed concentrations at Well ICPP-MON-A-230. A ten gpm flow rate from the location of highest Tc-99 within the 380-ft interbed was needed. The total amount of Tc-99 transferred directly from the 380-ft interbed to the aquifer at the ICPP-MON-A-230 well location was 1.87 Ci, which is approximately 53% of the total Tc-99 (3.56 Ci) that was released to the tank farm. This flow rate resulted in a maximum aquifer concentration of 3,842 pCi/L in the year 1986.

This simulation indicates a relatively small preferential flow pathway could bring aquifer concentrations to that observed at ICPP-MON-A-230, but the area influenced was smaller than the current area observed to be over the MCL. The recently drilled ICPP-2020 and ICPP-2021 indicate this area may extend from north of the tank farm to possibly 1,000 ft southeast of the tank farm. The simulated arrival time for the very high concentration was much earlier than the current time and had fallen to 307 pCi/L by the year 2005. The peak aquifer concentration in the year 2095 was 9 pCi/L. The horizontal aquifer concentrations near INTEC for this simulation are given in Figure A-10-38, and the peak aquifer concentrations are shown in Figure A-10-39.

Figure A-10-38. Tc-99 aquifer concentrations (pCi/L) for the 10-gpm preferential flow path to well ICPP-MON-A-230 (MCL*10 = thin red, MCL = thick red, MCL/10 = thin black, MCL/100 = thin black dashed).

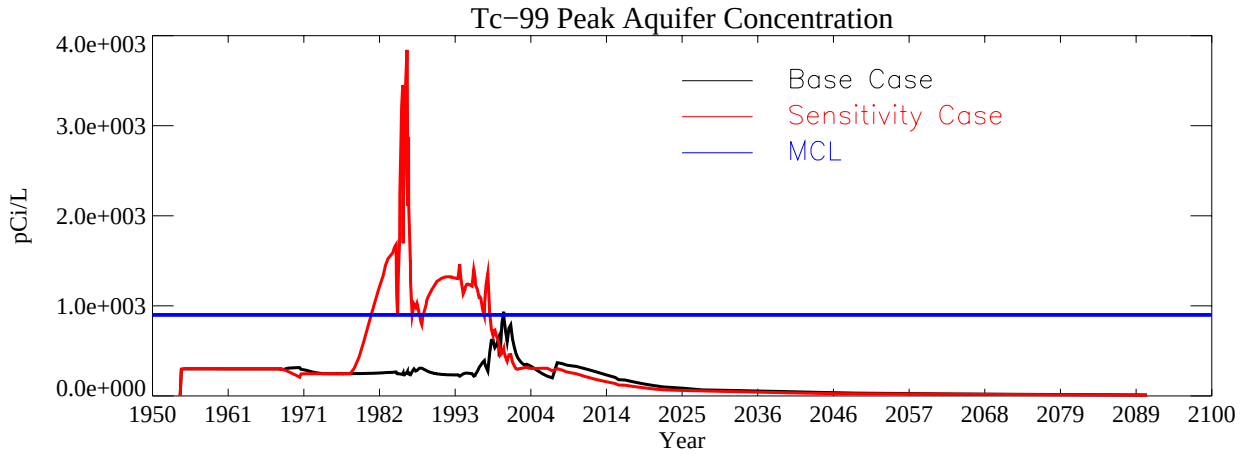

Figure A-10-39. Tc-99 peak aquifer concentration (pCi/L) for the 10-gpm preferential flow path to well ICPP-MON-A-230.

A-10.1.4 Tc-99 Service Waste Source Inventory

The Tc-99 concentrations were never monitored in the INTEC service waste. The service waste source term was estimated from the I-129 inventory and the ratio of Tc-99 to I-129 concentration measured in 2001 in the aquifer near the CFA (see Section A-9.2.3). As discussed in that section, I-129 and Tc-99 are very mobile and long-lived. If Tc-99 and I-129 are assumed to be transported identically from the CPP-3 injection well to the CFA monitoring wells, the ratio of measured values should be equal to the original disposal inventory. The aquifer wells north of the CFA were not used to obtain this estimate because the Tc-99 released in the tank farm may be influencing those ratios near INTEC.

The primary source of uncertainty is in how Tc-99 and I-129 are transported en route to the CFA. The sensitivity of the model to different Tc-99 service waste amounts was investigated by using the maximum concentration ratio found in the CFA wells. The maximum ratio was 25.1/1. This ratio resulted in a combined CPP-3 and percolation pond Tc-99 source of 37 Ci.

A-10.1.4.1 Maximum Service Waste Inventory for Tc-99

The peak simulated concentration in the vadose zone for this case was 1.64e+5 pCi/L in 1978 and coincides with the CPP-31 release date. The peak simulated concentration declined to 1.91e+4 pCi/L in 2005 and to 1.68e+3 pCi/L in 2095. Figures A-10-40 and A-10-41 illustrate the vertical and lateral extent of the simulated vadose zone concentrations.

Figure A-10-42 illustrates the peak vadose zone concentration through time. The peak vadose zone concentration is the result of the tank farm sources and increasing the service waste did not change these values. Therefore, both data appear as a single line on Figure A-10-42. The Tc-99 activity flux into the aquifer is illustrated in Figure A-10-43 and indicates that concentrations in the aquifer resulting from CPP-3 injection well failure and percolation ponds have nearly doubled. The Tc-99 concentration in key perched water wells is illustrated in Figure A-10-44. The shallow vadose zone contamination located immediately northwest of the former percolation ponds is due to the CPP-22 OU 3-13 soil site (0.1 Ci), which was placed in the model in 1990.

The increased Tc-99 service waste inventory had the most significant influence on the aquifer concentrations. Differences in the vadose zone model were only observable in a higher early activity concentration as a result of the CPP-3 injection well failure. The activity flux to the aquifer from the injection well failure increased from 0.001 Ci/day to 0.002 Ci/day.

Figure A-10-45 illustrates the horizontal aquifer concentrations, and peak aquifer concentrations through time are given in Figure A-10-46. The peak Tc-99 concentration in the year 2095 was 15 pCi/L, which is approximately 1.5 times the base case.

Figure A-10-40. Tc-99 horizontal vadose zone concentrations (pCi/L) for the maximum service waste inventory case (MCL = thick red, MCL/10 = thin black, MCL*10 = thin red).

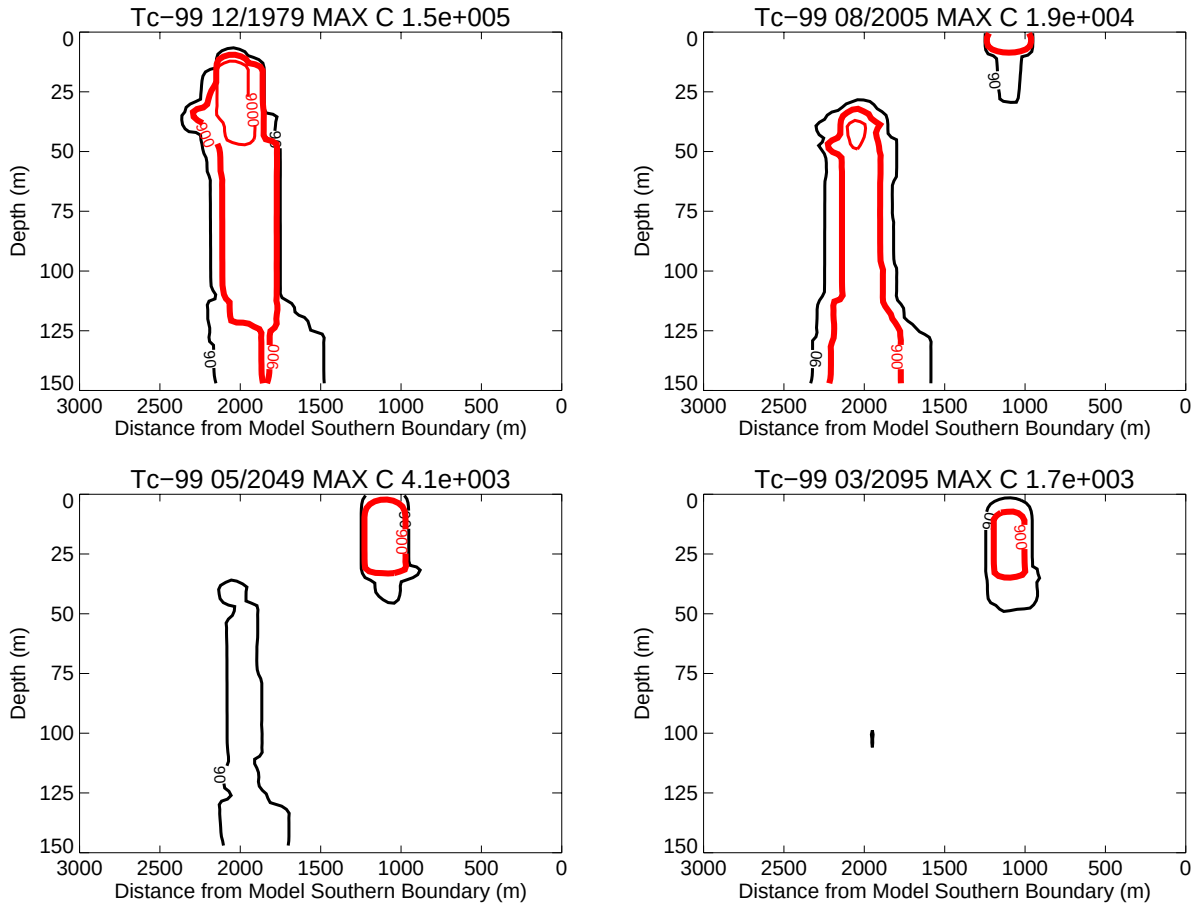

Figure A-10-41. Tc-99 vertical vadose zone concentrations (pCi/L) for the maximum service waste inventory case (MCL = thick red, MCL/10 = thin black, MCL*10 = thin red).

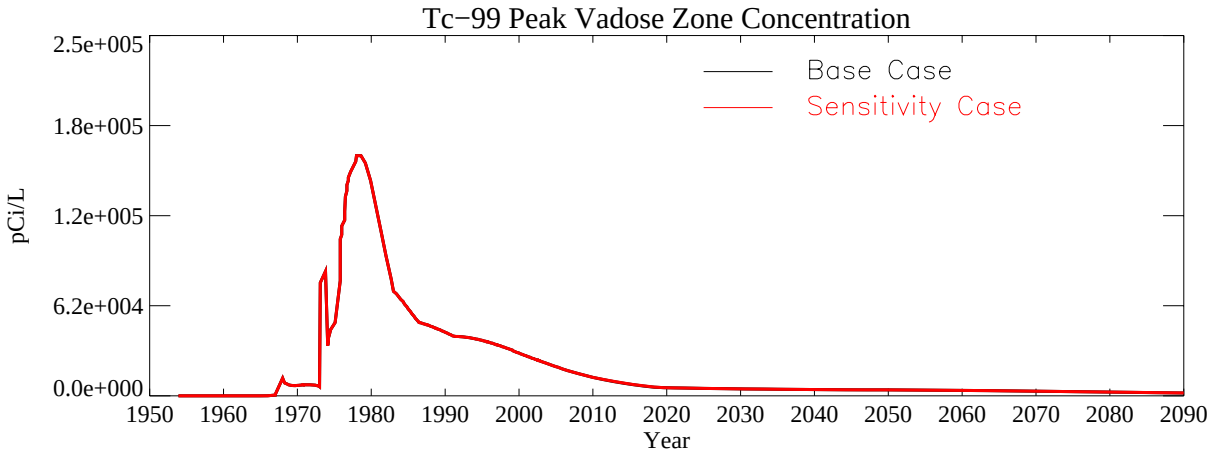

Figure A-10-42. Tc-99 peak vadose zone concentrations (excluding submodel area) (pCi/L) for the maximum service waste inventory case (sensitivity and base case data are identical).

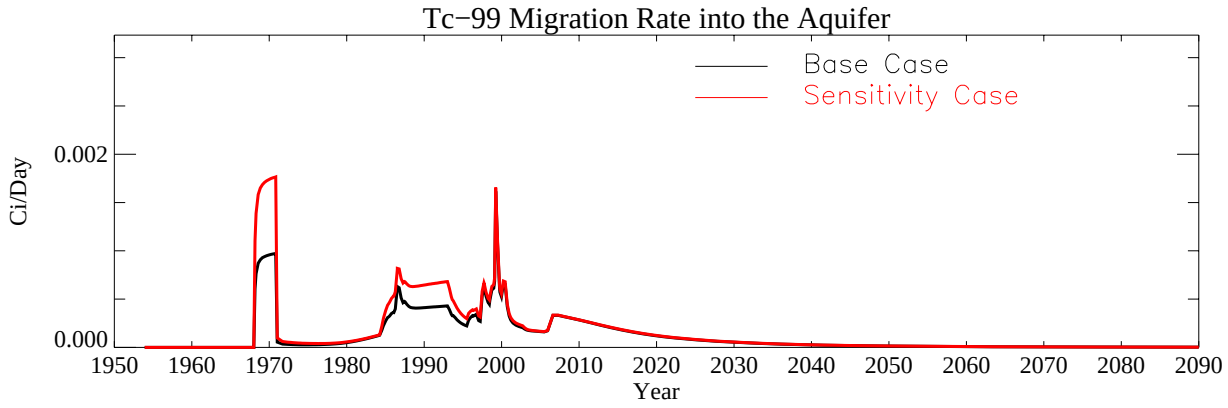

Figure A-10-43. Tc-99 flux into the aquifer (Ci/day) for the maximum service waste inventory case.

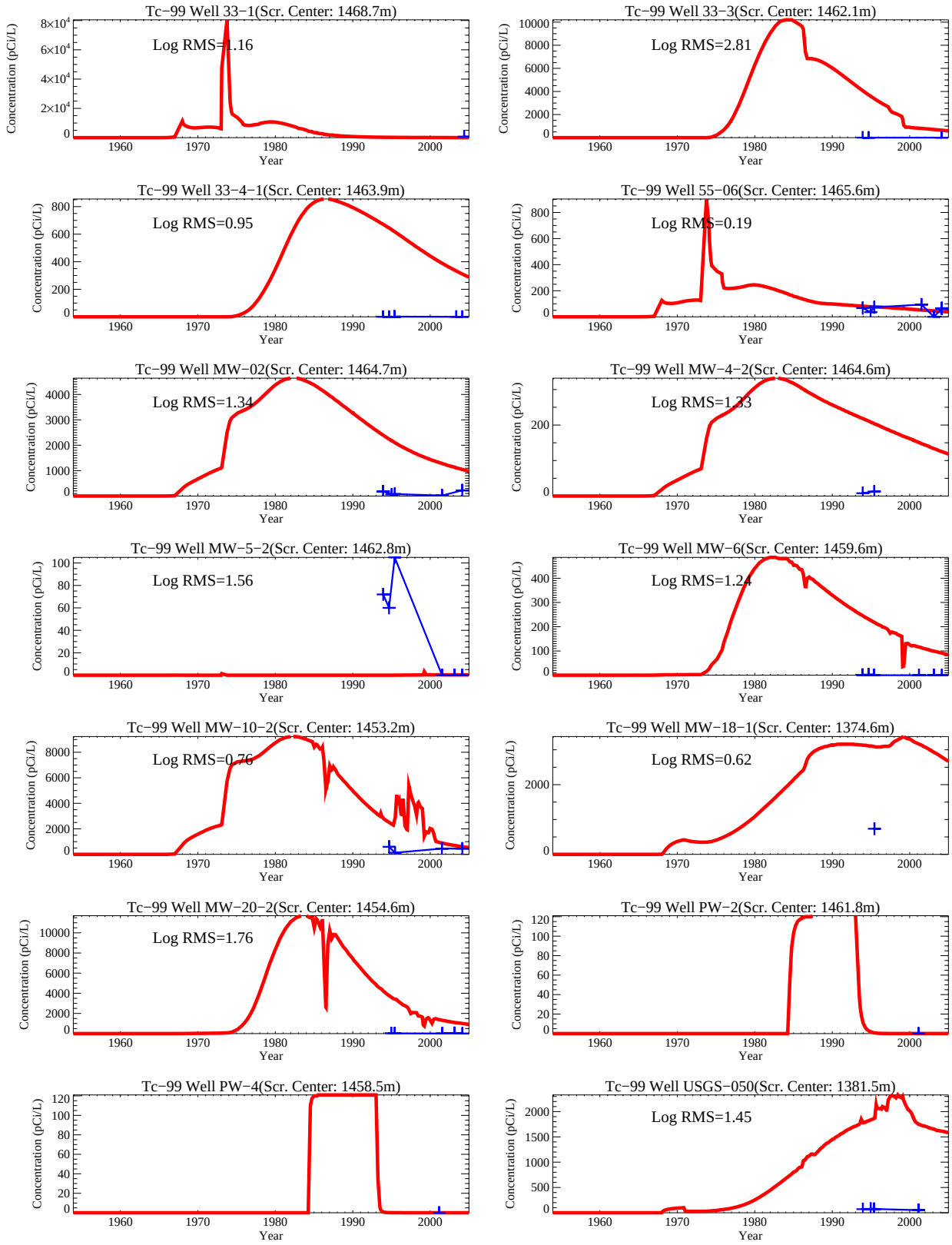

Figure A-10-44. Tc-99 concentration (pCi/L) in perched water wells for the maximum service waste inventory case. (measured values = blue crosses, red = model at screen center)

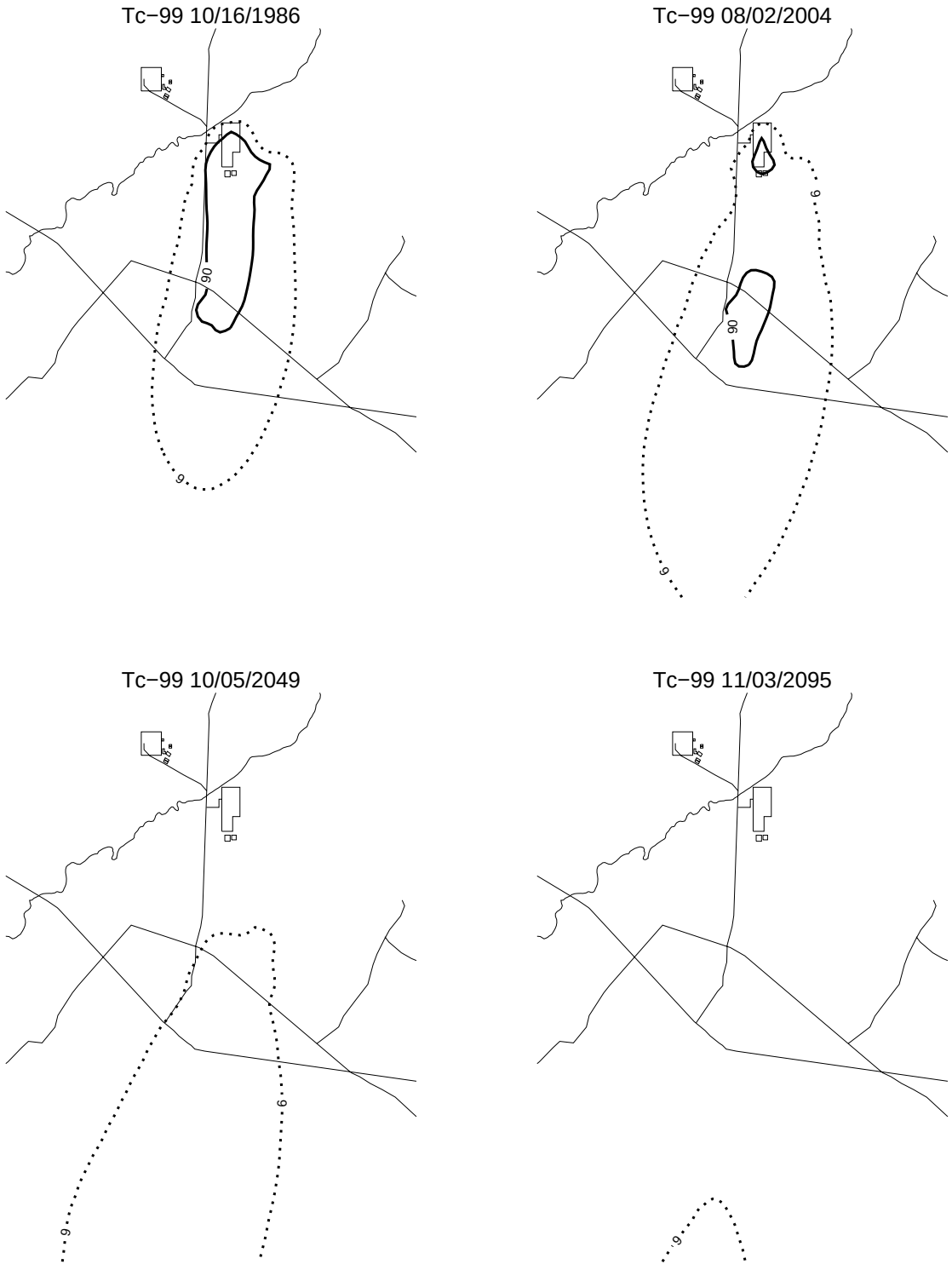

Figure A-10-45. Tc-99 concentrations (pCi/L) for the maximum service waste inventory case (MCL*10 = thin red, MCL = thick red, MCL/10 = thin black, MCL/100 = thin black dashed).

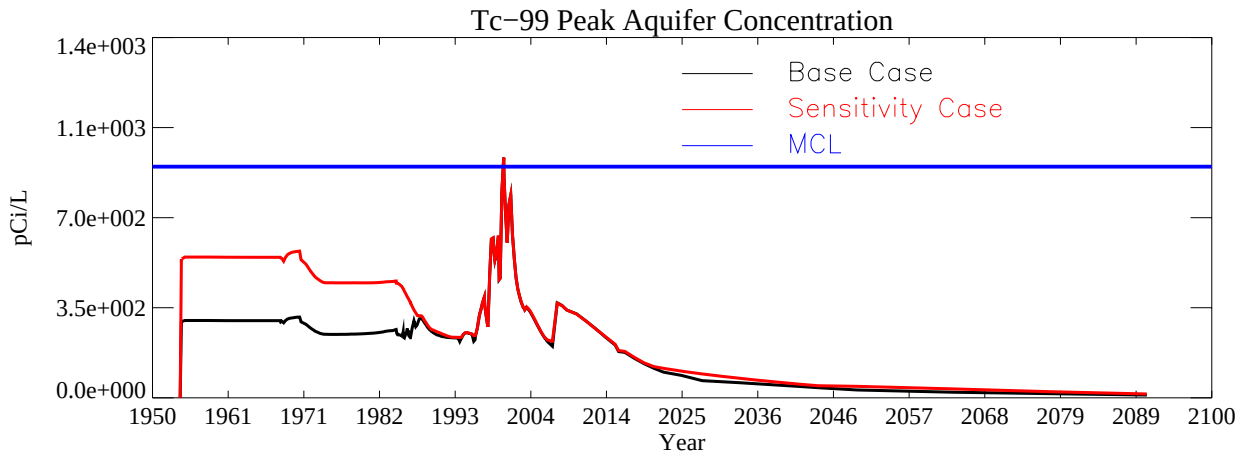

Figure A-10-46. Tc-99 peak aquifer concentration (pCi/L) for the maximum service waste inventory case.

A-10.1.5 Model Horizontal Grid Size

Contaminant concentrations and soil/rock saturations are functions of grid block discretization, primarily because of the implementation of the boundary conditions, where the incoming fluxes are assumed to be assigned to the node center. The incoming fluxes are partitioned within a given grid block (sorption), and phase velocities and pressures are calculated based on the pressure-saturation relationships within the grid blocks. Large grids can result in underpredicting contaminant concentrations and water saturations in addition to increasing numerical dispersion. Ideally, the model grid discretization should be determined by the minimum grid size required to obtain an invariant (size-to-size) result. However, limitations emplaced by computational resources typically dictate the minimum grid discretization. As a result of computational limitations, discretization is often a trade-off between larger block sizes, smaller simulation domains, and longer run times. Small simulation domains may have boundaries that influence the solution. For example, a lateral boundary could restrict lateral water movement and create deeper perched water, which would not occur in the larger domain, while more grid blocks of the same size necessary to represent the larger flow domain require excessive run times. The OU 3-14 model discretization was guided by the need to capture the very large Big Lost River and percolation pond recharge sources and the need to have a computationaly tractable model.

The model sensitivity to the horizontal grid discretization was assessed by simulating a subdomain of the northern INTEC using the same model parameters and a smaller horizontal grid block size. The OU 3-14 used a 100- x 100-m horizontal grid and the subdomain model used a 50- x 50-m horizontal grid. The submodel includes a smaller reach of the Big Lost River, which also may contribute to differences between the subdomain model and the base model. The submodel domain is illustrated in Figure A-10-47.

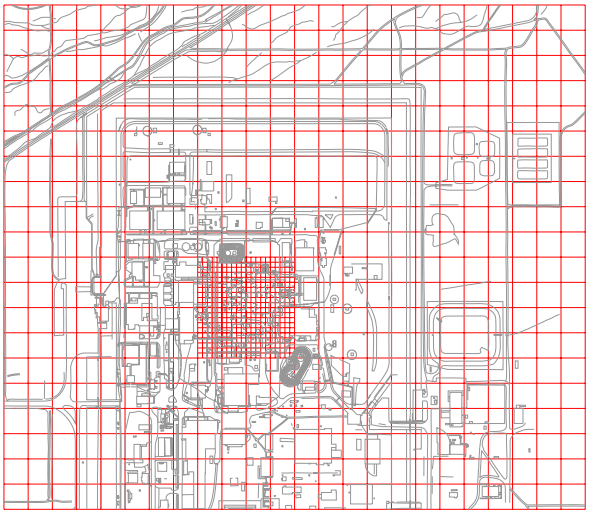

Figure A-10-47. Subdomain model horizontal discretization.

A-10.1.5.1 Tc-99 Horizontal Discretization Sensitivity Results

The peak simulated concentration in the vadose zone for this case was 6.42e+5 pCi/L in 1978 and occurs after the CPP-31 release date. The peak simulated concentration declined to 7.4e+4 pCi/L in 2005 and to 3.64e+3 pCi/L in 2095. Figures A-10-48 and A-10-49 illustrate the vertical and lateral extent of the simulated vadose zone concentrations.

Figure A-10-50 gives the peak vadose zone concentration through time. The peak concentration resulting from the CPP-31 release increased by a factor of 3.9 simply as a result of decreasing the grid size. The Tc-99 activity flux into the aquifer is illustrated in Figure A-10-51 and does not contain the service waste pond peak fluxes that occurred in the base case during the 1980s and 1990s because the submodel domain did not include the ponds. The Tc-99 concentration in key perched water wells is illustrated in Figure A-10-52.

The amount of horizontal spreading in this submodel is less than that predicted by the base case. As a result, the submodel overpredicted concentrations in the tank farm hot spot located south and east of the tank farm (i.e., CPP-33-1 and MW-10-2) but underpredicted concentrations further from the tank farm (i.e., wells MW-5-2 and MW-55-06). The submodel would require a higher dispersivity to match the far and near wells. This would result in lower peak concentrations and better agreement between the submodel and base case model. In general, the behavior of the submodel Tc-99 and the base case Tc-99 is similar. The tank farm contaminants move south and east of the tank farm in the upper shallow perched water. Both models predict the Big Lost River to have a large impact on Tc-99 flux into the aquifer. In both cases, the peak aquifer flux immediately follows the minimum peak flow year for the Big Lost River recorded at Lincoln Boulevard bridge gauge in 1999.

Aquifer concentrations for these simulations are given in Figure A-10-53, and Figure A-10-54 illustrates peak aquifer concentrations through time. The peak aquifer concentration was 783 pCi/L in 1970 and 192 pCi/L in 2005, which were very near the base case values. The peak aquifer concentration in the year 2095 was 14 pCi/L, which was slightly higher than the base case value.

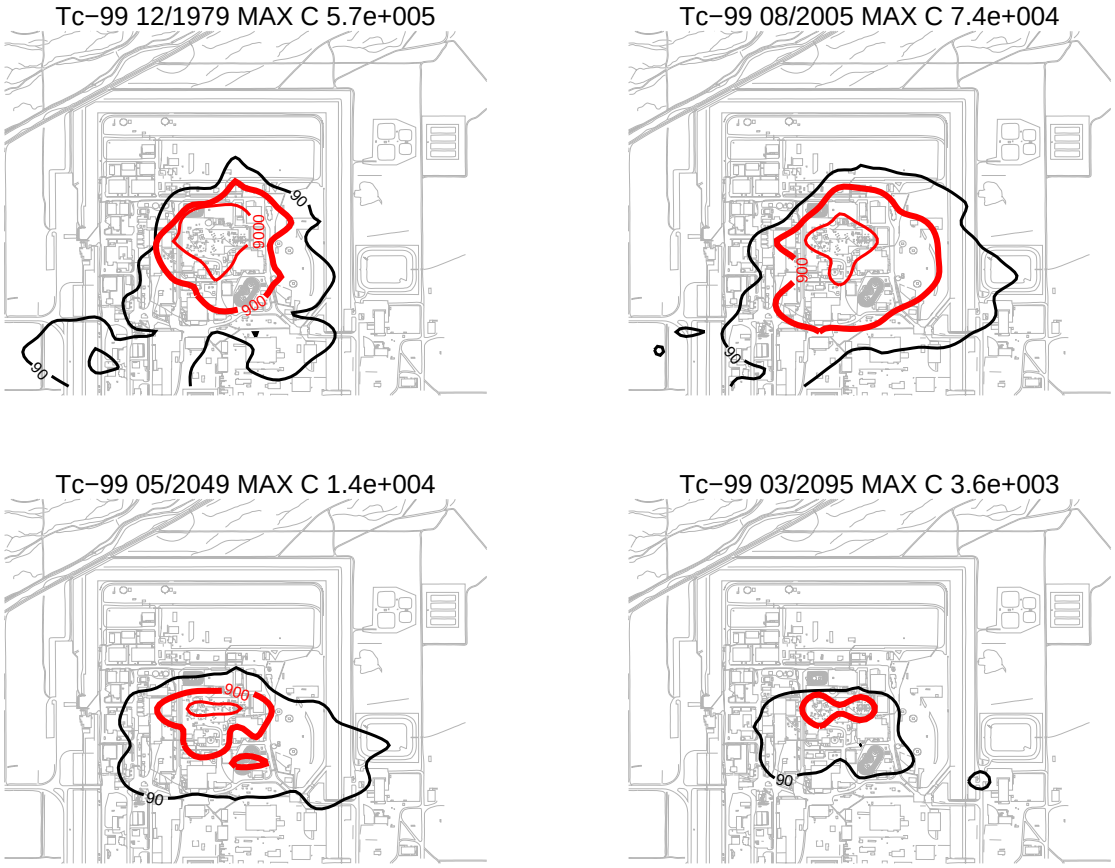

Figure A-10-48. Tc-99 horizontal vadose zone concentrations (pCi/L) for the 50- x 50-m submodel case (MCL = thick red, MCL/10 = dotted, MCL*10 = thin red).

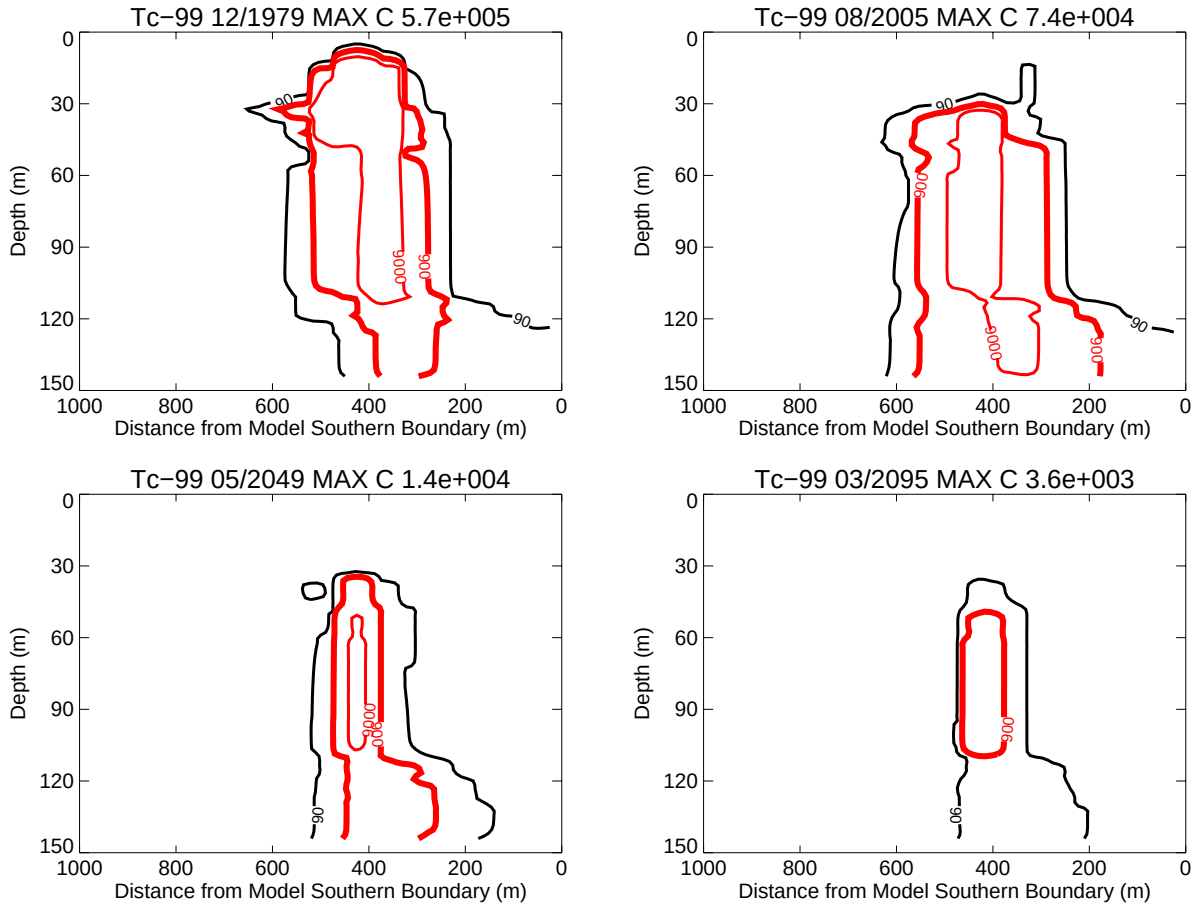

Figure A-10-49. Tc-99 vertical vadose zone concentrations (pCi/L) for the 50- x 50-m submodel case (MCL = thick red, MCL/10 = dotted, MCL*10 = thin red).

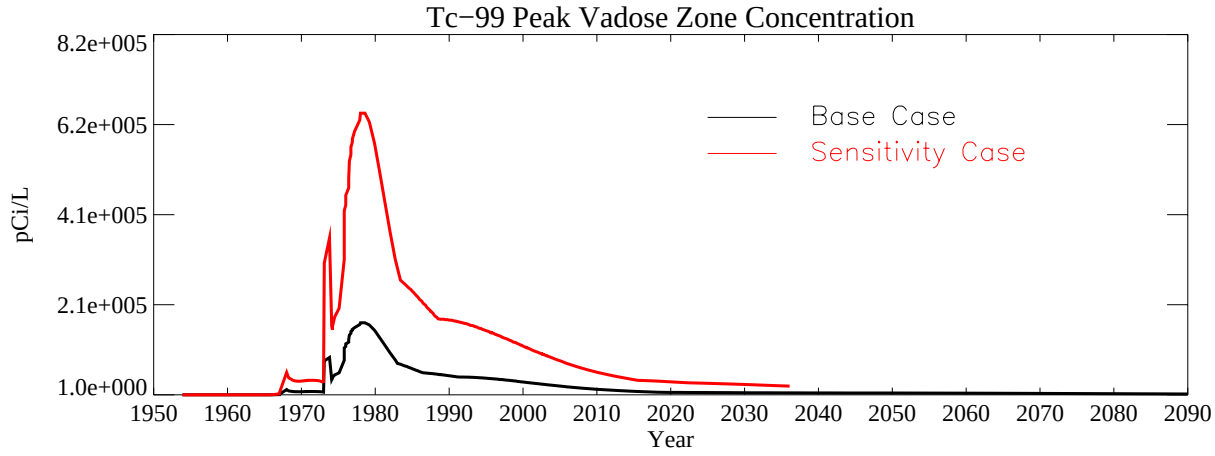

Figure A-10-50. Tc-99 peak vadose zone concentrations (excluding submodel area) (pCi/L) for the 50- x 50-m submodel case.

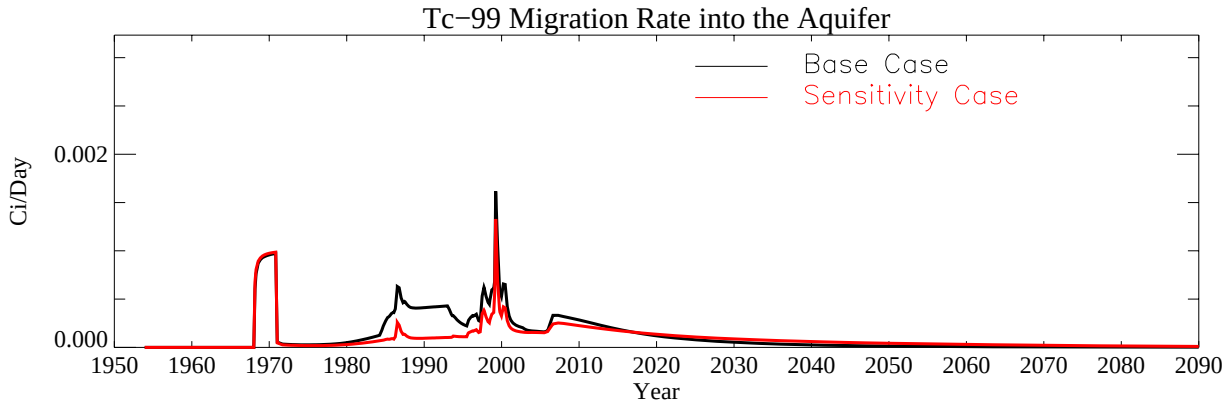

Figure A-10-51. Tc-99 flux into the aquifer (Ci/day) for the 50- x 50-m submodel case.

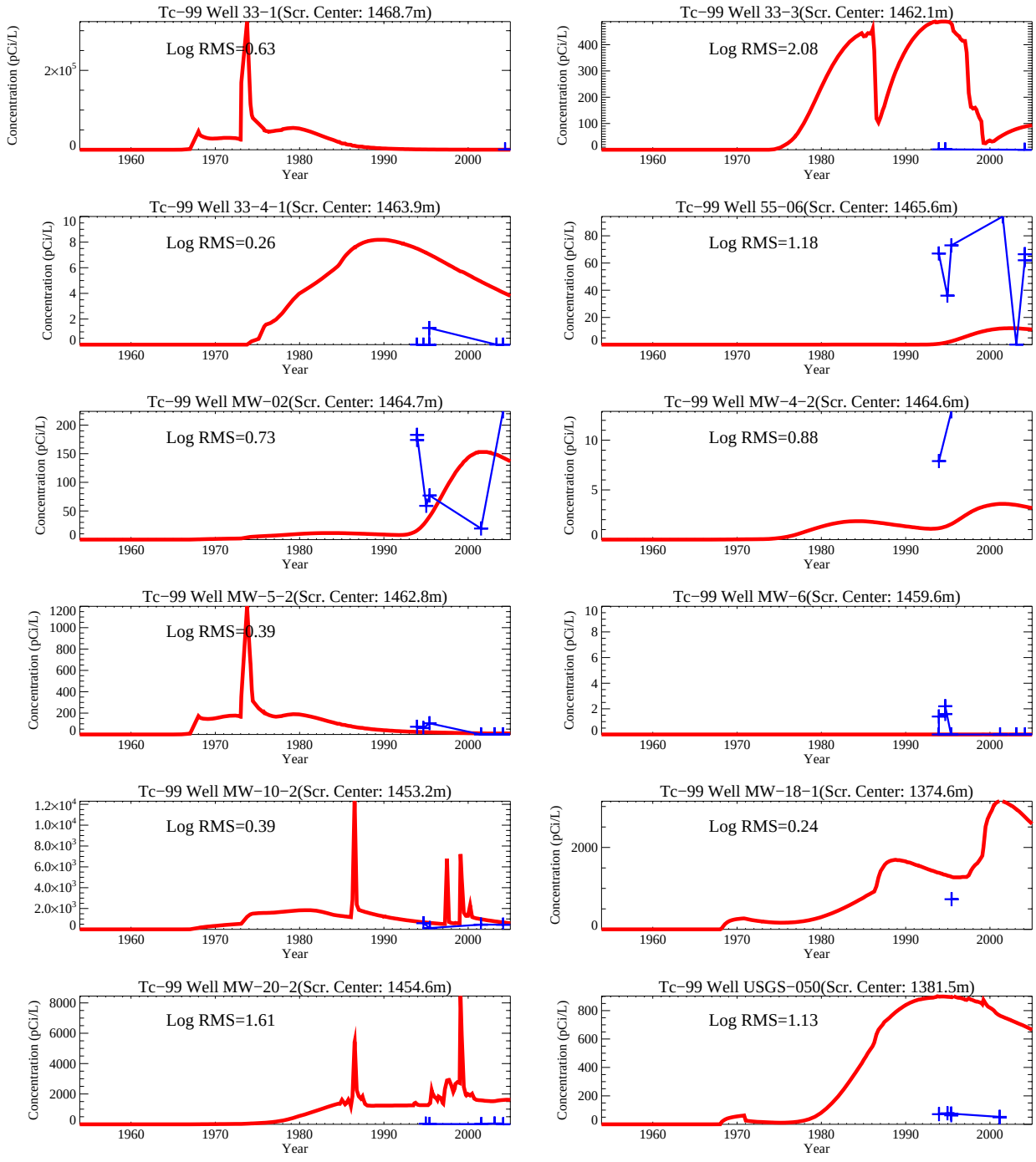

Figure A-10-52. Tc-99 concentration (pCi/L) in perched water wells for the 50- x 50-m submodel case (measured values = blue crosses, red = model at screen center).

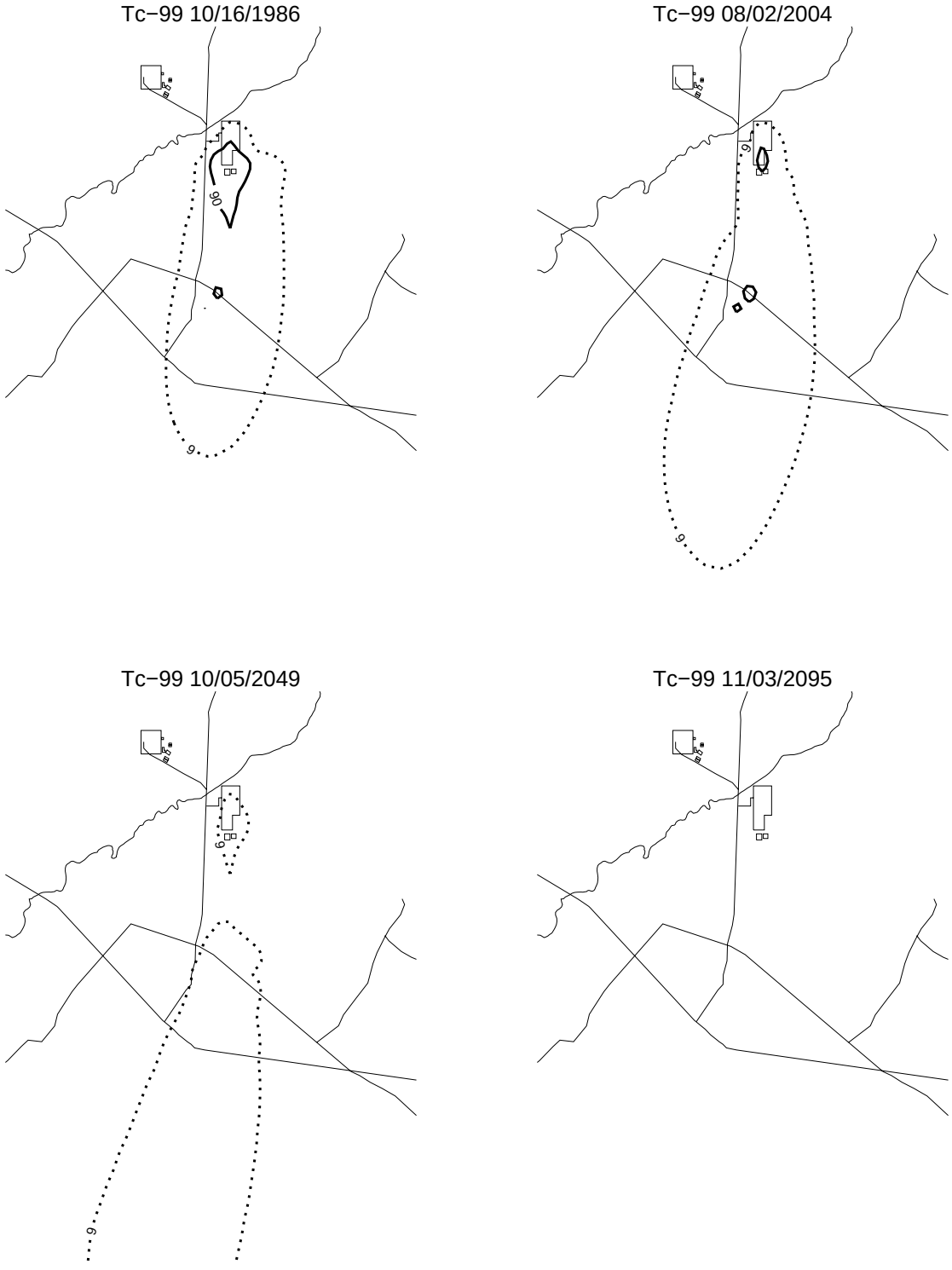

Figure A-10-53. Tc-99 aquifer concentrations (pCi/L) for the 50- x 50-m submodel case (MCL*10 = thin red, MCL = thick red, MCL/10 = thin black, MCL/100 = thin black dashed).

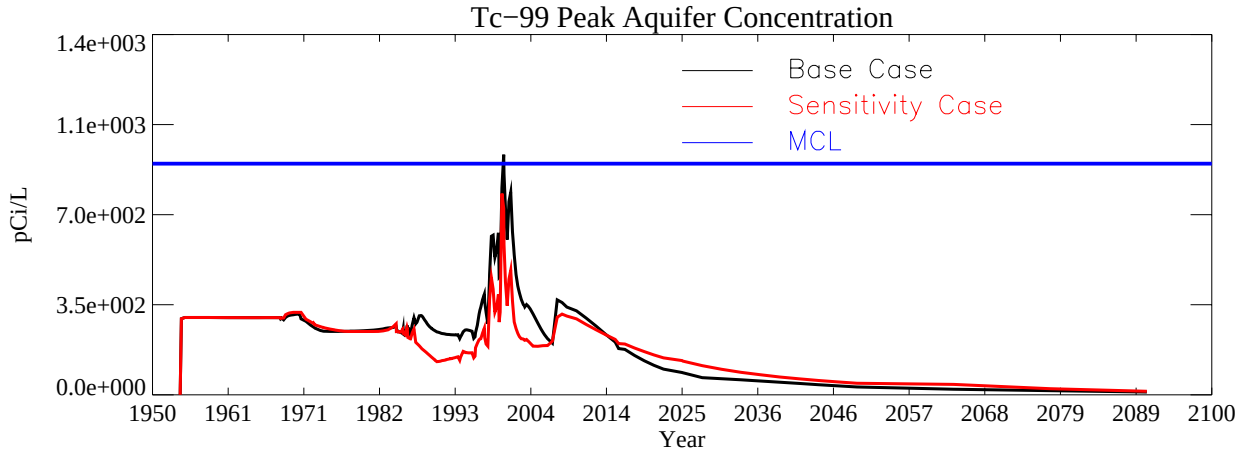

Figure A-10-54. Tc-99 peak aquifer concentration (pCi/L) for the 50- x 50-m submodel case.

A-10.1.6 Sensitivity Analysis Summary

Decreasing the tank farm recharge rate to 3 cm/year from 18 cm/year increases the travel time through the vadose zone and the peak Tc-99 concentrations by allowing a much longer and lower amplitude breakthrough to the aquifer. It also lessens the impact of the Big Lost River because less Tc-99 is deep in the vadose during the high flow years. Increasing the tank farm recharge to the maximum expected rate had a less dramatic effect than decreasing it to the minimum expected rate and did not significantly change the simulation results. This is because the recharge rate was only doubled, but the minimum expected rate decreased the recharge rate by a factor of six.

Tc-99 preferential flow path sensitivity simulations suggested a large fraction of the total tank farm Tc-99 must move from the 380-ft interbed directly to the aquifer near the ICPP-MON-A-230 well location to result in the high concentrations observed at this location. The peak Tc-99 concentrations in the 380-ft interbed were approximately 5,500 pCi/L in 1999 and a 10-gal/min flow rate from the 380-ft interbed resulted in a peak aquifer concentration of 3,842 pCi/L. The total amount of Tc-99 transferred from the 380-ft interbed at this flow rate was 2.87 Ci.

The highest and lowest interbed conductance simulations affected the influence of the Big Lost River and resulted in a lower amplitude and longer Tc-99 flux into the aquifer. The highest conductance interbed simulation reduced the horizontal spreading of the Big Lost River and allowed a smaller fraction of that flux to extend below the tank farm. The lowest conductance interbed simulation resulted in more horizontal spreading of the Big Lost River west of the tank farm but slightly less water reaching beneath the tank farm relative to the base case. However, agreement of the simulated and observed perched water concentrations was similar to the base case. The interbed conductance sensitivity simulations indicate that the model is more sensitive to interbed surface slope than permeability and thickness. Both the interbed conductance sensitivity realizations of the vadose zone lithology decreased the dip of the 140 ft interbed towards the tank farm and the resulting change in aquifer concentrations was similar.

Results of the horizontal discretization sensitivity simulations using smaller grid blocks resulted in higher concentrations, overprediction of concentrations in the nearest shallow perched water well (CPP-33-1), and underprediction of concentrations in the more distant wells (CPP-55-06 and MW-02). Matching the northern shallow perched water with the submodel would require a larger dispersivity value and the results would most likely be similar to the base case. This suggests the base case horizontal discretization was adequate to represent the vadose zone.

Table A-10-2 summarizes the sensitivity simulation results in the vadose zone and includes the peak concentration, time of peak, peak concentration in year 2005, and the peak concentration in the year 2095. Table A-10-3 presents the same information for the aquifer. Table A-10-4 presents the model calibration statistics for each sensitivity case and includes the average, minimum, maximum, and standard deviation of the log RMS for all vadose zone wells. The total number of simulated and observed pairs evaluated in calculating the calibration statistics is also included. This value is different for each sensitivity simulation because the log RMS was not calculated if simulated or observed values were zero. The statistics presented in Table A-10-4 allow evaluation of the agreement between the simulated and observed data. Sensitivity simulations that show a much worse agreement than the base case do not represent a true model sensitivity because the results are unrealistic.

Table A-10-2 Vadose zone model sensitivity analysis peak concentrations.

Section	Simulation	Year of Peak	Peak Concentration (pCi/L)	Peak Concentration in 2005 (pCi/L)	Peak Concentration in 2095 (pCi/L)
A-7.3.1	Tc-99 base case	1978	1.64e+5	1.91e+4	1.68e+3
A-10.1.2.1	Tc-99 high interbed conductance	1978	1.64e+5	2.61e+4	2.56e+3
A-10.1.2.2	Tc-99 low interbed conductance	1978	1.64e+5	2.71e+4	2.29e+3
A-10.1.3.1	Tc-99 3-cm/year tank farm recharge rate	1977	1.01e+6	5.47e+4	8.26e+3
A-10.1.3.3	Tc-99 39-cm/year tank farm recharge rate	1978	1.49e+5	7.60e+3	1.69e+3
A-10.1.3.4	Tc-99 maximum anthropogenic water recharge rate	1978	3.34e+4	7.60e+3	1.69e+3
A-10.1.4.1	Tc-99 10-gal/min preferential flow path from 380-ft Interbed[a]	1978	1.64e+5	1.91e+4	1.68e+3
A-10.1.5.2	Tc-99 estimate from 25.1 Tc-99/ I-129 ratio	1978	1.64e+5	1.91e+4	1.68e+3
A-10.1.6.1	Tc-99 50- x 50-m horizontal grid	1978	6.41e+5	7.40e+4	3.64e+3

a. Identical to base case.

Table A-10-3 Aquifer model sensitivity analysis peak concentrations.

Section	Simulation	Year of Peak	Peak Concentration (pCi/L)	Peak Concentration in 2005 (pCi/L)	Peak Concentration in 2095 (pCi/L)
A-8.3.2	Tc-99 base case	1999	935	234	11
A-10.1.2.1	Tc-99 high interbed conductance	1999	568	203	43
A-10.1.2.2	Tc-99 low interbed conductance	1999	628	169	45

Section	Simulation	Year of Peak	Peak Concentration (pCi/L)	Peak Concentration in 2005 (pCi/L)	Peak Concentration in 2095 (pCi/L)
A-10.1.3.1	Tc-99 3-cm/year tank farm recharge rate	1999	327	125	40
A-10.1.3.3	Tc-99 39-cm/year tank farm recharge rate	1999	970	220	10
A-10.1.3.4	Tc-99 maximum anthropogenic water recharge rate	1986	799	139	22
A-10.1.4.1	Tc-99 10 gal/min preferential flow path from 380-ft interbed	1986	3,842	307	9
A-10.1.5.2	Tc-99 estimate from 25.1 Tc-99/ I-129 ratio	1999	935	236	15
A-10.1.6.1	Tc-99 50- x 50-m horizontal grid	1999	783	192	14

Table A-10-4 Vadose zone model sensitivity analysis calibration statistics.

Section	Simulation	Average Log RMS Error	Minimum Log RMS Error	Maximum Log RMS Error	Standard Deviation Log RMS Error	Number of Pairs Evaluated
A-7.3.1	Tc-99 base case	1.14	0.193	2.81	0.603	54
A-10.1.2.1	Tc-99 high interbed conductance	0.984	0.0141	2.89	0.722	56
A-10.1.2.2	Tc-99 low interbed conductance	0.972	0.154	2.84	0.648	56
A-10.1.3.1	Tc-99 3-cm/year tank farm recharge rate	1.09	0.359	2.96	0.638	56
A-10.1.3.3	Tc-99 39-cm/year tank farm recharge rate	1.02	0.057	2.54	0.613	56
A-10.1.3.4	Tc-99 maximum anthropogenic water recharge rate	0.933	0.0304	2.91	0.634	56
A-10.1.4.1	Tc-99 10-gal/min preferential flow path from 380-ft interbed[a]	1.14	0.193	2.81	0.603	54
A-10.1.5.2	Tc-99 estimate from 25.1 Tc-99/ I-129 ratio	1.17	0.193	2.81	0.594	54
A-10.1.6.1	Tc-99 50- x 50-m horizontal grid	0.639	0.241	2.08	0.681	46

a. Identical to base case.

A-10.2 Model Uncertainty Analysis

Prediction uncertainty is comprised of (1) uncertainty in the conceptual model (i.e., a complex process oversimplified or not well understood) and (2) a lack of knowledge about the model parameter values. The conceptual model uncertainty can be qualitatively assessed by comparing simulation results to observations and assessing whether sufficient complexity exists to capture the observed behavior. Parametric uncertainty can be quantitatively assessed by using Monte Carlo simulation if sufficient data exist to define probability distributions for all parameters. This was not done here because (1) there are insufficient data to create probability distributions of the model parameters and (2) the most sensitive model parameters were adjusted to minimize the mismatch between prediction and observations during the model calibration process. The model's parametric uncertainty is qualitatively presented in the context of the sensitivity analysis results.

The primary purpose of the OU 3-14 model is to predict future Snake River Plain groundwater concentrations from the tank farm soil sites and to evaluate proposed remedial actions. Numerical simulation of aquifer and vadose zone transport is inherently uncertain because observations of subsurface conditions are very sparse as are the data gathered to parameterize the model. This section is included to discuss these uncertainties in context of the primary purpose. Conceptual model uncertainty is assessed in Section A-10.2.1, Section A-10.2.2 presents the parametric uncertainty, and Section A-10.2.3 summarizes the model uncertainty for each contaminant of concern simulated as being low, moderate, or high.

A-10.2.1 Conceptual Model Uncertainty

The uncertainty due to model conceptualization is assessed in terms of how successful the calibration was in matching the observed data. A good agreement between model and observations indicates the conceptual model included sufficient complexity to match the actual behavior and the modeled system was well understood. A summary of the model calibration is provided in this section to provide a basis for assessing the conceptual model uncertainty.

The conceptual model adopted for the INTEC vadose zone attributes surface recharge to the transient Big Lost River, uniformly distributed steady-state precipitation, and time-varying anthropogenic water sources. The magnitude of these recharge sources are larger than exist across the INL Site as a whole. Increased recharge in the INTEC area infiltrates downward through a heterogeneous vadose zone comprised of the alluvium; fractured basalt; and 110-ft, 140-ft, below middle massive basalt (BM), and 380-ft interbeds. There are additional discontinuous sediment units interspersed between these primary lithologic units. Near land surface, liquid spills have occurred, releasing contaminants into the environment. We have assumed that these spills occurred uniformly in time over the estimated release period. Contaminants are then allowed to partition onto the soil, and this partitioning is described using a linear sorption isotherm. Subsequent transport occurs under spatially and temporally varying conditions as the contaminants migrate downward to the aquifer. The ability of the OU 3-14 conceptual model to represent these subsurface conditions is illustrated in the vadose zone and aquifer model calibration sections (Sections A-7 and A-8, respectively).

The simulated recharge originating in the former percolation ponds and the Big Lost River resulted in the formation of extensive perched water bodies beneath these location. The simulated perched water occurs within and above the major interbeds and is consistent with observed perched water near the Big Lost River and below the former percolation ponds. The areal extent of the perched water below the percolation ponds is consistent with the observed extent and did not reach much beyond the MW-7 well. This extent is consistent with the geochemical analysis presented in the MWTS report (DOE-ID 2003a). The recharge from precipitation and facility-related discharges resulted in very high saturation (0.99) in the low-permeability interbeds beneath INTEC, but the water phase pressure is slightly negative. This is consistent with the ephemeral perched water behavior observed in many of the wells beneath the INTEC, but not all locations. A very high interbed saturation would result in the perched water screens behaving as a seepage face and resulting in only small amounts of water being able to be withdrawn without the well temporarily drying out. The locations of the simulated high saturation areas agree with the observed perched water locations. However,

some observed perched water locations beneath the northern INTEC and away from the Big Lost River contain substantial perched water depth and even have rapid lateral flow.

The simulated recharge from the Big Lost River and former percolation ponds resulted in perched water and positive water phase pressure in these locations. The observed perched water drained out after the percolation ponds were relocated in 2002, and this behavior is generally captured by the model. The agreement between simulated and observed perched water suggests that the OU 3-14 vadose zone conceptual model is sufficient and the uncertainty is acceptable, but it is not low because the model did not create positive water at the perched water locations near the tank farm.

The highest observed contaminant concentrations in the northern shallow perched water are located south, east, and southeast of the tank farm in wells CPP-33-1, MW-2, MW-10-2, MW-20-2, MW-5, and CPP-55-06. This was presented for both predicted and observed data in Section A-7.3. The model is consistent with this observed trend.

The simulated transport of Tc-99 from the tank farm release sites resulted in peak aquifer concentrations occurring in the year 1999. The highest measured aquifer concentrations were found in the first sampling of the ICPP-MON-A-230 in 2003. The observed aquifer concentrations in other aquifer wells near the tank farm suggest that Tc-99 concentrations in the aquifer have been either changing slowly or steady since the mid 1990s. However, there are insufficient data for conclusive model calibration to deep vadose zone or aquifer peak concentrations. Conclusive model calibration requires knowledge of the source and concentration history in observation wells. Most often, the perched water wells were monitored after the majority of Tc-99 passed the monitoring locations or the sampling period was too short to discern where on the concentration history the data lie.

Steady-state underflow is assumed to move beneath the INTEC through the fast-moving aquifer and recharge and contaminants from the vadose zone water are diluted and dispersed as they slowly percolate downward. The model includes the INTEC production and injection wells as sinks and sources at the well screen depths. The aquifer thickness was estimated based on deep well temperature profiles and is spatially varying. The aquifer model included the following three lithological layers: (1) H basalt from the water table to the HI interbed with permeability estimated from aquifer well test data, (2) HI interbed with permeability estimated from laboratory testing of core, and (3) I basalt with permeability estimated based on fitting the tritium, I-129, and Sr-90 data.

The simulated large-scale aquifer gradient near the INTEC is mostly due south. This matches the large-scale regional gradient predicted in the summer 2004 water level measurements. The aquifer model had good agreement with observed contaminant arrival in downgradient wells for contaminants discharged into the CPP-3 injection well. There are sufficient time histories for contaminants to discern the rising limb, peak concentration, and falling limb of the tritium and Sr-90 concentrations in the observed concentration histories. The agreement with the simulated and observed large-scale gradient and contaminant history data (specifically tritium) indicate that the OU 3-14 aquifer model has sufficient complexity to match the observed water behavior and the uncertainty is acceptable. The relatively poor match with Sr-90 concentrations in the aquifer suggest spatially varying sorption chemistry is occurring within the aquifer and the model does not contain this complexity/understanding. For this reason, the conceptual model uncertainty within the aquifer is only acceptable.

A-10.2.2 Parametric Uncertainty

The model parametric uncertainty analysis quantifies the model output uncertainty to the model's input parameters. The results of the sensitivity analysis forms most of the basis for the parametric uncertainty discussion presented in this section. The OU 3-14 source term was not included in the sensitivity analysis, but the OU 3-14 source term is an important model parameter and the uncertainty is discussed in this section. Contaminant transport scales linearly with an increase or decrease in source magnitude, and a linear increase or

decrease in the OU 3-14 source terms would result in a corresponding linear increase in the predicted groundwater concentrations.

In general, the most sensitive parameters suggest highest uncertainty. However, this is qualified here: If the sensitivity analysis was high for a specific parameter and that specific parameterization resulted in a greatly increased mismatch between observed and predicted data, the uncertainty is less than suggested by the sensitivity analysis. The parameters contributing most to uncertainty are (1) the source terms, (2) model transport parameters, (3) model hydraulic parameters, (4) infiltration rate, and (5) subsurface structure. Each of these are discussed in the next sections.

A-10.2.2.1 Contaminant Source Terms

The source terms used in the groundwater risk assessment included (1) the tank farm leaks and spills that created the OU 3-14 contaminated sites, (2) the service waste disposed of into the former CPP-3 injection well and percolation ponds, and (3) OU 3-13 soil sites. The uncertainty of each source is presented below. The service waste (except Tc-99) and the OU 3-13 soil sites source terms were taken from the OU 3-13 RI/FS (DOE-ID 1997), and much of the uncertainty discussion was taken from the OU 3-13 RI/FS.

A-10.2.2.1.1 OU 3-14 Sources

The source term uncertainty for most of the smaller tank farm sites is of no consequence because the activity released was insignificant compared to the few large releases. In the tank farm, there was one major release (CPP-31); three much lower and roughly equal releases (CPP-79 [deep]; CPP-27/31; and CPP-28); and several other minor releases that had a total activity several orders of magnitude lower than the four largest releases. Releases incorporated in the model included both measured and estimated waste volumes and waste compositions. The measured values are expected to be more accurate than the estimated values.

There are two main areas of uncertainty in the waste source terms: first is the volume of waste released; second is the activity per unit volume of waste released. The uncertainty in the specific activity varies among the radionuclides. In general, the activity of the fission products (Cs-137, Sr-90, Tc-99, etc.) can be accurately (within 5%) estimated or measured. Tritium and I-129 can be accurately measured or estimated in some wastes. However, due to their volatility, those radionuclides sometimes separate from the bulk of the fission products. When this occurs, the estimates become less accurate. The activity of the activation products (including the transuranic components) can be accurately measured, but estimates of the activation products are less accurate than those of the fission products due to difference in fuel design, reactor operation, etc., that affect the activity of activation products. The estimates of the activation products may be accurate within a factor of two.

In addition to the radionuclide activities, the waste compositions include nitrate concentrations. The nitrate concentrations for the major releases are either measured or estimated based upon waste generation and treatment flowsheets. Most of the nitrate estimates are likely accurate to within 20%. The nitrate concentrations are inherently more accurate than many of the radionuclide activities because of process and physical limits (solubility) on the nitrate concentration.

The uncertainty of each major release site is presented in the following:

- **CPP-31** – This is the source of the bulk of activity released at the tank farm. The uncertainties in its source term are larger than many of the other source terms. The CPP-31 source term (total activity) is an order of magnitude higher than even the second largest tank farm release source term. The volume of waste released was estimated to be 18,600 gal. This value is good to plus/minus 4,000 gal (about 20%). The radionuclide activity included measured values from waste sample analyses (variability of 10% or less) for Cs-137, Sr-90, H-3, U, Pu, and nitrate.

  Tc-99 was not measured but is expected to be accurately estimated based upon fission yield. The waste

had been concentrated in the process equipment waste evaporator, which depleted the H-3 and I-129 from the fission yield values. Therefore, the estimated I-129 activity was reduced by the same factor as the measured H-3 activity. This is probably accurate to within a factor of two for I-129. Other transuranic components (Np-237, Am-241, etc.) are likely within a factor of two, based on the ORIGEN2-based estimates documented in Appendix E.

- **CPP-27/33** – This leak consisted of Waste Calcining Facility scrub solution. In this case, neither the volume nor composition was measured at the time of the release. However, most of the contaminated soil was removed and the activity of Cs-137 in the contaminated soil was measured/estimated. A reasonable Waste Calcining Facility scrub solution activity was assumed (based on historical sample data), and the total Cs-137 activity released was divided by the Waste Calcining Facility scrub solution Cs-137 specific activity to get the volume of scrub solution released. In this case, the waste activity and waste volume do not have separate uncertainties. An error in one tends to be cancelled by a compensating error in the other. For example, if the assumed specific activity is too low, then the calculated waste volume is too high by a compensating percentage (and visa versa). Therefore, although errors are likely in both the activity and waste volume estimates, they are not necessarily additive. In this case, the greatest uncertainty lies with the estimate of the total Cs-137 activity in the soil that was removed. However, the model does not account for soil removal.

  The Cs-137 activity was estimated based upon average radiation readings taken from five (accessible) sides of the waste boxes as the soil was removed from the site in 1974. Basing the Cs-137 on such readings is likely accurate to within a factor of two. All other radionuclides were calculated based upon Cs-137; therefore, most fission products will be accurate to a factor of two. Due to their volatility, the H-3 and I-129 estimates may be less accurate than other fission products. The activation products are also likely good to a factor of two because they were a long-term average of fairly well-defined waste (first-cycle Al raffinate).

  The nitrate estimate for this release is not as good as other releases because the release consisted of two parts: (1) a high-activity stream for which the nitrate estimate is very good and (2) a low-activity (decon solution) stream for which the nitrate concentration estimate is good, but the volume is unknown. The second waste stream does not affect the radionuclide activity. In this case, the nitrate is likely good to only a factor of two as well.

- **CPP-28** – This leak consisted of first-cycle coprocessing raffinate. Such waste was well defined. The specific activity of the waste was based upon contemporary analyses of coprocessing wastes that included Cs-137, Sr-90, H-3, U, Pu, and Np-237. Tc-99 and I-129 were not included in the analyses but can be accurately estimated based upon fission yield. The specific activity estimate of these radionuclides is good. The activation products transuranics were estimated based upon the Cs-137 activity. The volume of waste released was estimated based upon the volume of contaminated soil, activity of the soil, and the specific activity of the waste. As with CPP-27/33, errors in the estimated volume released are somewhat compensated by the errors in the source term specific activity. If the estimated specific activity is too high, the estimated volume will be too low. So the errors in activity and volume are not additive. The major source of error is in the total activity originally in the contaminated soil. The total error (combined volume and specific activity) is accurate to about 50% for the fission products and a factor of two for the activation products.

- **CPP-79 (deep)** – This release is the least well defined of the four major tank farm releases and thus has the most uncertainty. The activity released was based upon blends of predominantly stainless-steel, first-cycle raffinate, with smaller amounts of Al, Zr, and other wastes. The fission product estimates are likely very accurate relative to each other (within 5%). Due to the blending of wastes, the activation product activity could vary significantly. However, all activity depends upon the estimate of the Cs-137 activity. The waste that leaked was assumed to have been first-cycle raffinate. In fact, a significant

portion of the waste was not first-cycle raffinate. Such waste would have a significantly lower Cs-137 activity. The estimated leak volume was based upon steam dilution estimates of waste transfers. Steam jet dilution is variable and those estimates could be off by a factor of two.

Although the total activity estimate for CPP-79 (deep) is potentially more variable than other releases, the assumption and estimates were on the conservative (high-activity) side. The ORIGEN simulations generated two potential waste source terms, based upon different blends of waste. Both estimates have similar fission product activity, but the transuranic content varies by about a factor of two (some slightly more, some slightly less). The stream with the highest Pu-239 activity was used, and the entire release was assumed to be first-cycle raffinate. This assumption is not correct because a portion of the waste released was not first-cycle raffinate but included some relativity process equipment waste solution and perhaps other relativity solution. Therefore, although the specific activity is variable, the fission product activity could be no more than 25% higher, but it could be considerably less (up to a factor of two). Likewise, the transuranic activity is likely no more than a factor of two higher than the estimate, but could be up to a factor of four less.

A-10.2.2.1.2 Service Waste

The injection well provided a direct source of contamination to the aquifer. However, during the injection well failure, a large fraction of the service waste stream entered the vadose zone. During this period, the depth of the discharge to the vadose zone is uncertain. The vadose zone disposal of the service waste could result in a delayed arrival to the aquifer and allow the contaminants to arrive in the aquifer after the well was repaired and receiving service waste again. This could result in a short period of higher concentrations due to superposition of the delayed and current disposal. The vadose zone and aquifer models should capture the behavior because, during the estimated well failure period, the injection well disposal was placed into the vadose zone model.

The discharges of H-3 and Sr-90 to the service waste stream were monitored regularly and the uncertainty in these two contaminant source terms should be small. The discharge of I-129 was also monitored but less frequently than H-3 and Sr-90. The source term for the other COPCs was estimated from less data and the uncertainty is higher. The H-3 and Sr-90 were regularly monitored in the downgradient wells and provide a check of the uncertainty in these two source terms. The aquifer model had good agreement with the observed H-3 and Sr-90 and verifies the uncertainty is not significant for these two COPCs.

The Tc-99 concentrations were never monitored in the INTEC service waste. The service waste source term was estimated from 2001 Tc-99-to-I-129 concentration ratios in the aquifer near the CFA and the I-129 source term (see Section A-9.2.3). The sensitivity of the model to an increased Tc-99 service waste was evaluated by using the maximum Tc-99-to-I-129 ratio to estimate the source term and can be used to assess effect of the Tc-99 service waste uncertainty. The uncertainty of the injection well Tc-99 source term will result in higher or lower concentrations far south of INTEC at the current time and should not significantly change predicted concentrations near INTEC now or into the future. The uncertainty of the other COPCs is recognized but cannot be quantified.

The arrival of each OU 3-14 tank farm COPC to the aquifer should occur long after the injection well component of that COPC has moved south of INTEC. This should not allow superposition of each COPC when evaluating whether the COPC is above the MCL, but superposition of different COPCs can occur for a risk calculation. Most of the Sr-90 currently in the aquifer beneath INTEC is the result of the CPP-3 injection well operation and will contribute to a higher cumulative risk as unretarded tank farm COPCs arrive in the aquifer. Thus, the injection well source term uncertainty would only contribute to total risk calculations from the tank farm sources and should not contribute to an MCL evaluation for each COPC, because the CPP-3 injection well source will have moved south of INTEC before the tank farm sources reach the aquifer.

As with the CPP-3 injection well, the former percolation pond sources were estimated from discharge records reported for the percolation ponds. The discharge records were not regularly reported over the years,

and an average daily discharge was used for the percolation ponds source terms. The uncertainty of the percolation pond source terms is recognized but cannot be quantified.

A-10.2.2.1.3 OU 3-13 Soil Sources

The OU 3-13 soil sources were estimated from the volume and contaminated soil concentration. These sources were implemented in the model on March 29, 1990, and represent radioactivity remaining in the soil at this time. The contaminated soil volume was assumed to be represented by a cube spanning the horizontal extent of measured contaminant and extending from land surface to the top of basalt. The soil concentration applied to this soil volume was typically the highest measured value. Using the spanning volume and maximum concentrations means that both the soil volume and concentration were conservatively estimated and that the total radioactivity assumed to be at each site is most likely much less. The uncertainty in the soil sources will result in overestimating the contribution to groundwater risk from these locations.

A-10.2.2.2 Transport Parameters

Simulating contaminant transport through porous media requires parameterizing the solute chemical interaction with the soil/rock matrix (sorption) and dispersion in the modeled system. The model's sensitivity to sorption and dispersivity were investigated simulating Sr-90 and is presented in Appendix J.

A-10.2.2.3 Hydraulic Parameters

Numerous cores of INTEC sediment have been taken, and laboratory analysis of the cores has been performed to estimate hydraulic conductivity, porosity, and soil moisture characteristics. However, hydrologic parameters tend to be scale-dependent. Cores represent nearly point-scale data, and the model represents a field scale. The model can be parameterized with the measured hydraulic properties, but disparity between measured and simulated scales requires adjustment of parameters to match observed conditions. The model was calibrated to perched water elevation, perched water temporal trends, and contaminant concentrations in the perched water and aquifer. The calibration process should reduce the model's uncertainty due to hydraulic parameters to a small amount.

A-10.2.2.4 Infiltration Rate

The model's infiltration rate was spatially varying and was estimated from known anthropogenic sources (i.e., lawn irrigation, steam vents, and line leaks) and from the natural water sources (i.e., Big Lost River and precipitation). There is a large amount of uncertainty in the amount and locations of the anthropogenic water sources and the recharge from precipitation because of the following reasons: (1) approximately 10-11% of the produced water is unaccounted for, (2) the accuracy of the flow meters on the production wells is unknown, and (3) very limited soil moisture data were used to estimate infiltration due to precipitation. The model's sensitivity to infiltration was investigated for a long-lived mobile contaminant (Tc-99) and for a short-lived relatively immobile contaminant (Sr-90, see Appendix J) for a high and low tank farm infiltration rate, and, for a worst case, anthropogenic infiltration rate.

The model's Tc-99 sensitivity to different infiltration rates was not great because a large fraction of the Tc-99 inventory was directly injected to the aquifer in the CPP-3 disposal well. This is probably a real source of uncertainty in the model predictions because the agreement between the simulated and observed perched water was comparable and either simulation could equally represent Tc-99 contaminant transport. The peak Tc-99 arrival in the northern shallow perched water was not observed in the field data and the higher and lower infiltration rates were in the tail of the observed data. Peak aquifer concentrations were within a factor of two to three of the base case and the uncertainty is acceptable.

The Sr-90 uncertainty due to infiltration rates is substantially greater because changes in vadose zone water velocity are multiplied by the retardation factor, and the average Sr-90 travel time through the vadose zone is several half-lives (see Appendix J).

A-10.2.2.5 Subsurface Structure

The INTEC subsurface is a highly complex layering of basalt flows and sedimentary interbeds, and an infinite number of possible structures could be inferred from the well log data. The sensitivity analysis used the most conducive for transport and least conducive for transport generated using stochastic simulation to evaluate model sensitivity to subsurface structure. The two structures were run with Sr-90 and Tc-99.

As with the infiltration rate sensitivity, the Tc-99 sensitivity to different subsurface structures was not great because a large fraction of the Tc-99 inventory was directly injected into the aquifer at the CPP-3 disposal well. This is probably a real source of uncertainty in the model predictions because the agreement between the simulated and observed perched water was comparable and either simulation could equally represent Tc-99 contaminant transport. Peak aquifer concentrations in the year 2095 were higher than the base case, but still an order of magnitude below the MCL.

A-10.2.3 Model Uncertainty Summary

The possible impact of the uncertainty is summarized for each COPC simulated in the groundwater risk pathway (except Sr-90, which may be found in Appendix J) as follows:

- **H-3** – The majority of the H-3 released to the INTEC subsurface originated from the CPP-3 injection well. The injection well contributed 20,100 Ci and the OU 3-14 tank farm sources contributed only 10 Ci out of a total 21,500 Ci released to the subsurface. Uncertainty due to vadose zone model parameters, vadose zone model structure, net infiltration rate, and tank farm source terms is insignificant. The aquifer model was calibrated to tritium concentrations in monitoring wells, and tritium discharges to the service waste water were monitored regularly. The tritium concentrations in downgradient wells were also regularly monitored. The overall uncertainty in the tritium aquifer concentrations predictions is low.

- **I-129** – The majority of the I-129 released to the INTEC subsurface also originated from the CPP-3 injection well. The injection well contributed 0.86 Ci and the OU 3-14 tank farm sources contributed only 0.001 Ci out of a total 0.98 Ci released to the subsurface. Uncertainty due to vadose zone model parameters, vadose zone model structure, net infiltration rate, and tank farm source terms is insignificant. The aquifer model was not calibrated to aquifer I-129 concentrations but was compared to observed concentrations. The simulated and observed concentrations were similar. I-129 discharges into the service waste stream and aquifer concentrations were monitored less frequently than tritium. The overall uncertainty in the I-129 predictions of groundwater concentration is low for sources originating from the injection well and the tank farm.

- **Np-237** – The majority of the Np-237 released to the INTEC subsurface also originated from the CPP-3 injection well. The CPP-3 injection well contributed 1.07 Ci and the OU 3-14 tank farm sources contributed only 0.03 Ci out of a total 1.2 Ci released to the subsurface. Uncertainty due to vadose zone model parameters, vadose zone model structure, net infiltration rate, and tank farm source terms is small. Np-237 discharges to the service were monitored infrequently and were estimated using process knowledge. The overall uncertainty in groundwater concentration prediction from Np-237 is moderate.

- **Pu-239** – The majority of the Pu-239 released into the INTEC subsurface originated from the OU 3-14 tank farm sources and the OU 3-13 soil contamination sites. The OU 3-14 sources contributed 6.9 Ci and the OU 3-13 soil contamination sites contributed 1.1 Ci out of 8.0 Ci released to the subsurface. The CPP-31 was the largest contributor to the Pu-239 inventory, which was estimated to be accurate within 30% (20% in liquid volume and 10% in activity concentration). Pu-239 is highly retarded in the subsurface and the travel time was estimated to be 90,000 years. The source uncertainty for Pu-239 is low, but the very long vadose zone travel time increases the predictive uncertainty and the overall uncertainty in groundwater concentration prediction is high. The uncertainty of exceeding the MCL is

low because the maximum predicted concentration is several orders of magnitude below the MCL.

- **Pu-240** – The majority of the Pu-240 released into the INTEC subsurface originated from the OU 3-14 tank farm sources and the OU 3-13 soil contamination sites. The OU 3-14 sources contributed 1.07 Ci and the OU 3-13 soil contamination sites contributed 0.12 Ci out of 1.2 Ci released to the subsurface. The Pu-240 source term uncertainty and vadose zone transport uncertainty are the same as that for Pu-239. The uncertainty for the Pu-240 prediction is high. The uncertainty of exceeding the MCL is low because the maximum predicted concentration is several orders of magnitude below the MCL.

- **Tc-99** – The majority of the Tc-99 released into the INTEC subsurface originated from the CPP-3 injection well, but the OU 3-14 tank farm source also contributed a significant fraction. The CPP-3 injection well contributed 11.9 Ci and the OU 3-14 tank farm source contributed 3.56 Ci out of 16.7 Ci released to the subsurface. The majority of the tank farm source is from the CPP-31 site and the source was estimated to be accurate within 30%. However, the CPP-3 injection well source was estimated from aquifer concentration ratios of I-129 to Tc-99 and the I-129 source. The calibration of the vadose zone model to the observed Tc-99 concentrations in the northern shallow perched water wells is uncertain because the data began after peak concentrations of Tc-99 had passed through. The aquifer model also underpredicts the concentrations at the ICPP-MON-A-230 well. For these reasons, the uncertainty of the Tc-99 prediction is high.

- **U-234** – The OU 3-14 tank farm sources, OU 3-13 soil contamination sources, and the CPP-3 injection well all contributed similar amounts to the total U-234 released to the subsurface. The OU 3-14 tank farm sources contributed 0.095 Ci, the OU 3-13 soil contamination sources contributed 0.140 Ci, and the injection well contributed 0.135 Ci out of 0.391 Ci released to the subsurface. The majority of the tank farm source is from the CPP-31 site and the source was estimated to be accurate within 30%. The OU 3-13 soil site sources were estimated to be grossly conservative. The injection well U-234 was estimated from very limited data. U-234 is retarded in the subsurface, but the half-life is 244,000 years and radioactive decay en route to the aquifer is negligible. Thus, uncertainty in the radioactive decay attenuation en route to the aquifer is negligible. However, the source term is believed to be overpredicted because of the grossly high OU 3-13 estimates and an overestimated OU 3-14 source term. The overall uncertainty of the U-234 groundwater concentration prediction is moderate because of the uncertainty in the injection well source term and conservative OU 3-13 and OU 3-14 source terms. The uncertainty of exceeding the MCL is low because the maximum predicted concentration is several orders of magnitude below the MCL.

- **Mercury** – The majority of the mercury released into the subsurface originated from the OU 3-13 soil sources and CPP-3 injection well. The OU 3-13 soil sources contributed 585 kg and the injection well contributed 400 kg. The OU 3-14 tank farm sources only contributed 72 kg. The injection well source term was estimated and the OU 3-13 soil site source term was grossly overestimated and was equal to that used for the OU 3-13 RI/BRA. As a result, the overall uncertainty of the mercury groundwater concentration prediction is high. The uncertainty of exceeding the MCL is low because the maximum predicted concentration after 2095 is an order of magnitude below the MCL and the OU 3-13 sources were grossly overestimated.

- **Nitrate** – The majority of the nitrate released into the INTEC subsurface originated from the CPP-3 injection well and the former percolation ponds. The injection well contributed 2,830,000 kg; the former percolation ponds contributed 1,310,000 kg; and the OU 3-14 tank farm sources only contributed 21,200 kg out of a total 4,160,000 kg released into the subsurface. Uncertainty due to vadose zone model parameters, vadose zone model structure, net infiltration rate, and tank farm source terms is insignificant. The aquifer model was not calibrated to aquifer nitrate concentrations but was compared to observed

concentrations. The simulated and observed concentrations were similar. The overall uncertainty in the nitrate prediction of groundwater concentration is low.

A-11 REFERENCES

Ackerman, D. J., 1991, "Transmissivity of the Snake River Plain Aquifer at the Idaho National Engineering Laboratory Idaho," U.S. Geological Survey-Water Resources Investigations Report 91-4058.

Anderson, S. R. and B. D. Lewis, 1989, "Stratigraphy of the Unsaturated Zone at the Radioactive Waste Management Complex, Idaho National Engineering Laboratory, Idaho," U.S. Geological Survey Water-Resources Investigations Report 89-4065, IDO-22080.

Anderson, S. R., 1991, "Stratigraphy of the Unsaturated Zone and Uppermost Part of the Snake River Plain Aquifer at the Idaho Chemical Processing Plant and Test Reactors Area, Idaho National Engineering Laboratory, Idaho," U. S. Geological Survey Water-Resources Investigations Report 91-4010.

Bear, J., 1972, *Dynamics of Fluids in Porous Media*, New York: American Elsevier Publishing.

Bennett, C. M., 1990, "Streamflow Losses and Ground-Water Level Changes Along the Big Lost River at the Idaho National Engineering Laboratory, Idaho," DOE/ID-22091, U.S. Geological Survey Water-Resources Investigations Report 90-4067.

Brooks, R. H. and A. T. Corey, 1966, "Properties of Porous Media Affecting Fluid Flow," *J. Irrig. Drain. Div*., Am Soc. Civil Eng., Vol. 92 (IR2), pp. 61-88.

Buckham, J. A., to C. W. Bills, Atomic Energy Commission, October 12, 1970, "Liner Construction Materials CPP No. 3 Injection Well," Buc-312-70.

Cahn, L. S., and S. L. Ansley, 2004, *Analysis of Perched Water Data from ICDF Monitoring Wells*, INEEL/EXT-03-00250, Rev. 0, Idaho National Engineering and Environmental Laboratory, Idaho Completion Project, September 2004.

DOE-ID, 1994, *Track 2 Sites: Guidance for Assessing Low Probability Hazard Sites at the INEL*, DOE/ID-10389, Rev. 6, U.S. Department of Energy Idaho Operations Office, January 1994.

DOE-ID, 1997, *Comprehensive RI/FS for the Idaho Chemical Processing Plant* OU *3-13 at the INEEL, Part A, RI/BRA Report (FINAL),* U.S. Department of Energy Idaho Operations Office, DOE/ID-10534, November 1997.

DOE-ID, 1999, *Final Record of Decision Idaho Nuclear Technology and Engineering Center Operable Unit 3-13*, DOE/ID-10660, Rev. 0, U.S. Department of Energy Idaho Operations Office, October 1999.

DOE-ID, 2002, *Annual INTEC Groundwater Monitoring Report for Group 5 - Snake River Plain Aquifer (2001)*, DOE/ID-10930, Rev. 0, U.S. Department of Energy Idaho Operations Office, February 2002.

DOE-ID, 2003a, *Phase I Monitoring Well and Tracer Study Report for* OU *3-13, Group 4, Perched Water*, DOE/ID-10967, Rev. 2, U.S. Department of Energy Idaho Operations Office, March 2003. [Note: Revision 2 is Offical Use Only; Revision 1 is publicly avaiable.]

DOE-ID, 2003b, *INTEC Water System Engineering Study*, DOE/ID-11115, Rev. 0, U. S. Department of Energy Idaho Operations Office, December 2003.

DOE-ID, 2003c, *Performance Assessment for the INEEL CERCLA Disposal Facility Landfill,* DOE/ID-10978, Rev. 0, U.S. Department of Energy Idaho Operations Office, August 2003.

DOE-ID, 2003d, *Composite Analysis for the INEEL CERCLA Disposal Facility Landfill,* DOE/ID-10979, Rev. 0, U.S. Department of Energy Idaho Operations Office, August 2003.

DOE-ID, 2004a, *Operable Unit 3-14 Tank Farm Soil and Groundwater Remedial Investigation/Feasibility Study Work Plan*, DOE/ID-10676, Rev 1, U.S. Department of Energy Idaho Operations Office, June 2004.

DOE-ID, 2004b, *Vicinity Discharges Elimination Work Plan for the HWMA/RCAR Post-Closure Permit for the INTEC Waste Calcining Facility at the INEEL*, DOE/NE-ID-11138, Rev. 0, U.S. Department of Energy Idaho Operations Office, April 2004.

DOE-ID, 2004c, *Monitoring Report/Decision Summary for Operable Unit 3-13, Group 5, Snake River Plain Aquifer*, DOE/ID-11098, Rev. 1, U.S. Department of Energy Idaho Operations Office, December 2004.

DOE-ID, 2004d, *Operable Unit 3-13, Group 3, Other Surface Soils Remediation Sets 1-3 (Phase 1) Remedial Design/Remedial Action Work Plan*, DOE/ID-11089, Rev. 0, U.S. Department of Energy Idaho Operations Office, February 2004.

DOE-ID, 2005a, *Response to the First Five-Year Review Report for the Test Reactor Area, Operable Unit 2-13, at the Idaho National Engineering and Environmental Laboratory*, DOE/NE-ID-11189, U.S. Department of Energy Idaho Operations Office, May 2005.

DOE-ID, 2005b, *Waste Area Group 10, Operable Unit 10-08, Remedial Investigation/Feasibility Study Annual Status Report for Fiscal Year 2004*, DOE/NE-ID-11198, U.S. Department of Energy Idaho Operations Office, March 2005.

DOE/ID, 2006, *Annual INTEC Water Monitoring Report for Group 4—Perched Water (2005)*, DOE/ID-11259, U.S. Department of Energy Idaho Operations Office, Revision 0, January 2006.

Cecil, L. D., J. R. Pittman, T. M. Beasley, R. L. Michel, P. W. Kubik, P. Sharma, U. Fehn, and H. Gove, 1992, "Water Infiltration Rates in the Unsaturated Zone at the Idaho National Engineering Laboratory Estimated from Chlorine-36 and Tritium Profiles, and Neutron Logging," Y. K. Kharaka and A. S. Meest, eds., *Proceedings of the 7th International Symposium on Water-Rock Interaction - WRI-7, Park City, Utah.*

EDF-5758, 2005, "Geochemical Study For Perched Water Source Identification At INTEC," Rev. 0, Idaho National Laboratory, Idaho Cleanup Project, May 2005.

EDF-ER-275, 2005, "Fate and Transport Modeling Results and Summary Report," Rev. 4, Idaho National Engineering and Environmental Laboratory, Idaho Completion Project, January 2005.

EPA, 1988, "Limiting Values of Radionuclide Intake And Air Concentration and Dose Conversion Factors For Inhalation, Submersion, And Ingestion," Federal Guidance Report No. 11, EPA 520/1-88-020, U.S. Environmental Protection Agency, September 1988.

Frederick, D. B. and G. S. Johnson, 1996, *Estimation of Hydraulic Properties and Development of a Layered Conceptual Model for the Snake River Plain Aquifer at the Idaho National Engineering Laboratory, Idaho*, State of Idaho INEL Oversight Program, Idaho Water Resources Research Institute, February 1996.

Gee, G. W., D. G. Felmy, J. C. Ritter, M. D. Campbell, J. L. Downs, M. J. Fayer, R. R. Kirkham, and S. O. Link, 1993, *Field Lysimeter Test Facility Status Report IV: FY 1993*, PNL-8911 UC-902, Pacific Northwest Laboratory, 1993.

Golder Associates, Inc, 1992, *Report for the Idaho Chemical Processing Plant Drilling and Sampling Program at Land Disposal Unit CPP-37 (DRAFT)*, Prepared for EG&G Idaho, Inc./Westinghouse Idaho Nuclear Company, under Contract No. C90 132739, 903-1161, March 1992.

Honkus, R. J., 1982, *ICPP CY-1981 Effluent Monitoring Report*, ENICO-1115, Exxon Nuclear Idaho, Inc., May 1982.

ICP, 2004, *Evaluation of Tc-99 in Groundwater at INTEC: Summary of Phase 1 Results*, ICP/EXT-04-00244, Rev. 0, Idaho National Engineering and Enivronmental Laboratory, Idaho Completion Project, September 2004.

INEEL, 2003a, *Analysis of Baseline Data from ICDF Detection Monitoring Wells*, INEEL/EXT-03-00251, Rev. 0, Idaho National Engineering and Environmental Laboratory, August 2003.

INEEL, 2003b, *Comprehensive Facility and Land Use Plan*, http://cflup.inel.gov/, Idaho National Engineering and Environmental Laboratory, Web page created 2003, Web page visited March 16, 2005.

INEL, 1995a, *Report of 1993/1994 Tank Farm Drilling and Sampling Investigation at the Idaho Chemical Processing Plant*, INEL-95/0064, Idaho National Engineering Laboratory, February 1995.

INEL, 1995b, *Waste Area Group 3 Comprehensive Remedial Investigation/Feasibility Study Work Plan (FINAL)*, INEL-95/0056, Vol.1, Idaho National Engineering Laboratory, August 1995.

Kehow, A. E., 2001, *Applied Chemical Hydrogeology*, Upper Saddle River, New Jersey: Prentice-Hall, Inc..

Knutson, C. F., K. A. McCormick, R. P. Smith, W. R. Hackett, J. P. O'Brien, and J. C. Crocker, 1990, *FY 89 Report RWMC Vadose Zone Basalt Characterization*, EGG-WM-8949, EG&G Idaho, Inc., Idaho National Engineering Laboratory, July 1990.

Magnuson, S. O., 1995, *Inverse Modeling for Field-Scale Hydrologic and Transport Parameters of Fractured Basalt*, INEL-95/0637, Idaho National Engineering Laboratory, December 1995.

Magnuson, S. O. and A. J. Sondrup, 1998, *Development, Calibration, and Predictive Results of a Simulator for Subsurface Pathway Fate and Transport of Aqueous- and Gaseous-Phase Contaminants in the Subsurface Disposal Area at the Idaho National Engineering and Environmental Laboratory*, INEEL/EXT-97-00609, Idaho National Engineering and Environmental Laboratory, July 1998.

Martian, P., 1995, *UNSAT-H Infiltration Model Calibration at the Subsurface Disposal Area, Idaho National Engineering Laboratory*, INEL-95/0596, Idaho National Engineering Laboratory, October 1995.

Martian, P., 1999, *Numerical Modeling Support of the Natural Attenuation Field Evaluation for Trichloethene at the Test Area North, Operable Unit 1-07B, Idaho National Engineering and Environmental Laboratory*, INEEL/EXT-97-01284, Rev. 1, Idaho National Engineering and Environmental Laboratory, January 1999.

NCRP, 1996, *Screening Models for Release of Radionuclides to Atmosphere, Surface Water, and Ground*, NCRP Report No. 123 I&II, National Council on Radiation Protection, January 1996.

Orr, B. R., L. D. Cecil, and L. L. Knoble, 1991, "Background Concentrations of Selected Radionuclides, Organic Compounds, and Chemical Constituents in Ground Water in the Vicinity of the Idaho National Engineering Laboratory," U. S. Geological Survey-Water Resources Investigations Report 91-4015.

Parker, J. C., R. J. Lenhard, and T. Kuppusamy, 1987, "A Parametric Model for Constitutive Properties Governing Multiphase Flow in Porous Media," *Water Resources Research*, Vol. 23, No. 4, pp. 618-624.

Perry, R. H., D. W. Green, and J. O. Maloney, 1984, *Perry's Chemical Engineers' Handbook, Sixth Edition*, New York: McGraw Hill Book Company.

Roback, R. C., T. M. Johnson, T. L. McLing, M. T. Murrell, S. Luo, and T. L. Ku, 2001, "Uranium Isotopic Evidence for Groundwater Evolution and Flow Patterns in the Eastern Snake River Plain Aquifer," *Idaho Geologic Society America Bulletin*, 113, pp. 1133-1141.

Robertson, J. B., R. Schoen, and J. T. Barraclough, 1974, "The Influence of Liquid Waste Disposal on the Geochemistry of Water at the National Reactor Testing Station, Idaho: 1952-1970," IDO-22053, TID-4500, U.S. Geological Survey Open File Report, February 1974.

Rood, A. S., 1999, *GWSCREEN: A Semi-Analytical Model for Assessment of the Groundwater Pathway from Surface or Buried Contamination*, INEEL/EXT-98-00750 (Revised July 17, 2002), Idaho National Engineering and Environmental Laboratory, February 1999.

Sheppard, M. J., and D. H. Thibault, 1990, "Default Soil Solid/Liquid Partition Coefficients Kd's for Four Major Soil Types: A Compendium," *Health Physics* 59(4), pp. 471-482, 1990.

Shook, G. M., 1995, *Development of an Environmental Simulator from Existing Petroleum Technology*, INEL-94/0283, Idaho National Engineering Laboratory.

Shook, G. M., J. H. Forsmann, M. E. Velasquez, and S. O. Magnuson, 2003, "Improving Numerical Model Efficiency of an Existing, In-House Simulation Model," *Laboratory-Directed Research and Development, FY-2003 Annual Report*, INEEL/EXT-04-01772, Idaho National Engineering and Environmental Laboratory, pp. 197-199.

Smith, R. P., 2002, *Aquifer Thickness Assessment for Use in WAG 10*, OU *10-08 Groundwater Modeling Activities*, INEEL/INT-01-01458, Rev. 0, Idaho National Engineering and Environmental Laboratory, February 2002.

USGS, 2004, *NWISWeb Data for the Nation*, http://waterdata.usgs.gov/nwis, U.S. Geological Survey, Web page visited December 15, 2005.

Vinsome, P. K. W. and G. M. Shook, 1993, "Multi-Purpose Simulation," *Journal of Petroleum Science and Engineering*, Vol. 9, pp. 29-38, Elsevier Science Publishers B. V., Amsterdam.

Wood, T. R., 1989, *Test Area North Pumping Tests 1953-1987*, EGG-ER-8438, EG& G Idaho, Idaho National Engineering Laboratory, January 1989.

Van Genuchten, M. Th., 1980, "A Closed-Form Equation for Predicting the Hydraulic Conductivity of Unsaturated Soils," *Soil Science Society of America Journal*, 44, pp. 892-898.